Petrography, geochemistry and sedimentology of sandstones from the Central Tertiary Basin of Svalbard – implications for diagenesis and temperature history

Master Thesis in Basin and Reservoir Studies

Elisabeth Osaland

Department of Earth Science
University of Bergen
September 2019

Abstract

Svalbard, representing an uplifted area of the north-western Barents Sea Shelf, provides a unique opportunity for studying on-shore outcrops of the shelf. The present study focuses on Paleocene-Eocene deposits of the Central Tertiary Basin (CTB), located in central-southern parts of Spitsbergen. Despite the large number of studies concerning diagenetic alteration of sedimentary rocks, parameters controlling the types and distribution of authigenic minerals are still not fully understood. Here, I systematically relate the early diagenetic minerals of the Firkanten, Grumantbyen and Aspelintoppen formations to sandstone composition and depositional environment. The identification of these diagenetic minerals integrates petrographic observations obtained from thin section analyses (optical microscopy and SEM) and XRD-analysis. Sedimentological analysis is supplemented by geochemical data, providing a better understanding of large- and small-scale variations in lithology and, thus, depositional environment.

The different authigenic mineral assemblages of the sandstones of the Firkanten, Grumantbyen and Aspelintoppen formations are related to their different detrital compositions and depositional environment. The generally higher porosity values of the Grumantbyen Formation sandstones may be ascribed to the occurrence of grain coating chlorite, preventing precipitation of quartz cement at great burial depths. The relatively homogenous nature of these sandstones provides conditions favourable for precipitation of early berthierine rims. At temperatures of about 90^{o}C (i.e. subsequent to the onset of quartz cementation) berthierine is altered into chlorite, suggesting that early diagenetic berthierine-rims, rather than later burial grain-coating chlorite, is responsible for preventing quartz cementation. The occurrence of glauconite in the lowermost part of the Firkanten Formation (Todalen Member), accompanied by abundant framboidal pyrite, may indicate the onset of transgressive conditions and deposition of the overlying marine Endalen Member. Burial diagenesis is largely influenced by the presence of early diagenetic products, in which they affect a variety of diagenetic processes. Burial diagenetic minerals, usually indicating a specific burial depth and minimum-temperature, can be used to cross-check temperatures derived from organic maturity indicators (e.g. vitrinite reflectance). The burial diagenetic signatures of the studied formations (e.g. quartz, Fe-chlorite, ankerite), suggest maximum temperatures of at least 100-110^{o}C. Extensive quartz cementation in sandstone samples from the Firkanten and Grumantbyen formations, however, may support higher temperatures, as suggested by vitrinite reflectance measurements of coals.

Acknowledgements

This thesis was conducted at the Department of Earth Science at the University of Bergen and, in part, at the University Centre in Svalbard. I would like to acknowledge several people for their contribution and encouragement – this research project would not have been possible without you.

First, I would like to express my sincerest gratitude to my supervisor Helge Hellevang (UiO) for his guidance, encouragement and support. A big thanks to my co-supervisors William Helland-Hansen (UiB), Malte Jochmann (UNIS), Snorre Olaussen (UNIS) and Maria Jensen (UNIS) for their feedback and interesting discussions. A special thanks to Malte for taking good care of me at UNIS and for helping me to collecting the cores in Endalen. Thanks to Helge for going all the way to Svalbard with me this winter for XRF-analysis of the cores. I would also like to express my appreciation to Beyene Girma Haile (UiO) for performing XRD-analysis of selected core-samples.

Furthermore, I would like to thank Store Norske Spitsbergen Kullkompani (SNSK) for giving me access to their core storage in Endalen and UNIS for letting me store more than 200 meters of cores at Logistics. A big thanks to the Department of Earth Science at the University of Bergen for generously funding parts of this research, and to the Department of Geosciences at the University of Oslo for thin section preparations.

Thanks to my fellow students and friends at the University of Bergen for five indelible years. A special thanks to the people at “Hovedkvarteret” and “Grotten”, and to my Svalbard-friends for making my stay at UNIS unforgettable. Last but not least, I would like to thank Anne-Brit and Malin for their encouragement and support, and for always believing in me. A big thanks to my fellow student May Britt for proof reading and good advices.

Elisabeth Osaland

Bergen, 2nd of September 2019

Table of Contents

1 Introduction

1.1 Aim of study

Temperature, being a crucial factor controlling diagenesis in sedimentary rocks, is important for assessing a range of different parameters, including fluid flow, petroleum generation, chemical compaction, and estimations of the amount uplift and erosion (Haile et al., 2018b). Constraining the thermal history of sedimentary basins is thus essential in forecasting the quality of reservoir rocks. Svalbard, representing an uplifted area of the north-western Barents Sea Shelf, provides a unique opportunity for studying on-shore outcrops of the shelf. Reconstructions of the thermal history of the Central Tertiary Basin (CTB), however, are chiefly restricted to vitrinite reflectance (VR) studies of coals (Manum and Throndsen, 1978; Throndsen, 1982) . Organic maturity indicators (i.e. VR) provide a direct measure of thermally induced changes rather than a direct measure of paleotemperatures. Temperatures derived from organic maturity indicators are thus calculated indirectly using various models or empirical regression equations, suggesting that it may be difficult to obtain accurate temperature estimates (Haile et al., 2018b). Diagenetic processes in sedimentary rocks, however, are strongly linked to a specific burial depth and temperature, suggesting that authigenic minerals usually indicate a specific burial depth and minimum-temperature or temperature interval (Worden and Burley, 2003; Bjørlykke and Jahren, 2015) .

Diagenetic processes (i.e. mechanical/chemical compaction and cementation) are largely influenced by the detrital composition of sandstones (Bjørlykke, 2001; Morad et al., 2012). The detrital composition of sandstones, in turn, is a function of depositional environment, transport and provenance. Common diagenetic processes, including mechanical compaction, grain dissolution (e.g. feldspar), formation of kaolinite and growth of pore-lining minerals (e.g. grain coating chlorite), can thus be linked to depositional facies and depositional environment (Morad et al., 2010). Depositional facies and depositional environment control a variety of parameters, including initial porosity and permeability, sand/mud ratio and sand-body geometry, which, in turn, affect the rate and path-ways of fluid flow (Morad et al., 2010). The amount and distribution of eogenetic alterations in sandstones is largely influenced by the rate and path-ways of fluid flow, whereas burial diagenesis is controlled by the amount of fluid flow through the remaining porosity and the presence of early diagenetic products. Early diagenetic products

affect, for instance, clay mineral transformations and precipitation of quartz cement, in which the latter is of great importance to reservoir quality (Morad et al., 2010).

Diagenetic alteration of reservoir rocks has frequently been studied in the Barents Sea region (e.g. Riis et al., 2008; Mørk, 2013). Nevertheless, paleotemperature estimates of the rocks are based on vitrinite reflectance studies of coals, Rock-Eval pyrolysis and fission track analyses rather than diagenetic signatures (e.g. Abay et al. cited in Haile et al., 2018b). Haile et al. (2018b), however, recently presented an integrated approach of thermal history reconstruction, utilising the middle to upper Triassic strata of Edgeøya, Svalbard. Paleotemperatures of the sedimentary sequence were estimated using Rock Eval pyrolysis parameters, fluid inclusions in diagenetic quartz and inorganic diagenetic signatures of sandstones. Furthermore, the study of Dörr et al. (2018) provides a basin model based on low-temperature thermochronology data, vitrinite reflectance measurements and clay mineralogy. The diagenetic signatures (clay minerals) seem to be consistent with vitrinite data, suggesting maximum temperatures of 90-100^{o}C for the Eocene coals and 120-130^{o}C for the Paleocene coals. Furthermore, Dörr et al. (2018) argued that nearly 4000 m of sediments have been removed from the Central Tertiary Basin since the Early Eocene. The present estimate is considerably higher than previous estimates, ranging from 1000 m to approximately 3500 m (Manum and Throndsen, 1978; Blythe and Kleinspehn, 1998; Marshall et al., 2015).

Despite the large number of studies concerning diagenetic alteration of sedimentary rocks, the parameters controlling their spatial and temporal distribution are still not fully understood (Morad et al., 2012). The study of Mørk (2013), however, discussing the diagenetic alteration of reservoir sandstones of the Upper Triassic-Middle Jurassic De Geerdalen and Knorringfjellet formations (Svalbard), demonstrates that diagenesis and distribution of quartz cement is strongly controlled by lithofacies and detrital composition. Furthermore, Haile et. al (2018a) provides a detailed study of the diagenetic alteration of the middle to late Triassic sandstones of Edgeøya, Svalbard, aiming to link diagenesis and reservoir quality to depositional facies. The study suggests that the variability of diagenetic signatures is a function of depositional facies, and that the diagenetic alteration variability between depositional facies results from differences in the quality of grain-coating chlorite, the extent and distribution of porefilling clays, quartz and carbonate cements, sorting, and distribution of grain sizes.

Initially, the main purpose of the present thesis was to investigate if authigenic minerals can be used to estimate the maximum temperature of reservoirs, requiring that the reservoir has experienced temperatures not higher than 130ºC and not lower than 60ºC. Authigenic minerals can thus be used to support previous estimates of paleotemperatures based on vitrinite reflectance and/or be used unattended where coal or other paleotemperature indicators are absent. The deep burial of the CTB and high degree of mechanical and chemical compaction, however, complicated the use of authigenic minerals as a paleothermometer. The main focus of this thesis was thus rather to investigate the importance of depositional environment to diagenesis in sandstones. The data was obtained from sedimentological and petrographic analyses of the Firkanten, upper part of Grumantbyen and Aspelintoppen formations, constituting the lower, lower-middle and upper part of the Van Mijenfjorden Group, respectively (often referred to as the Central Tertiary Basin). The sub-objectives of this thesis were to:

1. Discuss factors controlling the types and distribution of authigenic minerals
2. Identify geochemical trends in the sediment cores and to investigate whether these can be correlated to the sedimentary logs
3. Discuss the consistency between authigenic signatures and vitrinite reflectance measurements of coals/organic matter – do they tell the same temperature history?

1.2 Data background

Spitsbergen – the largest island of the Svalbard archipelago – is situated in the north-western corner of the Barents Shelf. The Central Tertiary Basin covers the central and southern parts of Spitsbergen, extending from north of Isfjorden to the Sørkapp area, and from near the east coast to the eastern front of the West Spitsbergen Fold and Thrust Belt (Fig. 1.1). The present thesis is based on data from drill cores of the Store Norske Spitsbergen Kullkompani (SNSK) wells 7-2006 and 11-2003, utilising the coal-bearing Firkanten Formation (7-2006), the upper part of Grumantbyen Formation (7-2006 and 11-2003) and the Aspelintoppen Formation (11-2003). The wells, located between Van Mijenfjorden and Isfjorden in the northern part of the Central Tertiary Basin, were drilled as a part of SNSKs coal-exploration (Fig. 1.1). The excellent-exposed outcrops of the Svalbard archipelago and abundance of extensive coal deposits, allowing comparison of results with vitrinite data, justify the choice of study area.

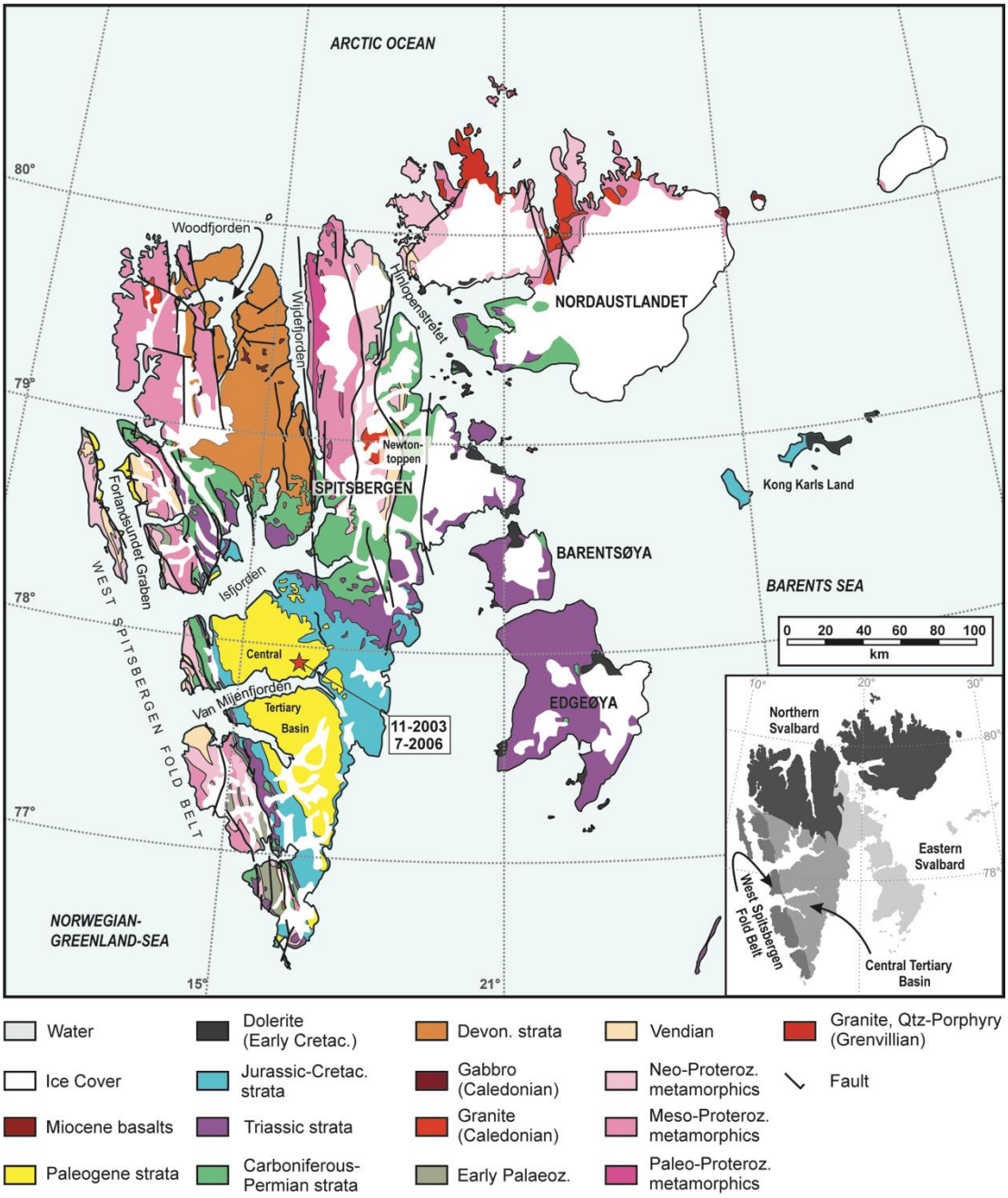

Figure 1.1: Geological map of Svalbard. The red star indicates the location of cores 11-2003 and 7-2006. Slightly modified from Dörr et al. (2018).

2 Geological framework

2.1 Introduction

The Svalbard archipelago comprises all islands between 74-81°N and 10-35°E, covering a land-area of more than 60 000 km^2. Svalbard, representing an uplifted area of the north-western Barents Sea Shelf, provides a unique opportunity for studying on-shore outcrops of the shelf, including Cenozoic deposits (Central Tertiary Basin). The geological record of Svalbard is well-preserved, ranging in age from Late Precambrian to Paleogene. Precambrian to Early Silurian metamorphic rocks are present in northern and western parts of Svalbard, Devonian grabens in the north, Late Paleozoic and Mesozoic platform sediments in the central and eastern parts, and Paleogene sediments in the central and southern parts of Spitsbergen. The geological record shows evidence of multiple tectonic events, in which the most prominent are the Grenvillian (Precambrian), Caledonian (Ordovician-Silurian) and the West Spitsbergen orogeny (Paleogene) (Dallmann, 1999). The late Paleozoic to Cenozoic record of Svalbard reflects the northwards movement of Svalbard from equatorial regions in the Devonian-Early Carboniferous to its current high-latitude position (Worsley, 2008).

The focus of the present thesis it the Paleocene-Eocene Central Tertiary Basin, reflecting the opening of the Norwegian-Greenland Sea and accompanying formation of the West Spitsbergen Fold and Thrust Belt.

2.2 The Cenozoic sedimentary system

The Central Tertiary Basin (CTB) – the focus of the present thesis – formed in response to the opening of the Norwegian Greenland Sea and formation of the West Spitsbergen Fold and Thrust Belt (Steel and Worsley, 1984). The CTB occupies an area of 200 x 60 km, extending from north of Isfjorden to the Sørkapp area, and from near the eastern coast of Spitsbergen to the eastern front of the West Spitsbergen Fold and Thrust Belt. The Paleogene sediment fill of the CTB, composing sandstones, siltstones, shales and subordinate coals and conglomerates, is called the Van Mijenfjorden Group. A Paleocene-Eocene age is generally accepted for the Van Mijenfjorden Group (Harland, 1969), although Livsic (cited in Steel and Worsley, 1984) suggested, in part, an Oligocene age for the succession. Vitrinite reflectance measurements of coals suggest that 1500-3000 m of sediments were removed by post-Oligocene erosion (Manum and Throndsen, 1978; Throndsen, 1982).

The formation of the CTB is firmly related to the large-scale Cenozoic Eurekan orogeny (Dörr et al., 2018). The concurrent spreading in the Baffin Bay-Labrador Sea and Norwegian-Greenland Sea, resulted in a northeast movement of Greenland from c. 55 Ma onwards. The latter caused compression along the western parts of Spitsbergen, resulting in extensive basement uplift and growth of a 300 km long NNW-SSE trending fold and thrust belt, referred to as the West Spitsbergen Fold and Thrust Belt (WSFTB) (Piepjohn et al., 2016). Furthermore, subsidence east of the WSFTB resulted in formation of a 60 km wide NNW-SSE trending trough – the Central Tertiary Basin (Steel et al., 1981; Grundvåg et al., 2014). The Eurekan deformation and accompanying northward movement of Greenland peaked at c. 50 Ma. At c. 49 Ma, however, changing spreading directions in the Baffin Bay-Labrador Sea caused Greenland to move northwestward, resulting in a change in the deformation regime from compression to dextral transpression in the west (Piepjohn et al., 2016; Dörr et al., 2018). Finally, at c. 36 Ma, seafloor spreading in the Baffin Bay-Labrador Sea terminated, eventually resulting in extension between Svalbard and Greenland.

The sediment fill of the CTB – the Van Mijenfjorden Group – can tectono-stratigraphically be divided into two parts: (1) a lower mainly Paleocene part and (2) an upper mainly Eocene part (Fig. 2.1). The succession composes wave- and tidal influenced deltaic deposits, showing a large scale landward-stepping-basinward-stepping depositional pattern (Bruhn and Steel, 2003). The succession thickens from 1500 m in the northeast to 2500 m in the southwestern

part, reflecting the asymmetric shape of the basin towards the western margin (Steel and Worsley, 1984). The CTB shows gently dipping strata in the east and steeply-vertically dipping strata in the western part, resulting from the folding and thrusting of the WSFTB. (Dallmann,1999).

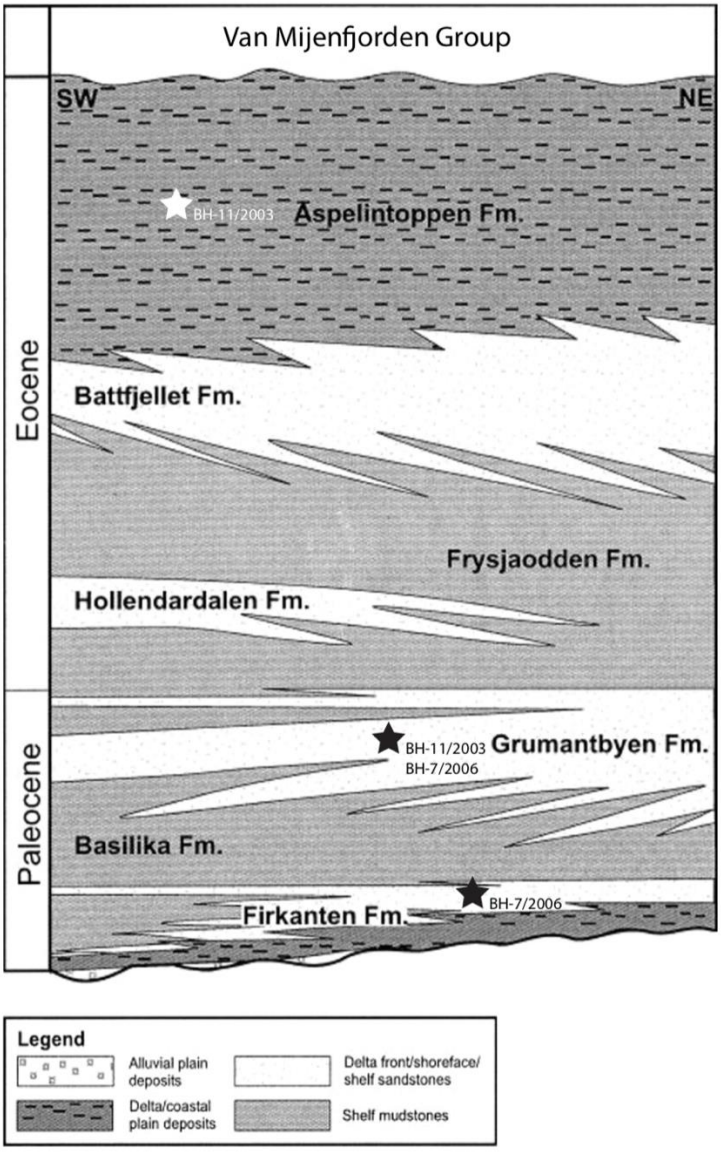

Figure 2.1: The Paleocene-Eocene Van Mijenfjorden Group, representing the sediment infill of the Central Tertiary Basin (CTB). The formations studied in this work are marked with a star and core-name. Slightly modified from Bruhn and Steel (2003).

The lowermost Paleocene succession, thickening from less than 300 m in the north-eastern parts of the basin to more than 800 m in the west, can be divided into the Firkanten Formation, Basilika Formation, Grumantbyen Formation and lowermost part of Frysjaodden Formation (Fig. 2.1). The uppermost Eocene succession is more than 1500 m thick, comprising the

Frysjaodden Formation, Hollenderdalen Formation, Battfjellet Formation and Aspelintoppen Formation (Fig. 2.1). The Frysjaodden Formation reflects the change in sediment supply from a probably eastern source area to the fold and thrust belt in the west (Steel et al., 1985). The lowermost Paleocene succession shows an overall landward-stepping (i.e. transgressive), east-migrating depositional pattern whereas the uppermost Eocene succession shows an overall basinward-stepping (i.e. regressive), east-migrating depositional pattern, reflecting the main infilling of the CTB (Bruhn and Steel, 2003). Shelf paleo water-depths of the CTB have been estimated to be less than 20 metre on the continental shelf and hundreds of meters across the shelf edge (Helland-Hansen, 2010; Mellere et al., 2002).

A westerly source is generally accepted for the Eocene-succession, reflecting the growth of the WSFTB (Petersen et al., 2016). The source area for the Paleocene-succession, however, is still not fully understood; both the WSFTB and a so-called peripheral bulge east of the basin (see section 2.3) have been suggested (Petersen et al., 2016). However, the occurrence of Cretaceous-aged zircon in the Paleocene Firkanten Formation indicate (at least in part) an easterly source for the Paleocene-succession, in which Cretaceous igneous rocks are exclusively occurring in the eastern and northeastern Svalbard (i.e. indicate sourcing from the east) (Petersen et al., 2016). Furthermore, the absence of Cretaceous-aged zircon in the Eocene Battfjellet Formation confirm a westerly source for the Eocene-succession.

2.3 Basin fill of the Central Tertiary Basin

The sedimentary succession of the Central Tertiary Basin provides an important record of the tectonic events associated with the opening of the Norwegian-Greenland Sea. Two general models have been established for the CTB formation: (1) Steel et al. (1981) suggested a two-step transtension-transpression scenario (Fig. 2.2), whereas Bruhn and Steel (2003) proposed a single, compressional foreland-basin scenario. The two-step transtension-transpression scenario presumes formation of several coal-forming basins, resulting from Late Cretaceous-Early Paleocene strike-slip movements along the Greenland-Svalbard plate boundary. Finally, Late Paleocene-Early Eocene transpression and thrust loading combined the basins into a single foreland basin. The model of Bruhn and Steel (2003) rather assumes formation of a flexural trough in front of the thrust wedge of the WSFTB. Furthermore, lithospheric loading resulted in formation of a peripheral bulge east of the WSFTB. The fold and thrust belt in the west (WSFTB), syndepositional tilting of the basin towards the orogen and later incorporation of the

orogenic flank into the deformation, support the model of Bruhn and Steel (2003). (Dickinson and Yarborough cited in Helland-Hansen, 1990). However, Steel et al. (1981) divided the stratigraphy of the CTB into three main depositional phases: (1) a transgressive phase reflecting episodic west and southwestward progradation of deltas, and (2) two regressive phases reflecting east and southeastward progradation of delta-systems. The different depositional stages will be further described in the following.

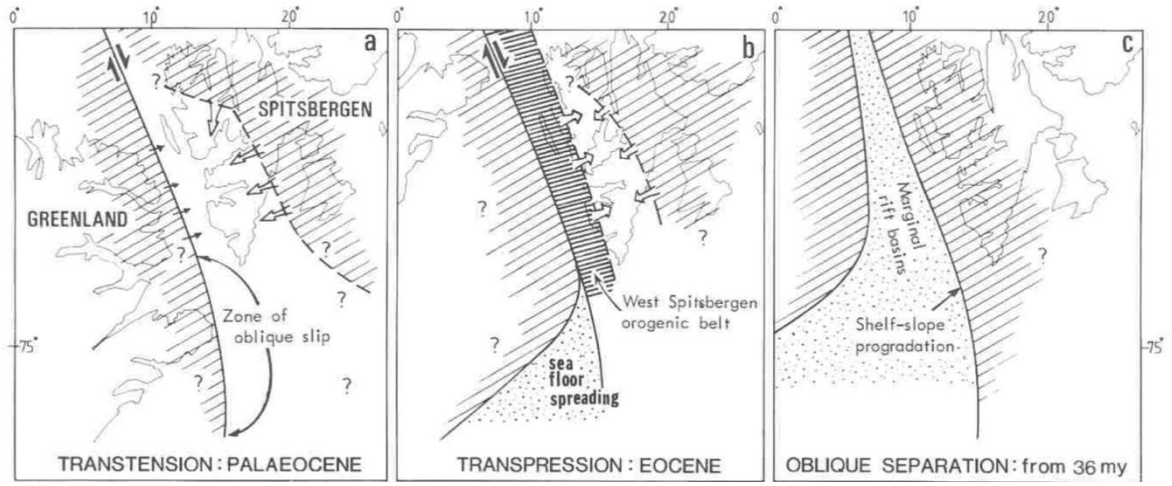

Figure 2.2: The two-step transtension-transpression model suggested by Steel et al. (1981). From Steel and Worsley (1984).

2.3.1 The transgressive phase of basin infilling – Firkanten and Basilika formations

The Firkanten and Basilika formations, representing the first phase of basin infilling, are of Paleocene age. Furthermore, the succession is thought to have been sourced from the peripheral bulge east of the WSFTB (Petersen et al., 2016).

The coal-bearing Firkanten Formation constitutes the lowermost part of the Van Mijenfjorden Group, representing the first basin infill of the Central Tertiary Basin. Analysis of fission-track ages from apatite grains suggest a Danian age (i.e. Early Paleocene) for the Firkanten Formation (Blythe and Kleinspehn, 1998; Bruhn and Steel, 2003). The succession, resting unconformably on the Early Cretaceous Carolinefjellet Formation, thickens from less than 100 m in the northeast to 200 m in the western part of the basin (Bruhn and Steel, 2003). The resultant hiatus suggests Late Cretaceous erosion or non-deposition in the northwestern part of the Barents Shelf (e.g. Harland cited in Dörr et al., 2018). The Firkanten Formation can be subdivided into three members: The Todalen Member, Endalen Member and Kolthoffberget Member. The

lowermost Todalen Member (less than 60 m thick), composes alternating mudstones, coal-beds, siltstones and fine-grained sandstones, representing fluvial-dominated delta deposits (Bruhn and Steel, 2003). Lüthje (2008), however, interpreted the lowermost part of the Firkanten Formation (i.e. Todalen Member) to represent wave-dominated coastal plain deposits of minor fluvial input. The overlying marine Endalen Member thickens from 40 m in the northeast to 100 m in the south and southwest. The succession composes shoreface deposits, reflecting the landward migration of the coastline. The mudstones of the Kolthoffberget Member, present in the western and southern parts of the Central Tertiary Basin, form the deep-marine equivalent to the Endalen Member (Steel et al., 1981). Despite the overall transgressive nature of the succession, several smaller-scale regressive units occur (Steel et al., 1981).

The overlying Basilika Formation composes black and grey shales, siltstones and interbedded very fine sandstones, representing outer shelf to deep marine deposits. The succession ranges in thickness from 430 m in the western part of the basin to about 30 m in the north and northeast (Steel et al., 1981). The lower part of the Basilika Formation composes mudstones and siltstones, showing fining- and deepening-upwards, whereas the upper part of the succession is composed of upwards-coarsening packages, each 2-15 m thick (Steel et al., 1981; Bruhn and Steel, 2003). Studies of foraminifera in the lower-middle part of the succession suggest a late Paleocene age for the Basilika Formation (Nagy et al., 2001) .

2.3.2 The first regressive phase of basin infilling – Grumantbyen and Hollenderdalen formations

The Grumantbyen and Hollenderdalen formations constitute the second phase of basin infilling. The regressive depositional pattern of the succession implies that sediment supply outpaced rates of subsidence, although the high degree of bioturbation of the Grumantbyen Formation sandstones indicates relatively low sediment supply.

The Grumantbyen Formation, constituting the lower part of the second phase of basin infilling, composes greenish-grey intensively bioturbated sandstones. The greenish colour of the sandstones reflects the high glauconite-content of the formation (Steel et al., 1981). The succession thickens from 200 m in the southwestern part of the basin to approximately 450 m in the northeast (Dallmann, 1999). Although the Grumantbyen Formation is poorly understood, Steel et al. (1985) suggested an offshore origin of the formation, probably representing offshore

bar deposits. The succeeding Hollenderdalen Formation, predominantly composing sandstones, is suggested to represent tide-influenced delta deposits (Dalland, 1976). The succession is up to 150 m thick in the west, pinching out into the marine shales of the Frysjaodden Formation in the north-eastern part of the basin (Dalland, 1976).

2.3.3 The second regressive phase of basin infilling – Frysjaodden, Battfjellet and Aspelintoppen formations

The Frysjaodden, Battfjellet and Aspelintoppen formations represent the third and final phase of basin infilling. The succession shows a total thickness of 1500 m, ranging in age from late Paleocene to Eocene.

The Frysjaodden Formation constitutes the lowermost part of the third phase of basin infilling. The succession reflects the long-term eastward migration of the basin depocenter and change in sediment supply from the source areas in the east to the fold and thrust belt in the west (Steel et al., 1985). The succession composes deep-marine shales, occasionally interbedded with turbiditic sandstones (Crabaugh and Steel, 2004). The succession is absent in the south-eastern parts of the basin and up to 150 m thick in the north-west (Steel et al., 1981).

The Battfjellet Formation, ranging in thickness from 60 m in the northeast to 200 meters in the southwestern part of the basin, composes upwards-coarsening packages of siltstones and sandstones. Steel (1977) interpreted the succession to represent prograding wave-dominated deltaic and barrier coastlines. The large-scale eastward prograding clinothems of the Battfjellet Formation reflects the high sediment influx from the WSFTB in the west.

The Aspelintoppen Formation, constituting the uppermost and thickest succession of the Van Mijenfjorden Group, represents the final basin infill of the Central Tertiary Basin. The formation is more than 1000 m thick south of Van Mijenfjorden; north of the Van Mijenfjorden, only thinner deposits are preserved (Steel et al., 1981). The succession, composing poorly sorted sandstones, siltstones and subordinate coal-layers, overlies and interfingers the marine Battfjellet Formation. Steel et al. (1981) interpreted the Aspelintoppen Formation to be of delta plain origin, predominantly composing flood plain and lacustrine deposits. Furthermore, high degree of soft-sediment deformation is a diagnostic feature of the formation, reflecting high

sediment supply and frequent earthquakes (Steel et al., 1981). The abundant soft sediment deformation often makes it difficult to distinguish the sedimentary structures during logging.

2.4 The Cenozoic climate

Climate, being a crucial factor controlling erosion and weathering, is important for the detrital mineral composition of sedimentary rocks. The mineral composition, in turn, is important for the types and distribution of diagenetic processes in sediments. Paleomagnetic data suggests a paleo-latitude of 71-72^{o}N for Svalbard in the Eocene (Dalland, 1976). The Paleogene climate was warm-temperate or moderately temperate (Golovneva, 2000). Based on analysis of conifers, Schweitzer (1980) suggested an annual mean temperature of 15-18^{o}C. The paleotemperature estimates of Schweitzer (1980) is consistent with more recently estimates; Golovneva (2000) suggested an annual temperature-range of about 13-19^{o}C. Schweitzer (1980) argued that precipitation was moderate to absent in the winter and heavy in the summer. The study of Golovneva (2000), however, suggests high precipitation equally distributed over the year. Compared to the present-day mean temperature for similar latitudes, e.g. Troms in Norway, the Paleocene-Eocene climate was considerably warmer (Dypvik et al., 2011). The relatively warm and humid Paleocene-Eocene climate, reflecting the PETM (Paleocene-Eocene Thermal Maximum), implies high degree of erosion and weathering. The study of Dypvik et al. (2011) shows a distinct decrease in feldspar content and accompanying increase in the relative amounts of kaolinite, reflecting higher temperatures and resultant increase in precipitation.

3 Theoretical background

3.1 Introduction

Diagenesis comprises all the chemical, physical and biologic processes occurring in a sediment after its initial deposition (Bjørlykke and Jahren, 2015). The primary composition of sandstones, which is a function of provenance, transport and depositional environment, is the starting point for diagenetic processes. The primary composition is thus an important factor controlling diagenetic alteration of sandstones (Bjørlykke and Jahren, 2015). In addition, the properties of sandstones are largely dependent on their temperature and stress history during burial; prolonged exposure to high temperatures and stresses results in a variety of diagenetic processes. The main diagenetic processes, however, are (1) near surface diagenesis, (2) mechanical compaction, (3) chemical compaction and (4) precipitation of cements and formation of authigenic minerals (Bjørlykke and Jahren, 2015). Mechanical compaction is the most important factor reducing porosity at shallow burial depths; at greater depths, chemical compaction (e.g. precipitation of quartz cement) prevents further mechanical compaction of the sandstone. In the literature, near surface diagenesis and burial diagenesis are often referred to as eogenesis and mesogenesis, respectively.

3.2 Factors controlling diagenesis

The distribution of diagenetic alterations in sandstones is largely controlled by detrital composition, texture (grain size, sorting, form), porewater chemistry and burial history. Other factors of importance to diagenesis include depositional environment, sequence stratigraphy and paleoclimatic conditions (Bjørlykke, 2001; Al-Ramadan et al., 2012). Changes in either porewater chemistry, temperature or stress results in diagenetic reactions and accompanying alteration of the sediment (Worden and Burley, 2003).

The detrital composition of sandstones is crucial for the types and distribution of diagenetic processes (Bjørlykke, 2001; Morad et al., 2012). Furthermore, the sandstone composition largely controls their mechanical- and chemical properties, in which sandstones composing ductile grains (e.g. mud intraclasts, low-grade metamorphic rock fragments) experience higher degree of mechanical compaction than sandstones rich in rigid grains (quartz and felspar). In addition, the degree of compaction, both mechanical and chemical, is dependent on grain size,

sorting and form, which, in turn, is dependent on depositional environment and transport. The abundance of quartz cement is, in part, a function of grain surfaces available for quartz precipitation; the more quartz grains and the bigger the surface area, the more quartz cement is precipitated. Assuming that the sand is well-sorted, the latter implies that fine-grained sand contains more quartz cement than coarser-grained sand (Bjørlykke, 2001).

Changes in the relative sea-level, resulting from changes in the eustatic sea level and/or tectonic uplift/subsidence and rate of sediment supply, controls the sequence stratigraphic framework and distribution of facies in siliciclastic deposits (Al-Ramadan et al., 2012). Factors controlling diagenesis, including detrital composition, porewater chemistry and residence time, is largely influenced by relative sea-level changes, suggesting that diagenesis can be systematically linked to sequence stratigraphy. Types of diagenetic reactions are often characteristic for specific systems tracts and boundaries, e.g. authigenic kaolinite is typical for sandstones localized immediately below erosional surfaces. The importance of porewater chemistry (meteoric water) and burial history will be further discussed in the following sections.

3.3 Early diagenesis

Early diagenetic reactions start to alter the detrital composition of sediments immediately after deposition. The ability of sediments to react with the atmosphere or water, either by fluid flow or diffusion, is highest at shallow burial depths (<1-10 m), suggesting that the potential for sediments to change their post-deposition composition is higher at shallow depths than greater burial depths (Bjørlykke and Jahren, 2015). The most important early diagenetic processes are (1) formation of biogenic carbonates and silica, (2) precipitation of authigenic minerals, e.g. carbonates, glauconite and iron minerals, and (3) flushing of meteoric water, resulting in leaching of unstable minerals and accompanying precipitation of more stable minerals (e.g. precipitation of kaolinite at the expense of feldspar).

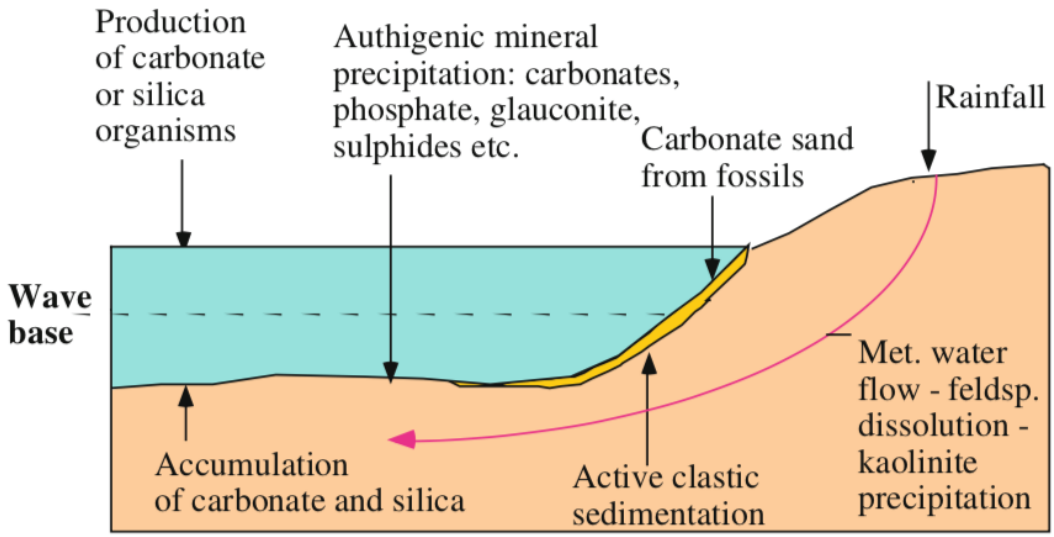

Figure 3.1: Schematic description of diagenetic processes in shallow marine environments. Feldspar dissolution and precipitation of kaolinite occur in response to meteoric water flushing. Slightly modified from Bjørlykke and Jahren (2015).

Flushing of slightly acidic meteoric water results in dissolution of carbonates and unstable minerals, e.g. feldspar and mica. (Fig. 3.1). The presence of carbonate cement in sandstones is commonly related to dissolution and reprecipitation of biogenic carbonate. The leaching rates of unstable minerals, such as felspar and mica, and precipitation of kaolinite depends on the amount of groundwater flowing through the sediments per unit of time. Furthermore, precipitation of kaolinite requires that Na+, K+ and silica are continuously removed from the solution and that new freshwater undersaturated with respect to feldspar and mica is supplied. If the porewater becomes oversaturated with respect to feldspar and mica, the reaction stops. Accordingly, if the silica-concentration in the porewater is very high, kaolinite is unstable and smectite is precipitated instead. Authigenic minerals formed at shallow burial depth, however, are not always stable at deeper burial and thus replaced by other more stable minerals, e.g. formation of illite at the expense of kaolinite and/or smectite.

3.4 Mechanical compaction

Mechanical compaction, resulting from grain rearrangement, plastic deformation of ductile grains, dissolution and brittle fracturing, is controlled by burial depth, fluid pressure, the ratio of brittle to ductile grains and texture (grain size and form), in which the two latter factors are strongly controlled by the depositional environment. Compaction occurs in response to increasing overburden load, in which the overburden load acts as an effective stress (Fig. 3.2) (Bjørlykke, 2001). Sandstones composing ductile grains are exposed to higher degree of

mechanical compaction than sandstones rich in rigid grains (quartz and feldspar), in which ductile grains are squeezed between the more rigid grains, sometimes resulting in formation of so called pseudomatrix (Mansurbeg, 2012). Furthermore, in well-sorted sand composed of spherical grains, the contact surface between the grains is small, suggesting that the pressure per unit area (kg/cm^3) is very large. Increasing overburden (i.e. effective stress) causes deformation of the grains and accompanying distribution of the load over a larger area. Furthermore, experimental compaction suggests that the porosity of loose sand is reduced from 40-42% (initial porosity) to 35-25% (intermediate burial depth), depending on grain strength and grain size. According to the experiment, well sorted coarse-grained sand is compacted more than fine-grained sand, in which the stress per grain contact is higher in coarse-grained sand (Chuhan et al., 2002, 2003; Bjørlykke and Jahren, 2015) .

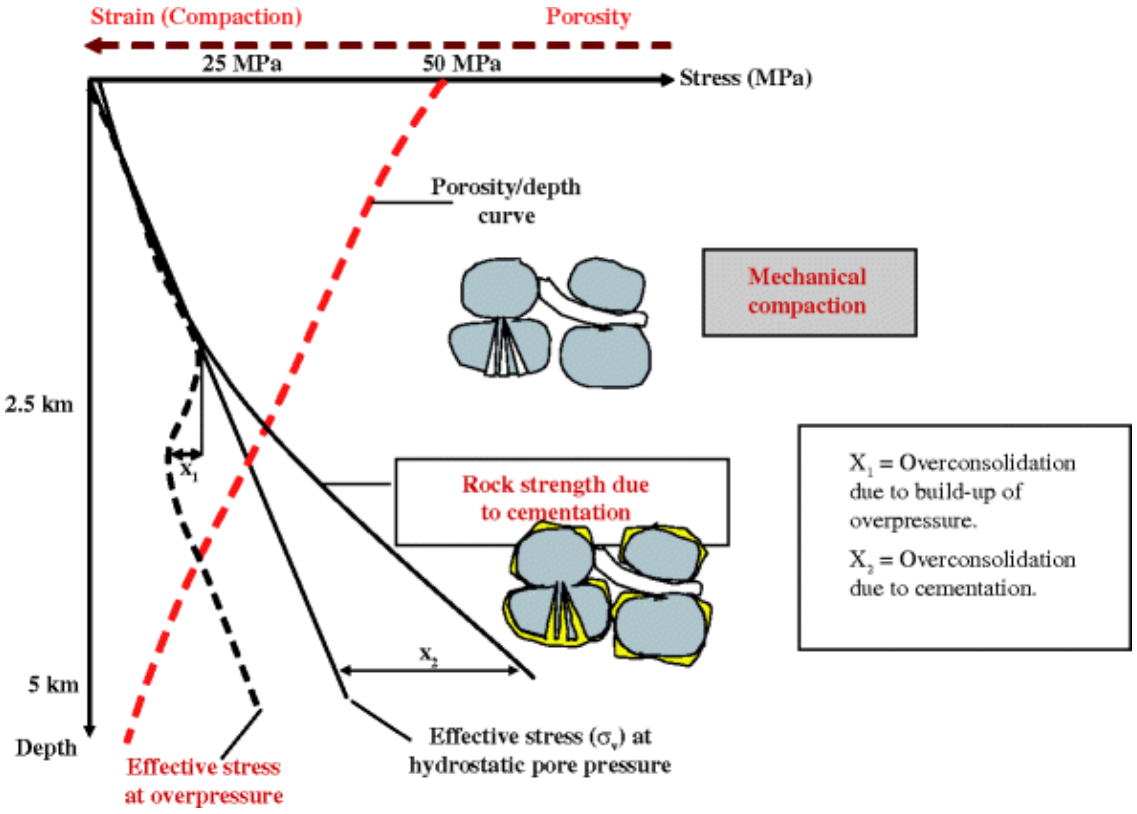

Figure 3.2: Prior to the onset of quartz cementation (about 70-80°C), sandstones experience mechanical compaction. Compaction occurs in response to increasing overburden load, in which the overburden load acts as an effective stress. At intermediate burial depths (>2,5 km), chemical compaction (i.e. quartz cementation) prevents further mechanical compaction. From Bjørlykke and Jahren (2015).

3.5 Sandstones buried to intermediate depths (2.0-3.5 km, 50-120ºC)

At intermediate burial depths (>2 km), chemical compaction (i.e. quartz cementation) prevents further mechanical compaction, in which only 2-4% quartz cement is required to stop mechanical compaction (Fig. 3.2). Compaction and porosity loss at greater burial depths is thus controlled by the rate of mineral dissolution and precipitation (i.e. chemical compaction). In well-sorted quartz- and feldspar-rich sandstones, precipitation of quartz cement is an important factor destroying porosity. The solubility of quartz is controlled by temperature and time; the higher the temperature and the slower the subsidence rates, the higher the solubility (Worden and Burley, 2003). In addition, precipitation of quartz is dependent on grain size, grain surfaces available for quartz precipitation and presence/absence of grain coatings (Mansurbeg, 2012). Grain coatings (e.g. grain coating chlorite) are suggested to retard precipitation of quartz and is thus of great importance to preservation of porosity and permeability at great burial depths (Bjørlykke, 2001). Furthermore, recrystallisation of detrital and/or eogenetic minerals is an important diagenetic process at burial depths. At temperatures higher than 100-120ºC and 70-80ºC, kaolinite is recrystallised to dickite and smectite is dissolved and replaced by illite, respectively. Furthermore, at depths greater than 3 km, K-feldspar and/or plagioclase are replaced by albite (i.e. albitisation). The replacement of feldspar is related to removal of potassium and accompanying increase in the relative amounts of Na+, suggesting that albite is more stable than feldspar.

3.6 Sandstones buried to great depths (>3.5-4 km, >120ºC)

Sandstones exposed to temperatures >120ºC (120-160ºC), corresponding to burial depths of 3-3.5 km to 4-4.5 km, generally show strong reduction in porosity and permeability (Bjørlykke and Jahren, 2015). The reduction in porosity and permeability is largely related to precipitation of quartz cement (i.e. quartz overgrowth) and authigenic illite. Quartz cementation is not shut down until nearly all the porosity is lost, or the temperature drops below 70-80ºC (Bjørlykke and Jahren, 2015). At temperatures >90ºC, kaolinite is replaced by illite, requiring that K-feldspar is present in the sediment. Pervasive precipitation of illite, however, occurs at temperatures >120 ºC. The characteristic fibrous crystal shape of illite reduces the permeability of sandstones significantly and is thus of great importance to reservoir quality.

4 Methods

4.1 Introduction

The present study is based on observations and interpretations obtained from sedimentological and petrographic analyses of cores 7-2006 and 11-2003, focusing on the Firkanten Formation (core 7-2006), upper part of Grumantbyen Formation (cores 7-2006 and 11-2003) and Aspelintoppen Formation (11-2003). The upper part of the Grumantbyen Formation was studied in both cores in order to identify any differences in burial history. The studied intervals of the upper part of Grumantbyen Formation is hereinafter referred to as the "Grumantbyen Formation". The sediment cores, provided by Store Norske Spitsbergen Kullkompani (SNSK), were collected in Endalen and brought to the University Centre in Svalbard (UNIS) for sedimentary logging and sampling. Mineralogical and petrographic data was obtained from optical thin section-, SEM- and XRD-analyses. XRD-analysis was performed by Beyene Girma Haile (University of Oslo). In addition, a handheld XRF-analyser was used for elemental analysis of the sediment cores.

4.2 Sedimentary logging

Logging of the sediment cores was performed in order to (1) get an overview of the lithology and depositional environment of the Firkanten, Grumantbyen and Aspelintoppen formations and (2) choose sampling intervals for mineralogical and petrographic analyses. Core logging was performed in 1:20 scale, focusing on lithology, grain size, sedimentary structures, colour, bioturbation intensity and trace fossils. Formation boundaries were identified prior to collection of the cores, based on the paper of Dörr et al. (2018) and SNSK's pictures of cores 7-2006 and 11-2003. Grain size was determined using a grain-size identification sheet and hand lens. Furthermore, every 20 cm of the cores was acid tested in order to detect possible carbonate cement. The sedimentary logs were redrawn digitally in Adobe Illustrator CC.

4.3 Sampling and cutting of sediment cores

Based on the core logging, a total of 44 selected rock-samples were taken; 28 from the Firkanten Formation, 6 from the Grumantbyen Formation (3 from each core) and 10 from the Aspelintoppen Formation (Appendix I). Sampling intervals were chosen based on lithology,

mineral composition and facies associations. Two different types of "key"-rocks were sampled: (1) quartz-rich sandstones in order to identify possible authigenic quartz cement and (2) sandstones rich in carbonate in order to investigate the types and distribution of carbonate cement. Furthermore, the sandstone samples represent different facies associations, allowing linkage of diagenesis and depositional environment. Prior to cutting, the samples were marked with numbers and top/bottom. A mobile saw was used to cut the sediment cores and split the samples into two pieces, in which one half was sampled for petrographic analysis and the other half was put back in the core-box. The samples, each approximately 4 cm in diameter, were put in small plastic bags, sealed and sent to the University of Oslo (UiO) for thin section preparations. The sampling intervals are displayed in Fig. 5.2, Fig. 5.6 and Fig. 5.9 (sedimentary logs).

4.4 Petrographic analyses

Optical microscopy

The collected sandstone-samples from the Firkanten, Grumantbyen and Aspelintoppen formations were sent to the University of Oslo for thin section preparations. The samples were polished to a thickness of 30 microns and stained blue to highlight porosity. The thin sections were analysed using an optical microscope. Petrographic properties, including mineralogy, grain-sizes, sorting and roundness, were analysed in both plane-polarized light (PPL) and cross-polarized light (XPL).

Scanning Electron Microscopy (SEM)

A total of eight thin sections were chosen for SEM backscattered electron (BSE) imaging and energy dispersive (EDS) analysis. SEM-analysis aimed to help fill in gaps in data obtained from optical microscopy and thus get a better understanding of the detrital- and authigenic mineral compositions of the Firkanten, Grumantbyen and Aspelintoppen formations. Using a focused beam of high-energy electrons, various signals are generated at the surface of the analysed sample, including BSE and EDS, revealing information regarding texture and elemental composition (Fig. 4.1) (Swapp, 2017). Prior to SEM-analysis, the thin sections were covered with a thin layer of carbon in order to prevent accumulation of charge.

Electron-sample interactions produce elastic and inelastic collisions between electrons and atoms in the sample. Backscattered electrons (BSE) – elastically scattered incident electrons –

provide a useful signal for imaging the sample (Zhou et al., 2006). The number of backscattered electrons (BSE) reaching the BSE detector is proportional to the mean atomic number of the sample, suggesting that "brighter" BSE-intensities correlates with large atoms and vice versa (Goodge, 2016). BSE-images was used to obtain high-resolution compositional maps and distinguish the different mineral phases present in the samples. The elemental composition of minerals was obtained using electron dispersive spectroscopy (EDS), performing both point- and area (element map) analyses.

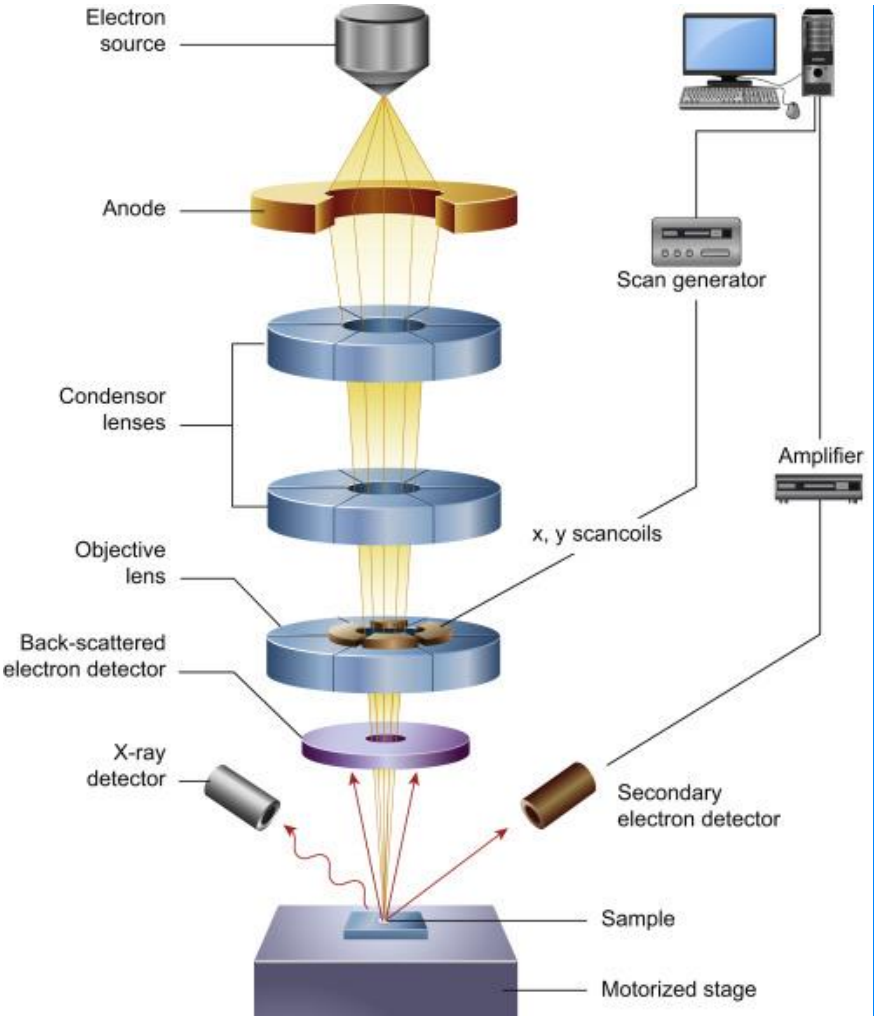

Figure 4.1: Simplified sketch of a Scanning Electron Microscope (SEM). The microscope composes an electron source in the top, lenses to control the electron beam and a variety of detectors, including BSE- and X-ray detector. From Inkson (2016).

4.5 X-ray Fluorescence (XRF) analysis

A handheld X-Ray Fluorescence (XRF) spectrometer – Thermo NITON XL5 – provided by Holger Hartmann AS, was used to determine the elemental composition of cores 7-2006 and 11-2003. The XRF-analysis aimed to (1) identify geochemical trends in the sediment cores and (2) investigate whether these can be correlated to the sedimentary logs (i.e. changes in lithology, sand/mud ratio). The geochemical data can thus be used to support sedimentological interpretations and/or help fill in gaps in the sedimentary logs (i.e. trends that cannot be seen during logging, e.g. in heavy bioturbated intervals).

XRF spectrometry is an efficient and non-destructive analytical technique used to quantify the elemental composition of materials (e.g. sediment cores) (Thermo Fisher Scientific, 2019). Depending on specific instrument configurations, the XRF analyser is capable of quantifying a range of elements. Fluorescent (or secondary) X-rays emitted from an excited sample is used to determine its chemical composition. The sample is irradiated with high-energy X-rays, causing each of the elements present in the sample to produce a set of fluorescent X-rays (Thermo Fisher Scientific, 2019). The emitted sets of X-rays, each being characteristic for a specific element, are detected by a detector and amplified. Handheld XRF spectrometers, however, analyse groups of elements simultaneously in order to efficiently determine the elements present in the sample and their relative concentrations. Prior to analysis, the XRF-spectrometer was set up for maximum counts of light elements, such as calcium, potassium, silica and aluminium. XRF was performed for every core-metre, each analysis running for approximately three minutes. Elemental concentrations were presented in parts per million (ppm).

5 Results

5.1 Sedimentological analysis

5.1.1 Introduction

Prior to sampling and cutting of the sediment cores (7-2006 and 11-2003), sedimentological logging was performed. Logging was required in order to (1) get an overview of the lithology and depositional environment of the Firkanten, Grumantbyen and Aspelintoppen formations (Fig. 5.1a,b) and (2) choose sampling intervals for thin section- (optical microscopy and SEM) and XRD-analyses. The present chapter provides a brief overview of the studied successions rather than a detailed sedimentological description. In the following, each of the studied formations will be described, focusing on lithological observations, including grain size, sedimentary structures, colour, bioturbation and trace-fossils. In addition, facies associations and depositional environment(s) for each of the studied formations will be discussed. As defined by Collinson (1969), facies associations are assemblages of genetically related facies, interpreted based on depositional origin. The formation-boundaries were identified prior to collection of the cores, based on the study of Dörr et al. (2018) and SNSK's pictures of cores 7-2006 and 11-2003.

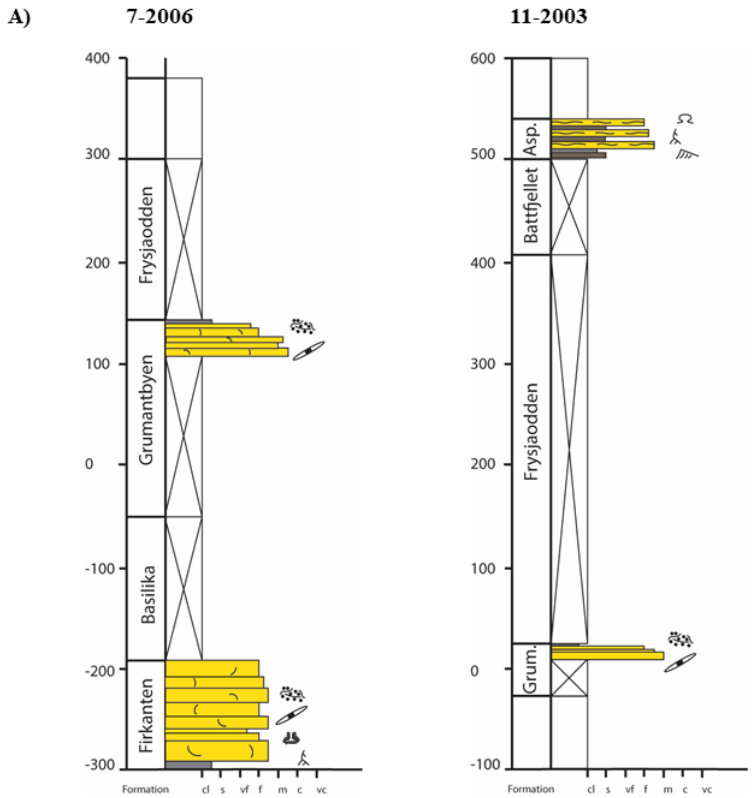

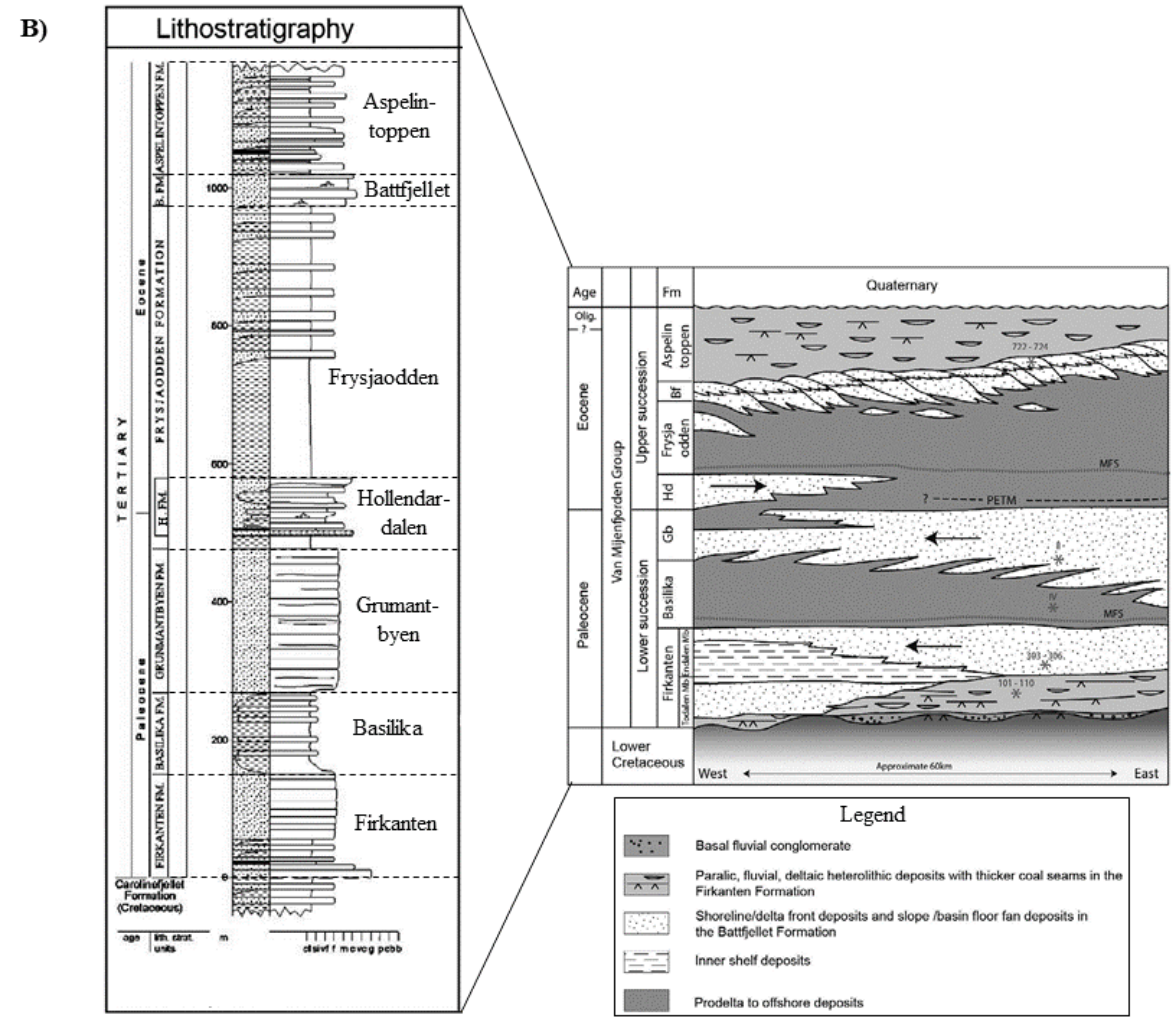

Figure 5.1: (A) Core intervals studied in the present work (core 7-2006 and 11-2003). Depth is presented in elevation (metres above sea level). Grum. = Grumantbyen Formation; Asp. = Aspelintoppen Formation. (B) Generalised stratigraphy of the Paleocene-Eocene Van Mijenfjorden Group (Central Tertiary Basin). Slightly modified from Petersen et al. (2016).

5.1.2 Firkanten Formation (core 7-2006)

Unit 1 (690,60-678,20 m)

Description

The lowermost approximately 12 m of the Firkanten Formation (690,60-678,20 m) is composed of alternating mudstones and coal-layers, occasionally interbedded with silt and thin (a few cm) very fine sand-layers (Fig. 5.2 and Fig. 5.3a). The mudstones are dark brown to black, suggesting high organic content. The coal-layers are typically whiteish and/or yellowish in colour. Abundant plant roots and coal-fragments are observed within the mudstones.

Interpretation

The abundance of interbedded coal-layers and plant roots indicate prolonged periods of terrestrial exposure, probably in a paralic depositional environment close to the shore. Lüthje (2008) describes high sulphur- and ash contents in similar thin coal-layers of the Firkanten Formation, indicating marine influence. Accumulation of peat, the precursor to humic coal, typically occurs in humid, vegetated environments, requiring a standing body of water, absence of siliciclastic sedimentation and creation of accommodation (Ward, 1984; Bohacs and Suter, 1997). Thick and laterally extensive coal deposits of the Firkanten Formation have previously been interpreted to represent raised mires complexes (Lüthje, 2008). The modest thickness of the coal-layers observed in the core, however, suggests formation at the marine influenced outer rim of a mire or in a poorly developed mire (i.e. marsh or swamp) (Lüthje, 2008). The organic rich mudstones are interpreted to represent periods of high terrigenous clastic input to the marsh/swamp, preventing generation of coal.

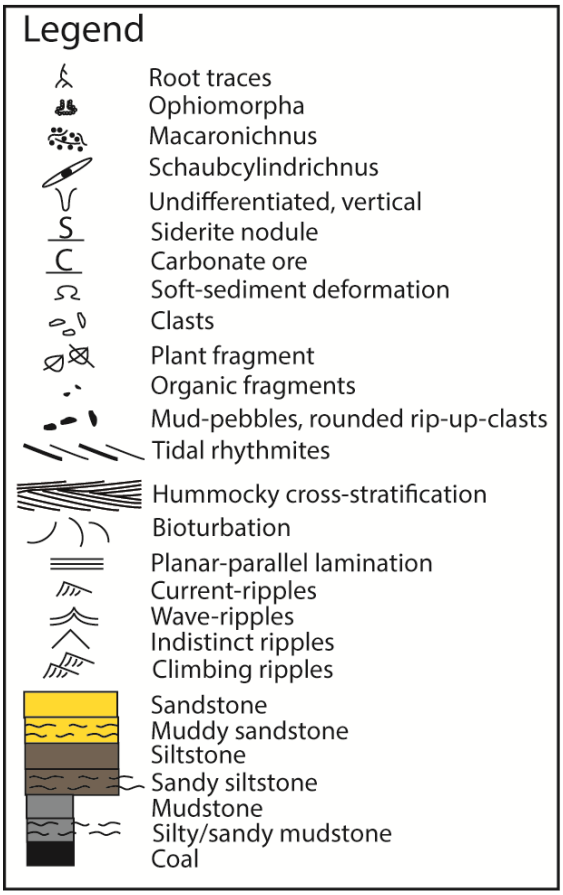

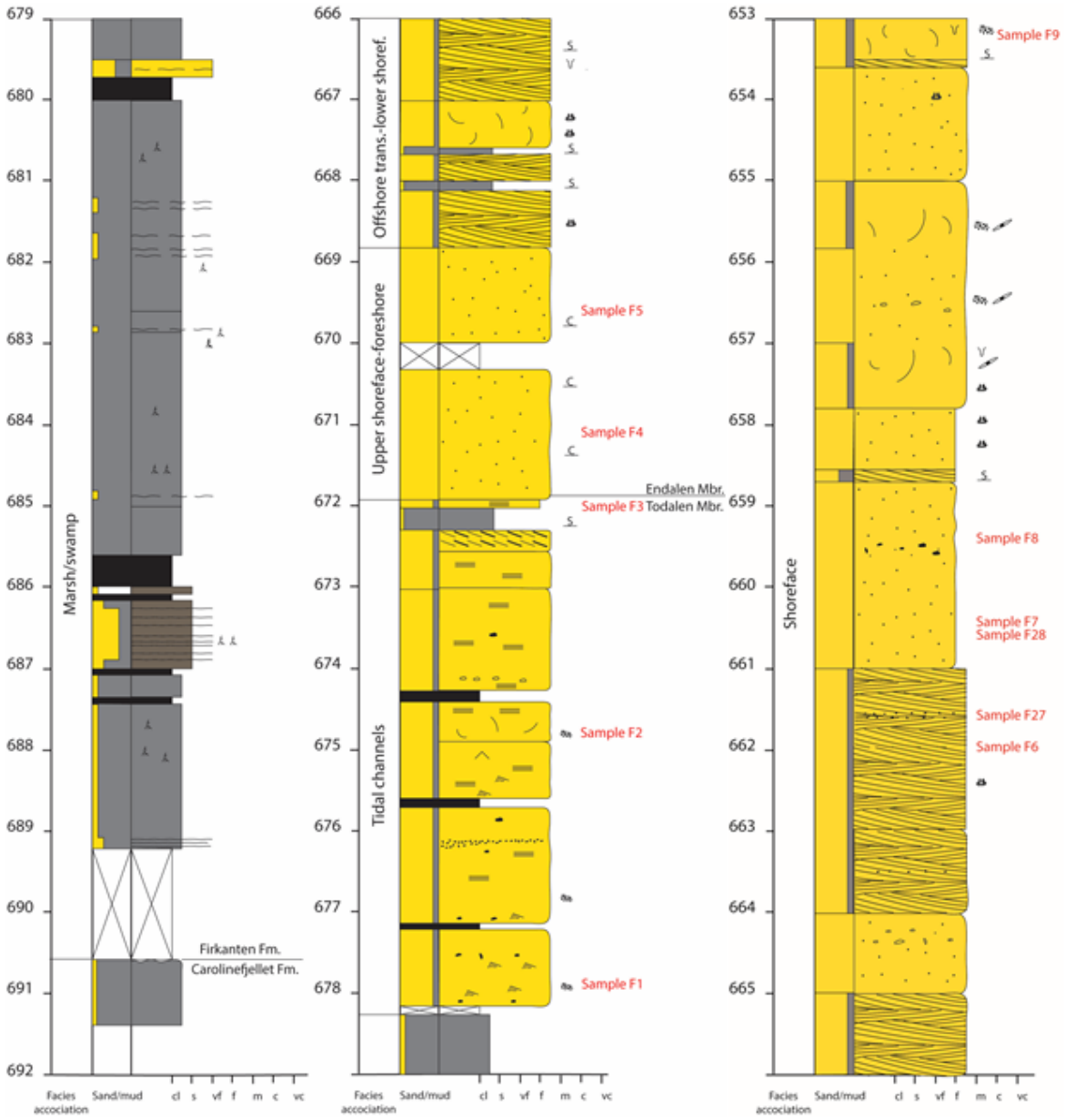
679
680
681
682
683
684
685
686
687
688
689
690
691
692
Marsh/swamp
Firkanten Fm.
Carolinefjellet Fm.
Facies accociation
Sand/mud
cl s vf f m c vc
666
667
668
669
670
671
672
673
674
675
676
677
678
Offshore trans.-lower shoref.
Upper shoreface-foreshore
Tidal channels
Sample F5
Sample F4
Endalen Mbr.
Sample F3 Todalen Mbr.
Sample F2
Sample F1
Facies accociation
Sand/mud
cl s vf f m c vc
653
654
655
656
657
658
659
660
661
662
663
664
665
Shoreface
Sample F9
Sample F8
Sample F7
Sample F28
Sample F27
Sample F6
Facies accociation
Sand/mud
cl s vf f m c vc

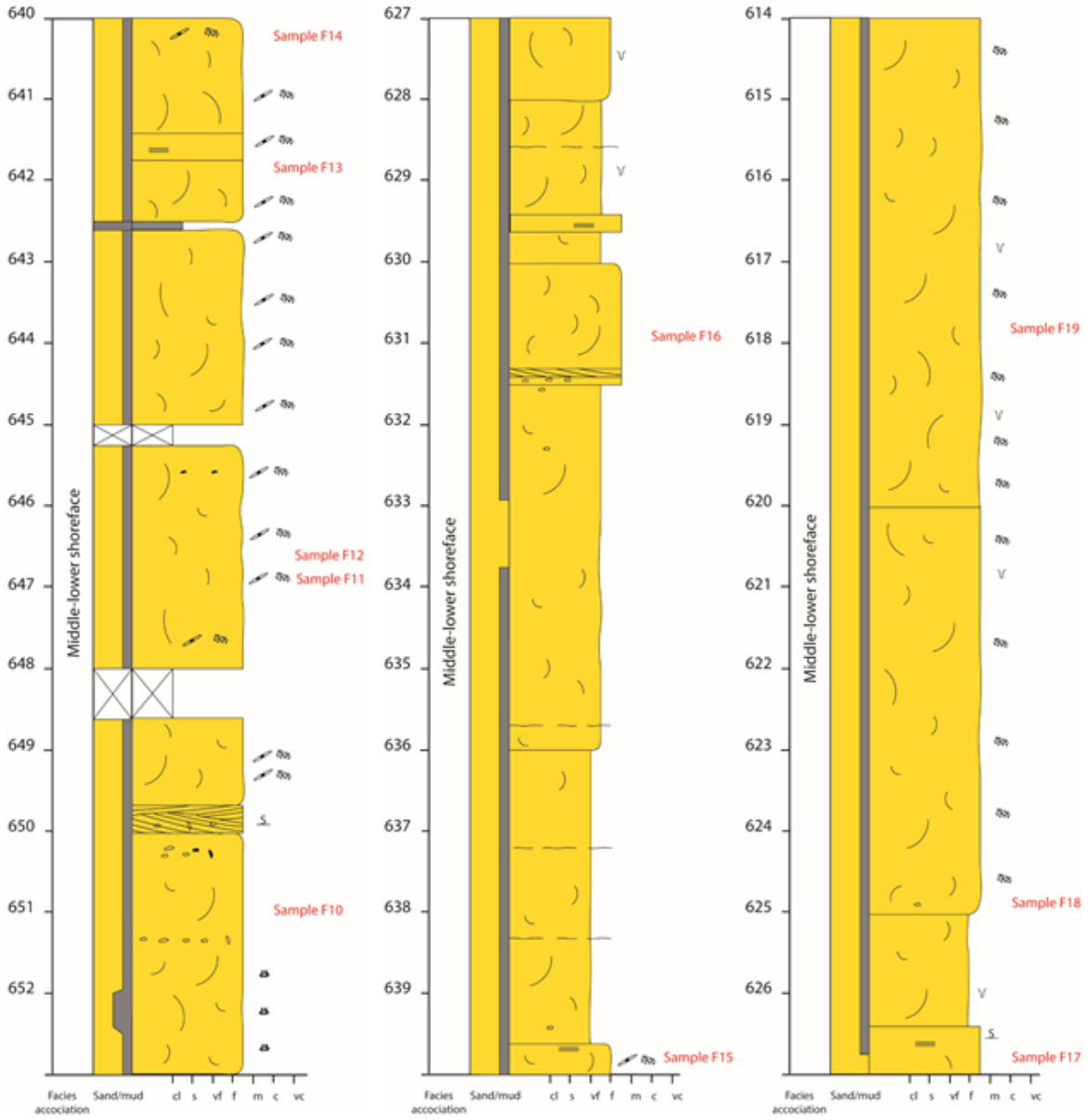
640
641
642
643
644
645
646
647
648
649
650
651
652
Sample F14
Sample F13
Sample F12
Sample F11
Sample F10
Middle-lower shoreface
Facies accociation
Sand/mud
cl s vf f m c vc
627
628
629
630
631
632
633
634
635
636
637
638
639
Sample F16
Sample F15
Middle-lower shoreface
Facies accociation
Sand/mud
cl s vf f m c vc
614
615
616
617
618
619
620
621
622
623
624
625
626
Sample F19
Sample F18
Sample F17
Middle-lower shoreface
Facies accociation
Sand/mud
cl s vf f m c vc

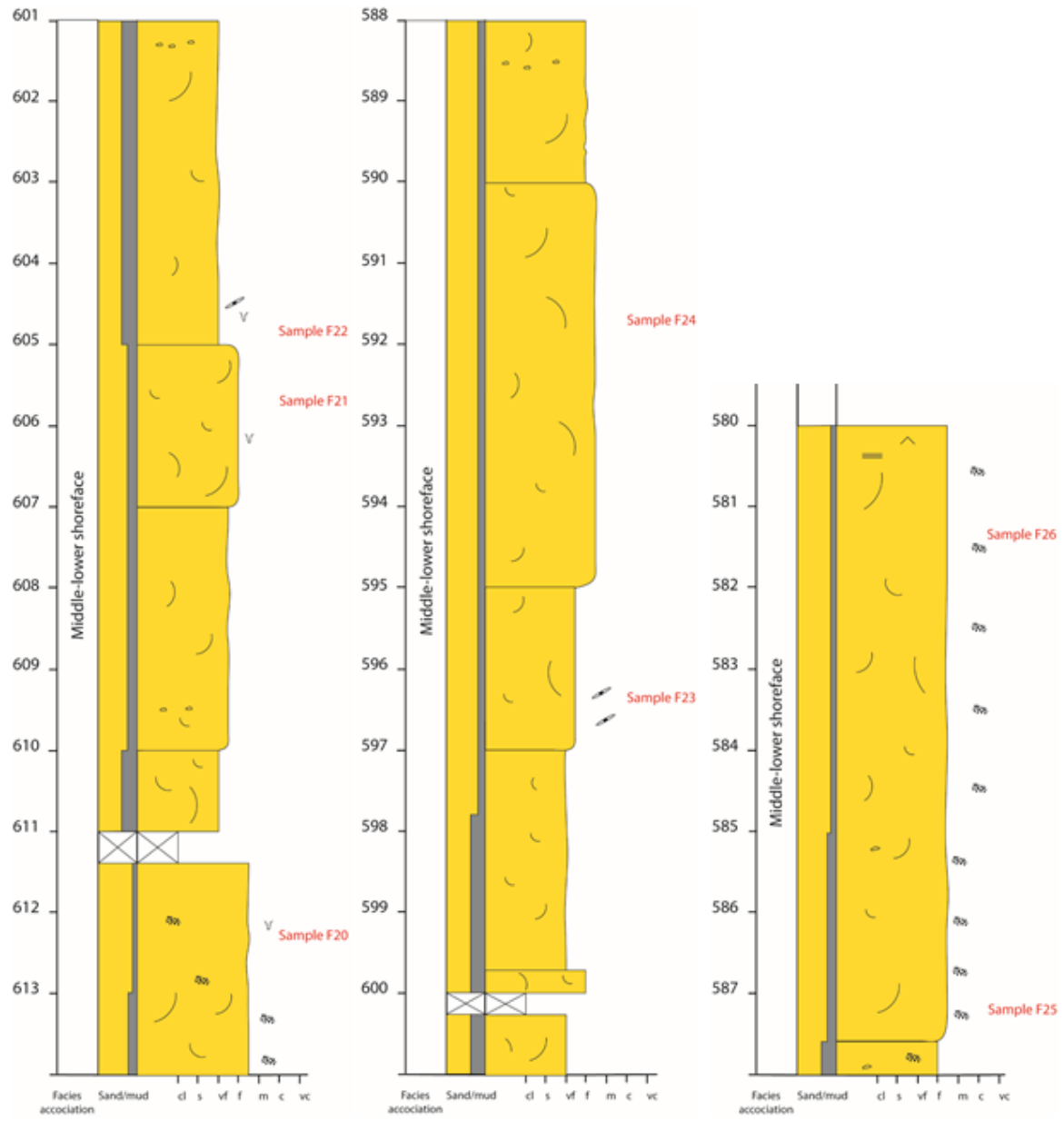

Figure 5.2: Sedimentary log of the Firkanten Formation (1:20 scale). The change in facies association, from tidal channels to upper shoreface-foreshore deposits (c. 671,90 m), is interpreted to represent the transition between the paralic Todalen Member and the overlying marine Endalen Member.

Unit 2 (678,20-668,80 m)

Description

An interval of muddy fine-medium grained sandstones, each separated by a thin coal-layer, overlies the alternating mudstones and coal-layers (678,20-671,90 m; Fig. 5.2 and Fig. 5.3a). The three lowermost sandstone-bodies (678,20-674,40 m; Fig. 5.3a) are greenish-grey in colour, showing evidence of weak lamination. The form of the lamination indicates presence of ripple and planar lamination and mud-drapes (Fig. 5.3b). Rip-up mud-clasts and pebbles are observed sporadically throughout the interval. Furthermore, *Macaronichnus* occurs in clusters

of 5-10 cm (Fig. 5.3c). The uppermost muddy sandstones (674,30-671,90 m) show evidence of planar lamination and rhythmites (Fig. 5.3d). A lag of pebbles and siderite concretion is observed in the lowermost planar laminated sandstone (c. 674,20 m) and upper sandstone (c. 672,30 m), respectively. Finally, a well-sorted massive sandstone (671,90-668,80 m) overlies the muddy sandstone-interval (Fig. 5.3d).

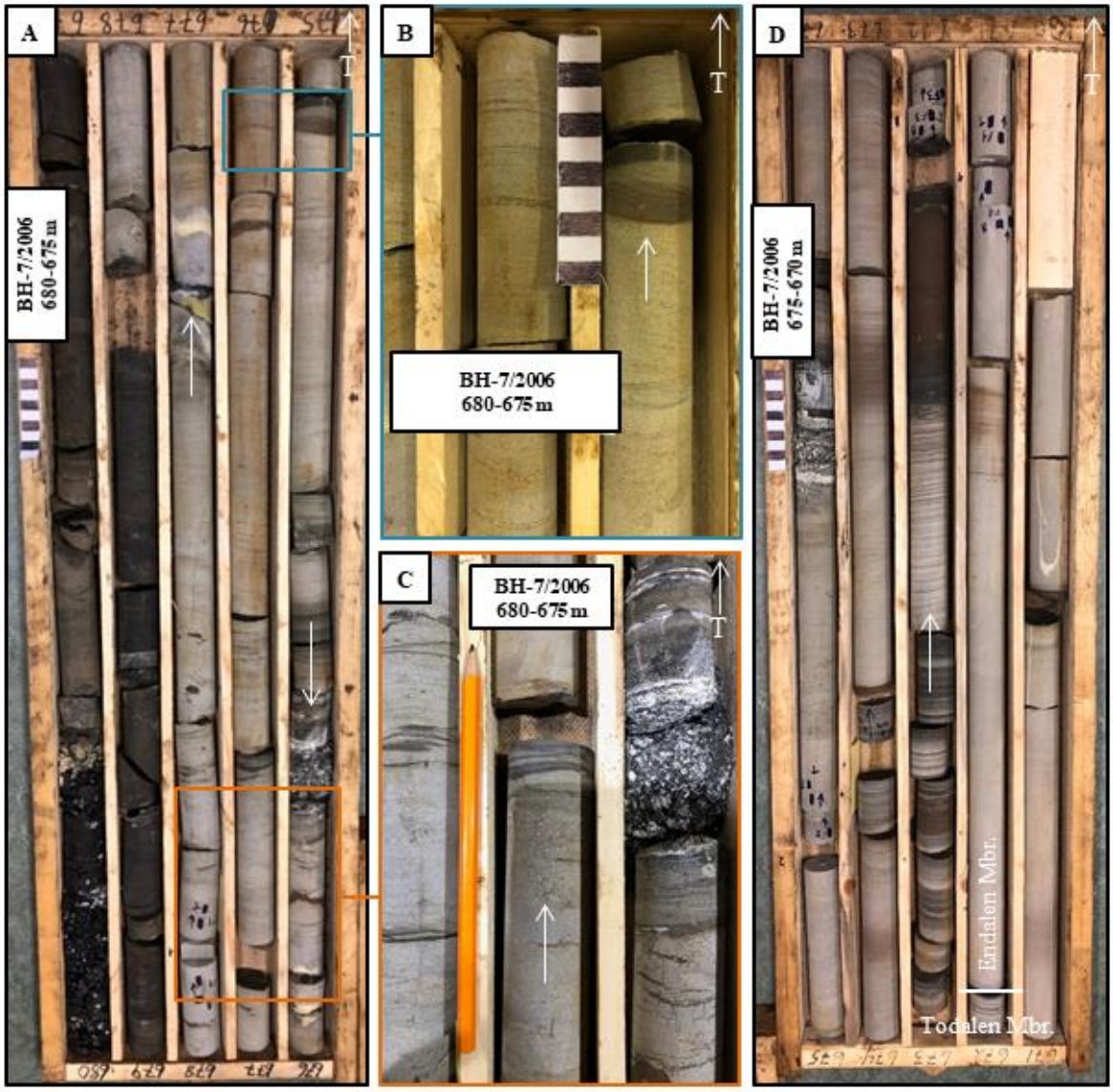

Figure 5.3: Sedimentary features of units 1 and 2 of the Firkanten Formation (core 7-2006). (A) Lower part of the Firkanten Formation (Todalen Mbr.). Abrupt change in lithology, from alternating mudstones and thin coal-layers to muddy sandstones (tidal channels). (B) Ripple-cross lamination in tidal channel. (C) Cluster of *Macaronichnus* trace fossils in tidal channel. (D) Rhythmites in the uppermost muddy sandstone (arrow).

Interpretation

The muddy sandstones of unit 2 are interpreted to represent tidal channels. The sharp boundary to the underlying mudstone-coal interval, rip-up mud-clasts, marine/brackish trace fossils (*Macaronichnus*), mud drapes and rhythmites support the present interpretation. The thin coal-layers probably indicate abandonment of the channels. The well-sorted and massive nature of the overlying sandstone implies deposition in a moderate to high energy shallow marine environment. The apparent absence of sedimentary structures is typical for foreshore and upper shoreface (Walker and Plint, 1992; Reading and Collinson, 1996). The change in facies association, from tidal channels to foreshore-upper shoreface deposits (c. 671,90 m), is interpreted to represent the transition between the paralic Todalen Member and the overlying marine Endalen Member (Fig. 5.3d).

Unit 3 (668,80-653,40 m)

Description

The succeeding approximately 15 m of the Firkanten Formation (668,80-653,40 m) composes alternating hummocky and/or swaley cross stratified sandstones and well-sorted massive sandstones (Fig. 5.2 and Fig. 5.4a). Thin intervals of bioturbated sandstones are observed in the lowermost and uppermost part of the unit (e.g. 657,50-657 m), often showing presence of *Macaronichnus* and *Schaubcylindrichnus* trace fossils. Mudclasts and pebbles occur sporadically within the non-bioturbated sandstones (Fig. 5.4d). Furthermore, *Ophiomorpha* trace fossils and siderite concretions are observed scattered throughout the interval (Fig. 5.4b,c).

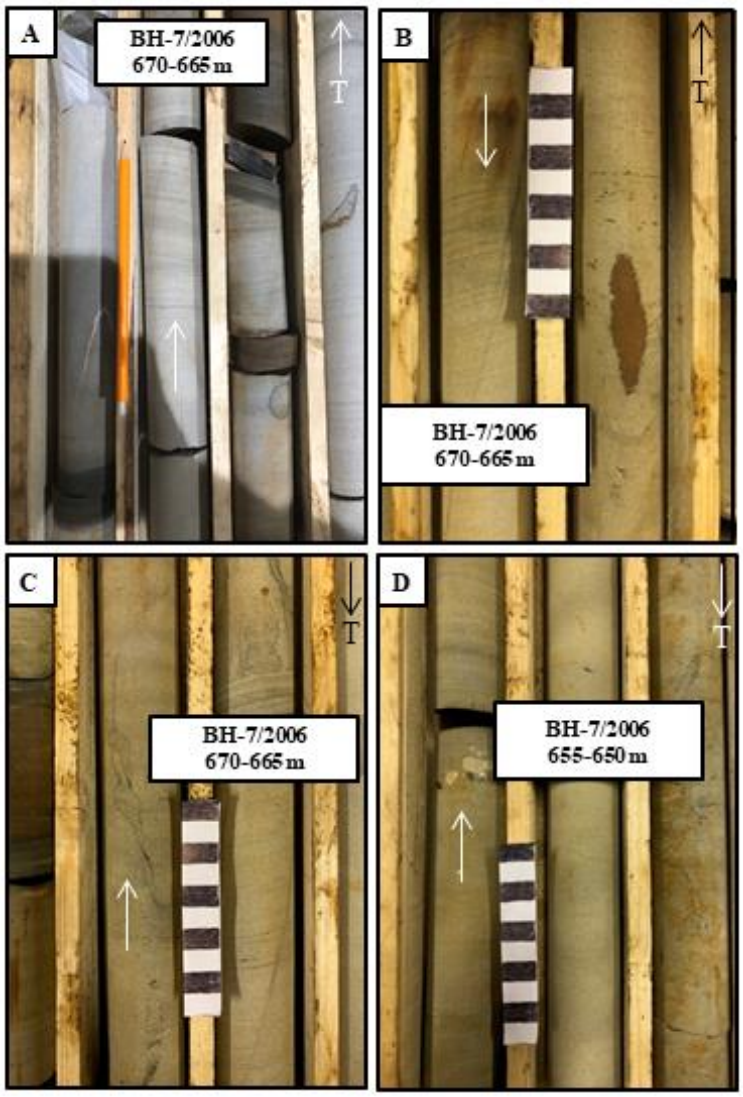

Figure 5.4: Sedimentary features of unit 3 of the Firkanten Formation (core 7-2006). (A) Hummocky and/or swaley cross-stratified sandstone (arrow). (B) Hummocky and/or swaley cross-stratification (arrow) and *Ophiomorpha* trace fossil (right). (C) *Ophiomorpha* trace fossil. (D) Lag of pebbles (storm deposits).

Interpretation

The hummocky and/or swaley cross-stratified sandstones are interpreted to represent storm-influenced offshore-transition to lower shoreface deposits (Walker and Plint, 1992). Plint and Norris (cited in Lüthje, 2008), however, considered similar deposits to be of middle-upper shoreface origin. The presence of *Ophiomorpha*, typical for moderate to high energy shallow marine environments, supports the present interpretation (Knaust, 2017). The well-sorted massive sandstones resemble foreshore-upper shoreface deposits (see unit 2). The mudclasts and pebbles probably represent laminated storm deposits, reflecting storm-induced erosion of the sea-floor (Reineck and Singh, 1972). The bioturbated intervals are suggested to represent periods of low sedimentation rates, allowing biogenic activity.

Unit 4 (653,40-580)

Description

The middle and upper part of the Firkanten Formation (653,40-580 m) is composed of highly bioturbated sandstones, leaving only weak indications of the initial lamination. The bioturbated sandstones, however, are sometimes interspersed with less bioturbated and/or weakly laminated sandstones (Fig. 5.5c). The lamination resembles hummocky- and/or swaley cross-stratification. Trace fossils occur frequently throughout the interval, in which *Macaronichnus* and *Schaubcylindrichnus* are most prominent (Fig. 5.5b). Mud-clasts and pebbles are observed sporadically. The interval shows several shallowing-upwards sequences, from dark mud-rich and less bioturbated sandstones to light grey-grey coarser-grained and heavily bioturbated sandstones (e.g. 600-590 m; Fig. 5.5a). Generally, the degree of bioturbation seems to slightly decrease towards the top of the core.

In the uppermost approximately 8 m of the core, however, a grey-brownish sandstone showing evidence of mottling occurs (Fig. 5.5e). Furthermore, a coalified piece of wood and ripple-cross lamination are observed (Fig. 5.5d).

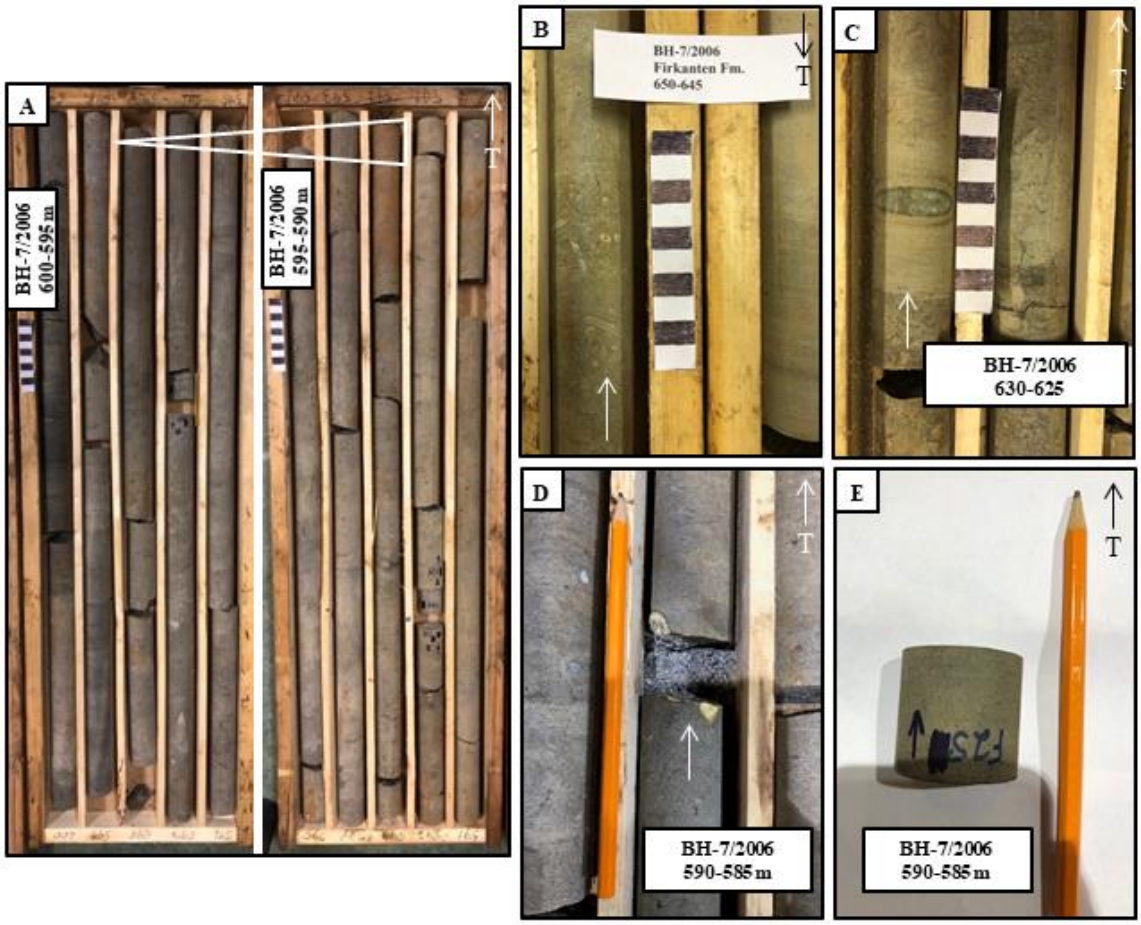

Figure 5.5: Sedimentary features of unit 4 of the Firkanten Formation (core 7-2006). (A) Example of shallowing upwards unit (i.e. parasequence) in the uppermost part of the core (600-590 m). (B) *Macaronichnus* and *Schaubcylindrichnus* trace fossils (arrow). (C) Interbedded hummocky and/or swaley cross stratified sandstone. (D) Coalified piece of wood. (E) Possible soil profile in the uppermost part of the core (Endalen Mbr.).

Interpretation

The muddy nature and high degree of bioturbation of unit 4 implies that deposition alternated with periods of low sedimentation rates (Lüthje, 2008). The bioturbated sandstones are probably of middle-lower shoreface origin (Lüthje, 2008). The presence of interbedded hummocky and/or swaley cross-stratified sandstones, however, implies periodically storm-influence (see unit 3). In periods of quiescence, oxygenated bottom conditions and low sedimentation rates allowed burrowing activity. The shallowing-upwards sequences, from mud-rich very fine-fine sandstones to fine-medium bioturbated sandstones, are interpreted to represent parasequences, reflecting small fluctuations in the relative sea-level. Possible mottling, typical for soil-profiles, in the uppermost part of the core indicate deposition close to the coast and, thus, possibly a significant fall in the relative sea level.

Depositional environment

The interpretations of unit 1-4 are consistent with previous studies of the Firkanten Formation (e.g. Lüthje, 2008), suggesting a coastal plain (Todalen Member) to shallow marine (Endalen Member) depositional environment for the formation.

5.1.3 Grumantbyen Formation (cores 7-2006 and 11-2003)

The upper part of Grumantbyen Formation was studied in both cores 7-2006 and 11-2003 (Fig. 5.6), aiming to identify any differences in temperature- and burial history.

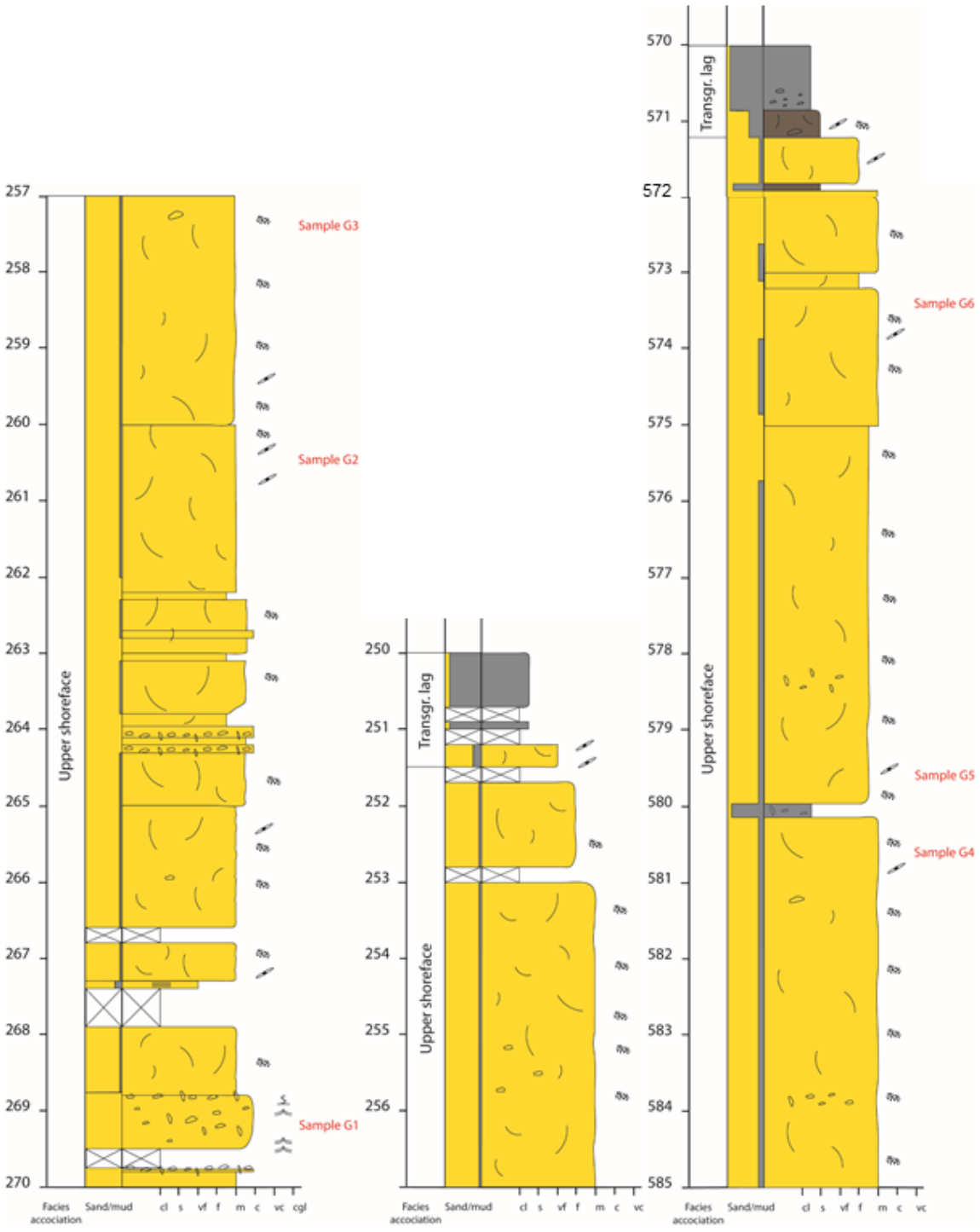

Figure 5.6: Sedimentary log of the upper part of Grumantbyen Formation (1:20 scale). Left and middle: Core 7-2006; right: Core 11-2003. The change in lithology from bioturbated sandstone to mudstone indicates the transition between the shallow-marine Grumantbyen Formation and the overlying deep-marine Frysjaodden Formation. See section 5.1.2 for legend.

Unit 1 (270-251 m in core 7-2006/585-571,20 m in core 11-2003)

Description

The lowermost part of the Grumantbyen Formation (core 7-2006) composes a light grey gravelly coarse-grained sandstone (269,80-268,80 m; Fig. 5.7a,b). Clasts, up to 1 cm in diameter, occur scattered throughout the sandstone. Although rare, ripple cross-lamination is observed in the uppermost part of the sandstone (Fig. 5.7c). The form of the lamination indicates presence of wave-ripple cross-lamination. An interval of greenish-grey well-sorted medium-coarse grained sandstones (268,80-251,20), occasionally interbedded with thin (approximately 10 cm) gravelly layers, overlies the gravelly coarse-grained sandstone. The sandstones generally show moderate-high, although varying, degree of bioturbation, leaving only few indications of the original lamination. Trace fossils include *Macaronichnus* and *Schaubcylindrichnus*, in which the former is the most prominent type (Fig. 5.8b,c). White and blackish clasts (millimetre to centimetre scale) occur sporadically throughout the interval (Fig. 5.8e). The bioturbated sandstone-interval is somewhat finer-grained in core 11-2003 (585-571,20 m) and lacks the interbedded gravelly sandstone-layers observed in core 7-2006.

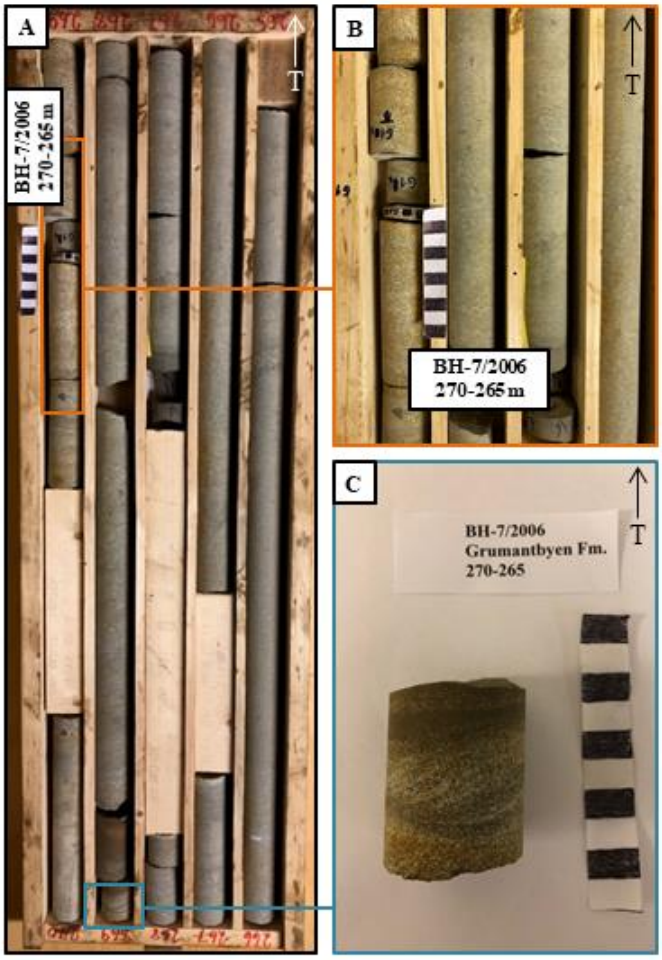

Figure 5.7: Sedimentary features of the lowermost part of the Grumantbyen Formation in core 7-2006 (unit 1). (A) Overview of lowermost part of the Grumantbyen Formation (270-265 m). (B) Gravelly sandstone in the lowermost part of the interval (269,80-268,80 m). (C) Wave-ripple cross-lamination in the uppermost part of the interval (c. 269 m).

Interpretation

The relatively coarse grain-sizes and variation in bioturbation intensity, from absent in the lowermost gravelly sandstone (core 7-2006) to moderate-high in the overlying bioturbated sandstone-interval, suggests high-energy conditions and a proximal rather than distal origin. The occurrence of wave-ripple cross-lamination indicates deposition in a wave-dominated shallow-marine environment. Furthermore, the slightly greenish colour of the bioturbated sandstones indicate presence of glauconite (Steel et al., 1981). The relatively homogeneous nature of the sandstones, moderate-high degree of bioturbation and presence of glauconite imply low sedimentation rates (Odin and Matter, 1981). Low-sedimentation rates allow burrowing activity despite high-energy conditions. The clasts observed sporadically throughout the interval probably originate from the Permian Kapp Starostin Formation and are thought to have been deposited by seasonal winter ice across the shelf (Dalland, 1976).

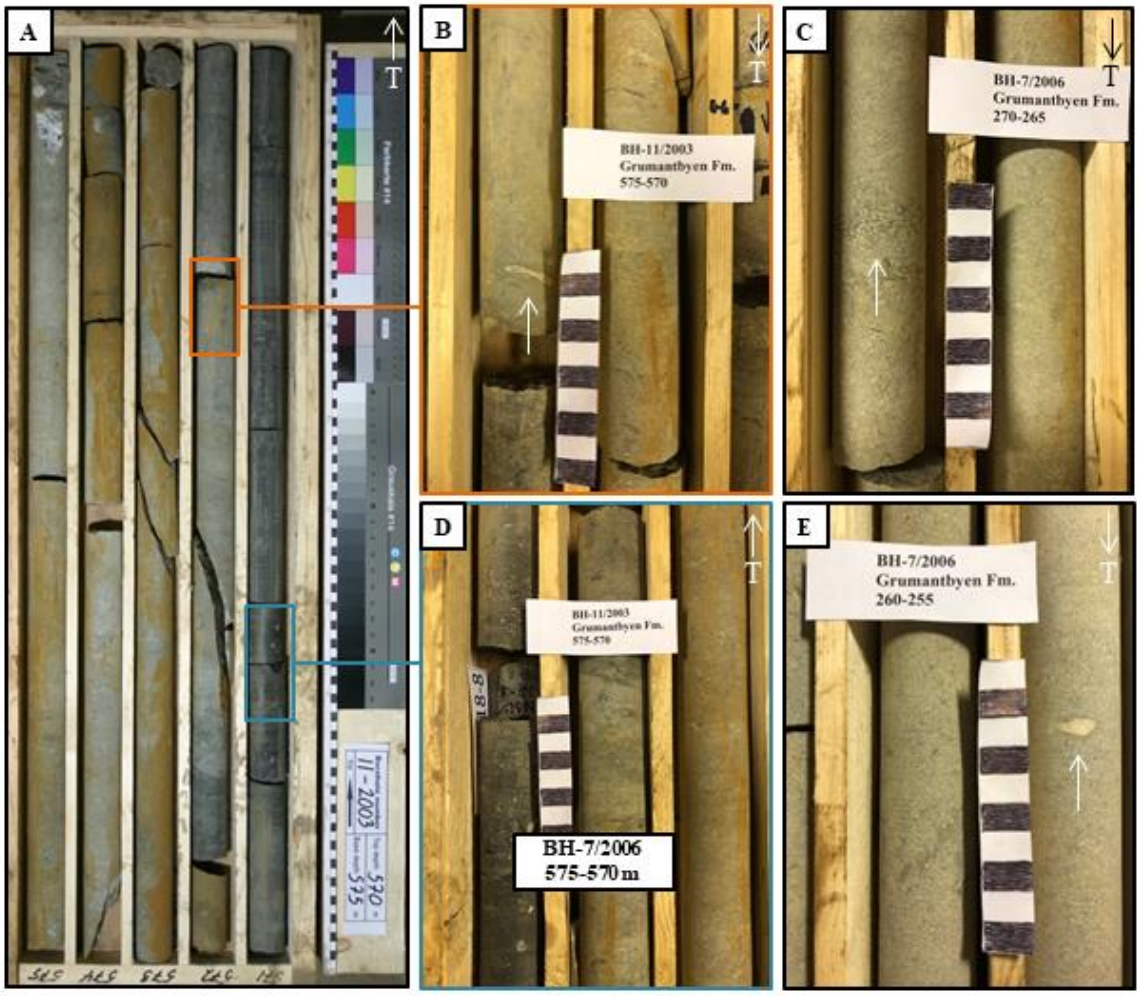

Figure 5.8: Sedimentary features of units 1 and 2 of the Grumantbyen Formation (cores 7-2006 and 11-2003). (A) Overview of the uppermost part of the formation in core 11-2003. The change in lithology, from bioturbated sandstone to mudstone, indicate the transition between the shallow-marine Grumantbyen Formation and the overlying deep-marine Frysjaodden Formation. (B) *Schaubcylindrichnus* trace fossil in the uppermost part of the formation in core 11-2003. (C) *Macaronichnus* and *Schaubcylindrichnus* trace fossils in core 7-2006 (arrow). (D) Transgressive lag, reflecting marine flooding. (E) Clasts observed sporadically throughout the interval.

Unit 2 (251-250 m in core 7-2006/571,20-570 m in core 11-2003)

Description

A dark grey-blackish mudstone, approximately 1 m thick in both of the cores, occurs in the uppermost part of the Grumantbyen Formation (Fig. 5.8a). In core 11-2003, a lag of pebbles is observed in the lowermost part of the mudstone (Fig. 5.8d).

Interpretation

The pebbly layer observed in the lowermost part of the mudstone (core 11-2003) is interpreted to represent a transgressive lag, reflecting marine flooding and accompanying erosion of the

sea-floor. This transgressive lag probably represents the transition between the shallow marine Grumantbyen Formation and the overlying deep-marine Frysjaodden Formation.

Depositional environment

The high degree of bioturbation, leaving only few indications of the original lamination, makes it difficult to precisely interpret the depositional environment of the upper part of Grumantbyen Formation. However, the overall nature of the succession, including grain size and occurrence of wave ripple cross-lamination, suggests deposition in a shallow-marine environment, probably upper shoreface. The abundance of *Macaronichnus*, a characteristic shallow-marine trace fossil often occurring in middle-upper shoreface and foreshore deposits, supports the present interpretation (Clifton and Thompson, 1978; Knaust, 2017).

5.1.4 Aspelintoppen Formation (core 11-2003)

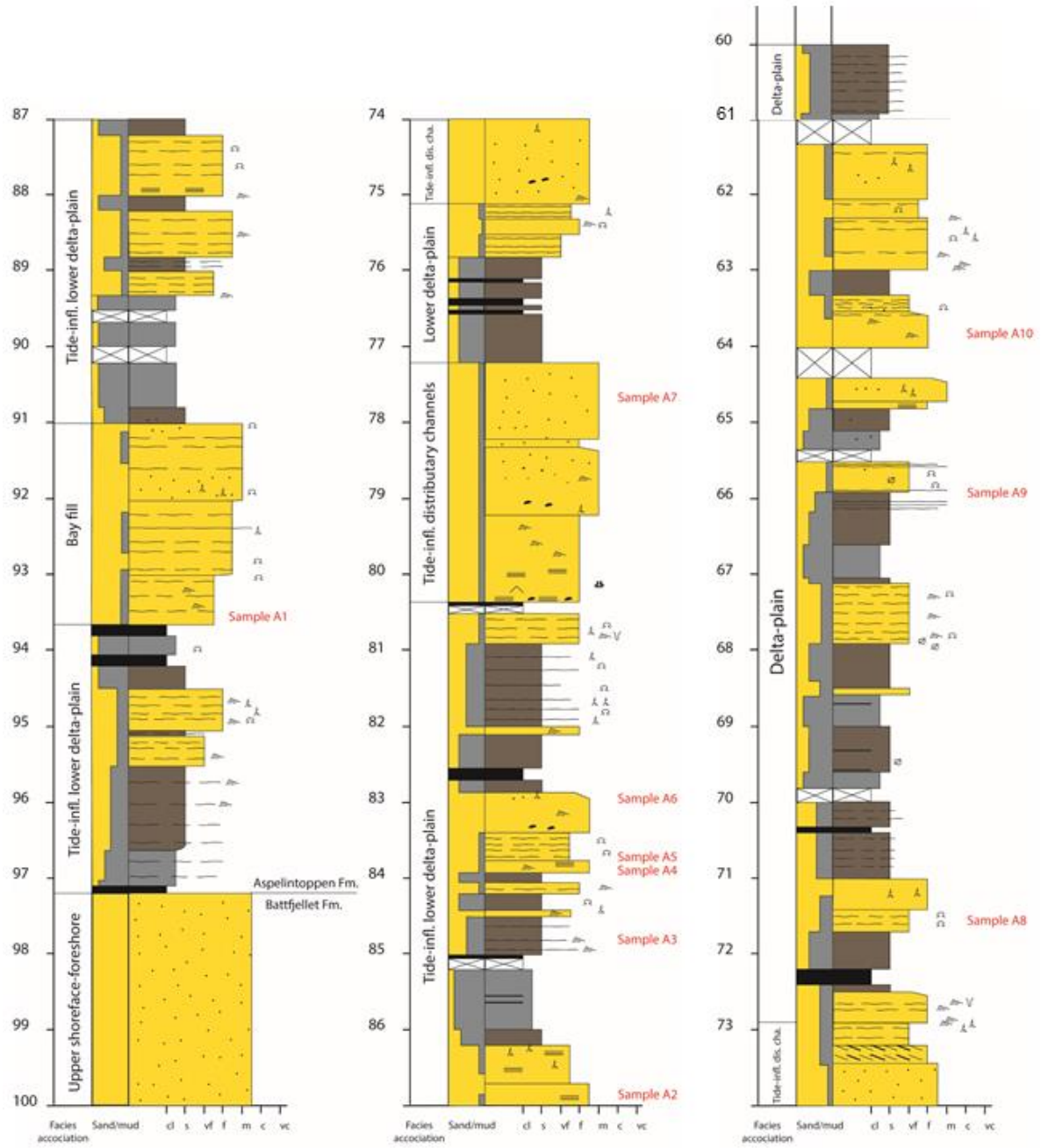

Figure 5.9: Sedimentary log of the Aspelintoppen Formation (1:20 scale). The lowermost coal-bed (c. 97 m) indicates the transition between the marine Battfjellet Formation and the paralic Aspelintoppen Formation. See section 5.1.2 for legend.

Unit 1 (100-93,70 m)

Description

The lowermost part of the core composes a thick well-sorted massive sandstone (100-97,20 m). The sandstone is capped with a thin layer of coal, probably indicating the transition between the marine Battfjellet Formation and the paralic Aspelintoppen Formation (Fig. 5.9 and Fig. 5.10a). A heterolithic interval, composing alternating muddy very fine-fine sandstones, siltstones and sandy mudstones (97,20-93,70 m) overlies the coal-layer. The muddy sandstones, each approximately 30 cm thick, contains current-ripple cross-lamination and root traces. Furthermore, the sandstones show evidence of soft sediment deformation. The mudstones and siltstones are occasionally interbedded with lenses of ripple cross-laminated very fine-fine grained sandstone, sometimes showing opposing migration directions (Fig. 5.10b,d). Two coal-layers are observed in the uppermost part of the interval (Fig. 5.10c)

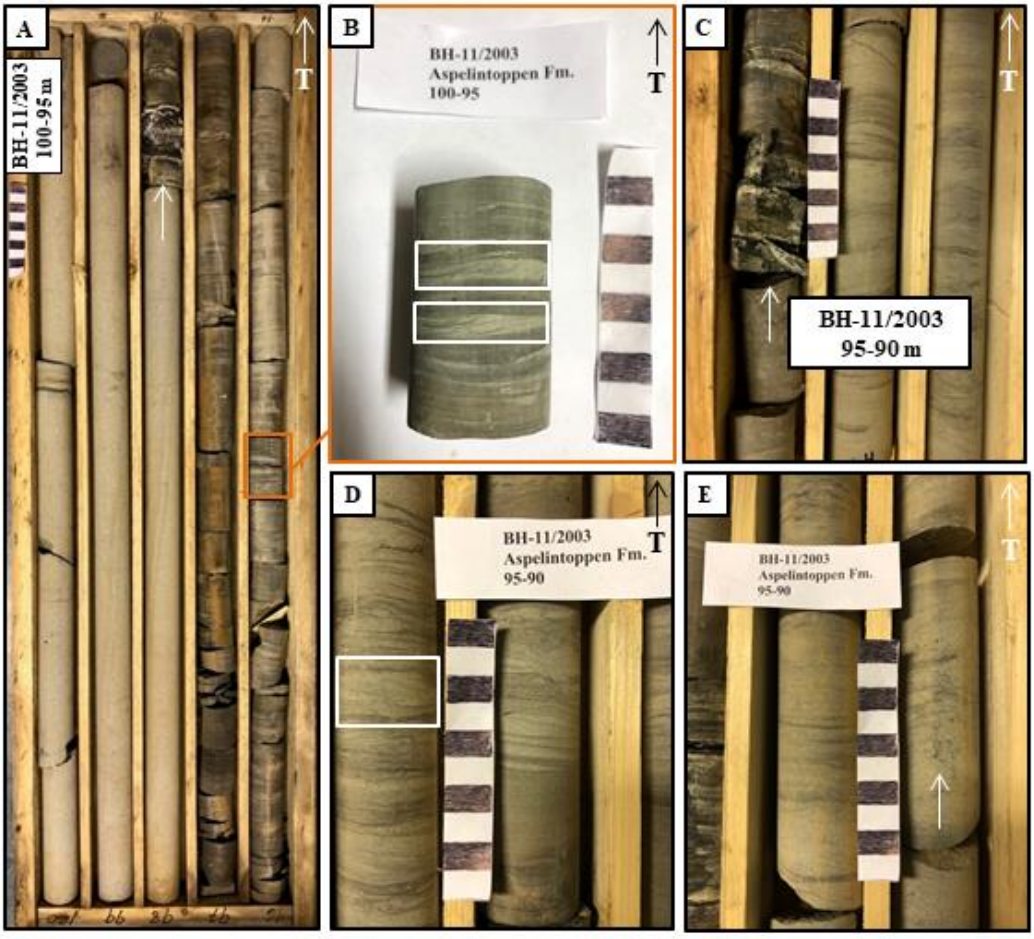

Figure 5.10: Sedimentary features of units 1 and 2 of the Aspelintoppen Formation (core 11-2003). (A) Overview of the lowermost part of the Aspelintoppen formation (unit1). The thin coal-layer (arrow) indicates the transition between the marine Battfjellet Formation and paralic Aspelintoppen Formation. (B) Lenticular bedding in the middle part of unit 1 (c. 95, 50 m). (C) Coal layer in the upper part of unit 1. (D) Wavy bedding in the upper part of unit 1. (E) Root traces in the uppermost part of the bay-fill deposits (93,70-91 m; unit 2).

Interpretation

The well-sorted and mature character of the lowermost sandstone-body suggests deposition in a moderate-high energy shallow marine environment. The apparent absence of sedimentary structures is typical for foreshore and uppermost part of shoreface (Walker and Plint, 1992; Reading and Collinson, 1996). The sandstone is interpreted to represent upper shoreface-foreshore deposits of the uppermost part of the Battfjellet Formation. The overlying heterolithic interval, composing alternating muddy sandstones, siltstones and sandy mudstones, are interpreted to represent tidally induced lenticular-, wavy- and flaser bedding. The occurrence of current ripple cross-lamination, sometimes showing opposing migration directions, supports the latter interpretation. The coal-beds observed in the uppermost part of the interval is suggested to represent prolonged periods of terrestrial exposure. Flaser, wavy and lenticular bedding (typical for near-shore tidal deposits), however, are not exclusively occurring in tidal zones; similar deposits are also occurring in overbank areas of episodic flooding (Reineck and Singh, 1980). However, tide induced lenticular-, wavy- and flaser bedding is consistent with previous studies of the Aspelintoppen Formation, suggesting tide-influence on the lower part (Naurstad, 2014).

Unit 2 (93,70-80,30)

Description

The lowermost approximately three meters of unit 2 composes a mud-rich fine-medium grained sandstone showing overall coarsening upwards (93,70-91 m; Fig. 5.9). Ripple cross-lamination and root-traces are observed in the lowermost- and middle-upper part of the sandstone, respectively (Fig. 5.10e). Furthermore, the sandstone generally shows high degree of soft sediment deformation, leaving few indications of the original lamination. A thick interval of alternating muddy sandstones, siltstones and mudstones (91-80,30 m) overlies the overall coarsening upwards sandstone. The muddy sandstones are sometimes normal-graded and soft-sediment deformed. Furthermore, current-ripple cross-lamination and root traces are observed within the muddy sandstones and siltstones. Three thin coal-beds occur in the middle-upper part of the interval (Fig. 5.9).

Interpretation

The muddy fine-medium grained sandstone, showing overall coarsening upwards, is interpreted to represent tide-influenced bay fill deposits. The succeeding heterolithic interval resemble tidally induced lenticular- and flaser bedding (see unit 1).

Unit 3 (80,30-72,80 m)

Description

The lower-middle part of unit 3 composes an interval of fine-medium grained sandstones (80,30-77,20 m; Fig. 5.9). The lowermost sandstone shows a sharp boundary to the underlying coal-bed (Fig. 5.11a). Furthermore, thin lenses of coal, planar lamination, ripple cross-lamination and *Ophiomorpha* trace fossil are observed in the lowermost part of the sandstone (Fig. 5.11b,c). An abrupt change in colour and grain size occurs at approximately 79,20 m. Mudclasts and/or coalified wood pieces and root traces are observed in the lowermost part; ripple cross-lamination occurs throughout the sandstone. Furthermore, the sandstone shows overall fining upwards. The uppermost sandstone (78,20-77,20 m) is massive, showing no/few signs of lamination. An interval of alternating siltstones and coal-layers and muddy very fine-fine sandstones (77,20-75,10 m) overlies the three sandstone bodies. The uppermost part of unit 3 (75,10-72,80) comprises a muddy sandstone showing upwards-fining. The sandstone contains mud-clasts in the lowermost part and show evidence of rhythmites in the uppermost part (73,40-73,20 m; Figure 5.11d).

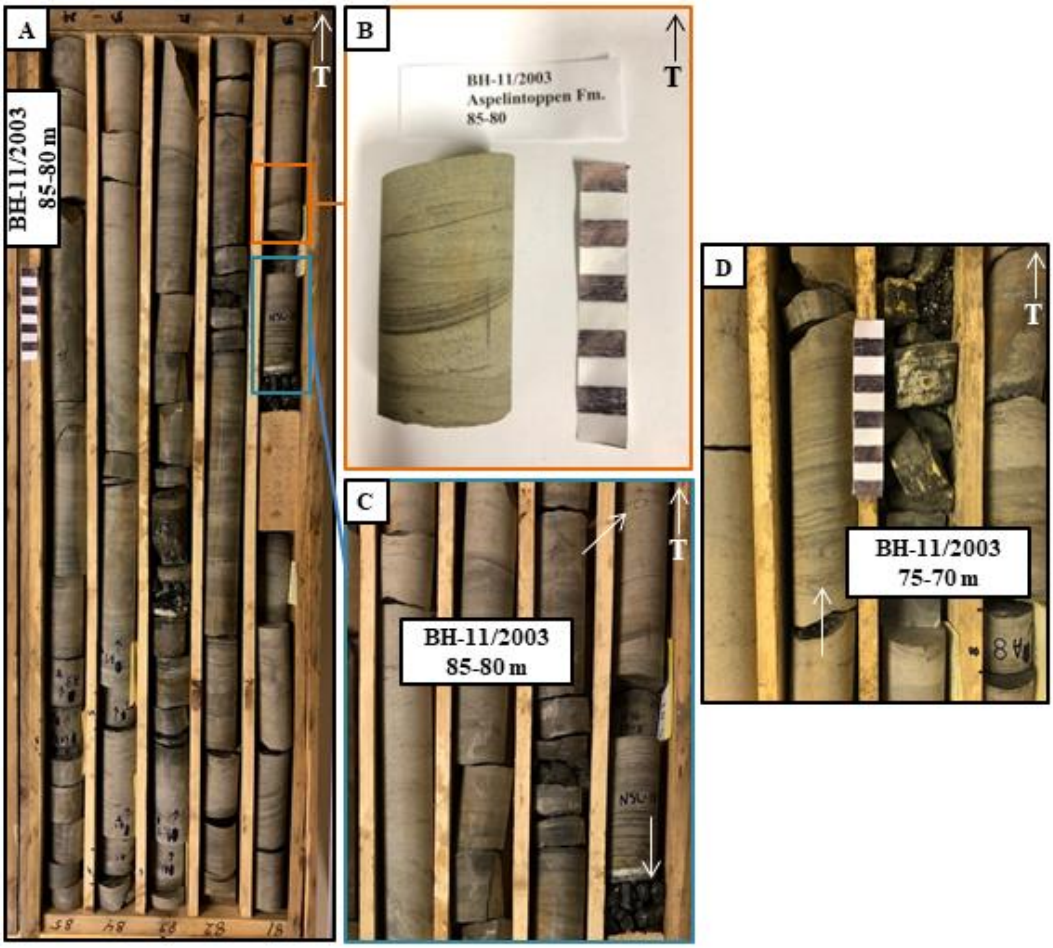

Figure 5.11: Sedimentary features of unit 3 of the Aspelintoppen Formation (core 11-2003). (A) Upper part of unit 2 (85-80,50 m) and lower 0,5 m (80,50-80 m) of unit 3. (B) Ripple cross-lamination in the lowermost tide-influenced distributary channel. (C) Sharp boundary between coal-layer and overlying laminated sandstone (lower arrow). *Ophiomorpha* trace fossil in the lowermost tide-influenced distributary channel (upper arrow). (D) Rhythmites in the uppermost part of unit 3 (73,40-73,20 m).

Interpretation

The muddy sandstones occurring in the lower-middle part of the unit are interpreted to represent tide-influenced distributary channel fill deposits. The sharp boundary to the underlying coal-layer and the observation of rip-up mudclasts, plane parallel lamination, ripple cross-lamination and marine/brackish trace fossils (*Ophiomorpha*) support the present interpretation. The overlying interval, composing siltstones, thin coal-layers and sandstones, probably represent lower delta-plain deposits. The overall nature of the uppermost sandstone and the presence of rhythmites suggests tide-influenced distributary channel fill deposits.

Unit 4 (72,80-60 m)

Description

The upper part of the core comprises alternating sandy mudstones, siltstones and muddy sandstones, occasionally interbedded with thin coal-beds (72,80-60 m; Fig. 5.9). The sandstones are relatively thin and sometimes show normal-grading. Furthermore, current-ripple cross lamination, climbing ripples and root traces are observed within the sandstones (Fig. 5.12b). In addition, at least one reddish-brown soil profile is observed within the interval (68,50-68,40 m). Well-preserved leaf prints occur within some of the muddy sandstones and siltstones (Fig. 5.12a).

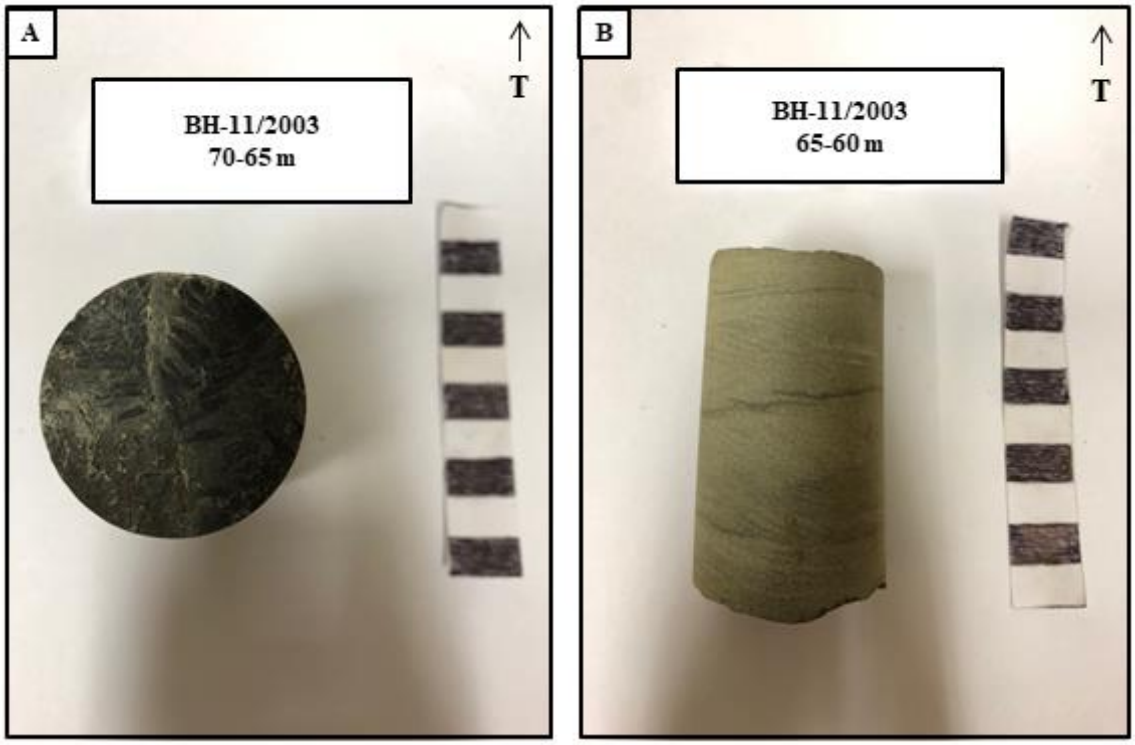

Figure 5.12: Sedimentary features of unit 4 of the Aspelintoppen Formation (core 11-2003). (A) Well-preserved leaf print in muddy siltstone. (B) Climbing ripples in the uppermost part of unit 4 (crevasse splay deposits).

Interpretation

The abundance of mud and silt-material in the upper part of the Aspelintoppen Formation suggests deposition dominantly from suspension, i.e. in a low-energy environment. The suspended material is brought to the floodplain by overbank flooding of nearby fluvial channels. The red-brownish sandstone occurring at approximately 68,50 m is suggested to represent a soil profile. The presence of root traces, leaf prints, coal-beds and a soil profile implies periodically subaerial exposure of the deposits, indicating deposition in a distal delta-plain setting. The interbedded mud-rich and sometimes normal-graded sandstones, containing current-ripple cross-lamination, climbing ripples and root traces, are interpreted to represent distal crevasse splay deposits.

Depositional environment

The overall nature of unit 1-3 (100-72,80 m) indicate a tide-influenced lower delta-plain depositional setting for the lower-middle part of the Aspelintoppen Formation. The latter interpretation is consistent with previous studies of the succession (e.g. Naurstad, 2014), suggesting tide-influence on the lower part. The upper part of the succession (unit 4; 72,80-60 m) is interpreted to represent distal delta-plain deposits. The observation of abundant root

traces, leaf prints and a soil profile, indicating periodically subaerial exposure of the deposits, support the latter interpretation. Although no distinct tide-induced structures are observed in unit 4, the presence of carbonate cement in sample A8 indicate some marine influence (see section 5.3)

5.2 Geochemical trends

5.2.1 Introduction

A handheld XRF-analyser were used to measure the elemental composition of core 7-2006 and 11-2003, aiming to identify geochemical trends in the sediment cores and to investigate whether these can be correlated to the sedimentary logs. Large- and small-scale geochemical trends can thus be used to support sedimentological interpretations and to help fill in gaps in the sedimentary logs (e.g. in heavy bioturbated intervals). In addition, the elemental composition of the cores provides information regarding the mineral composition of the studied formations, e.g. presence of feldspar, which, in turn, can be used to predict the formation of authigenic illite at the expense of kaolinite at great burial depths. Geochemical data can thus be used to get a better understanding of the types and distribution of authigenic minerals. However, combining the geochemical signatures of the rocks with the sedimentary logs and thin section analyses, provide a more complete "history" of the Firkanten, Grumantbyen and Aspelintoppen formations. In the following, the geochemical signatures (i.e. trends, peaks, troughs) of the studied formations will be discussed in detail, focusing on elements showing large and/or small-scale geochemical trends. The red and green trend-lines (Fig. 5.13-5.15) are based on visual inspection rather than scientific calculations, requiring at least three measurements on a (more or less) straight line. Elemental concentrations are represented in parts per million (ppm). In addition to Fig. 5.13-5.15, selected element plots are attached in Appendix II.

5.2.2 Firkanten Formation

The Firkanten Formation is interpreted to represent coastal plain- (Todalen Member) and shallow marine deposits (Endalen Member), reflecting the early Paleocene large-scale transgressive phase of basin infilling. The XRF-data reveals clear geochemical trends, both large- and small-scale. The most prominent trends, representing the large-scale evolution of the Firkanten Formation, are (1) a small decrease in silica (Si) concentration towards the top of the core and (2) accompanying increase in aluminium (Al), barium (Ba), rubidium (Rb), potassium

(K), strontium (Sr) and yttrium (Y) concentrations (Fig. 5.13 and Appendix II). The decrease in Si-content indicates a reduction in the relative amounts of quartz (i.e. sand), suggesting a more distal depositional setting towards the top of the core. The increase in Al-, Ba-, Rb-, K-, Sr- and Y-concentrations towards the top of the core, implying an increase in the amount of clayey material, correlates well with the decreasing Si-concentration. In the uppermost part of the core (c. 590 m), however, a distinct increase in the Si-content and accompanying decrease in the Al-, Rb- and K-concentrations occur, disturbing the large-scale trends discussed above (Fig. 5.13). Furthermore, the lowermost approximately 10 m of the core displays a cluster of relatively low Si-concentrations and high Al-, Ba-, Rb-, K-, Sr- and Y-values. The latter observation is consistent with the sedimentary log, showing an interval of alternating mudstones and coal-beds.

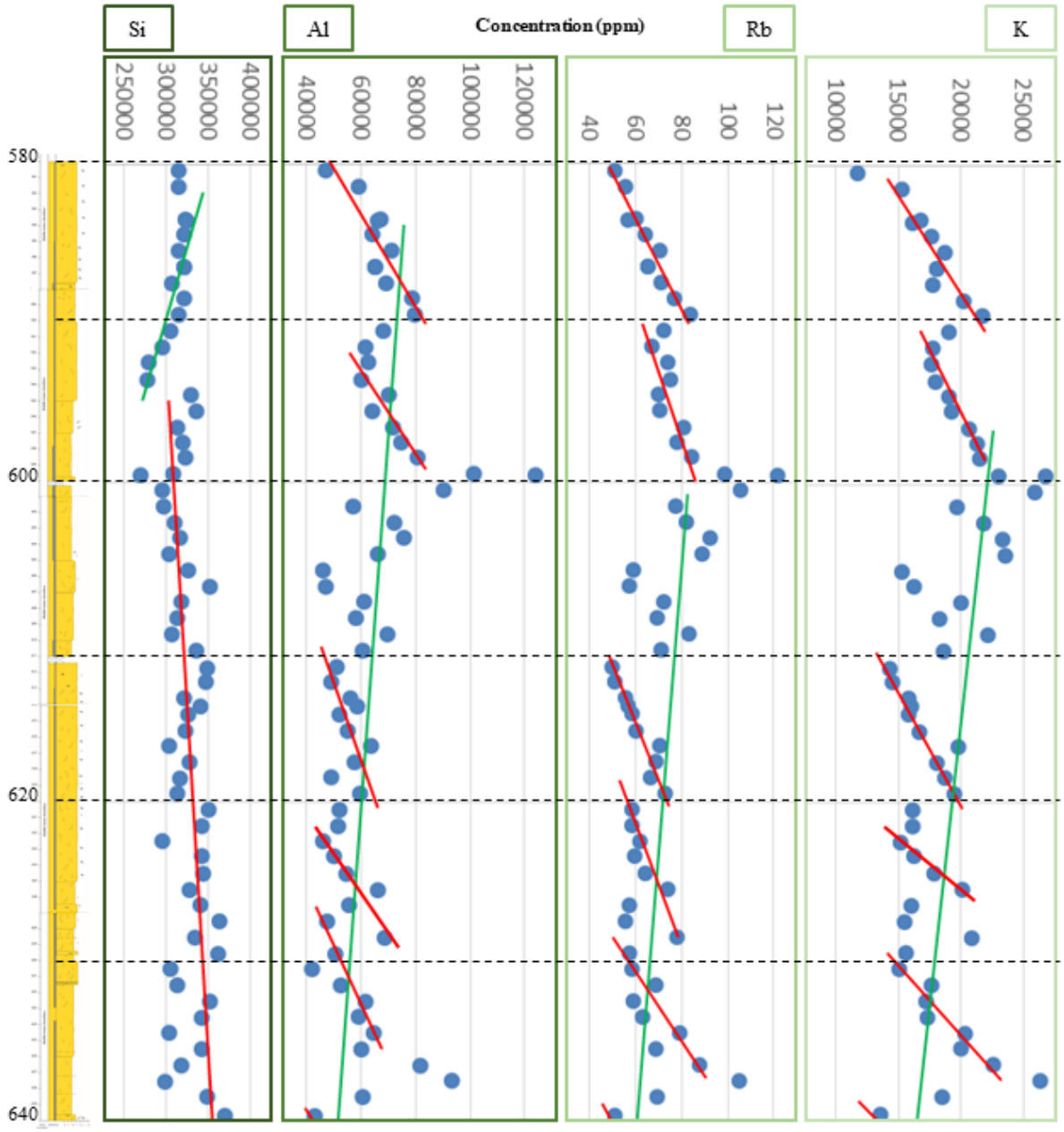

Figure 5.13: Geochemical trends identified in the middle-upper part of the Firkanten Formation (Endalen Mbr.). Sub-trends, showing decreasing Al, Rb and K element concentrations seem to correlate well with intervals of coarsening upwards (i.e. parasequences) in the sedimentary log.

The large-scale geochemical trends are occasionally interrupted by sub-trends, reflecting smaller changes in lithology. In particular, repeating sub-trends are observed in the Al-, Ba-, Rb- and K-profiles (Fig. 5.13 and Appendix II). The sub-trends, showing decreasing element concentrations, e.g. from 600-590 m and from 639-630 m (Fig. 5.13), seems to correlate well with intervals of coarsening upwards in the sedimentary log (i.e. parasequences). The sharp increase in the Al-, Rb- and K-concentrations at c. 605-600 m is probably related to the very

high mud-content of this interval. In addition, the geochemical profiles suggest decreasing concentrations in Al, Ba, Rb and K from approximately 655-645 m (bioturbated and, in part, cross-stratified sandstone; Fig. 5.2), although a coarsening upwards trend was not observed in the core. The latter observation suggests that the geochemical signatures of the Firkanten Formation, notably changes in elements typical for clay-bearing minerals, possibly can be used to help fill in gaps in the sedimentary log.

5.2.3 Grumantbyen Formation

The Grumantbyen Formation, interpreted to represent shallow-marine deposits, was studied in both cores 7-2006 and 11-2003. The geochemical signatures of core 7-2006 (Appendix II) shows several small-scale trends rather than continuous large-scale trends, whereas both large-scale and smaller-scale trends are observed in core 11-2003 (Fig. 5.14). Nevertheless, changes in element concentrations observed in the Grumantbyen Formation are modest compared to the underlying Firkanten Formation, probably reflecting the relatively stable depositional environment of the formation. The uppermost part of the Grumantbyen Formation (cores 7-2006 and 11-2003), however, composes an interval of fining upwards, capped with a thin mudstone. The resultant decrease in lithology and sand/mud-ratio is reflected in the geochemical signatures of the cores, revealing a steep increase in the Al-, Rb- and K-concentrations and a decrease in the Si-content (Fig. 5.14 and Appendix II). The muddy intervals are interpreted to represent transgressive lags, reflecting the onset of marine flooding and deposition of the overlying Frysjaodden Formation (see section 5.1).

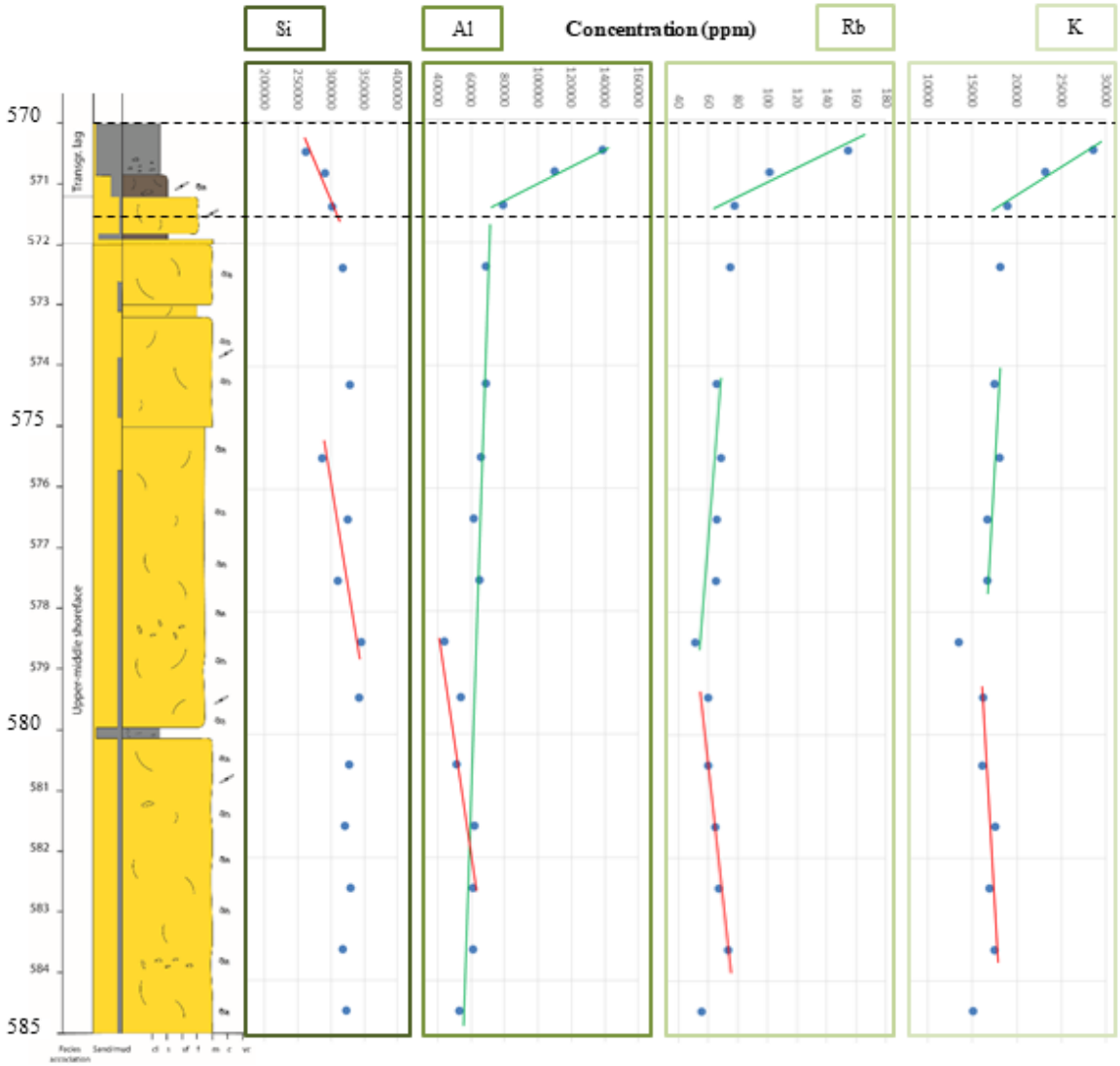

Figure 5.14: Geochemical trends identified in the Grumantbyen Formation (core 11-2003). The abrupt increase in Al, Rb and K element concentrations indicate the transition between the shallow-marine Grumantbyen Formation and overlying deep-marine Frysjaodden Formation.

5.2.4 Aspelintoppen Formation

The Aspelintoppen Formation, constituting the uppermost part of the Van Mijenfjorden Group, is interpreted to represent tide-influenced deltaic deposits. The XRF-analysis of the formation shows frequent variations in element concentrations rather than distinct small- and large-scale trends (Fig. 5.15), probably reflecting the muddy and chaotic nature of the deposits. The Si-profile displays relatively scattered measurements, although sets of smaller-scale geochemical trends are observed. The smaller-scale trends, predominantly showing increasing Si-concentration, seem to coincide, at least in part, with intervals showing increasing sand/mud ratios, e.g. from c. 83-77 m and from c. 95-91 m (Fig. 5.15). The Al-, Rb- and K-profiles are inverse proportional to the Si-profile, in which decreasing concentrations coincide with intervals of increasing sand/mud ratios and vice versa. The geochemical signatures of the Aspelintoppen Formation, however, are less distinct than similar signatures of the Firkanten Formation. The latter is probably related to the muddy character and frequent variations in lithology of the Aspelintoppen Formation.

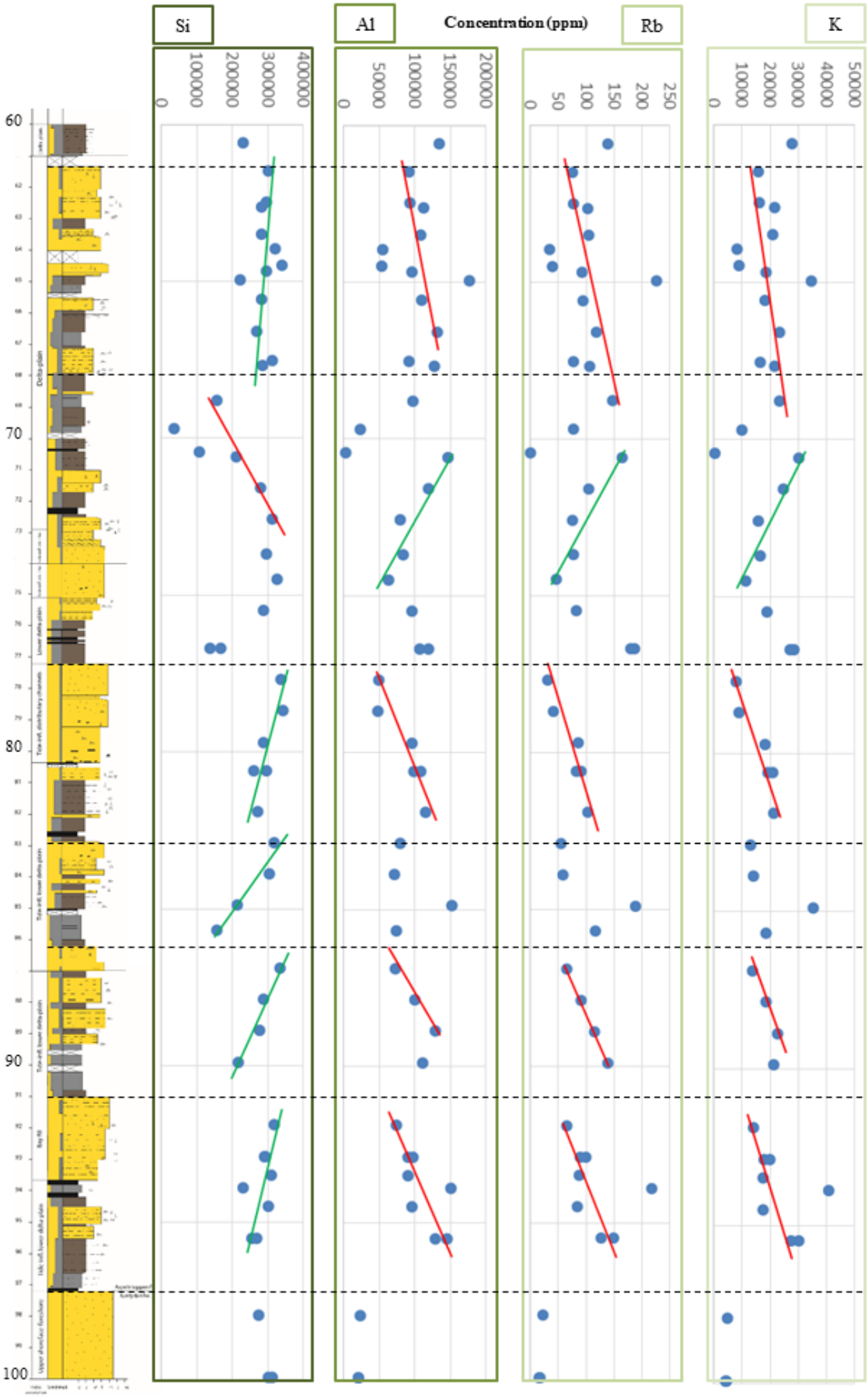
Si
Al
Concentration (ppm)
Rb
K
0
100000
200000
300000
400000
0
50000
100000
150000
200000
0
50
100
150
200
250
0
10000
20000
30000
40000
50000
60
70
80
90
100

Figure 5.15: Geochemical trends identified in the Aspelintoppen Formation (core 11-2003). Although less clear than in the Firkanten Formation, increasing Si-content and decreasing Al, Rb and K element ratios seem to sometimes coincide with intervals of increasing sand/mud ratios. The frequent variations in element concentrations probably reflect the muddy and "chaotic" nature of the Aspelintoppen Formation.

5.2.5 Authigenic minerals

The linkage between elements and mineral composition (e.g. high Si-content suggests abundant quartz etc.) suggests that the geochemical signatures of the cores can be used to predict the occurrence of certain authigenic minerals, including the formation of burial diagenetic illite at the expense of kaolinite in potassium-rich formation waters. The K/Rb and Rb/Sr element ratios are controlled by feldspars and micas, in which Rb and Sr often substitute for K and Na, suggesting that these ratios are indicative for feldspar-content (Fig. 5.16) (Schlegel et al., 2013). The sandstones of the Firkanten and Grumantbyen formations (higher feldspar contents) show higher element ratio of K/Rb and lower Rb/Sr ratio than the Aspelintoppen Formation (lower feldspar content). The latter observations are in agreement with thin section analyses (see section 5.3).

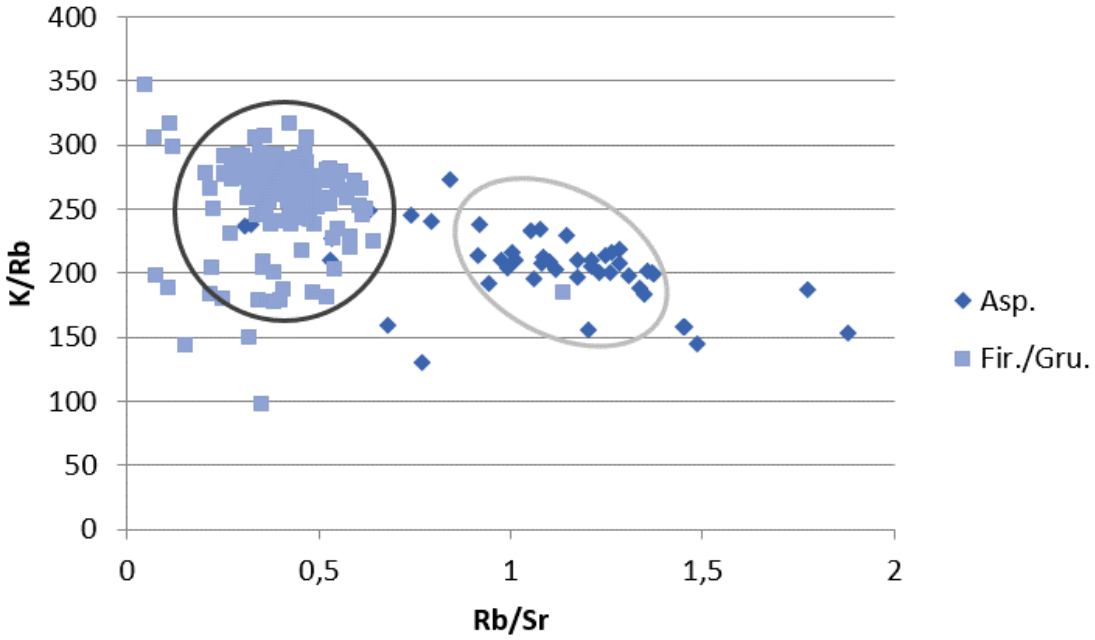

Figure 5.16: Distribution of the Rb/Sr and K/Rb element ratios in the Paleocene Firkanten and Grumantbyen formations (black circle) and the Eocene Aspelintoppen Formation (grey circle).

5.3 Petrographic analyses

5.3.1 Introduction

A total of 44 thin-sections, one from each sandstone-sample, were analysed using an optical microscope. In addition, eight of the samples were selected for Scanning Electron Microscope (SEM) and X-ray diffraction (XRD) analyses (Appendix I). The purpose of the thin section analysis was to investigate the composition (i.e. texture, detrital minerals, authigenic phases, cement and porosity) of the samples and thus get a better understanding of depositional environment, diagenesis and temperature history of the Firkanten, Grumantbyen and Aspelintoppen formations. Furthermore, SEM- and XRD-analyses aimed to help fill in gaps in optical microscopy and to identify uncertain minerals. Schlegel et al. (2013) generally classified sandstones of the Central Tertiary Basin (cores 7-2006 and 11-2003) as feldsphatic sandstones.

Detrital minerals – minerals present initially in sediments – were predominantly identified using optical microscope, whereas authigenic minerals – minerals formed "in situ" subsequent to deposition of detrital minerals – were identified using both optical microscope, SEM and XRD. The most prevalent cement types in sandstones are quartz, carbonate and clay minerals, although smaller amounts of pyrite, feldspar, hematite, apatite and Ti-rich minerals are locally important (Worden and Burley, 2003). Grain sizes- and porosity values were roughly estimated by visual inspection, using the scale appearing in the lower right/left corner of optical micrographs and quantifying the blue spots (i.e. epoxy) present in the samples, respectively. Optical micrographs (2,5x, PPL and close ups) of most samples are attached in Appendix III; SEM- and XRD-analyses of selected samples are attached in Appendix II.

5.3.2 Firkanten Formation

Table 5.1: Detrital and authigenic mineralogy of sample F1, F3, F11, F19 and F25 (Firkanten Formation) obtained from SEM EDS analysis.

Sample	Minerals	Origin
F1	Quartz	Detrital
	Pyrite	Authigenic
	Glauconite	Authigenic
	K-feldspar	Detrital
	Mica	Detrital
	Plagioclase	Detrital
	Rutile	Detrital
F3	Pyrite	Authigenic
	Apatite	Authigenic
	Chlorite	Authigenic
	Mica	Detrital
	Albite	Authigenic
	Glauconite	Authigenic
	Rutile	Detrital
	Calcite	Authigenic
	K-feldspar	Detrital
	Quartz	Detrital
F11	Quartz	Detrital
	K-feldspar	Detrital
	Glauconite	Authigenic
	Pyrite	Authigenic
	Albite	Detrital
	Calcite	Authigenic
	Clays	Authigenic
	Rutile	Detrital
F19	Rutile	Detrital
	Calcite	Authigenic
	Clays	Authigenic
	Quartz	Detrital
	K-feldspar	Detrital
	Chlorite	Authigenic
	Pyrite	Authigenic
	Ca-phosphate (apatite)	Authigenic
	Mica	Detrital
	Albite	Authigenic
F25	Quartz	Detrital
	Calcite	Authigenic
	Mica	Detrital
	Siderite	Authigenic
	Rutile	Detrital
	Albite	Detrital
	K-feldspar	Detrital
	Clay	Authigenic

Detrital sandstone composition

The analysed samples of the Firkanten Formation compose grain sizes ranging from very fine-medium sand, in which the majority of the samples composes fine grain-sizes. Furthermore, the thin section analysis suggests presence of several intervals of shallowing-upwards (i.e. parasequences; Fig. 5.17). The latter observation is consistent with the sedimentary log (see section 5.1.2) and XRF-analysis (see section 5.2.2). The sandstones are generally well-very well sorted; the uppermost part of the core is moderately-well sorted. The quartz grains are commonly subangular rounded, suggesting deposition close to the source area.

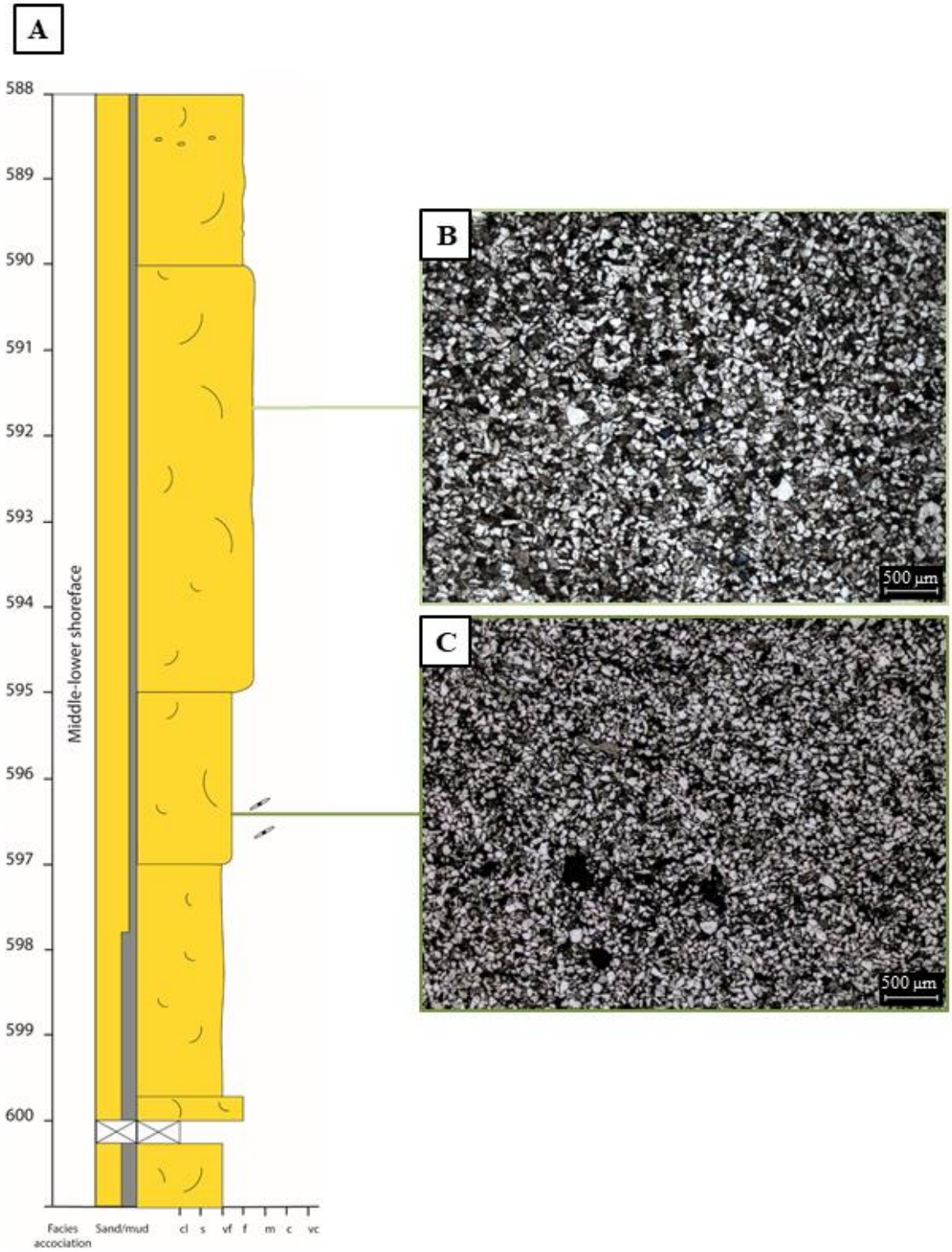

Figure 5.17: Alignment of sedimentary log and optical micrographs. (A) Sedimentary log of the upper part of Firkanten Formation (Endalen Mbr.). Gradual increase in grain size from c. 600-590 m (parasequence). (B) and (C) Optical micrographs (PPL) of sample F24 and F23, respectively, confirming an upwards increase in grain size.

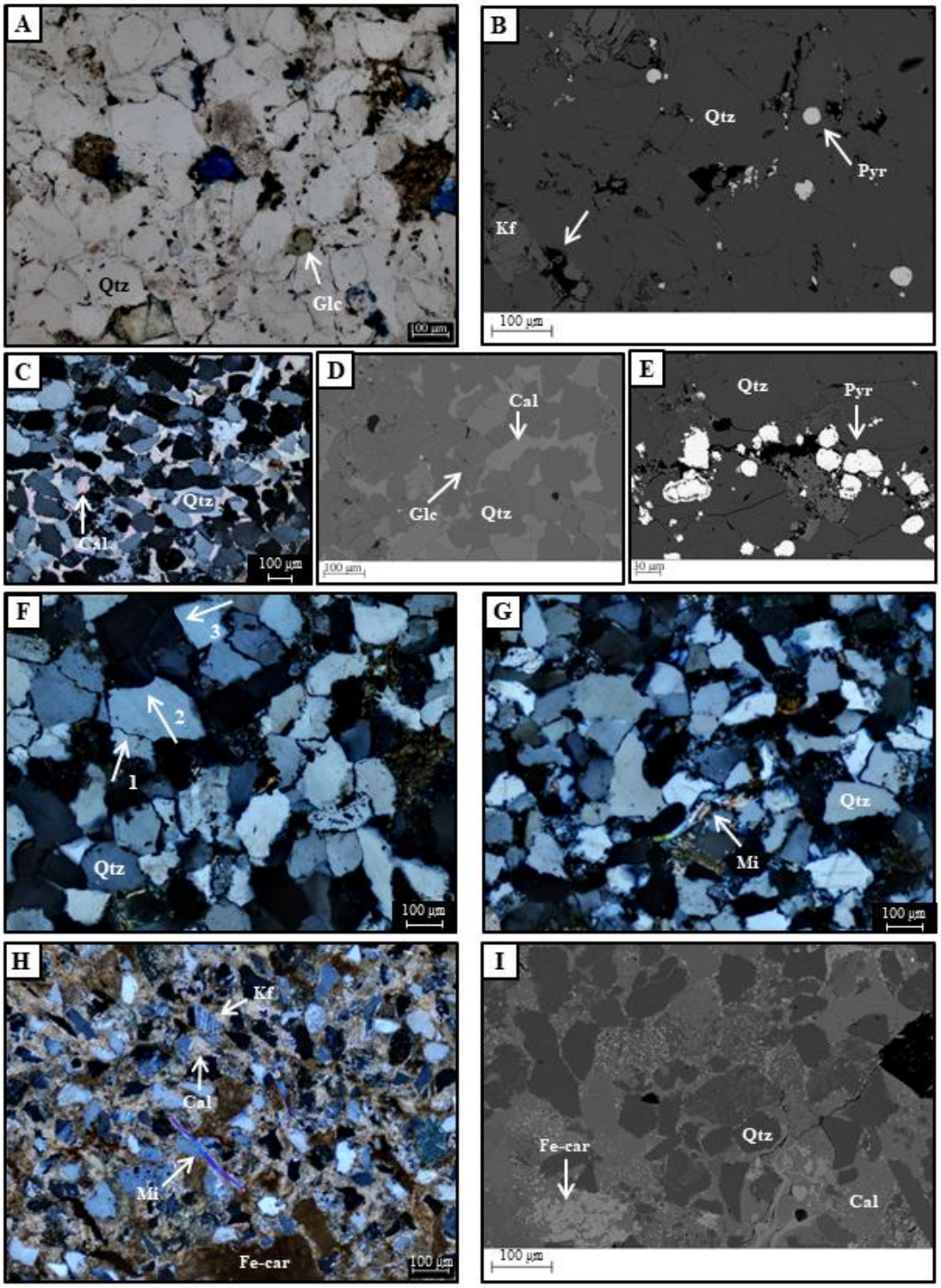

Figure 5.18: Micrographs of selected sandstone-samples from the Firkanten Formation (core 7-2006). Qtz = quartz; Glc = glauconite; Pyr = pyrite; Kf = K-feldspar; Cal = calcite cement; Mi = mica; Fe-car = Fe-carbonate (siderite). (A) Extensive quartz cementation and minor glauconite in sample F1 (optical microscopy; PPL). (B) SEM BSE image of sample F1, showing abundant quartz cement, K-feldspar, framboidal pyrite and dissolution porosity (arrow). (C)/(D) Optical micrograph (XPL)/SEM BSE image of carbonate (calcite) cemented sandstone (sample F3). (E) Abundant framboidal pyrite in laminated sandstone (sample F3; SEM BSE). (F) Optical micrograph (XPL) showing presence of sutured (1), concavo-convex (2) and long (3) grain contacts in quartz cemented sandstone (sample F1). (G) Bended mica grain in sample F4 (optical microscopy; XPL). (H)/(I) Optical micrograph (XPL)/SEM BSE image of muddy carbonate (siderite) cemented sandstone (sample F25).

Quartz is the most prominent detrital mineral in the Firkanten Formation, constituting >50% of the mineral assemblage. The majority of quartz grains are monocrystalline, although smaller amounts of polycrystalline grains are observed, and show undulatory extinction angle (cross-polarized light; XPL). Furthermore, quartz commonly show point contacts to adjacent grains. Both long, concavo-convex and sutured grain contacts are observed, in which the two formers are the most prominent types (Fig. 5.18f). In sample F13 and F25, however, grains are (partially) floating in a matrix of carbonate cement (Fig.5.18c). Generally, the samples show abundant quartz cement (e.g. Fig. 5.18a).

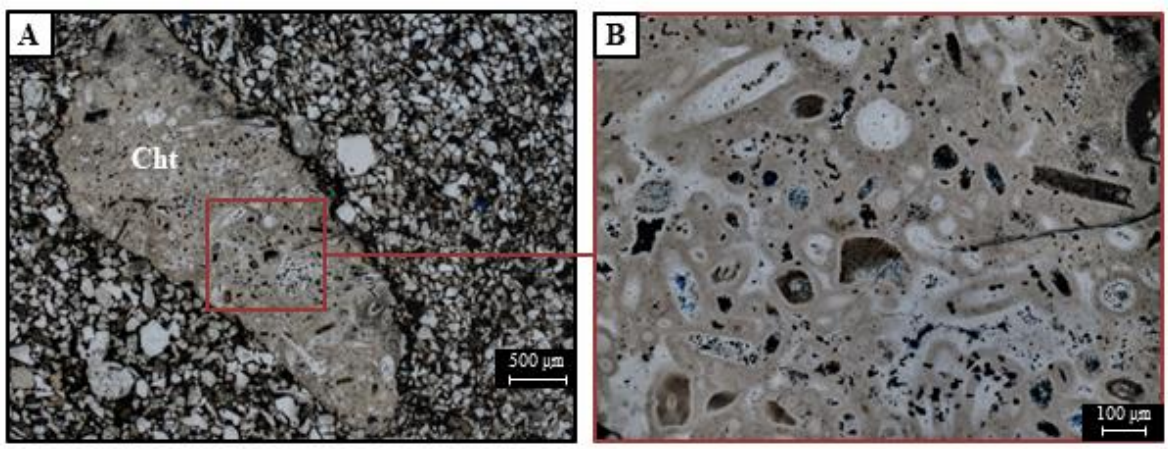

Figure 5.19: Optical micrographs (PPL) of sample F22 from the uppermost part of Firkanten Formation (core 7-2006). (A) Chert fragment (Cht) composing microfossils *(Spiculites)*. The chert fragment is thought to originate from the upper Permian Kapp Starostin Formation. (B) Close up optical micrograph of chert fragment in (A).

Feldspars, in particular plagioclase, is the second most abundant detrital mineral observed in the analysed samples. Plagioclase and K-feldspar appear colourless in plane-polarized light (PPL) and show inclined extinction angle in XPL. Polysynthetic- and tartan twinning are observed in plagioclase and K-feldspar, respectively. Furthermore, smaller amounts of mica (muscovite and biotite), rock fragments, chert and coal fragments are observed in the samples. Mica, both muscovite and biotite, show distinct colours and parallel extinction angle in XPL. Mica grains are often bended and/or broken, suggesting significant compaction. Chert fragments occur scattered throughout the formation, composing distinct microcrystalline quartz or microfossils (Fig. 5.19a,b). The microfossils observed in some of the chert fragments resemble *Spiculites,* suggesting that these fragments originate from the upper Permian Kapp Starostin Formation (S. Olaussen 2019, pers. comm., 22. Aug.). Coal fragments, typically small in size, occur scattered in some of the analysed samples. The coal fragments appear opaque (black) in PPL, showing softer edges than opaque heavy minerals (i.e. pyrite).

Authigenic mineralogy

The sandstones of the Firkanten Formation, representing coastal plain to shallow-marine deposits, are strongly influenced by compaction and cementation. Mechanical compaction, evidenced by dense grain packing and bending/breakage of mica, resulted in low porosity values, ranging from absent to approximately 5%. In addition, extensive quartz cementation probably played an important role in destroying porosity. The highest porosity value (approximately 5%) was estimated in sample F5, constituting upper shoreface-foreshore deposits (Fig. 5.2).

Authigenic quartz and calcite are the most prominent cement types, although smaller amounts of other authigenic minerals occur, including pyrite, glauconite, kaolinite and albite. Quartz cement, forming syntaxial overgrowths on the detrital quartz grains, locally fills the pore spaces between quartz and adjoining grains. Calcite occurs as extensive, continuous pore-filling cement, varying from absent in some samples to abundant in other samples (e.g. sample F3; Fig. 5.18c). Pyrite occurs as scattered euhedral grains or in clusters of euhedral and/or framboidal pyrite (Fig. 5.18b,e). Furthermore, authigenic pyrite seems to be more abundant in the lowermost part of the formation, although scattered grains are observed in most of the samples (except for in sample F25). Minor glauconite, appearing greenish in PPL, are observed in the lowermost part of the Firkanten Formation. Although a clear identification of glauconite was difficult, the greenish colour of the mineral (PPL) indicates presence of glauconite. Furthermore, Lüthje (2008) describes glauconite in the lowermost part of the Firkanten Formation, supporting the latter interpretation. Dissolution porosity is sometimes observed in K-feldspar grains (Fig. 5.18b).

SEM- (Table 5.1) and XRD-analyses (Appendix II) suggests presence of phosphate minerals, including apatite, Al-phosphate and Ba-phosphate, and Ti-oxides (rutile). The shape of the rutile grains, however, indicate a rather detrital origin. Phosphate is commonly observed within other minerals, typically chert fragments and quartz. Furthermore, XRD-analysis indicate presence of kaolinite, ankerite and illite/muscovite (Appendix II). Due to the small grain size of illite (reffered to as “clays” in table 5.1), mixing with other phases and low-resolution images, a clear identification of this mineral was not possible in SEM. Finally, SEM-analysis reveals presence of possible siderite in the uppermost part of the formation (sample F25; Fig. 5.18i).

5.3.3 Grumantbyen Formation

Table 5.2: Mineralogical composition of sample G6 (Grumantbyen Formation) obtained from SEM EDS analysis.

Sample	Minerals	Origin
G6	Quartz	Detrital
	Calcite	Authigenic
	K-feldspar	Detrital
	Albite	Authigenic
	Fe-chlorite	Authigenic
	Rutile	Detrital
	Glauconite	Authigenic
	Mica	Detrital

Detrital composition

The analysed samples of the Grumantbyen Formation compose grain-sizes ranging from fine-coarse sand, in which sample G1-G3 (core 7-2006) are slightly coarser-grained than sample G4-G6 (core 11-2003). The thin section analysis is in agreement with the sedimentary logs, showing only smaller changes in grain sizes (except for in the uppermost part of the formation). The analysed samples are well-very well sorted, predominantly showing subangular grains. The latter observation suggests deposition close to the source area.

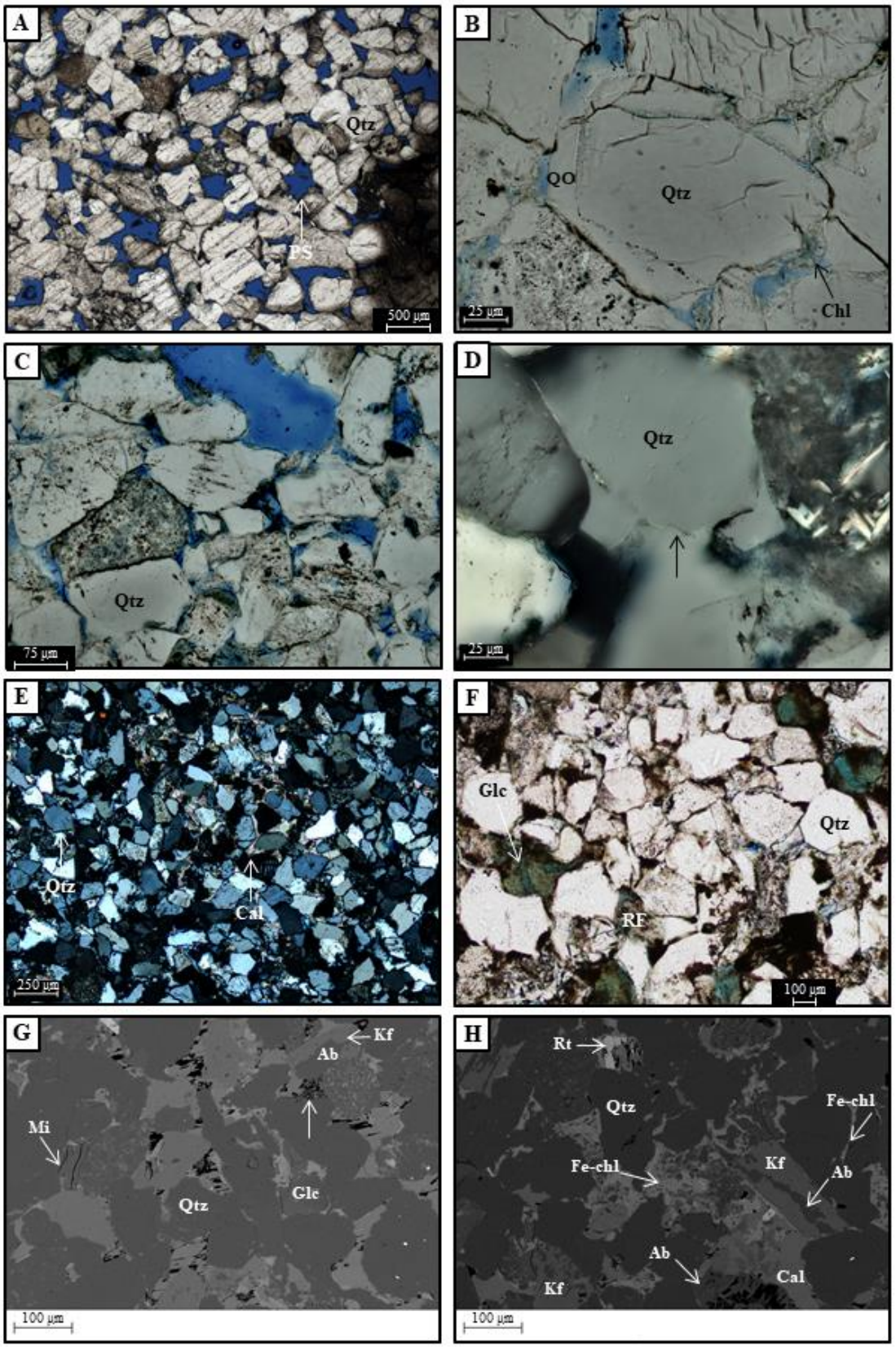

Figure 5.20: Micrographs of selected sandstone-samples of the Grumantbyen Formation (cores 7-2006 and 11-2003). Qtz = quartz; PS = pore space; QO = quartz overgrowth; Chl = chlorite; Cal = calcite; Glc = glauconite; RF = rock fragment; Mi = mica; Kf = K-feldspar; Ab = albite; Rt = rutile. (A) Optical micrograph (PPL) of gravelly sandstone (sample G1; core 7-2006). The relatively high porosity-values of the sandstone may be ascribed to the presence of grain-coating chlorite. (B) Optical micrograph (PPL) of discontinuous grain-coating chlorite in sample

G2 (core 7-2006). (C) Optical micrograph (PPL) of quartz cemented sandstone (sample G3; core 7-2006). Grain coating chlorite seems to have, at least in part, retarded quartz cementation. (D) High-resolution optical micrograph (XPL) of sample G5 (core 11-2003). Sutured grain-contact (arrow) and quartz overgrowth. (E) Sample F5 (core 11-2003), showing presence of both quartz- and carbonate cement (optical microscopy; XPL). (F) Optical micrograph (PPL) of quartz cemented sandstone (sample G6; core 11-2003), composing detrital quartz, rock fragments and minor glauconite. (G) and (H) SEM BSE images of sample G6 (core 11-2003), showing main mineral constituents and dissolution porosity (black areas; arrow in left picture).

Quartz is the most prominent detrital mineral in the Grumantbyen Formation, constituting more than 50% of the mineral assemblage. The quartz grains, showing undulatory extinction angle (XPL), are commonly monocrystalline, although minor polycrystalline quartz is observed. Furthermore, the quartz grains show point-contacts, in which both long, concavo-convex and sutured grain contacts occur (Fig. 5.20d). Quartz cement (i.e. quartz overgrowth) is observed in all of the analysed samples. Feldspar, both plagioclase and K-feldspar, is probably the second most abundant detrital mineral occurring. Plagioclase typically shows polysynthetic twinning, whereas K-feldspar shows tartan twinning. In addition, smaller amounts of mica, rock fragments and chert occur throughout the formation. The low mica-content of the samples probably reflect the high-energy depositional environment interpreted for the Grumantbyen Formation. The “fractures” observed in sample G1 (Fig. 5.20a) are probably an artefact from the polishing of thin sections.

Authigenic mineralogy

The bioturbated sandstones of the Grumantbyen Formation show high degree of compaction and cementation, in which compaction is evidenced by dense grain packing and squeezing of ductile grains. Generally, the porosity of the analysed samples is considerably higher than for the Firkanten and Aspelintoppen formations, in particular in samples G1, G3 and G4. The highest porosity value (up to 15%) was measured in sample G1, comprising gravelly coarse-grained sandstone (Fig. 5.6).

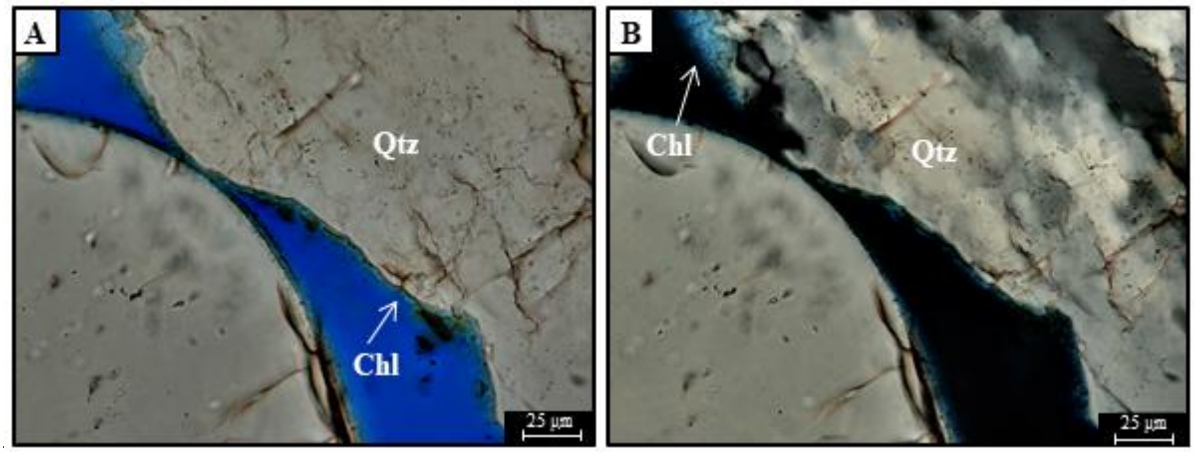

Figure 5.21: Optical micrographs of gravelly coarse-grained sandstone (sample G1; core 7-2006), showing presence of continuous grain-coating chlorite. (A) PPL. (B) XPL.

Quarts cement, forming syntaxial overgrowths on detrital quartz grains, is the most prominent type of cement occurring in the analysed samples. Quartz cement locally fills the pore spaces between quartz and adjacent grains (Fig. 5.20b). Furthermore, smaller amounts of pore-filling carbonate cement and glauconite are observed, in which carbonate cement is most prominent in core 11-2003 (Fig. 5.20e). Although a clear identification of glauconite was difficult, the greenish colour of the mineral (PPL) and previous studies of the Grumantbyen Formation (e.g. Steel et al., 1981), describing high glauconite-content, support presence of glauconite. Furthermore, SEM- and XRD analyses suggest presence of porefilling chlorite, albite and minor kaolinite and illite/muscovite (Fig. 520g,h). However, a clear identification of illite was not possible in SEM (see section 5.3.2). Calcite cement and feldspar often show dissolution porosity (Fig. 5.20g). Albite is sometimes observed within K-feldspar grains/seems to (partially) replace K-feldspar grains, indicating an authigenic origin of this mineral (Fig. 5.20g).

Optical microscopy suggests presence of grain-coating chlorite in sample G1, G2 and G3 (core 7-2006; Fig. 5.20b,c and Fig. 5.21a,b). In addition, SEM-analysis indicate presence of grain-coating chlorite in sample G6 (core 11-2003; Fig. 5.20h). Two different types of grain coating chlorite are observed: (1) continuous grain coating chlorite (sample G1; Fig. 5.21a,b) and (2) discontinuous grain coating chlorite (samples G2, G3 and G6; Fig. 5.20b,c,h). Grains showing continuous grain coating chlorite seem to lack quartz overgrowth (sample G1), whereas grains showing discontinuous grain coating chlorite are, at least in part, quartz cemented (e.g. sample G2). The latter observation is probably, in part, related to grain size, in which coarser grain sizes provide favourable conditions for precipitation of grain coating chlorite. Furthermore, grain coating chlorite seems to be absent at point contacts, implying that the coatings formed

subsequent to some compaction (Fig. 5.20b) (Gould et al., 2010). The generally higher porosity values estimated for the Grumantbyen Formation are probably related to the presence of grain-coating chlorite, preventing/retarding precipitation of quartz cement and, thus, preservation of porosity (Bjørlykke and Jahren, 2015).

5.3.4 Aspelintoppen Formation

Table 5.3: Mineral composition of sample A1 and A7 (Aspelintoppen Formation) obtained from SEM EDS analysis.

Sample	Minerals	Origin
A1	Pyrite	Authigenic
	Quartz	Detrital
	K-feldspar	Detrital
	Fe-oxide	Authigenic
	Kaolinite	Authigenic
	Fe-dolomite	Authigenic
	Chlorite	Authigenic
	Mica	Detrital
	Rutile	Detrital
	Fe-oxide	Authigenic
	Calcite	Authigenic
	Apatite (Ca-phosphate)	Authigenic
A7	Mica	Detrital
	Chlorite	Authigenic
	Kaolinite	Authigenic
	Fe-dolomite	Authigenic
	Rutile	Detrital
	Quartz	Detrital
	Phosphate	Authigenic
	K-feldspar	Detrital

Detrital sandstone composition

The thin section analysis reveals great variability in grain-size, ranging from coarse silt to fine-medium sand. The grain-size distribution is rather random, suggesting a chaotic nature of the succession. The latter observation is consistent with the sedimentary log, showing alternating muddy sandstones, siltstones and mudstones, occasionally interbedded with thin coal-beds. The samples are muddy and moderately sorted, generally showing subangular grains. The poor roundness of the grains and apparent immature character of the sediments suggest deposition close to the source area and limited reworking.

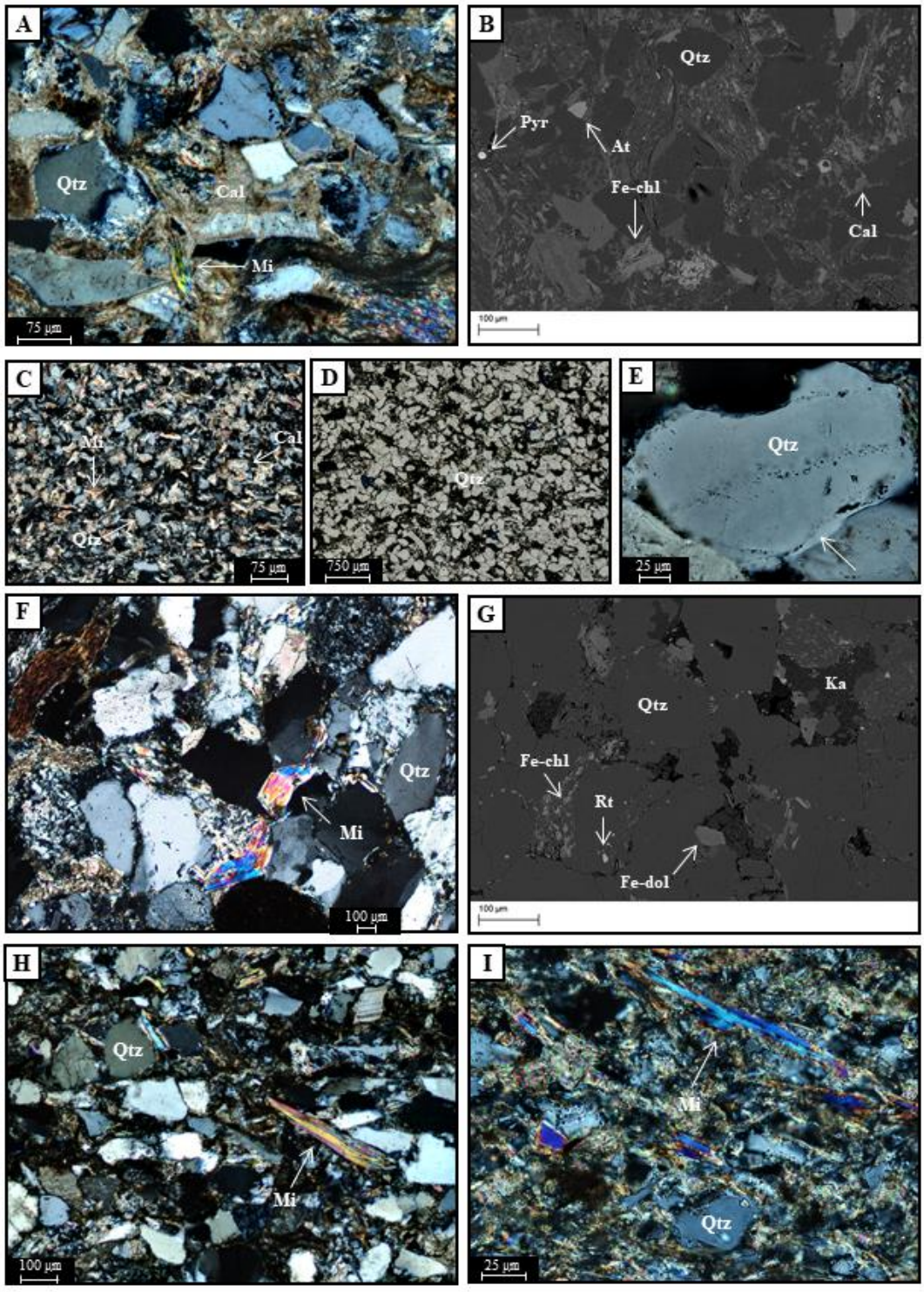

Figure 5.22: Micrographs of selected sandstone-samples of the Aspelintoppen Formation (core 11-2003). Qtz = quartz; Cal = calcite; Mi = Mica; Pyr = pyrite; At = apatite; Fe-chl = Fe-chlorite; Fe-dol = Fe-dolomite; Ka = kaolinite. (A) Muddy carbonate cemented sandstone (sample A1; optical microscopy; XPL). (B) SEM BSE image of sample A1, revealing presence of Fe-chlorite, calcite, pyrite and apatite. (C) Optical micrograph (XPL) of carbonate-cemented muddy siltstone. (D) Optical micrograph (PPL) of quartz-rich sandstone (sample A7). (E) High-resolution optical micrograph (XPL) of sample A7, showing quartz overgrowth (arrow). (F) Optical micrograph (XPL) of bended/broken mica grain in sample A7, suggesting sufficient compaction. (G) SEM BSE image of sample A7, showing mineral constituents. Fe-chlorite seems to (partially) replace quartz. Kaolinite occurs as extensive porefilling cement. (H)/(I) Optical micrographs (XPL) of muddy carbonate cemented sandstones (samples A6 and A8, respectively.). Non-deformed mica-grains suggest early diagenetic carbonate cementation.

The amount of detrital quartz varies significantly throughout the formation, from very small amounts in some samples (e.g. sample A8; Fig. 5.22i) to around 50% in other samples (e.g. sample A7; Fig. 5.22d). The majority of grains are monocrystalline, although polycrystalline quartz occurs, and show undulatory extinction angle in XPL. Quartz overgrowth is observed in most of the samples, notably in the quartz-rich sandstones. Furthermore, varying amounts of feldspar (both plagioclase and K-feldspar) occur. The feldspar-content, however, are generally low compared to the underlying formations, notably the Firkanten Formation. The latter observation may be related to the formation of early diagenetic kaolinite at the expense of k-feldspar. Generally, the thin section analysis shows high mica-content throughout the formation, reflecting the low-energy depositional setting interpreted for the Aspelintoppen Formation. Most of the samples show point contacts; the muddiest samples and/or samples showing abundant carbonate-cement are matrix supported or show a combination of point contacts and floating grains (e.g. sample A8; Fig. 5.22i).

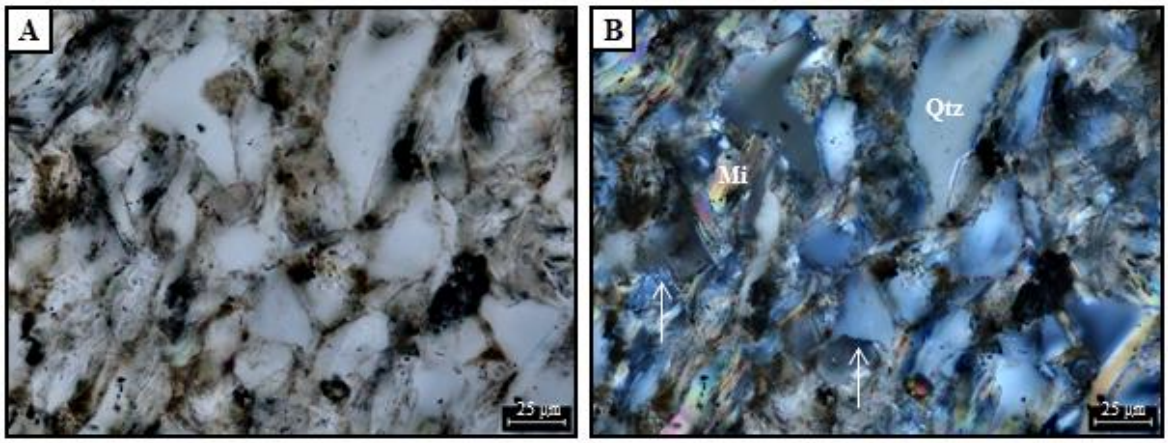

Figure 5.23: Optical micrographs of muddy, mica-rich sandstone (sample A4; core 11-2003). (A) PPL. (B) Styolitisation (arrows), causing additional loss of volume and porosity (XPL).

Authigenic mineralogy

The muddy sandstones of the Aspelintoppen Formation show high degree of compaction and cementation. Mechanical compaction is evidenced by dense grain packing and, sometimes, bending of mica grains (Fig. 5.22f). The thin section analysis suggests extremely low porosity values for the succession, ranging from absent to 1-2%. The highest porosity value (approximately 2%) was estimated in sample A7, constituting moderately-well sorted fine-medium grained sandstone.

Authigenic quartz, carbonate and kaolinite are the most prominent cement types occurring in the Aspelintoppen Formation. Quartz cement, forming syntaxial overgrowths on the detrital quartz grains, locally fills the pore spaces between quartz and adjacent grains. Although observed in most of the analysed samples, quartz cement is more abundant in sandstones rich in detrital quartz and/or showing little carbonate cement (e.g. sample A7; Fig. 5.22d,e). Carbonate cement contains both Fe-dolomite and calcite, in which Fe-dolomite commonly occurs as relatively large grains (Fig. 5.22g). In the very muddy sandstone-samples, calcite cement seems to be (partially) "hidden" behind clayey material (e.g. Fig. 5.22i). Generally, carbonate cement is abundant in all of the analysed samples, except for in sample A7. High intergranular volumes in these samples suggest early diagenetic origin of the carbonate cement. The presence of "non-deformed" mica grains support the latter assertion, in which early diagenetic carbonate cement "stiffen" the sediment at shallow burial (Fig. 5.22h,i) (Worden and Burley, 2003). Furthermore, muddy, mica-rich sandstones sometimes show evidence of styolitisation (e.g. sample A4; Fig. 5.23a,b).

Porefilling kaolinite, appearing dark grey in SEM BSE, is probably an alteration product of detrital K-feldspar (Fig. 5.22g). Furthermore, SEM- and XRD-analyses reveal presence of chlorite and minor pyrite and apatite. Chlorite is observed either as (1) relatively large fibrous grains occupying pore spaces (Fig. 5.22b) or (2) partially replacing detrital quartz grains (Fig. 5.22g). Pyrite occurs as scattered small spherical grains, filling pore spaces between grains, whereas apatite typically occur within matrix and/or other grains (Fig. 5.22b).

6 Discussion

6.1 Introduction

The results obtained from sedimentological, petrographic and geochemical analyses are further analysed and discussed in the present chapter, aiming to understand the importance of depositional environment to diagenesis and evaluate the use of authigenic minerals as a paleothermometer. Large- and small-scale trends in XRF geochemical signatures are assigned to changes in the sedimentary logs and mineral composition, the authigenic mineralogy of the Firkanten, Grumantbyen and Aspelintoppen formations are systematically linked to sandstone composition and depositional environment, and, finally, burial diagenetic signatures are compared to vitrinite reflectance measurements. Vitrinite reflectance measurements of coals and organic material from wells 11-2003 and 7-2006 were obtained from the recently published paper of Dörr et al. (2018).

6.2 Trends in geochemical data (XRF-analysis)

Although the Firkanten, Grumantbyen and Aspelintoppen formations are of different depositional origin, the geochemical data shows similar large-and small-scale trends. Generally, increasing Si-concentrations seem to correlate well with increasing sand/mud ratios (i.e. increasing quartz and feldspar contents) in the sedimentary logs, whereas high Al, Rb and K contents correlate well with mud-rich intervals. Al is often found as oxides and silicates, constituting an important component of kaolinite and other clay minerals, whereas Si is mainly incorporated in quartz and feldspar, justifying the use of these elements as proxies for changes in lithology and sand/mud ratios.

The repetitive sub-trends in elemental concentrations (Al, Rb, K and Si) observed in the Endalen Member. (Firkanten Formation) tend to coincide with intervals of shallowing upwards in the sedimentary log, suggesting that the geochemical signatures of the core may be used to identify parasequences (Fig. 5.13). The latter is particularly helpful in intensively bioturbated sandstones such as in the Endalen Member. The geochemical signatures of the Grumantbyen and Aspelintoppen formations, however, are less distinct and/or continuous than of the Firkanten Formation. The latter is probably related to the muddy nature and frequent variations in lithology, and the short interval of study in the Aspelintoppen Formation and Grumantbyen

Formation, respectively. Analysis of geochemical signatures is thus preferable for sedimentary rocks showing rather gradual and continuous changes in lithology and sand/mud ratios.

The present observations and interpretations are in agreement with previous studies of geochemical signatures in sediment cores (e.g. Schlegel et al., 2013), relating the distribution of major and trace elements in sandstone- and shale samples to their general mineralogical compositions. Schlegel et al. (2013) describes higher SiO_2 and lower Al_2O_3 contents in sandstone samples than shale samples, reflecting the abundance of quartz and feldspar in sandstones, and aluminous clayey material and mica (muscovite and biotite) in shales, respectively. Furthermore, the study suggests higher MgO, Fe_2O_3 and TiO_2 values and higher Cr, Ni, V and Rb contents in the shale-samples, resulting from abundant sheet silicates in the shales. The higher Rb-content of the shales is consistent with the present study, in which intervals of increasing sand/mud ratios in the Endalen Member show decreasing Rb values (Fig. 5.13). Finally, the study of Schlegel et al. (2013) relates comparable K_2O content of the shales and most of the sandstones to the incorporation of K in K-feldspar, muscovite and illite (i.e. not exclusively in clay minerals). The present study, however, suggests that decreasing K-values correlate well with increasing sand/mud ratios in the Firkanten and Aspelintoppen formations (Fig. 5.13, Fig. 5.15).

The higher K/Rb element ratio and lower Rb/Sr ratio of the sandstone-samples from the Firkanten and Grumantbyen formations than the Aspelintoppen Formation (Fig. 5.16) is consistent with the thin section analysis, showing higher feldspar-contents in the Firkanten and Grumantbyen formations (see section 5.2.5). Although significantly more abundant in the Aspelintoppen Formation, XRD-analysis indicated presence of kaolinite also in the Firkanten and Grumantbyen formations. Formation of illite at the expense of kaolinite at deep burial depths can thus not be excluded.

6.3 Linking diagenesis to depositional environment

Diagenetic processes (i.e. mechanical/chemical compaction and cementation) are largely controlled by the detrital composition of sandstones (Bjørlykke, 2001; Morad et al., 2012). The detrital composition of sandstones, in turn, is a function of depositional environment, transport and provenance (Bjørlykke and Jahren, 2015). Common diagenetic processes, including mechanical compaction and formation of pseudomatrix, grain dissolution (e.g. feldspars),

formation of kaolinite and growth of pore-lining minerals (e.g. grain-coating chlorite), can thus be linked to depositional facies and depositional environment (Morad et al., 2010). The presence of early diagenetic products, however, are of great importance to burial diagenesis, in which they affect, for instance, clay mineral transformations and precipitation of quartz cement (Morad et al., 2010). A variety of early diagenetic minerals are observed in the analysed samples of the Firkanten, Grumantbyen and Aspelintoppen formations, including quartz- and carbonate cement, kaolinite, pyrite and apatite. In the following, the authigenic mineral assemblage of each of the studied formations will be linked to depositional environment, focusing on early diagenetic processes.

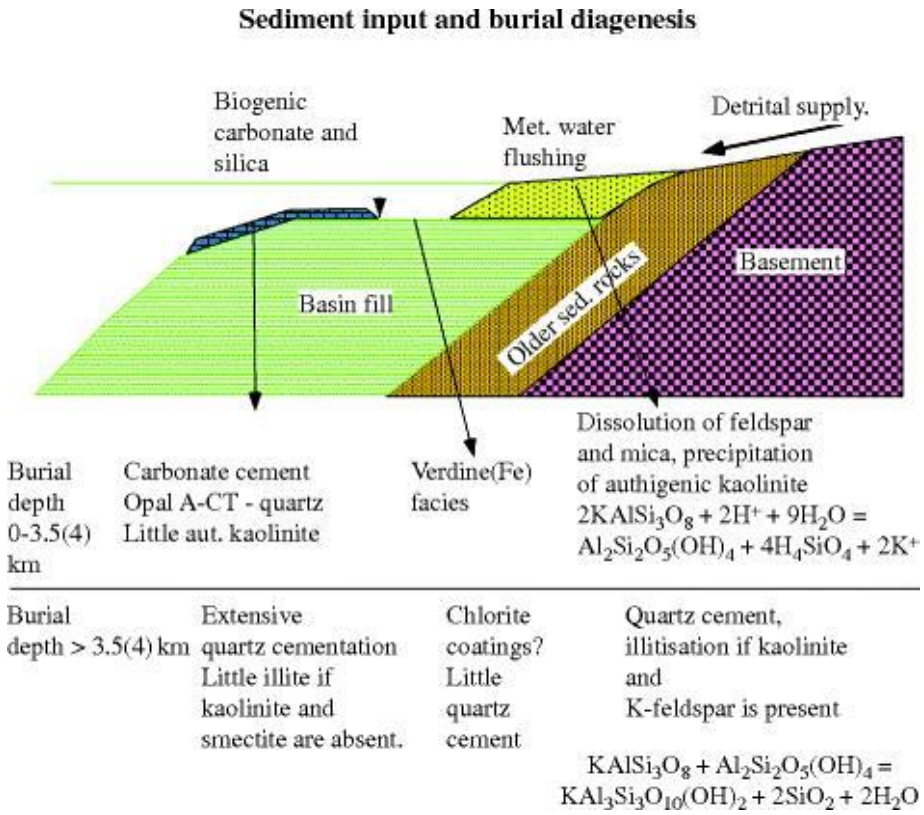

Figure 6.1: Common early- and burial diagenetic processes in sandstones. Early diagenetic processes, including dissolution of unstable minerals (feldspar and mica) and precipitation of authigenic kaolinite, start to alter the detrital composition of sediments immediately after deposition. The presence of early diagenetic products is of great importance to burial diagenesis, in which they affect a variety of diagenetic processes. From Bjørlykke and Jahren (2015).

6.3.1 Firkanten Formation

The eogenetic minerals identified in the Firkanten Formation sandstones (e.g. carbonate cement, framboidal pyrite, glauconite and phosphate minerals) indicate a marine depositional setting for the succession. *Carbonate cement* (i.e. calcite, dolomite and siderite) are commonly

related to dissolution and reprecipitation of biogenic carbonate, typically in alkaline waters (Bjørlykke and Jahren, 2015). Carbonate forms in both eogenetic and mesogenetic regimes, in which the formation of burial diagenetic carbonate results from recrystallisation of eogenetic calcite and dolomite in a ferroan form (Worden and Burley, 2003). Carbonate cement, predominantly non-ferroan calcite, was found to be most prominent in the lowermost samples (except for in sample F1 and F2), although sporadically occurring throughout the formation. Early diagenetic calcite cement is not evenly distributed within sandstones; it is rather concentrated in pore-systems capable of being completely filled (Bjørkum and Walderhaug, 1990). High intergranular volumes (i.e. porosity prior to chemical compaction) in the carbonate cemented sandstones suggest that carbonate cementation occurred prior to mechanical compaction (Worden and Burley, 2003).

Furthermore, the thin section analysis suggested presence of *siderite* in sample F25 (uppermost part of the Firkanten Formation). Eogenetic siderite commonly forms in iron-rich, partially reduced systems of minimal marine influence (Worden and Burley, 2003). The apparent lack of pyrite in sample F25 supports presence of siderite, in which available Fe was, possibly, incorporated into siderite. The latter indicate deposition in terrestrial/coastal environments rather than shallow marine environments for the uppermost part of the Firkanten Formation. The latter assertion is consistent with the sedimentological analysis, suggesting presence of possible mottling, a coalified piece of wood and ripple-cross lamination (see section 5.1.2). The relatively abrupt increase in Si-content and accompanying decrease in the Al-, Rb- and K-concentrations (Fig. 5.13) can thus possibly be ascribed to changing depositional conditions.

Pyrite occurs in all of the analysed samples (except for in sample F25), either as clusters of framboidal pyrite or scattered euhedral pyrite grains. Pyrite forms in both eogenetic and mesogenetic regimes, in which burial diagenetic pyrite is coarser than early diagenetic (often framboidal) pyrite (Worden and Burley, 2003). Pyrite formation, typical for anoxic environments, is related to the reaction of detrital iron minerals with H_2S (sulphide). The H_2S, in turn, originates from the bacterial reduction of dissolved sulphate, in which the bacteria use organic matter present in the sediment as a reducing agent (Berner, 1984).

Despite the large number of studies, an exclusive model for framboidal pyrite formation is still not established. Several previous studies (e.g. Wilkin and Barnes, 1997) relate pyrite framboid formation to the replacement of early diagenetic greigite framboids. Butler and Rickard (2000),

however, suggests that pyrite formation is rather controlled by the redox potential (Eh) of the initial reaction system. Depending on the redox potential, three different pyrite morphologies are generated: (1) euhedral pyrite, (2) protoframboidal clusters and (3) framboidal pyrite (Butler and Rickard, 2000). Furthermore, the amount of pyrite formation is a function of the rates of organic matter supply, dissolved sulphate and reactive detrital iron minerals, in which organic matter is thought to be the major factor controlling pyrite formation in normal (non-euxinic) terrigenous marine sediments (Berner, 1984). The latter assertion is in agreement with the present study, in which pyrite is more abundant in the muddy sandstones of the Todalen Member than the Endalen Member. Extensive framboidal pyrite cementation was observed in sample F3 (muddy laminated sandstone; Fig. 5.18e).

Early diagenetic *glauconite,* predominantly occurring in the lowermost sandstones of the Firkanten Formation (Todalen Member.), is indicative for suboxic marine environments. The occurrence of glauconite is often related to transgressive conditions, in which low sedimentations rates provide favourable conditions for glauconite formation (Odin and Matter, 1981; Cattaneo and Steel, 2003). Glauconite typically forms in granular siliciclastic substrates, either replacing unstable grains, filling pore spaces or coating individual grains (Udgata, 2007). The most common type of precursor substrate is fecal pellets, although glauconite has been found to replace a variety of other grain types, including micas, quartz, chert, feldspar, calcite and volcanic rock fragments (McRae, 1972; Odin and Matter, 1981). Furthermore, glauconite formation is favourable at water depths greater than 50 m (50-300 m), typically in shelf-slope settings (Odin and Matter, 1981). Chafetz and Reid, 2000, however, describe glauconite formation in considerably shallower water depths (between 10 m and tidal-flat depths) and high-energy conditions.

The presence of glauconite is not always indicative for transgressions; a nonselective distribution of glauconite of the same maturity rather than a vertical grading or concentration in laminae of varying maturity is required. Furthermore, transgressive deposits typically show an upward increase in autochthonous (i.e. in situ) and more mature glauconite (Cattaneo and Steel, 2003). The glauconite grains observed in the lowermost sandstones of the Firkanten Formation (tidal channels) seem to be randomly distributed, possibly indicating transgressive conditions. The accompanying high pyrite-content in the lowermost sandstone-samples and squeezing of glauconite grains, in which the latter indicates that the grains were still soft during compaction (Lüthje, 2008), supports the latter interpretation (Worden and Burley, 2003).

Although Chafetz and Reid (2000) describes glauconite formation in tide-influenced environments, they may have been reworked from a contemporaneous marine environment and incorporated into the tidal channel deposits (Lüthje, 2008).

6.3.2 Upper part of Grumantbyen Formation

The authigenic mineral assemblage (carbonate cement, glauconite and grain coating chlorite) of the Grumantbyen Formation sandstones is indicative for marine depositional environments. The *Carbonate cement* identified in the analysed samples predominantly composes non-ferroan calcite, suggesting an early diagenetic origin. Calcite cement was found to be more abundant in the sandstone samples from core 11-2003 than core 7-2006. *Glauconite* was observed scattered throughout the Grumantbyen Formation in both of the cores. Glauconite formation, however, have previously been discussed in section 6.3.1.

Authigenic chlorite was found to occur in all of the analysed samples, either as porefilling cement or grain-coatings. Chlorite forms in both eogenetic and mesogenetic regimes, often in reduced marine waters (Worden and Burley, 2003). Grain coating chlorite was observed in sample G1, G2 and G3 (core 7-2006), constituting upper shoreface deposits. Chlorite coatings are thought to retard or prevent later quartz cementation, sometimes resulting in abnormally high porosity values in deeply buried sandstones. Formation of grain coating chlorite require (1) a Fe-rich clay mineral precursor (e.g. odinite or berthierine) and (2) a threshold temperature (90-120^{o}C) (Aagaard et al., 2000; Gould et al., 2010). The formation of berthierine, in turn, requires presence of labile Fe, for instance from tropical weathering (Ehrenberga et al., 1998) or volcanic supply (Grigsby, 2001). The experiments of Aagaard et al. (2000) suggests that the alteration of berthierine to chlorite occurs at about 90 ^{o}C, i.e. subsequent to the formation of quartz overgrowth. The latter implies that early diagenetic berthierine-coatings, rather than burial diagenetic grain-coating chlorite, are responsible for preventing quartz cementation (Gould et al., 2010).

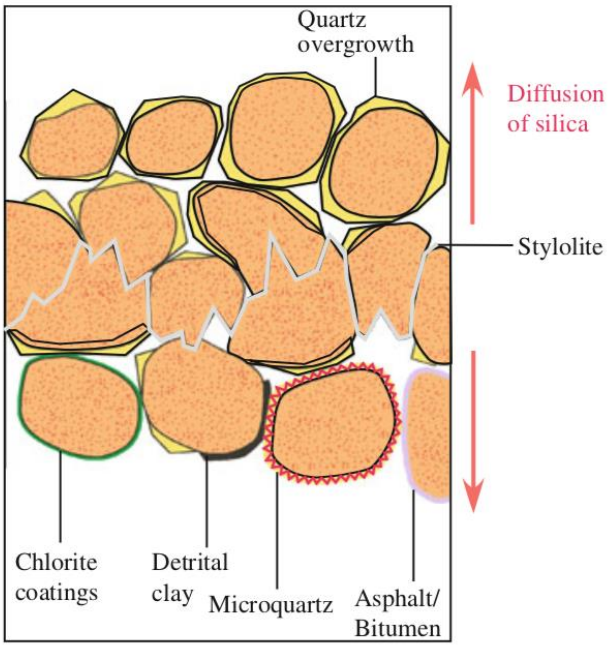

Figure 6.2: Schematic illustration of grain-coating chlorite. Early diagenetic berthierine-coating, rather than burial diagenetic chlorite-coating, is responsible for preventing precipitation of quartz cement. The berthierine-coating is replaced by chlorite at temperatures of 90-120°C, corresponding to intermediate burial depths. From Bjørlykke and Jahren (2015).

Two different types of grain coating chlorite were observed in the Grumantbyen Formation: (1) continuous (i.e. high-quality) grain coating chlorite and (2) discontinuous (i.e. low-quality) grain coating chlorite. Grains showing continuous chlorite-coating seemed to lack quartz overgrowth, whereas grains showing discontinuous chlorite-coating were found to be, at least in part, quartz cemented. High-quality chlorite coatings were observed in the massive pebbly sandstone (sample G1) in core 7-2006 (Fig. 5.20a and Fig. 5.21a,b), whereas low-quality chlorite coatings were observed in the bioturbated medium-grained sandstones (sample G2, G3 and G6) in cores 7-2006 and 11-2003 (Fig. 5.20b,c,h). The latter observations are in agreement with previous studies concerning formation of grain-coating chlorite (e.g. Gould et al., 2010), suggesting that high-quality chlorite rims are restricted to "clean" sandstones, showing few or no clay-rich laminae, mud drapes or muddy bioturbation. The high porosity and permeability of "clean" sandstones, in which permeability is enhanced by coarse grain-sizes, provide conditions favourable for precipitation of early diagenetic berthierine rims.

6.3.3 Aspelintoppen Formation

The early diagenetic minerals (i.e. kaolinite, calcite cement, pyrite, chlorite and apatite) identified in the muddy sandstones of the Aspelintoppen Formation indicate a mixed terrestrial-

marine depositional environment for the formation. *Carbonate cement,* composing both early diagenetic calcite and later burial Fe-dolomite, was found to occur in all of the analysed samples, suggesting marine/brackish influence. *Kaolinite* formation will be discussed in the following; the resisting authigenic minerals have previously been discussed in section 6.3.1 and 6.3.2.

Early diagenetic kaolinite, typically forming in warm, wet, low pH environments, is an alteration product of unstable detrital minerals, often feldspars and micas (Worden and Burley, 2003). The replacement of feldspars and micas by kaolinite is commonly related to meteoric-water flushing (Mansurbeg et al., 2012). SEM- and XRD analyses revealed presence of kaolinite in sample A1, A6 and A7. The relatively low feldspar content of the Aspelintoppen Formation sandstones, however, indicate that kaolinite is probably present throughout the formation. Recent petrographic studies of cores 11-2003 and 7-2006 (Schlegel et al., 2013) suggested that authigenic kaolinite is restricted to the Paleocene-Eocene sandstones of the Battfjellet and Aspelintoppen formations, i.e. absent in the older Paleocene sandstones of the Firkanten, Basilika and Grumantbyen formations. XRD-analysis performed in the present study, nevertheless, suggested presence of minor kaolinite in both the Firkanten and Grumantbyen formations. The lower kaolinite-content of the Firkanten and Grumantbyen formations may be ascribed to alteration of kaolinite at deep burial depths and/or changing climatic conditions.

6.3.4 Compaction

Compaction – reduction of volume and resultant pore-water expulsion within sediments – occurs in response to grain rearrangement, plastic deformation of ductile grains, dissolution and brittle fracturing, and is a crucial factor controlling the porosity of sandstones at greater burial depths (Worden and Burley, 2003). The degree of compaction is controlled by burial depth, fluid pressure and the ratio of brittle to ductile grains, in which the latter factor is strongly influenced by depositional environment. The sandstones of the Firkanten, upper part of Grumantbyen and Aspelintoppen formations were found to be strongly influenced by compaction and cementation, in which compaction is evidenced by dense grain packing, bending/breakage of mica and squeezing of ductile grains. Furthermore, both long, concavo-convex and sutured grain contacts were observed in the analysed sandstone-samples, in which the two formers are the most prominent types. Sutured contacts indicate diagenesis and deep

burial, whereas long and concavo-convex contacts indicate intermediate depths, suggesting that the sandstones have experienced substantial compaction (Heidari et al., 2013). Non-contacts (i.e. grain-cement and grain-matrix boundaries) are rare, although observed in some of the carbonate-cemented samples of the Firkanten and Aspelintoppen formations (e.g. sample F25 and A8; Fig. 5.18h and 5.22i).

The high degree of compaction resulted in low porosity values, ranging from absent to approximately 15%, in which the highest porosity values were estimated in the Grumantbyen Formation (Appendix III). The extremely low porosity values of the Aspelintoppen Formation are probably related to the abundance of mud and ductile grains, in which ductile grains are compacted more than rigid grains. Additional loss of porosity, notably in the muddy, mica-rich sandstone samples, may be ascribed to styolitisation, resulting in loss of volume. Furthermore, formation of quartz overgrowth and, in some samples, precipitation of early diagenetic carbonate cement, probably played an important role in destroying porosity. The generally low porosity values of the Firkanten and Grumantbyen formations are ascribed to abundant quartz cement and, in some samples, carbonate cement, enhanced by the relatively high amounts of ductile grains, notably in the Firkanten Formation. Quartz cement (i.e. quartz overgrowth) was found to fill most of the pore spaces in the quartz-rich samples (e.g. Fig. 5.18a and 5.20b,f). Although the present study suggests extensive quartz cementation, notably in the sandstones of the Firkanten and Grumantbyen formations, optical microscopy indicated that not all of the pore spaces have been filled (Appendix III, Fig. III.1a).

The thin section analyses, however, revealed slightly higher porosity values for the Grumantbyen Formation than for the Firkanten and Aspelintoppen formations. The latter observation is probably related to the presence of grain-coating chlorite in the sandstone samples of the Grumantbyen Formation (see section 6.3.2). Compaction was probably more important in destroying porosity than cementation, although precipitation of cement, including quartz- and carbonate cement, were important contributors. Previous studies of the Eocene Central Basin (e.g. Mansurbeg et al., 2012) suggests that compaction was far more important in porosity destruction than cementation, supporting the latter interpretation.

6.4 Use of authigenic minerals as a paleothermometer

Diagenetic processes in sedimentary rocks are strongly linked to a specific burial depth and temperature, suggesting that authigenic minerals usually indicates a specific burial depth and minimum-temperature or temperature interval (Worden and Burley, 2003; Bjørlykke and Jahren, 2015). Authigenic minerals can thus be used to cross-check temperatures derived from organic maturity indicators (e.g. vitrinite reflectance); are they telling the same temperature history? A variety of diagenetic signatures are routinely used in reconstructions of the thermal history of sedimentary basins, including (1) illite/smectite diagenesis, (2) formation of grain-coating chlorite, (3) formation of quartz cements, (4) albitization of feldspars (plagioclase and K-feldspar) and (5) ankerite cement formation, in which the three former are most frequently used (Haile et al., 2018b).

6.4.1 Burial diagenetic signatures

The authigenic mineral assemblage, high degree of mechanical compaction and low porosity of the Firkanten, Grumantbyen and Aspelintoppen formations suggests deep burial of the succession. Burial diagenesis is largely influenced by the amount of fluid flow through the remaining porosity and the presence of early diagenetic products, in which the latter affect, for instance, clay mineral transformations and precipitation of quartz cement (Morad et al., 2010). Quartz cement (i.e. quartz overgrowth) is the most prominent burial diagenetic mineral in the studied formations, although smaller amounts of albite, grain coating chlorite, Fe-dolomite and illite/muscovite were found to occur (Table 6.1).

Table 6.1: Burial diagenetic signatures of the Firkanten, Grumantbyen and Aspelintoppen formations.

Formation	Burial diagenetic signature
Aspelintoppen	Quartz overgrowth
	Fe-dolomite
Grumantbyen	Quartz overgrowth
	Albite
	Grain coating chlorite
	Illite/muscovite
Firkanten	Quartz overgrowth
	Albite
	Ankerite
	Illite/muscovite

The replacement of k-feldspar or plagioclase by *diagenetic albite* and the growth of *grain-coating chlorite* occur at depths greater than 3 km, corresponding to temperatures of about 90-100^{o}C (Bjørlykke and Jahren, 2015). Clay mineral reactions remove potassium from the solution, resulting in a relative increase in the Na+ concentration. Albite is thus more stable than k-feldspar and plagioclase, favoring dissolution of k-feldspar and/or plagioclase and precipitation of albite. Grain-coating chlorite is suggested to originate from Fe-rich clays, primarily berthierine (see section 6.3.2).

Quartz cementation (i.e. quartz overgrowths) and formation of *illite* at the expense of kaolinite occur at depths greater than 2-2,5 km, corresponding to temperatures of about 70-80^{o}C. Pervasive illite formation, however, occurs at temperatures greater than 130^{o}C (3-3,5 km to 4-4,5 km; Worden and Burley, 2003). Quartz cement is thought to originate from a variety of silica sources, including biogenic silica, mineral transformations (e.g. smectite to illite reactions) and pressure solution of detrital quartz grains at microstyolites (Xi et al., 2015). The rate of quartz cementation is largely influenced by temperature; the higher the temperature, the higher the rate of precipitation. Bjørlykke and Jahren (2015) estimated that the rate of quartz cementation increases by a factor of 1,7 for every 10 ^{o}C temperature increase (Walderhaug, 1996). Quartz cementation does not cease until roughly all the porosity is lost, or the temperature drops below 70-80^{o}C (Bjørlykke and Jahren, 2015). Sandstones buried to depths greater than about 3-3,5 km to 4-4,5 km, corresponding to temperatures of about 120 to 160 ^{o}C, thus often show strong reduction in porosity and permeability.

SEM- and XRD-analysis indicated presence of illite in the sandstones of the Firkanten and Grumantbyen formations, although a clear identification of this mineral was not possible. The formation of illite at the expense of kaolinite (i.e. illitisation) requires a source of potassium, commonly K-feldspar (Bjørlykke and Jahren, 2015). In potassium-depleted systems, kaolinite remains stable at greater burial depths, preventing formation of illite. Illite in low-potassium sandstones are thought to rather originate from smectite to illite reactions (Bjørlykke and Jahren, 2015). Illitisation of smectite occurs at temperatures greater than 70-90^{o}C (Worden and Burley, 2003). However, optical microscopy suggested presence of K-feldspar in all of the analysed samples, in which it is more abundant in the sandstones of the Firkanten and Grumantbyen formations than the overlying Aspelintoppen Formation. Authigenic kaolinite, replacing unstable feldspars and micas at shallow burial depths, predominantly occurs in the Aspelintoppen Formation, although SEM- and XRD-analysis indicated presence of minor

kaolinite in the Firkanten and Grumantbyen formations. The latter observations are consistent with the geochemical signatures of the formations, in which the sandstone samples of the Firkanten and Grumantbyen formations (higher feldspar contents) show higher element ratio of K/Rb and lower Rb/Sr ratio than the Aspelintoppen Formation (lower feldspar contents). Furthermore, the lower K/Rb and higher Rb/Sr element ratios of the Aspelintoppen Formation suggest that (1) the initial detrital feldspar-content of the Aspelintoppen Formation was lower or (2) feldspars have been replaced by other diagenetic minerals (e.g. kaolinite). The abundance of kaolinite in the Aspelintoppen Formation supports the latter assertion. Although thin section analyses showed that plagioclase is slightly more abundant than K-feldspar, a source of potassium, allowing illitisation of kaolinite at greater burial depths, cannot be excluded.

Carbonate cements grow over a wide range of diagenetic conditions. Burial diagenetic carbonate, originating from recrystallisation of early diagenetic carbonate minerals, composes coarser grained, locally pore-filling crystals, often of *ferroan dolomite*. Fe-dolomite grows at similar or somewhat higher temperatures than illite and quartz cement (about 100^{o}C). The Fe-dolomite cement identified in the Aspelintoppen Formation resembles the latter description, indicating a rather burial diagenetic origin of this mineral (Fig. 5.22g).

Although *ankerite* is a common burial diagenetic mineral in sandstones, it appears in relatively small amounts (Hendry, 1978) . Ankerite formation is thought to occur at temperatures around 100-110^{o}C (e.g. Morad et al. cited in Haile et al. 2018b). In subsurface Eocene Wilcox sandstones, however, ankerite was found to occur at depths from 2560 m (125^{o}C) to at least 4650 m (210^{o}C) (Boles, 1978). Radiogenic $^{87}Sr/^{86}Sr$ values suggest that ankerite formation occurs subsequent to a certain amount of silicate diagenesis. Furthermore, its formation has previously been related to mobilization of Mg^{2+} and Fe^{2+} following illitisation of smectite and thermal reduction of ferric oxides (Hendry, 1978).

6.4.2 Vitrinite reflectance studies of coals

Dörr et al. (2018) recently presented a reconstruction of the thermal and erosional history of the Central Tertiary Basin, utilising core 11-2003 and 7-2006. The study, providing vitrinite reflectance measurements of coals/organic material, allow comparison of the authigenic minerals of the Firkanten, Grumantbyen and Aspelintoppen formations with vitrinite reflectance measurements. The petrographic, chemical and physical properties of macerals (i.e.

coal) are highly temperature and pressure-dependent; increasing temperature and pressure results in removal of liquid and gaseous components and accompanying increasing carbon-content. The transformation is an irreversible maturation process, which is a function of temperature, time and chemical composition (e.g. Ritter, 1984; Burnham and Sweeney, 1989). Vitrinite reflectance (VR) is a measure of the maturation of organic material; the higher the maturation, the higher the reflectance. VR can thus be used to assess the rank of coalification, which, in turn, can be transformed into maximum paleotemperatures. Furthermore, maximum paleotemperatures can be used to estimate maximum burial depths and paleo-thermal gradients (Dörr et al., 2018).

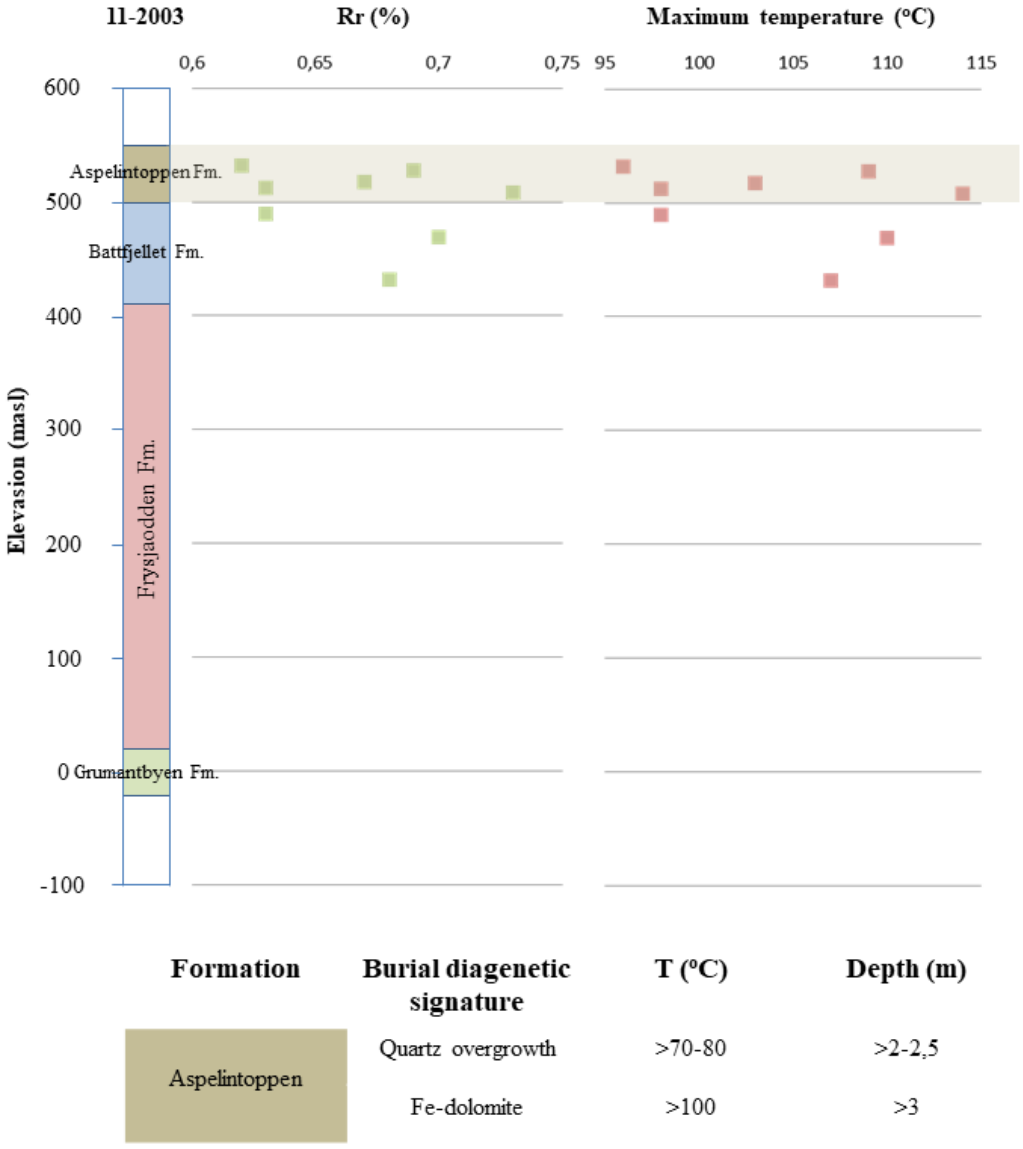

Figure 6.3: Comparison of Rr (mean random vitrinite reflectance values) and inorganic burial diagenetic signatures of the Aspelintoppen Formation (core 11-2003). Vitrinite reflectance measurements (Rr) and maximum temperatures are obtained from Dörr et al. (2018).

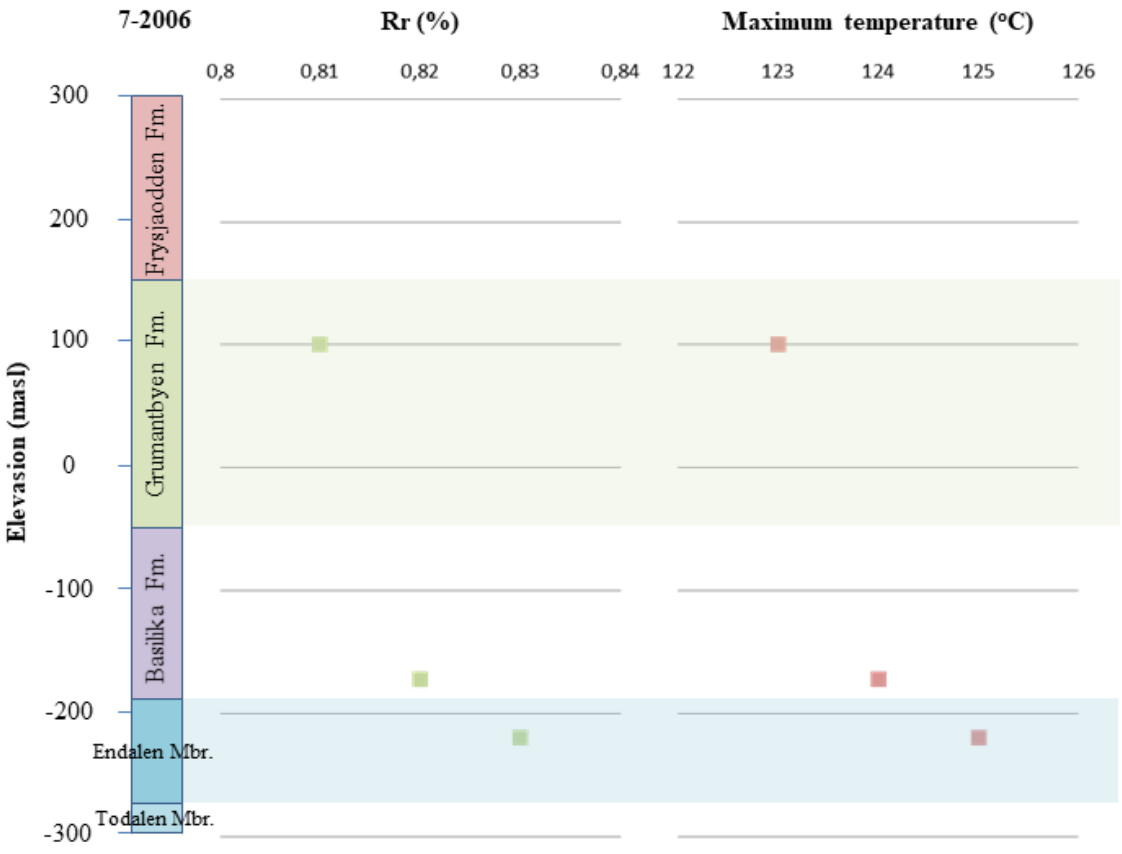

Formation	Burial diagenetic signature	T (°C)	Depth (km)
Grumantbyen	Quartz overgrowth	>70-80	>2-2,5
	Grain-coating chlorite	>90	>3
	Illite/muscovite	>120-130	>3,5
Firkanten (Endalen Mbr.)	Quartz overgrowth	>70-80	>2-2,5
	Ankerite	>100-110	>3
	Illite/muscovite	>120-130	>3,5

Figure 6.4: Comparison of Rr (mean random vitrinite reflectance values) and inorganic burial diagenetic signatures of the Firkanten (Endalen Member) and Grumantbyen formations (7-2006). Vitrinite reflectance measurements (Rr) and maximum temperatures are obtained from Dörr et al. (2018).

In core 11-2003, Rr values range from 0,62-0,73% in the Aspelintoppen and Battfjellet Formations. Core 7-2006 shows slightly higher Rr values than core 11-2003, increasing from 0,81% in the Grumantbyen Formation to 0,83% in the underlying Firkanten Formation (Endalen Member). The slightly higher Rr values reflect the deeper burial of the Firkanten and Grumantbyen formations. In addition, Dörr et al. (2018) performed vitrinite reflectance measurements in core 9-2007, located about l13 km northeast of cores 11-2003 and 7-2006.

The highest VR value (Rr = 0,76%) in core 9-2007 was measured in the Todalen Member (Firkanten Formation). This value, however, is not consistent with Rr values measured in the Endalen Member (0,40% and 0,35%), situated just c. 100 m above the Todalen sample. Marshall et al. (2015), however, relates (unlikely) low Rr values for Tertiary Svalbard coals to high bitumen content, causing suppression of vitrinite reflectance. However, Dörr et al. (2018) suggests maximum temperatures of c. 90-110^{o}C for the Eocene coals and c. 120-130^{o}C for the Paleocene coals.

6.4.3 Are VR measurements consistent with authigenic signatures?

Dörr et al. (2018) suggests maximum temperatures of 120-130^{o}C for the CTB, corresponding to burial depths of 4-4,5 (Fig. 6.5a). This is in agreement with the presence of grain-coating chlorite, ankerite and illite, indicating intermediate-deep burial depths. The existence of ankerite in the Firkanten Formation and grain-coating chlorite in the Grumantbyen Formation, show that the CTB have been subjected to temperatures of at least 100-110^{o}C (Fig. 6.4). Although a clear identification of illite was not possible, formation of illite at the expense of kaolinite, occurring at temperatures higher than 120-130^{o}C, cannot be excluded. Extensive quartz cementation in the sandstones of the Firkanten and Grumantbyen formations, nevertheless, may support maximum temperatures of 120-130^{o}C, in which the rate of quartz cementation increases with increasing temperatures (Bjørlykke and Jahren, 2015). Furthermore, the burial diagenetic mineral assemblage of the Grumantbyen Formation sandstones in (1) core 11-2003 and (2) core 7-2006 indicate a rather similar temperature/burial history for the individual intervals. In the absence of high-resolution SEM BSE images and fluid inclusions, nevertheless, any differences cannot be entirely excluded. The presence of Fe-dolomite in the overlying Aspelintoppen Formation indicate temperatures of at least 100^{o}C. This is in agreement with vitrinite reflectance measurements, suggesting maximum temperatures of 90-110^{o}C for the Eocene coals (Fig. 6.3).

The estimated low porosity values of the Firkanten, Grumantbyen and Aspelintoppen formations, nevertheless, may indicate deeper burial of the succession. The “Walderhaug model” (Bjørkum et al.,1998) shows porosity values of 15-20% for Miocene sandstones buried to 4 km depth, assuming a temperature gradient of 35^{o}C (i.e. considerably higher than the estimated porosity values in the present study). However, the abundance of clayey material and ductile grains in the analysed samples (notably in the Aspelintoppen Formation sandstones)

suggest high degree of mechanical compaction, in which ductile grains are more compressible than rigid grains (Bjørlykke and Jahren, 2015). The low porosity values are thus though to result from strong mechanical compaction rather than deeper burial of the studied formations. Due to the high content of clay material and ductile grains in the analysed samples and low porosity values, a "Walderhaug modelling" of the Firkanten, Grumantbyen and Aspelintoppen formations was not expedient (H. Hellevang 2019, pers. comm., 20. Aug.).

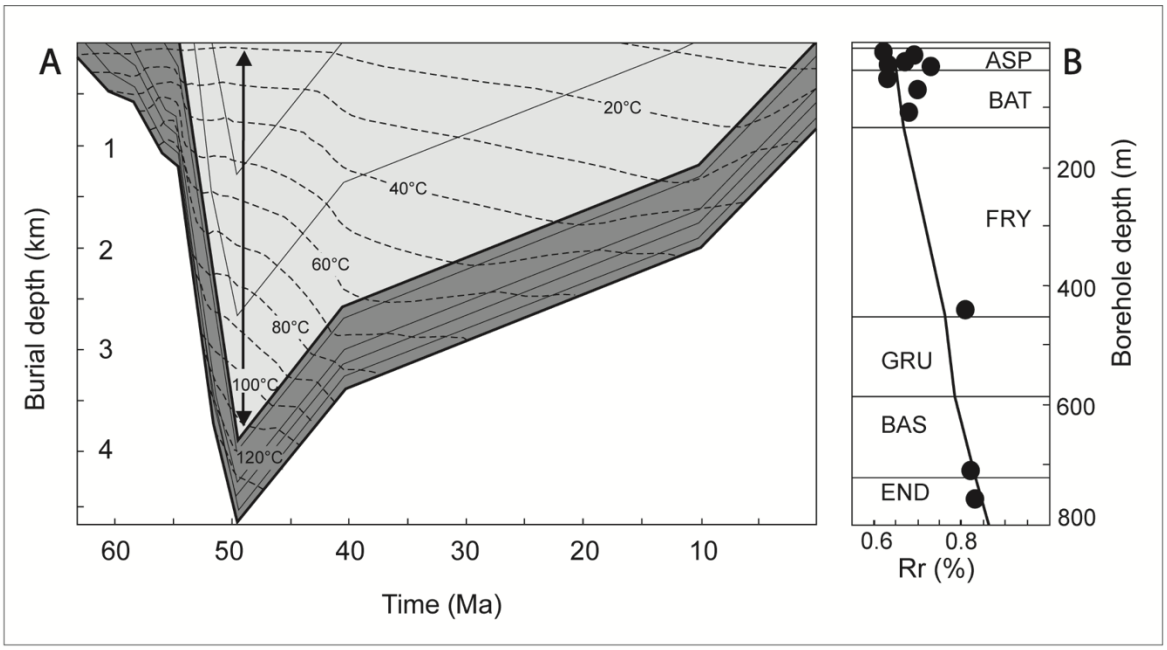

Figure 6.5: (A) Burial- and temperature history of the CTB. The dark-grey area represents the preserved sediment infill of the CTB, whereas the light-grey area represents the removed overburden. (B) Vitrinite reflectance measurements from cores 11-2003 and 7-2006. Slightly modified from Dörr et al. (2019).

7 Conclusions and further work

7.1 Conclusions

The main objective of this thesis was to investigate the importance of depositional environment to diagenesis in sandstones of the Firkanten, Grumantbyen and Aspelintoppen formations. The sedimentological and petrographic observation, and geochemical data from these sandstones allow the following conclusions:

- The Firkanten Formation constitute coastal plain (Todalen Mbr.) to shallow marine (Endalen Mbr.) deposits (1), the Grumantbyen Formation shallow marine deposits (2) and the Aspelintoppen Formation tide-influenced deltaic deposits (3)
- Geochemical trends in the sediment cores can, at least in part, be correlated to changes in lithology and sand/mud ratios in the sedimentary logs. The repetitive sub-trends observed in the Endalen Member. (upper Firkanten Formation) tend to coincide with intervals of shallowing upwards (i.e. parasequences)
- Use of geochemical signatures is preferable for sedimentary rocks showing gradual and continuous changes in lithology and sand/mud ratios, rather than abrupt changes
- The abundance of calcite cement in the Aspelintoppen Formation sandstones strongly support marine influence, as suggested by sedimentological analysis
- The presence of glauconite and abundant framboidal pyrite in the lowermost part of the Firkanten Formation (Todalen Mbr.) may indicate transgressive conditions
- The sandstones of the Firkanten, upper part of Grumantbyen and Aspelintoppen formations is strongly influenced by compaction and cementation, in which compaction is evidenced by dense grain packing, bending/breakage of mica and squeezing of ductile grains.
- The high degree of compaction resulted in low porosity values, ranging from absent to approximately 10-15%. The significant low porosity values of the Aspelintoppen Formation sandstones are ascribed to the abundance of clayey material and ductile grains. The generally low porosity values of the Firkanten and Grumantbyen formations resulted from extensive quartz cementation and, in some samples, carbonate cement, enhanced by the presence of ductile grains

- The considerably higher porosity values of the Grumantbyen Formation sandstones may be ascribed to the presence of grain-coating chlorite, preventing further quartz cementation at great burial depths. Variations in coating-quality is related to sandstone-type, in which high-quality chlorite rims are restricted to "clean" sandstones, showing few or no clay-rich laminae, mud drapes or muddy bioturbation.
- The burial diagenetic signatures of the analysed sandstones are in agreement with vitrinite reflectance measurements, suggesting temperatures of at least 100-110^{o}C for the Firkanten and Grumantbyen formations and temperatures of around 100^{o}C for the overlying Aspelintoppen Formation. However, extensive quartz cementation in the sandstones of the Firkanten and Grumantbyen formations may support maximum temperatures of 120-130^{o}C, as suggested by vitrinite reflectance measurements.

7.2 Suggestions for further work

Based on the results obtained from the present study, these are my recommendations for further work:

- Study the Firkanten, Grumantbyen and Aspelintoppen formations in the field. In the present study, sedimentological analysis was restricted to logging (and XRF-analysis) of core 7-2006 and 11-2003. Fieldwork would possibly provide a more detailed understanding of depositional environment/facies associations and, thus, a better understanding of the types and distribution of authigenic minerals. Furthermore, it would have been interesting to further investigate the upper part of the Endalen Member (Firkanten Formation) – are there evidence of fluvial incision or other terrestrial indicators in the field?
- Perform fluid inclusion analysis of authigenic minerals (e.g. quartz cement) in order to better constrain the thermal history of the CTB. In addition, higher-resolution SEM BSE images of the sandstone-samples could possibly confirm presence of illite

References

Aagaard, P., Jahren, J. S., Harstad, A. O., Nilsen, O. & Ramm, M. 2000. Formation of grain-coating chlorite in sandstones. Laboratory synthesized vs. natural occurrences. *Clay Minerals,* 35, p. 261-269.

Al-Ramadan, K., Morad, S. & Plink-Bjørklund, P. 2012. Distribution of Diagenetic Alterations in Relationship to Depositional Facies and Sequence Stratigraphy of a Wave-and Tide-Dominated Siliciclastic Shoreline Complex: Upper Cretaceous Chimney Rock Sandstones, Wyoming and Utah, USA. *In:* Morad, S., Ketzer, J. M. & De Ros, L. F. (eds.) *Linking Diagenesis to Sequence Stratigraphy*. International Association of Sedimentologists Special Publication, p. 271-296.

Berner, R. A. 1984. Sedimentary pyrite formation: an update. *Geochimica et cosmochimica Acta,* 48, p. 605-615.

Bjørkum, P. A., Oelkers, E. H., Nadeau, P. H., Walderhaug, O. & Murphy, W. M. 1998. Porosity prediction in quartzose sandstones as a function of time, temperature, depth, stylolite frequency, and hydrocarbon saturation. *AAPG Bulletin,* 82, p. 637-648.

Bjørkum, P. A. & Walderhaug, O. 1990. Geometrical arrangement of calcite cementation within shallow marine sandstones. *Earth-Science Reviews,* 29, p. 145-161.

Bjørlykke, K. 2001. *Sedimentologi og petroleumsgeologi 2nd ed.* Oslo, Gyldendal yrkesopplæring.

Bjørlykke, K. & Jahren, J. 2015. Sandstones and sandstone reservoirs. *In:* Bjørlykke, K. (ed.) *Petroleum Geoscience: From Sedimentary Environments to Rock Physics*. Heidelberg: Springer, p. 113-140.

Blythe, A. E. & Kleinspehn, K. L. 1998. Tectonically versus climatically driven Cenozoic exhumation of the Eurasian plate margin, Svalbard: Fission track analyses. *Tectonics,* 17, p. 621-639.

Bohacs, K. & Suter, J. 1997. Sequence stratigraphic distribution of coaly rocks: fundamental controls and paralic examples. *AAPG Bulletin,* 81, p. 1612-1639.

Boles, J. R. 1978. Active ankerite cementation in the subsurface Eocene of southwest Texas. *Contributions to Mineralogy and Petrology,* 68, p. 13-22.

Bruhn, R. & Steel, R. 2003. High-resolution sequence stratigraphy of a clastic foredeep succession (Paleocene, Spitsbergen): An example of peripheral-bulge-controlled depositional architecture. *Journal of Sedimentary Research,* 73, p. 745-755.

Burnham, A. K. & Sweeney, J. J. 1989. A chemical kinetic model of vitrinite maturation and reflectance. *Geochimica et Cosmochimica Acta,* 53, p. 2649-2657.

Butler, I. B. & Rickard, D. 2000. Framboidal pyrite formation via the oxidation of iron (II) monosulfide by hydrogen sulphide. *Geochimica et Cosmochimica Acta,* 64, p. 2665-2672.

Cattaneo, A. & Steel, R. J. 2003. Transgressive deposits: a review of their variability. *Earth-Science Reviews,* 62, p. 187-228.

Chafetz, H. S. & Reid, A. 2000. Syndepositional shallow-water precipitation of glauconitic minerals. *Sedimentary Geology,* 136, p. 29-42.

Chuhan, F. A., Kjeldstad, A., Bjørlykke, K. & Høeg, K. 2002. Porosity loss in sand by grain crushing—Experimental evidence and relevance to reservoir quality. *Marine and Petroleum Geology,* 19, p. 39-53.

Chuhan, F. A., Kjeldstad, A., Bjørlykke, K. & Høeg, K. 2003. Experimental compression of loose sands: Relevance to porosity reduction during burial in sedimentary basins. *Canadian Geotechnical Journal,* 40, p. 995-1011.

Clifton, H. E. & Thompson, J. K. 1978. Macaronichnus segregatis; a feeding structure of shallow marine polychaetes. *Journal of Sedimentary Research,* 48, p. 1293-1302.

Collinson, J. D. 1969. The sedimentology of the Grindslow Shales and the Kinderscout Grit: a deltaic complex in the Namurian of northern England. *Journal of Sedimentary Research,* 39, p. 194-221.

Crabaugh, J. P. & Steel, R. J. 2004. Basin-floor fans of the Central Tertiary Basin, Spitsbergen: relationship of basin-floor sand-bodies to prograding clinoforms in a structurally active basin. *Geological Society London Special Publication,* 222, p. 187-208.

Dalland, A. 1976. Erratic clasts in the Lower Tertiary deposits of Svalbard - evidence of transport by winter ice. *Norsk Polarinstitutt,* Årbok 1976, p. 151-165.

Dallmann, W. K. 1999. *Lithostratigraphic lexicon of Svalbard: review and recommendations for nomenclature use: Upper Palaeozoic to Quaternary bedrock.* Tromsø, Norwegian Polar Institute, 318 p.

Dörr, N., Lisker, F., Jochmann, M., Rainer, T., Schlegel, A., Schubert, K. & Spiegel, C. 2018. Subsidence, rapid inversion and slow erosion of the Central Tertiary Basin of Svalbard: Evidence from the thermal evolution and basin modeling. *In:* Piepjohn, K., Strauss, J. V., Reinhardt, L. & Mcclelland, W. C. (eds.) *Circum-Arctic Structural Events: Tectonic Evolution of the Arctic Margins and Trans-Arctic Links with Adjacent Orogens*. Geological Society of America Special paper 541, p. 1-20.

Dypvik, H., Riber, L., Burca, F., Rüther, D., Jargvoll, D., Nagy, J. & Jochmann, M. 2011. The Paleocene–Eocene thermal maximum (PETM) in Svalbard—clay mineral and geochemical signals. *Palaeogeography, Palaeoclimatology, Palaeoecology,* 302, p. 156-169.

Ehrenberga, S. N., Dalland, A., Nadeau, P. H., Mearns, E. W. & Amundsen, E. F. 1998. Origin of chlorite enrichment and neodymium isotopic anomalies in Haltenbanken sandstones. *Marine Petroleum Geology,* 15, p. 403-425.

Golovneva, L. B. 2000. Palaeogene climates of Spitsbergen. *GFF,* 122, p. 62-63.

Gould, K., Pe-Piper, G. & Piper, D. J. W. 2010. Relationship of diagenetic chlorite rims to depositional facies in Lower Cretaceous reservoir sandstones of the Scotian Basin. *Sedimentology,* 57, p. 587-610.

Grigsby, J. D. 2001. Origin and growth mechanism of authigenic chlorite in sandstones of the lower Vicksburg Formation, south Texas. *Journal of Sedimentary Research,* 71, p. 27-36.

Grundvåg, S. A., Helland-Hansen, W., Johannessen, E. P., Olsen, A. H. & Stene, S. A. K. 2014. The depositional architecture and facies variability of shelf deltas in the Eocene Battfjellet Formation, Nathorst Land, Spitsbergen. *Sedimentology,* 61, p. 2172-2204.

Haile, B. G., Klausen, T. G., Czarniecka, U., Xi, K., Jahren, J. & Hellevang, H. 2018a. How are diagenesis and reservoir quality linked to depositional facies? A deltaic succession, Edgeøya, Svalbard. *Marine and Petroleum Geology,* 92, p. 519-546.

Haile, B. G., Klausen, T. G., Jahren, J., Braathen, A. & Hellevang, H. 2018b. Thermal history of a Triassic sedimentary sequence verified by a multi-method approach: Edgeøya, Svalbard, Norway. *Basin Research,* 30, p. 1075-1097.

Harland, W. B. 1969. Contribution of Spitsbergen to Understanding of Tectonic Evolution of North Atlantic Region. *In:* Kay, M. (ed.) *North Atlantic: Geology and Continental Drift*. AAPG Memoir 12, p. 817-851.

Heidari, M., Momeni, A. A., Rafiei, B., Khodabakhsh, S. & Torabi-Kaveh, M. 2013. Relationship between petrographic characteristics and the engineering properties of Jurassic sandstones, Hamedan, Iran. *Rock mechanics and rock engineering,* 46, p. 1091-1101.

Helland-Hansen, W. 1990. Sedimentation in Paleogene Foreland Basin, Spitsbergen. *The American Association of Petroleum Geologists Bulletin,* 74, p. 260-272.

Helland-Hansen, W. 2010. Facies and stacking patterns of shelf-deltas within the Palaeogene Battfjellet Formation, Nordenskiöld Land, Svalbard: implications for subsurface reservoir prediction. *Sedimentology,* 57, p. 190-208.

Hendry, J. P. 1978. Ankerite (in sediments). *In:* Fairbridge, R. W. (ed.) *Sedimentology. Encyclopedia of Earth Science*. Heidelberg: Springer.

Inkson, B. J. 2016. Scanning electron microscopy (SEM) and transmission electron microscopy (TEM) for materials characterization. *In:* Hübschen, G., Altpeter, I., Tschuncky, R. & Herrmann, H. G. (eds.) *Materials Characterization Using Nondestructive Evaluation (NDE) Methods*. Sheffield: Woodhead Publishing, p. 17-43.

Knaust, D. 2017. *Atlas of Trace Fossils in Well Core: Appearance, Taxonomy and Interpretation.* Springer.

Lüthje, C. J. 2008. *Transgressive development of coal-bearing coastal plain to shallow marine setting in a flexural compressional basin, Paleocene, Svalbard, Arctic Norway.* Ph.D., University Centre in Svalbard/University of Bergen.

Mansurbeg, H., Morad, S., Plink-Björklund, P., El-Ghali, M., Caja, M. & Marfil, R. 2012. Diagenetic alterations related to falling stage and lowstand systems tracts of shelf, slope and basin floor sandstones (Eocene Central Basin, Spitsbergen). *International Association of Sedimentologists Special Publication,* 45, p. 353-378.

Manum, S. B. & Throndsen, T. 1978. Rank of coal and dispersed organic matter and its geological bearing in the Spitsbergen Tertiary. *Norsk Polarinstitutt,* Årbok 1977, p. 159-177.

Marshall, C., Uguna, J., Large, D. J., Meredith, W., Jochmann, M., Friis, B., Vane, C., Spiro, B. F., Snape, C. E. & Orheim, A. 2015. Geochemistry and petrology of palaeocene coals from Spitzbergen - Part 2: Maturity variations and implications for local and regional burial models. *International Journal of Coal Geology,* 143, p. 1-10.

McRae, S. G. 1972. Glauconite. *Earth-Science Reviews,* 8, p. 397-440.

Mellere, D., Plink-Björklund, P. & Steel, R. 2002. Anatomy of shelf deltas at the edge of a prograding Eocene shelf margin, Spitsbergen. *Sedimentology,* 49, p. 1181-1206.

Morad, S., Al-Ramadan, K., Ketzer, J. M. & De Ros, L. 2010. The impact of diagenesis on the heterogeneity of sandstone reservoirs: A review of the role of depositional facies and sequence stratigraphy. *AAPG Bulletin,* 94, p. 1267-1309.

Morad, S., Ketzer, J. M. & De Ros, L. F. 2012. Linking diagenesis to sequence stratigraphy: an integrated tool for understanding and predicting reservoir quality distribution. *International Association of Sedimentologists,* 45, p. 1-36.

Mørk, M. B. E. 2013. Diagenesis and quartz cement distribution of low-permeability Upper Triassic–Middle Jurassic reservoir sandstones, Longyearbyen CO2 lab well site in Svalbard, Norway. *AAPG Bulletin,* 97, p. 577-596.

Nagy, J., Kaminski, M., Kuhnt, W. & Bremer, M. A. 2001. Agglutinated foraminifera from neritic to bathyal facies in the Palaeogene of Spitsbergen and the Barents Sea. *In:* Hart, M., Kaminski, M. A. & Smart, C. (eds.) *Proceedings of the Fifth International Workshop on Agglutinated Foraminifera*. Plymouth, p. 333-361.

Naurstad, O. A. 2014. *Sedimentology of the Aspelintoppen Formation (Eocene-Oligocene), Brogniartfjella, Svalbard.* Master Thesis, University of Bergen

Odin, G. S. & Matter, A. 1981. De glauconiarum origine. *Sedimentology,* 28, p. 611-641.

Petersen, T. G., Thomsen, T. B., Olaussen, S. & Stemmerik, L. 2016. Provenance shifts in an evolving Eurekan foreland basin: the Tertiary Central Basin, Spitsbergen. *Journal of the Geological Society,* 173, p. 634-648.

Piepjohn, K., von Gosen, W. & Tessensohn, F. 2016. The Eurekan deformation in the Arctic: an outline. *Journal of the Geological Society,* 173, p. 1007-1024.

Reading, H. G. & Collinson, J. D. 1996. Clastic coasts. *In:* Reading, H. G. (ed.) *Sedimentary Environments: Processes, Facies and Stratigraphy,* 3rd ed. Oxford: Blackwell Science, p. 154-231.

Reineck, H. E. & Singh, I. B. 1972. Genesis of laminated sand and graded rhythmites in storm-sand layers of shelf mud. *Sedimentology,* 18, p. 123-128.

Reineck, H. E. & Singh, I. B. 1980. Tidal flats. *In:* Reineck, H. E. & Singh, I. B. (eds.) *Depositional sedimentary environments*. Heidelberg: Springer, p. 430-456.

Riis, F., Lundschien, B. A., Høy, T., Mørk, A. & Mørk, M. B. E. 2008. Evolution of the Triassic shelf in the northern Barents Sea region. *Polar Research,* 27, p. 318-338.

Ritter, U. 1984. The influence of time and temperature on vitrinite reflectance. *Organic Geochemistry,* 6, p. 473-480.

Schlegel, A., Lisker, F., Dörr, N., Jochmann, M., Schubert, K. & Spiegel, C. 2013. Petrography and geochemistry of siliciclastic rocks from the Central Tertiary Basin of Svalbard - implications for provenance, tectonic setting and climate. *German Journal of Geology,* 164, p. 173-186.

Schweitzer, H. J. 1980. Environment and climate in the Early Tertiary of Spitsbergen. *Palaeogeography, Palaeoclimatology, Palaeoecology,* 30, p. 297-311.

Steel, R., Gjelberg, J., Helland-Hansen, W., Kleinspehn, K., Nøttvedt, A. & Rye-Larsen, M. 1985. The Tertiary strike-slip basins and orogenic belt of Spitsbergen. *SEPM Special Publication,* 37, p. 339-359.

Steel, R. J. 1977. Observations on some Cretaceous and Tertiary sandstone bodies in Nordenskiold Land, Svalbard. *Norsk Polarinstitutt,* Årbok 1976, p. 43-67.

Steel, R. J., Dalland, A., Kalgraff, K. & Larsen, V. 1981. The Central Tertiary Basin of Spitsbergen: sedimentary development of a sheared-margin basin. *In:* Kerr, J. W. & Ferguson, A. J. (eds.) *Geology of the North Atlantic Borderland*. Can. Soc. Petrol. Geol., p. 647-664.

Steel, R. J. & Worsley, D. 1984. Svalbard's post-Caledonian strata - an atlas of sedimentational patterns and palaeogeographic evolution. *In:* Spencer, A. M. (ed.) *Petroleum Geology of the North European Margin*. Dordrecht: Springer, p. 109-135.

Throndsen, T. 1982. Vitrinite reflectance studies of coals and dispersed organic matter in Tertiary deposits in the Adventdalen area, Svalbard. *Polar Research,* 2, p. 77-91.

Udgata, D. 2007. *Glauconite as an indicator of sequence stratigraphic packages in a lower Paleocene passive-margin shelf succession, Central Alabama.* Master Thesis, Auburn University.

Walderhaug, O. 1996. Kinetic modeling of quartz cementation and porosity loss in deeply buried sandstone reservoirs. *AAPG Bulletin,* 80, p. 731-745.

Walker, R. G. & Plint, A. G. 1992. Wave- and storm-dominated shallow marine systems. *In:* Walker, R. G. & James, N. P. (eds.) *Facies Models: response to sea level change*. St Johns: Geological Association of Canada, p. 219-238.

Ward, C. R. 1984. *Coal geology and coal technology.* Oxford, Blackwell Scientific Publications, 345 p.

Wilkin, R. T. & Barnes, H. L. 1997. Formation processes of framboidal pyrite. *Geochimica et Cosmochimica Acta,* 61, p. 323-339.

Worden, R. H. & Burley, S. D. 2003. Sandstone diagenesis: the evolution of sand to stone. *In:* Burley, S. D. & Worden, R. H. (eds.) *Sandstone diagenesis: Recent and ancient*. Oxford: Blackwell Publishing Ltd., p. 3-44.

Worsley, D. 2008. The post-Caledonian development of Svalbard and the western Barents Sea. *Polar Research,* 27, p. 298-317.

Xi, K., Cao, Y., Jahren, J., Zhu, R., Bjørlykke, K., Zhang, X., Cai, L. & Hellevang, H. 2015. Quartz cement and its origin in tight sandstone reservoirs of the Cretaceous Quantou formation in the southern Songliao basin, China. *Marine Petroleum Geology,* 66, p. 748-763.

Zhou, W., Apkarian, R., Wang, Z. L. & Joy, D. 2006. Fundamentals of scanning electron microscopy (SEM). *In:* Zhou, W. & Wang, Z. L. (eds.) *Scanning microscopy for nanotechnology*. Springer, p. 1-40.

Electronic references

Swapp, S. (2017). Scanning Electron Microscopy (SEM). Retrieved from https://serc.carleton.edu/research_education/geochemsheets/techniques/SEM.html [Accessed: 22.02.2019]

Goodge, J (2016). Back-scattered Electron Detector (BSE). Retrieved from https://serc.carleton.edu/research_education/geochemsheets/bse.html [Accessed: 22.02.2019]

Thermo Fisher Scientific (2019). XRF Technology. Retrieved from https://www.thermofisher.com/no/en/home/industrial/spectroscopy-elemental-isotope-analysis/spectroscopy-elemental-isotope-analysis-learning-center/elemental-analysis-information/xrf-technology.html [Accessed: 12.03.2019]

APPENDIX I: *Sampling intervals*

Table I.1: Sampling intervals.

Sample	Depth interval	Core	Formation	Optical microscopy	SEM	XRD
F1	677,88-677,92	7-2006	Firkanten	X	X	
F2	674,80-674,84			X		
F3	672,00-672,04			X	X	
F4	671,10-671,14			X		
F5	669,60-669,64			X		X
F6	661,96-662,00					
F7	660,46-660,50			X		
F8	659,40-659,44			X		
F9	653,20-653,24			X		
F10	650,96-651,00			X		
F11	646,94-646,98			X	X	
F12	646,60-646,64			X		
F13	641,96-642,00			X		
F14	640,20-640,24			X		
F15	639,80-639,84			X		
F16	630,90-630,94			X		
F17	626,80-626,84			X		
F18	624,87-624,91			X		
F19	617,80-617,84			X	X	
F20	612,27-612,31			X		
F21	605,71-605,75					
F22	604,82-604,86			X		
F23	596,35-596,39			X		
F24	591,68-591,72			X		
F25	587,20-587,24			X	X	
F26	581,33-581,37			X		
F27	661,50-661,54					
F28	660,55-660-59					
G1	269,18-269,22	7-2006	Grumantbyen	X		
G2	260,46-260,50			X		

G3	257,37-257,41			X		
G4	580,57-580,61	11-2003	Grumantbyen	X		
G5	579,58-579,62			X		X
G6	573,38-573,42			X	X	
A1	93,50-93,52	11-2003	Aspelintoppen	X	X	
A2	86,80-86,84			X		
A3	84,76-84,80			X		
A4	83,92-83,96			X		
A5	83,74-83,78			X		
A6	82,92-82,96			X		X
A7	77,60-77,62			X	X	
A8	71,47-71,51			X		
A9	65,84-65,88			X		
A10	63,90-63,92			X		

APPENDIX II: *Petrographic analyses*

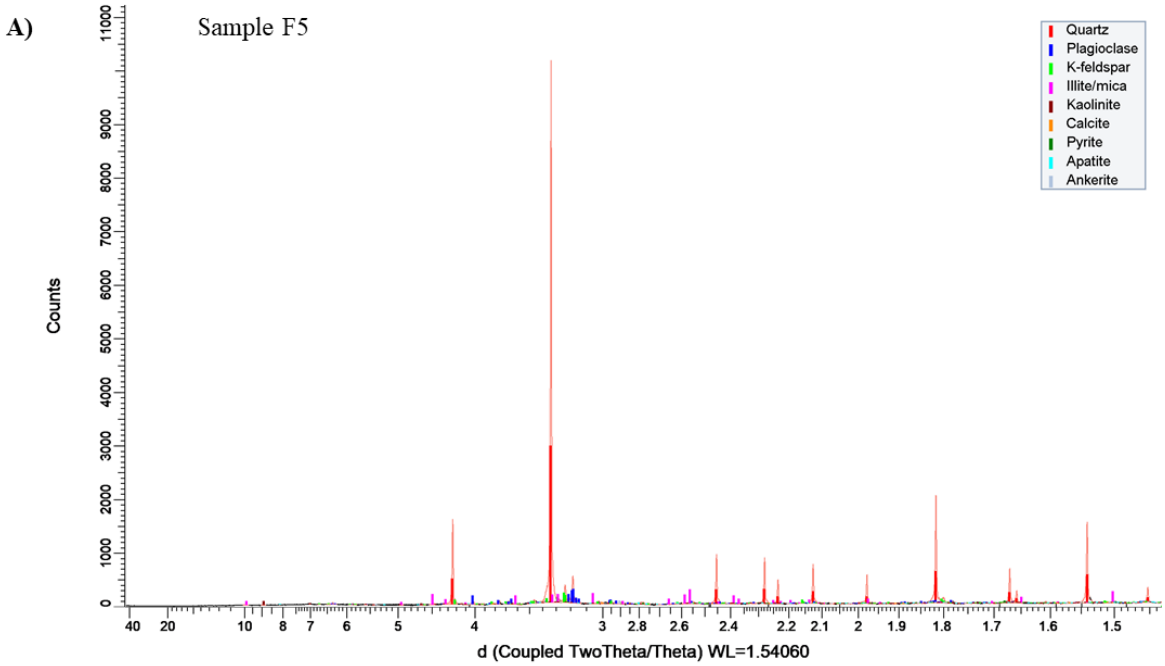
A)
Sample F5
Quartz
Plagioclase
K-feldspar
Illite/mica
Kaolinite
Calcite
Pyrite
Apatite
Ankerite
Counts
d (Coupled TwoTheta/Theta) WL=1.54060

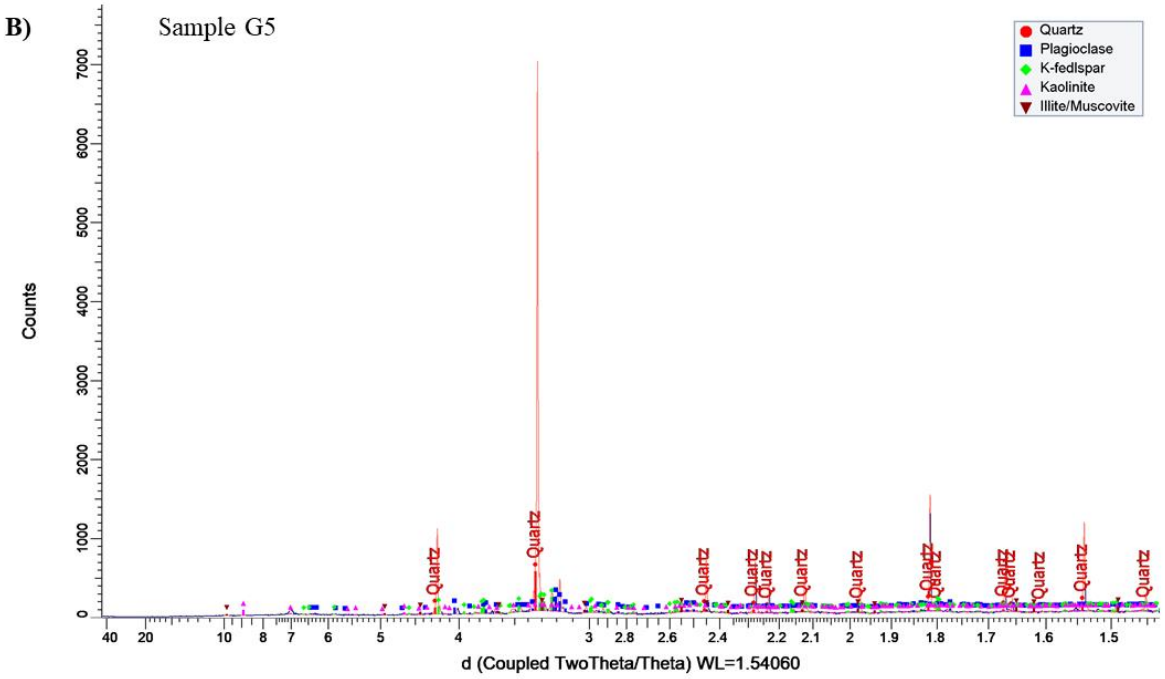
B)
Sample G5
Quartz
Plagioclase
K-fedlspar
Kaolinite
Illite/Muscovite
Counts
d (Coupled TwoTheta/Theta) WL=1.54060

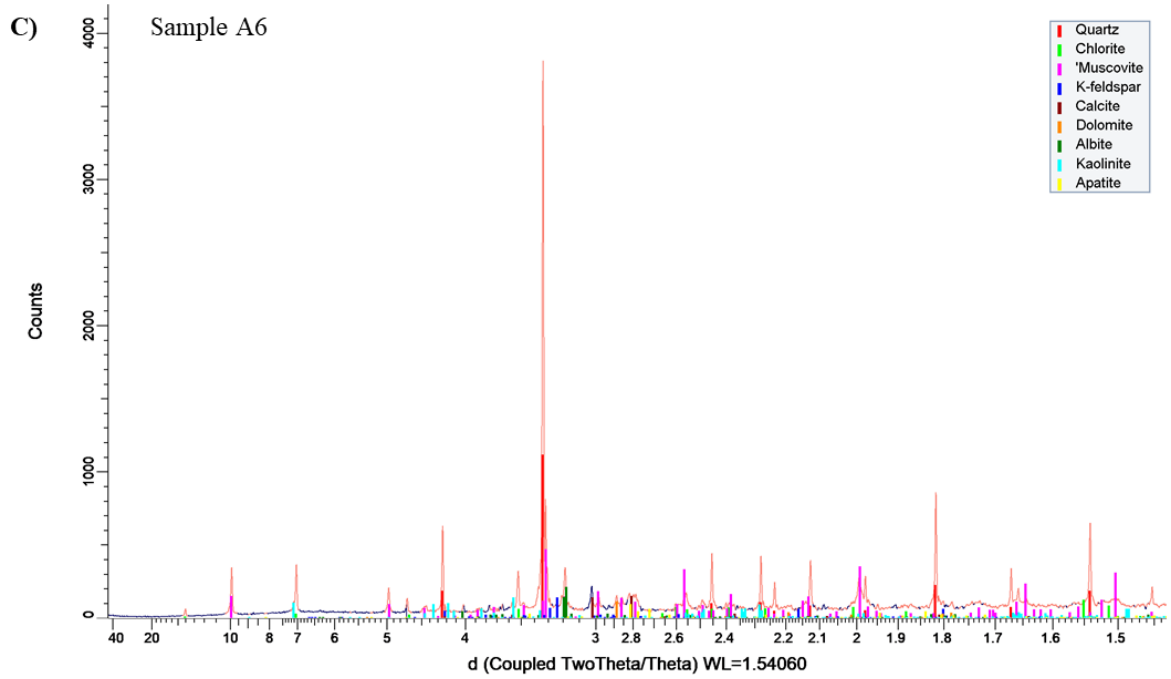

Figure II.1: XRD-analysis. (A) Sample F5 from the Firkanten Formation (core 7-2006). (B) Sample G5 from the Grumantbyen Formation (core 11-2003). (C) sample A6 from the Aspelintoppen Formation (core 11-2003).

A)

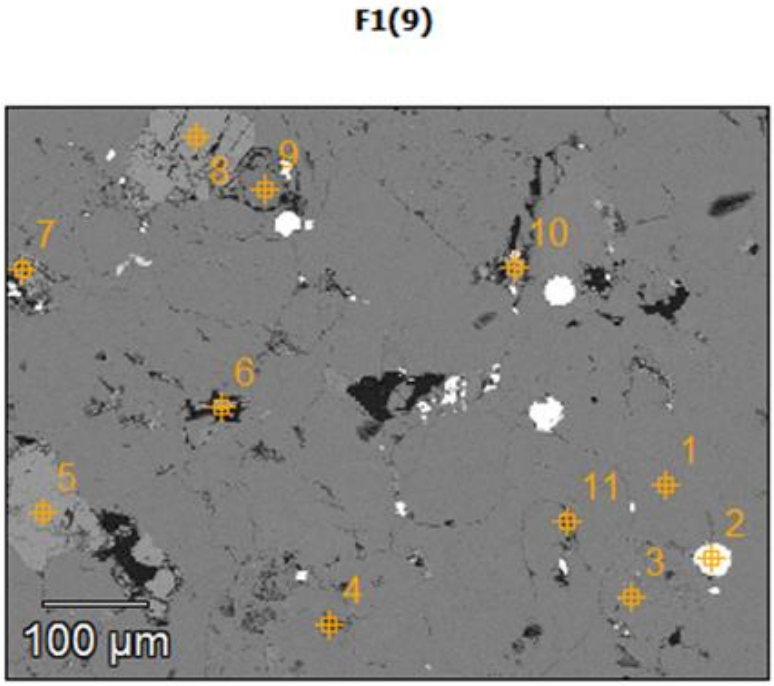
F1(9)
1
2
3
4
5
6
7
8
9
10
11
100 µm

B)

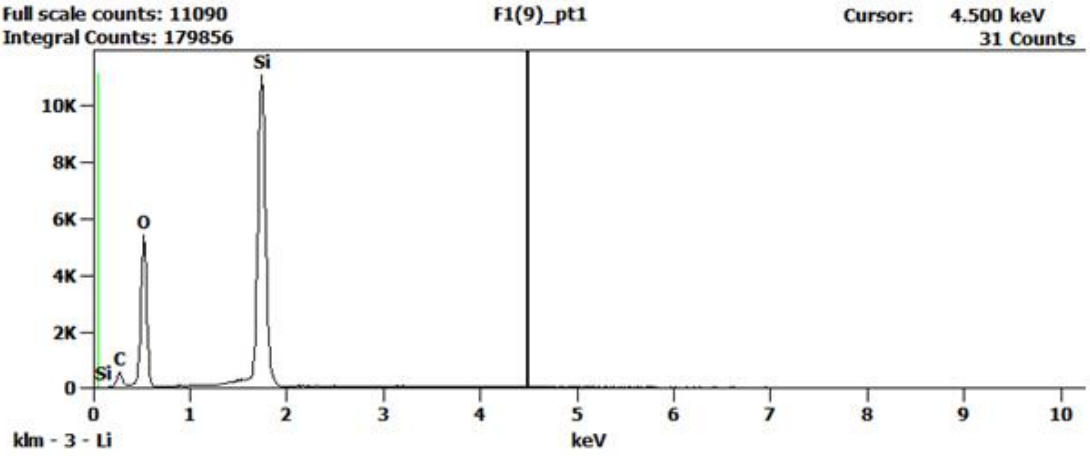
Full scale counts: 11090
Integral Counts: 179856
F1(9)_pt1
Cursor: 4.500 keV
31 Counts
Si
O
C
Si
10K
8K
6K
4K
2K
0
0 1 2 3 4 5 6 7 8 9 10
klm - 3 - Li
keV

C)

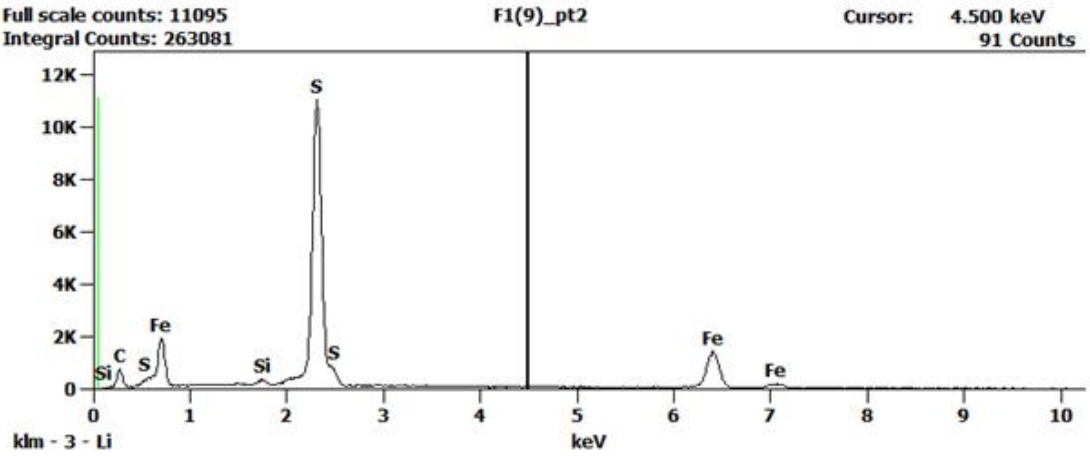
Full scale counts: 11095
Integral Counts: 263081
F1(9)_pt2
Cursor: 4.500 keV
91 Counts
S
Fe
C
S
Si
Si
S
Fe
Fe
12K
10K
8K
6K
4K
2K
0
0 1 2 3 4 5 6 7 8 9 10
klm - 3 - Li
keV

D)

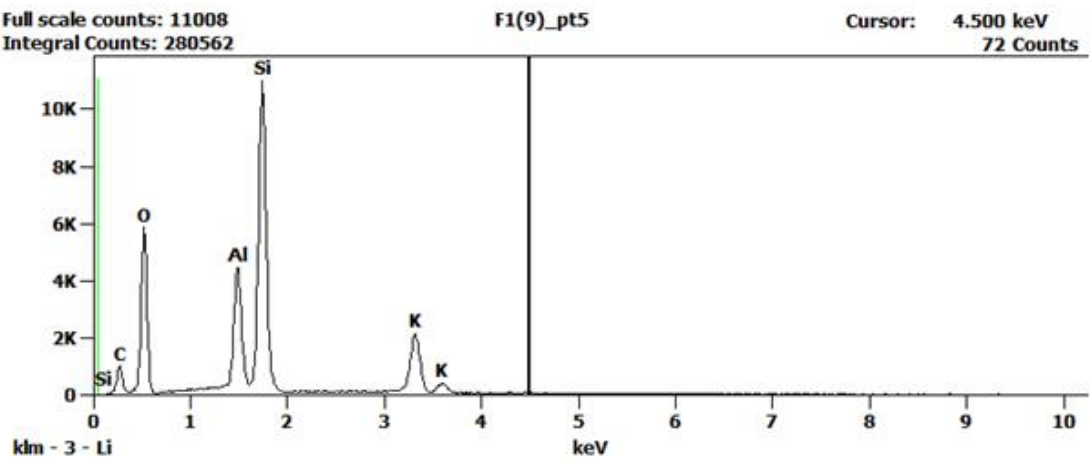
Full scale counts: 11008
Integral Counts: 280562
F1(9)_pt5
Cursor: 4.500 keV
72 Counts
Si
O
Al
K
C
Si
K
10K
8K
6K
4K
2K
0
0 1 2 3 4 5 6 7 8 9 10
keV
klm - 3 - Li

E)

F1(21)

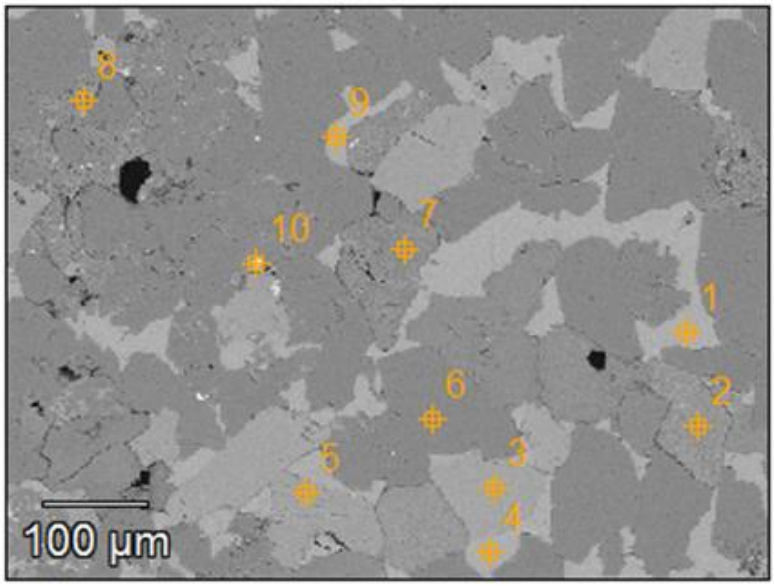
8
9
10
7
1
6
2
5
3
4
100 µm

F)

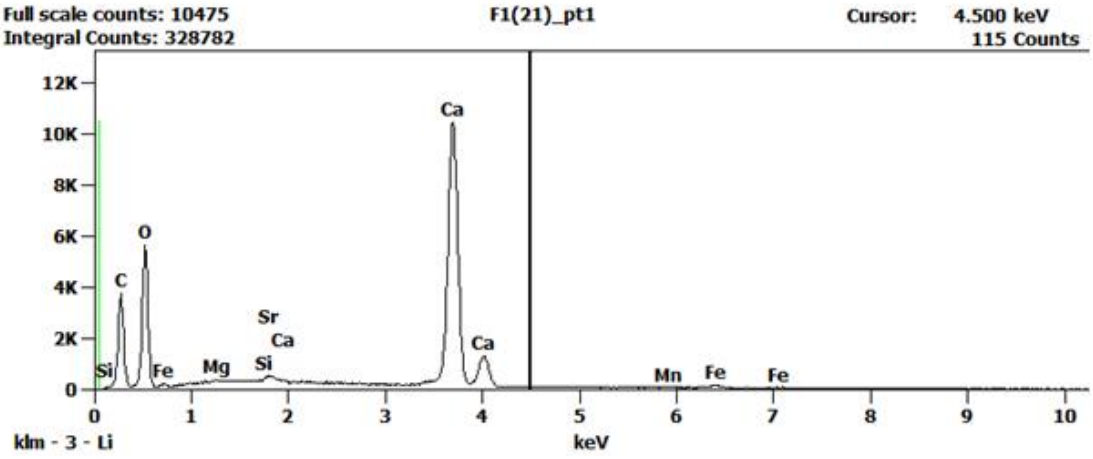
Full scale counts: 10475
Integral Counts: 328782
F1(21)_pt1
Cursor: 4.500 keV
115 Counts
Ca
O
C
Sr
Ca
Si
Fe
Mg
Si
Ca
Mn
Fe
Fe
12K
10K
8K
6K
4K
2K
0
0 1 2 3 4 5 6 7 8 9 10
keV
klm - 3 - Li

G)

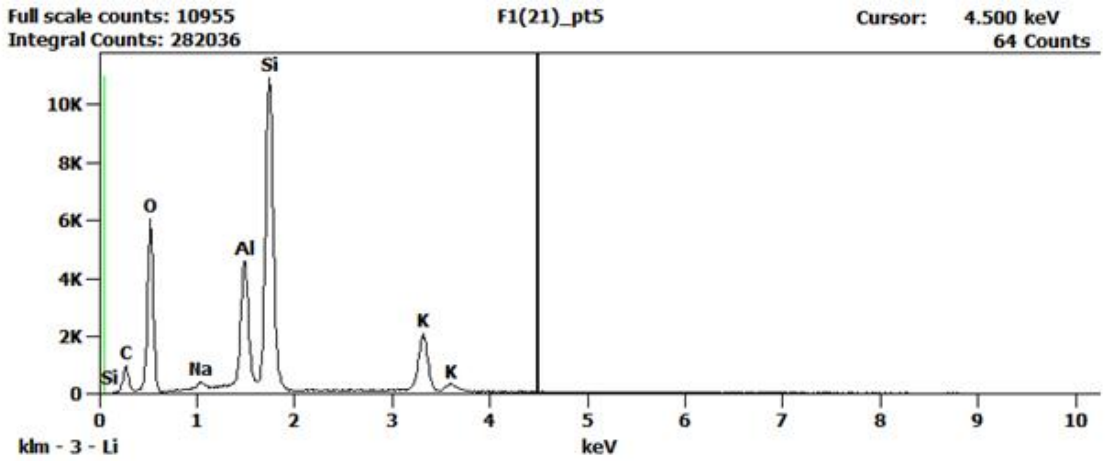
Full scale counts: 10955
Integral Counts: 282036
F1(21)_pt5
Cursor: 4.500 keV
64 Counts
Si
O
Al
C
Na
K
K
Si
10K
8K
6K
4K
2K
0
0 1 2 3 4 5 6 7 8 9 10
keV
klm - 3 - Li

H)

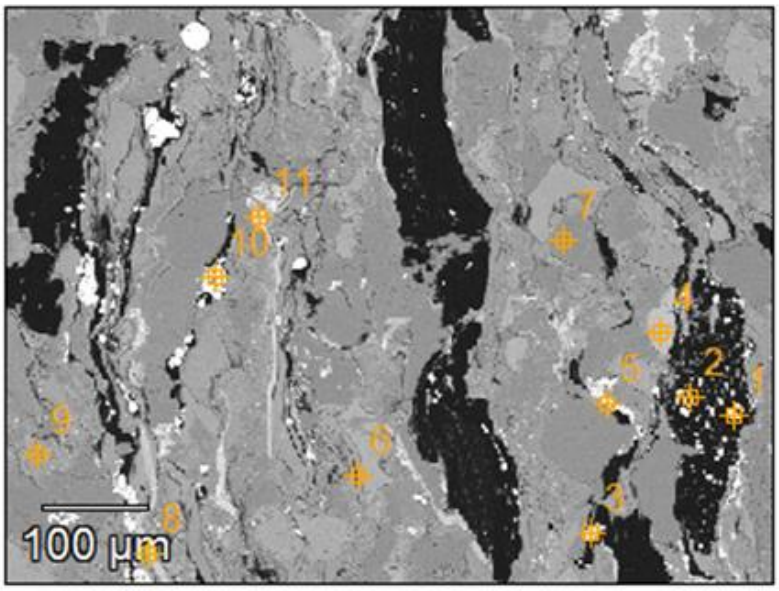
F1(19)
11
10
7
4
5
2
1
9
6
3
8
100 µm

I)

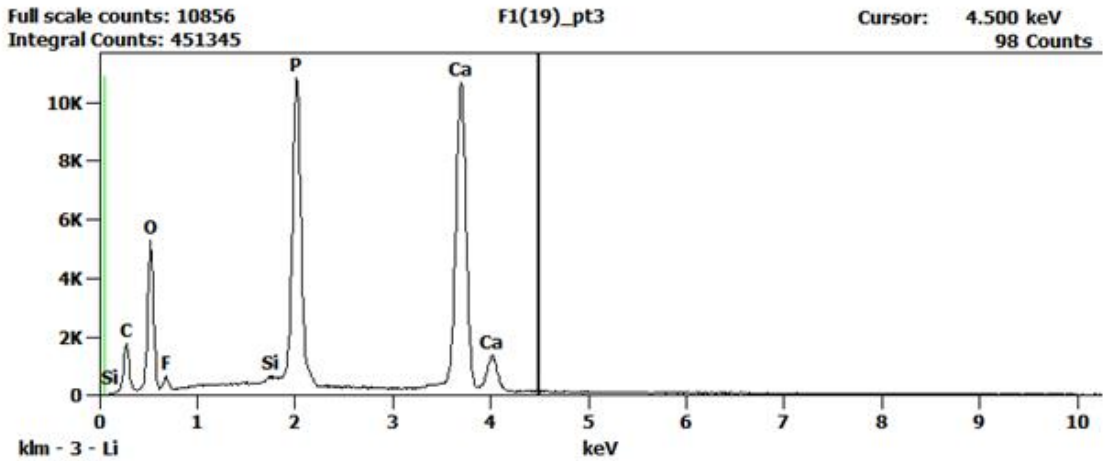
Full scale counts: 10856
Integral Counts: 451345
F1(19)_pt3
Cursor: 4.500 keV
98 Counts
P
Ca
O
C
F
Si
Si
Ca
10K
8K
6K
4K
2K
0
0 1 2 3 4 5 6 7 8 9 10
keV
klm - 3 - Li

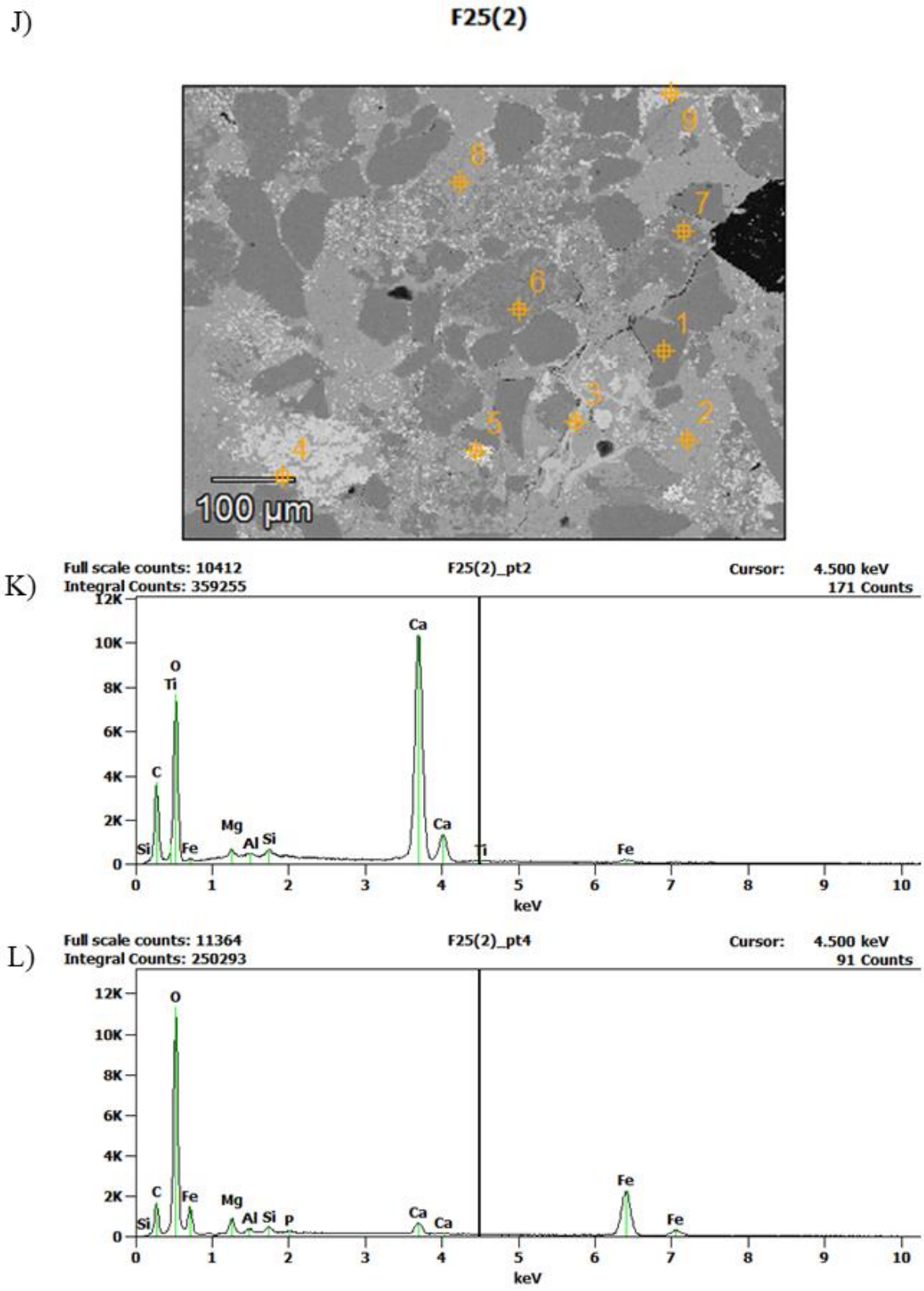

Figure II.2: SEM EDS analysis (examples) of sample F1, F3 and F25 from the Firkanten Formation (core 7-2006). (A)-(D) Sample F1. (E)-(I) Sample F3. (J)-(L) Sample F25.

A)

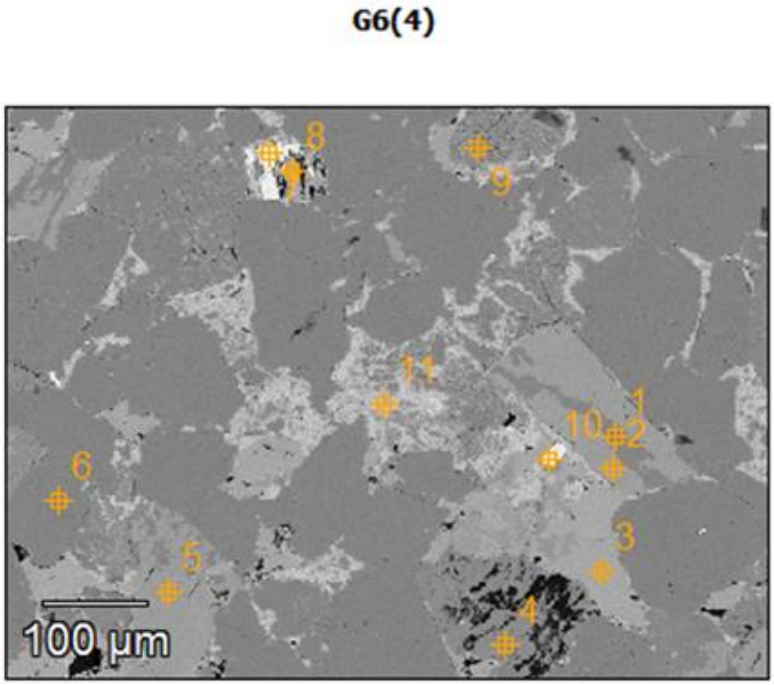
G6(4)
8
9
11
10
1
2
6
3
5
4
100 µm

B)

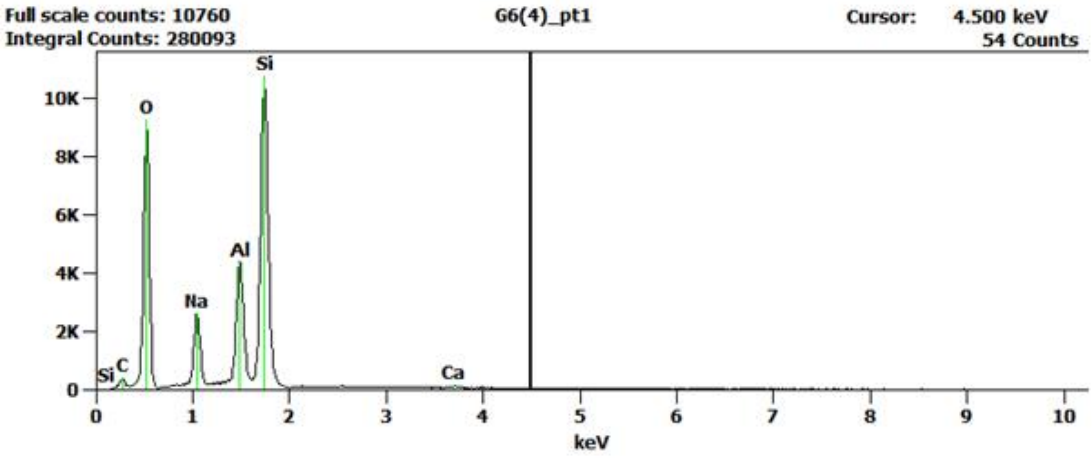
Full scale counts: 10760
Integral Counts: 280093
G6(4)_pt1
Cursor: 4.500 keV
54 Counts
Si
O
Al
Na
C
Si
Ca
10K
8K
6K
4K
2K
0
0 1 2 3 4 5 6 7 8 9 10
keV

C)

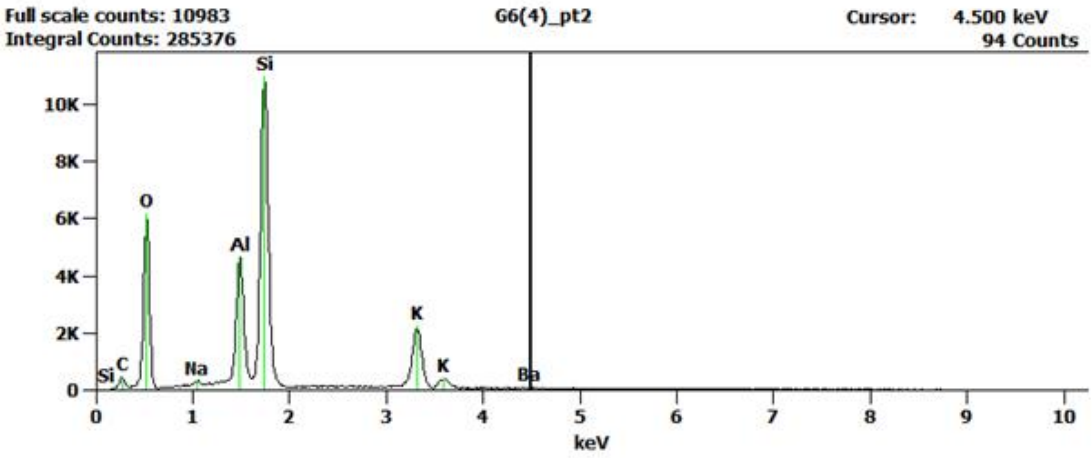
Full scale counts: 10983
Integral Counts: 285376
G6(4)_pt2
Cursor: 4.500 keV
94 Counts
Si
O
Al
K
K
Na
C
Si
Ba
10K
8K
6K
4K
2K
0
0 1 2 3 4 5 6 7 8 9 10
keV

D)

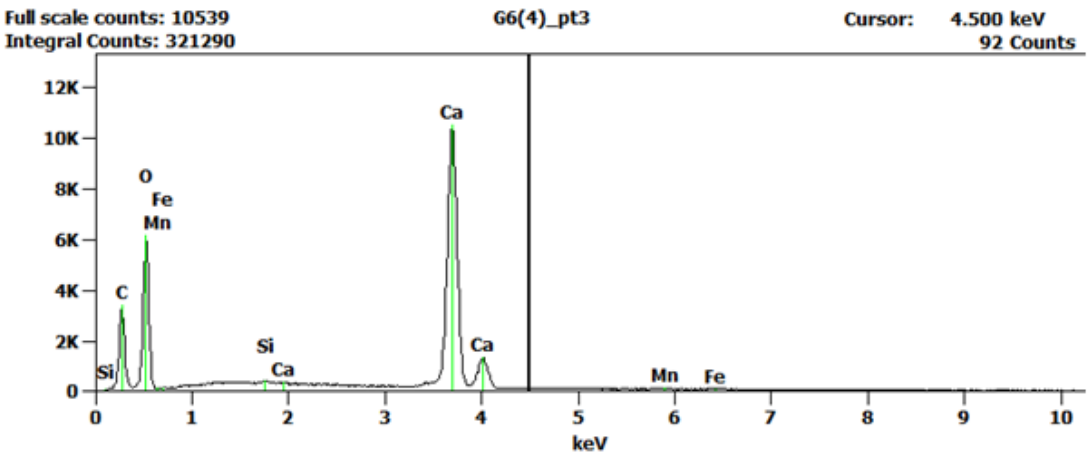
Full scale counts: 10539
Integral Counts: 321290
G6(4)_pt3
Cursor: 4.500 keV
92 Counts
12K
10K
8K
6K
4K
2K
0
O
Fe
Mn
C
Si
Ca
Si
Ca
Ca
Mn
Fe
0 1 2 3 4 5 6 7 8 9 10
keV

E)

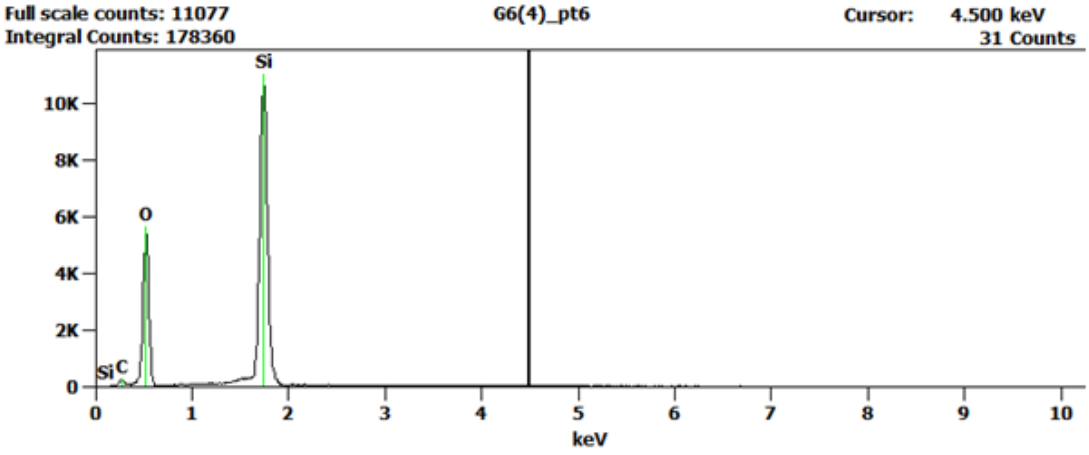
Full scale counts: 11077
Integral Counts: 178360
G6(4)_pt6
Cursor: 4.500 keV
31 Counts
10K
8K
6K
4K
2K
0
Si
O
Si
C
0 1 2 3 4 5 6 7 8 9 10
keV

F)

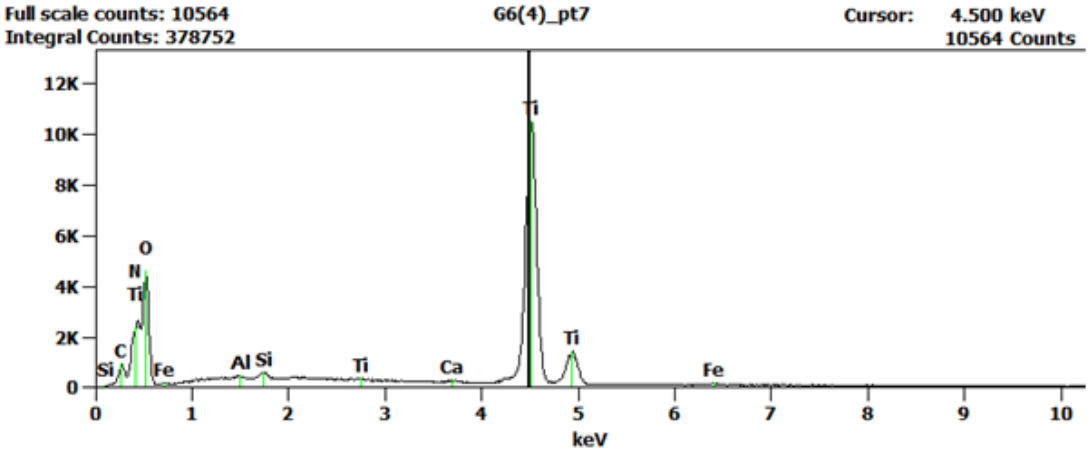
Full scale counts: 10564
Integral Counts: 378752
G6(4)_pt7
Cursor: 4.500 keV
10564 Counts
12K
10K
8K
6K
4K
2K
0
Ti
O
N
Ti
C
Si
Fe
Al
Si
Ti
Ca
Ti
Fe
0 1 2 3 4 5 6 7 8 9 10
keV

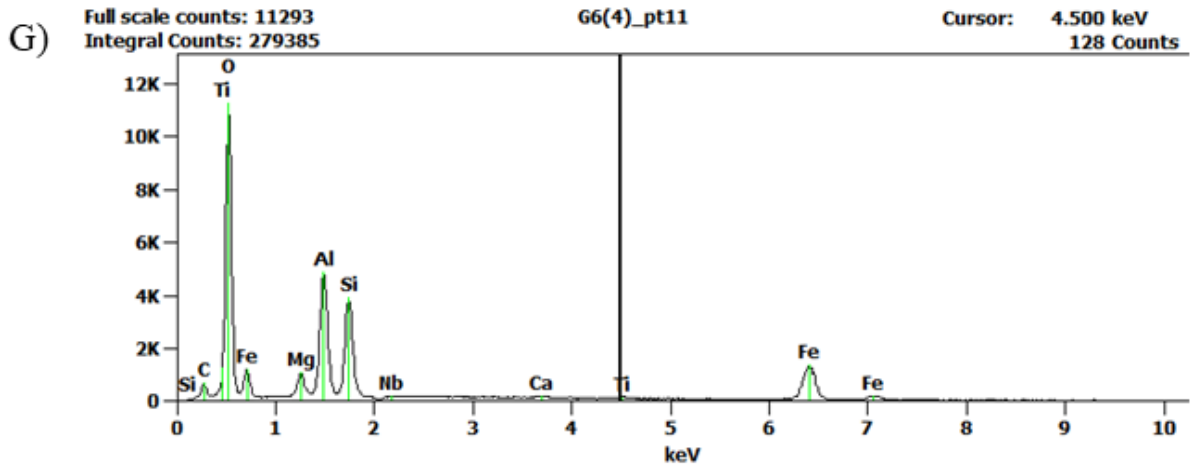

Figure II.3: (A)-(G) SEM EDS analysis (examples) of sample G6 from the Grumantbyen Formation (core 11-2003).

A)

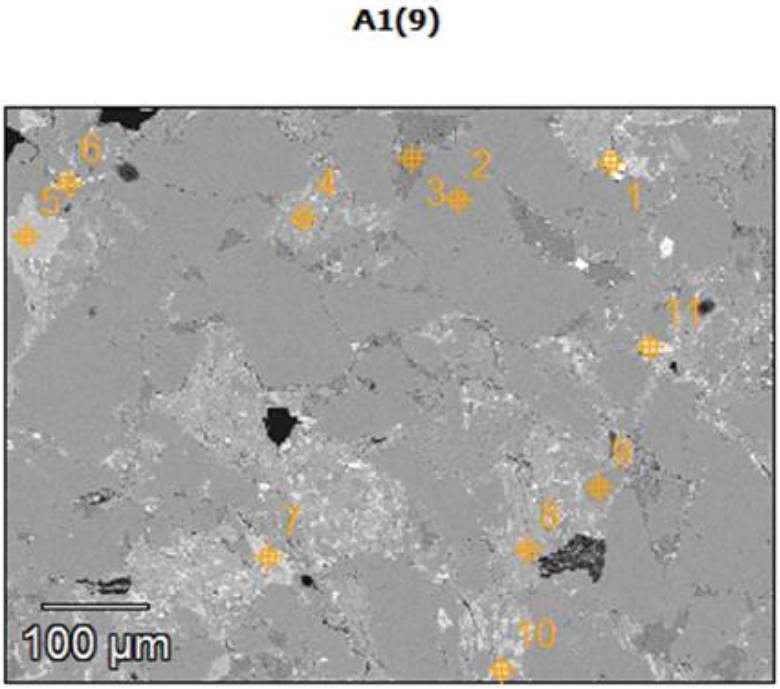
A1(9)
1
2
3
4
5
6
7
8
9
10
11
100 µm

B)

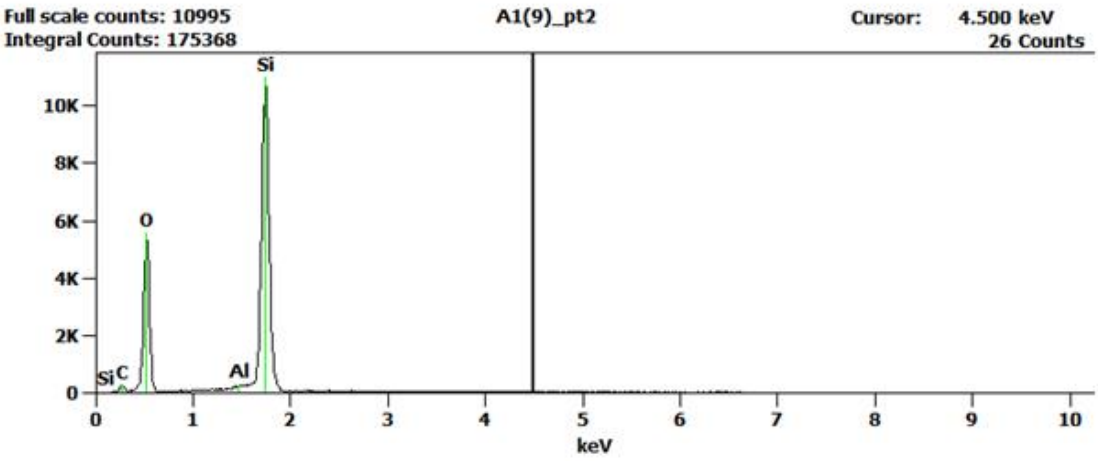
Full scale counts: 10995
Integral Counts: 175368
A1(9)_pt2
Cursor: 4.500 keV
26 Counts
Si
O
Al
Si
C
10K
8K
6K
4K
2K
0
0 1 2 3 4 5 6 7 8 9 10
keV

C) **A1(15)**

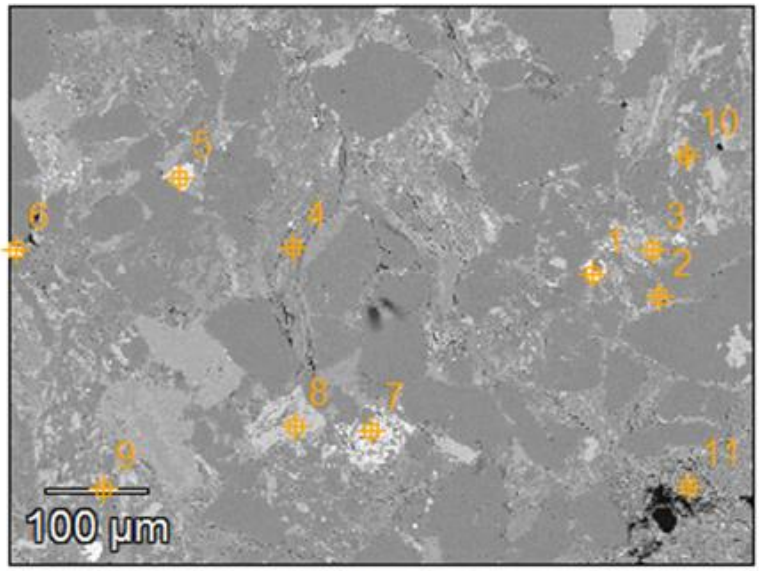
1
2
3
4
5
6
7
8
9
10
11
100 µm

D)

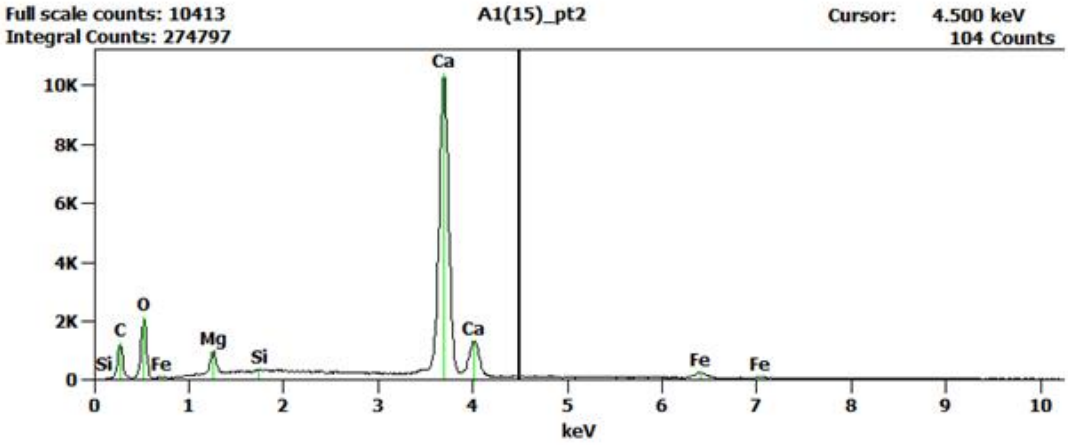
Full scale counts: 10413
Integral Counts: 274797
A1(15)_pt2
Cursor: 4.500 keV
104 Counts
Ca
O
C
Mg
Si
Fe
Si
Ca
Fe
Fe
10K
8K
6K
4K
2K
0
0 1 2 3 4 5 6 7 8 9 10
keV

E)

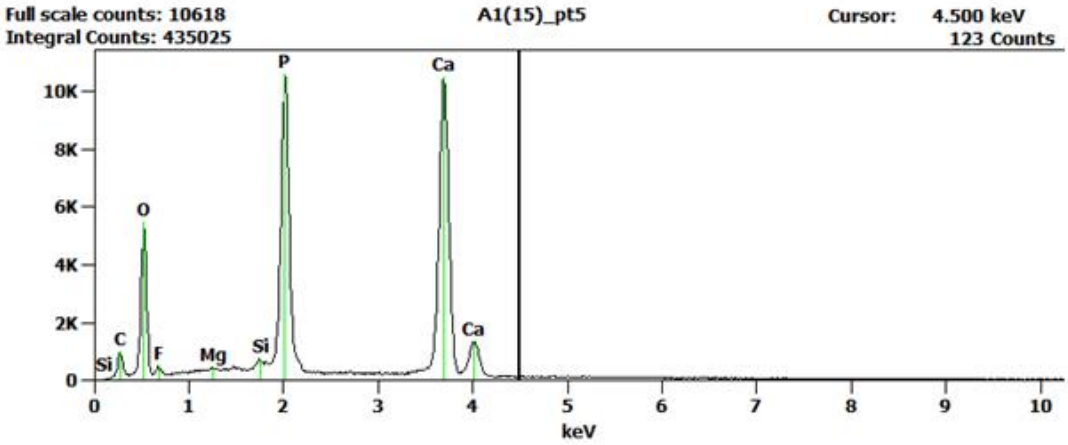
Full scale counts: 10618
Integral Counts: 435025
A1(15)_pt5
Cursor: 4.500 keV
123 Counts
P
Ca
O
C
F
Mg
Si
Si
Ca
10K
8K
6K
4K
2K
0
0 1 2 3 4 5 6 7 8 9 10
keV

F)

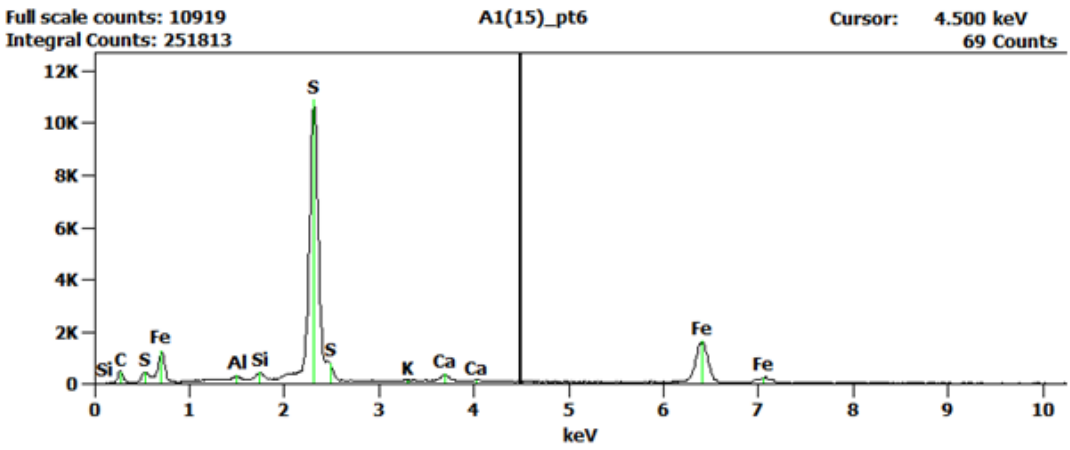
Full scale counts: 10919
Integral Counts: 251813
A1(15)_pt6
Cursor: 4.500 keV
69 Counts
12K
10K
8K
6K
4K
2K
0
Si
C
S
Fe
Al
Si
S
S
K
Ca
Ca
Fe
Fe
0 1 2 3 4 5 6 7 8 9 10
keV

G)

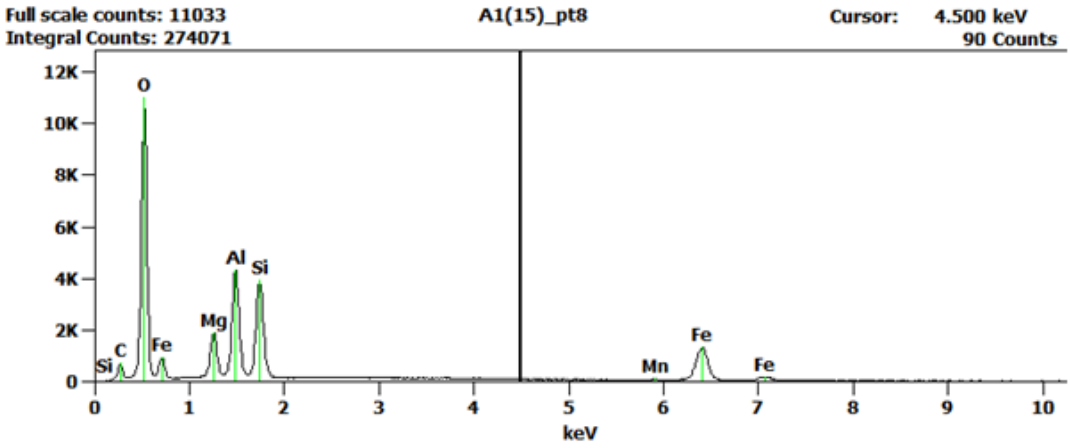
Full scale counts: 11033
Integral Counts: 274071
A1(15)_pt8
Cursor: 4.500 keV
90 Counts
12K
10K
8K
6K
4K
2K
0
O
Si
C
Fe
Mg
Al
Si
Mn
Fe
Fe
0 1 2 3 4 5 6 7 8 9 10
keV

H)

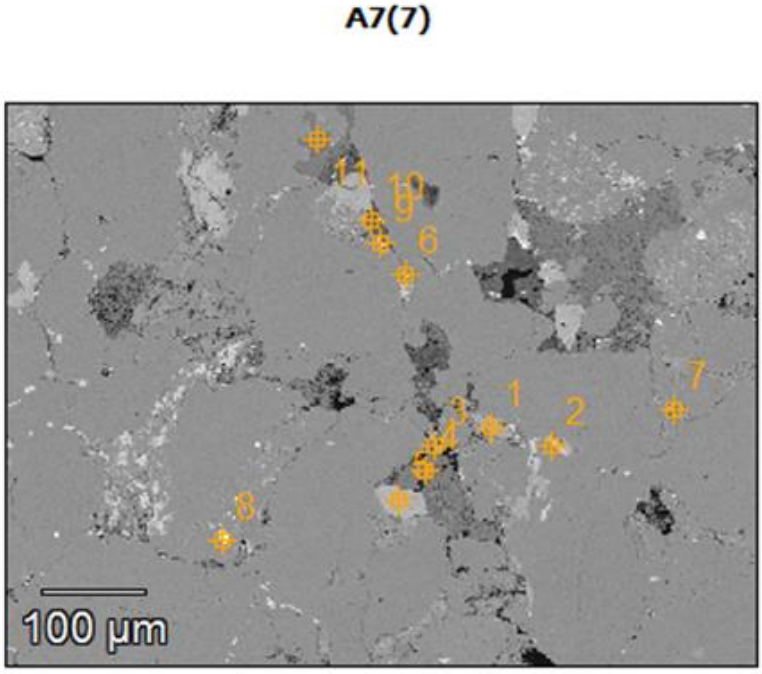
A7(7)
11
10
9
6
7
1
3
2
4
8
100 µm

I)

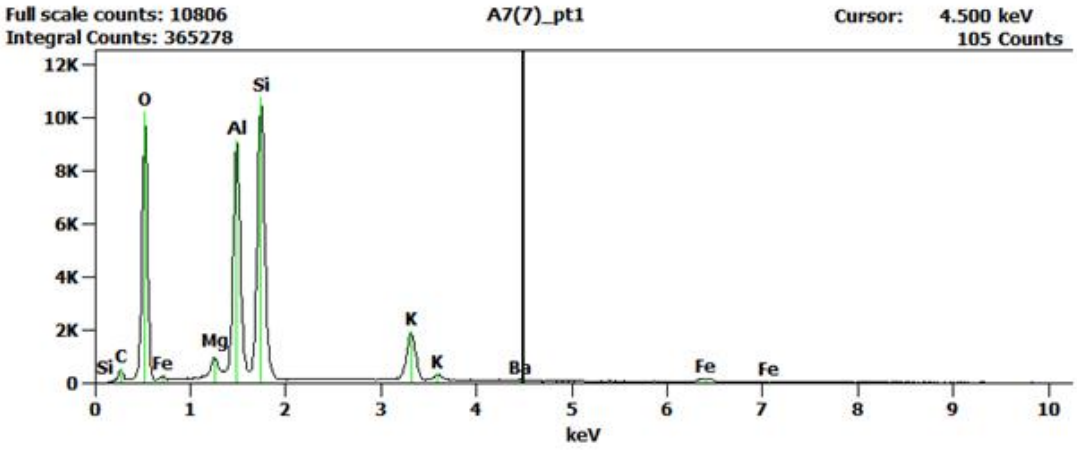
Full scale counts: 10806
Integral Counts: 365278
A7(7)_pt1
Cursor: 4.500 keV
105 Counts
12K
10K
8K
6K
4K
2K
0
O
Si
Al
K
Mg
C
Fe
Ba
0 1 2 3 4 5 6 7 8 9 10
keV

J)

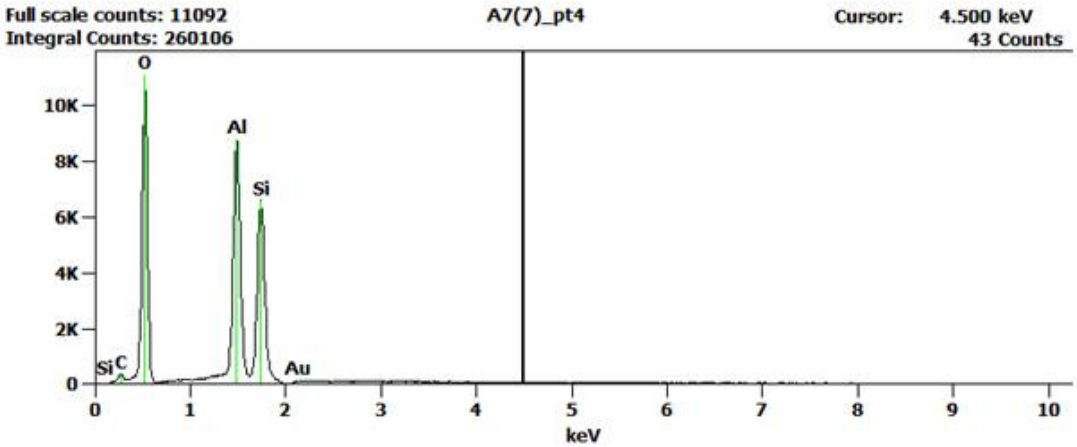
Full scale counts: 11092
Integral Counts: 260106
A7(7)_pt4
Cursor: 4.500 keV
43 Counts
10K
8K
6K
4K
2K
0
O
Al
Si
C
Au
0 1 2 3 4 5 6 7 8 9 10
keV

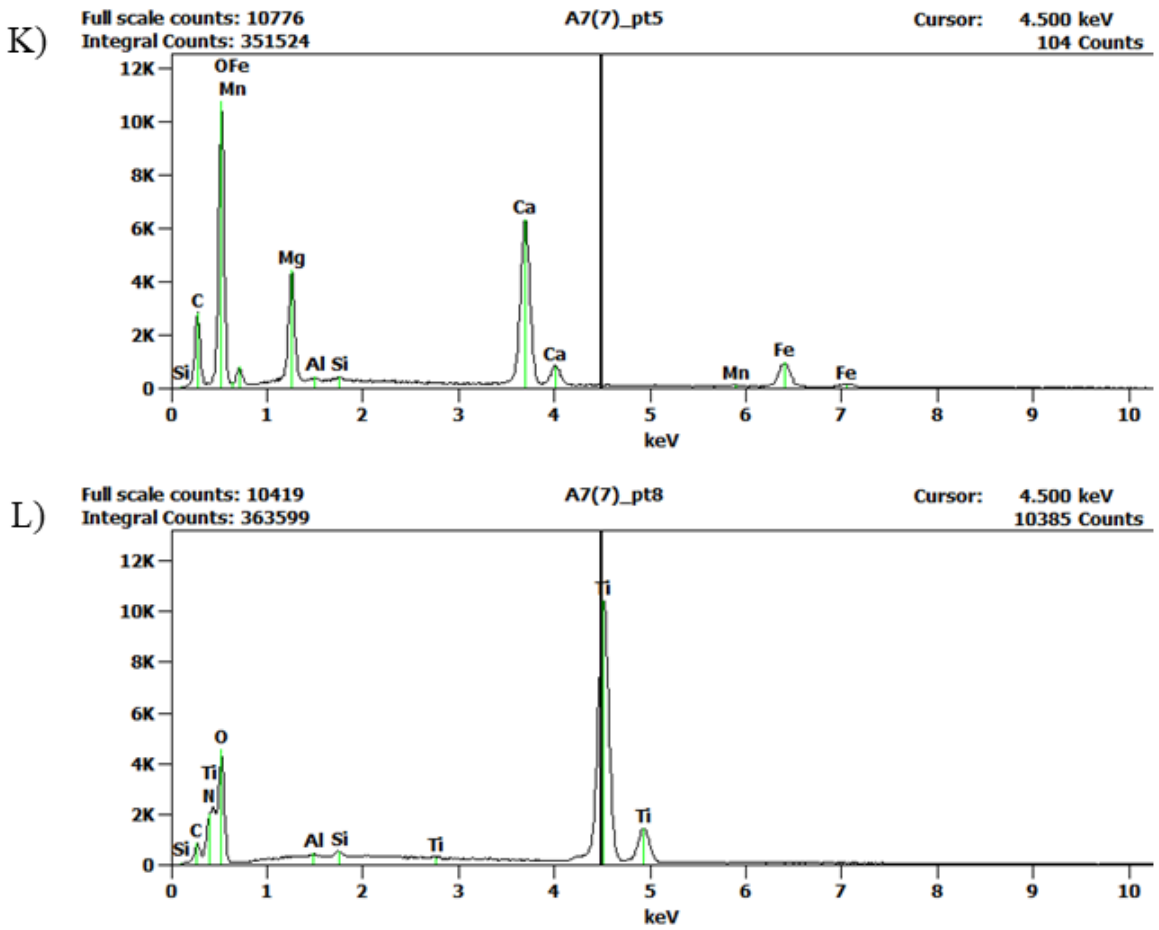

Figure II.4: SEM EDS analysis (examples) of sample A1 and A7 from the Aspelintoppen Formation (core 11-2003). (A)-(G) Sample A1. (H)-(L) Sample A7.

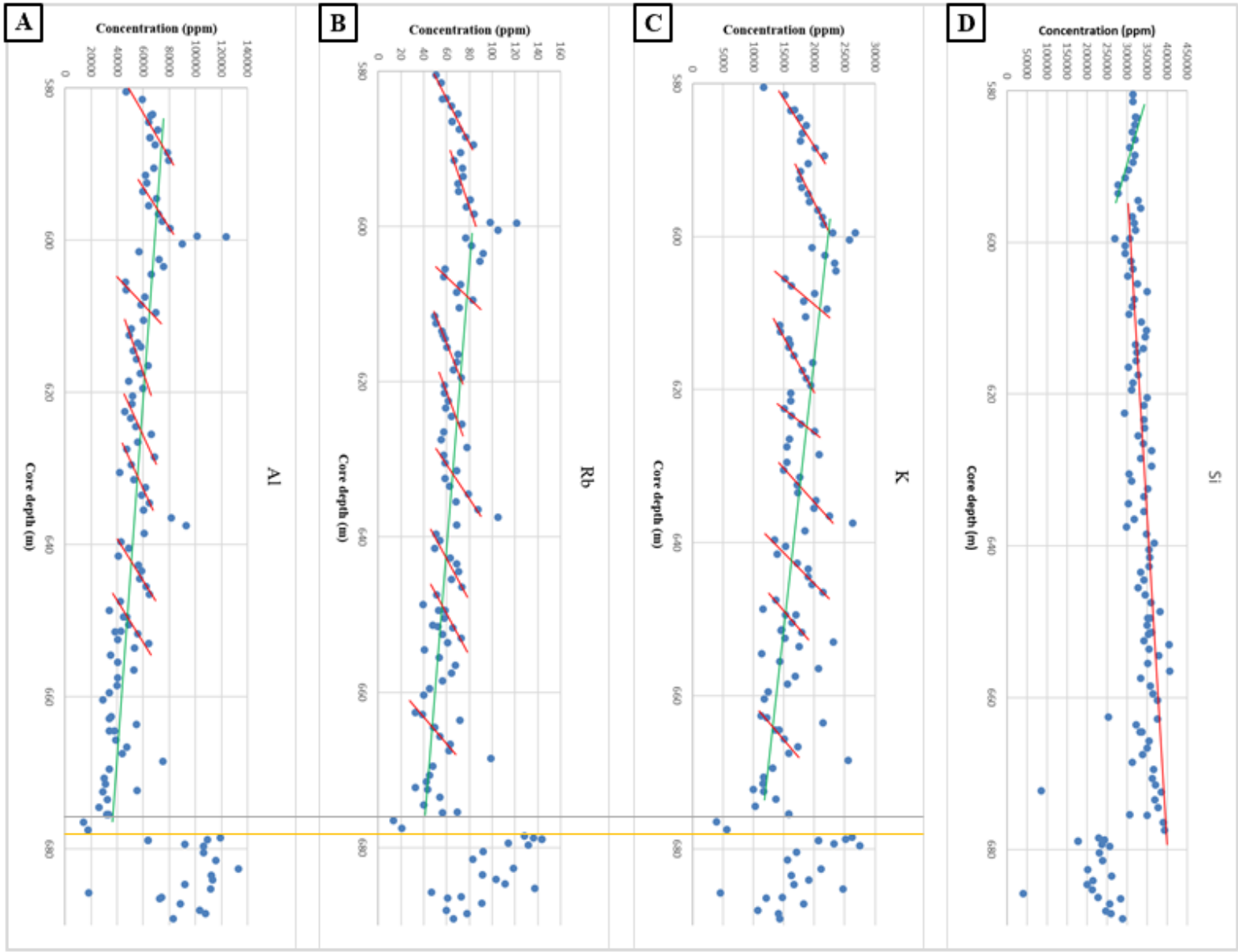
A
Concentration (ppm)
0
20000
40000
60000
80000
100000
120000
140000
Core depth (m)
580
600
620
640
660
680
Al
B
Concentration (ppm)
0
20
40
60
80
100
120
140
160
Core depth (m)
580
600
620
640
660
680
Rb
C
Concentration (ppm)
0
5000
10000
15000
20000
25000
30000
Core depth (m)
580
600
620
640
660
680
K
D
Concentration (ppm)
0
50000
100000
150000
200000
250000
300000
350000
400000
450000
Core depth (m)
580
600
620
640
660
680
Si

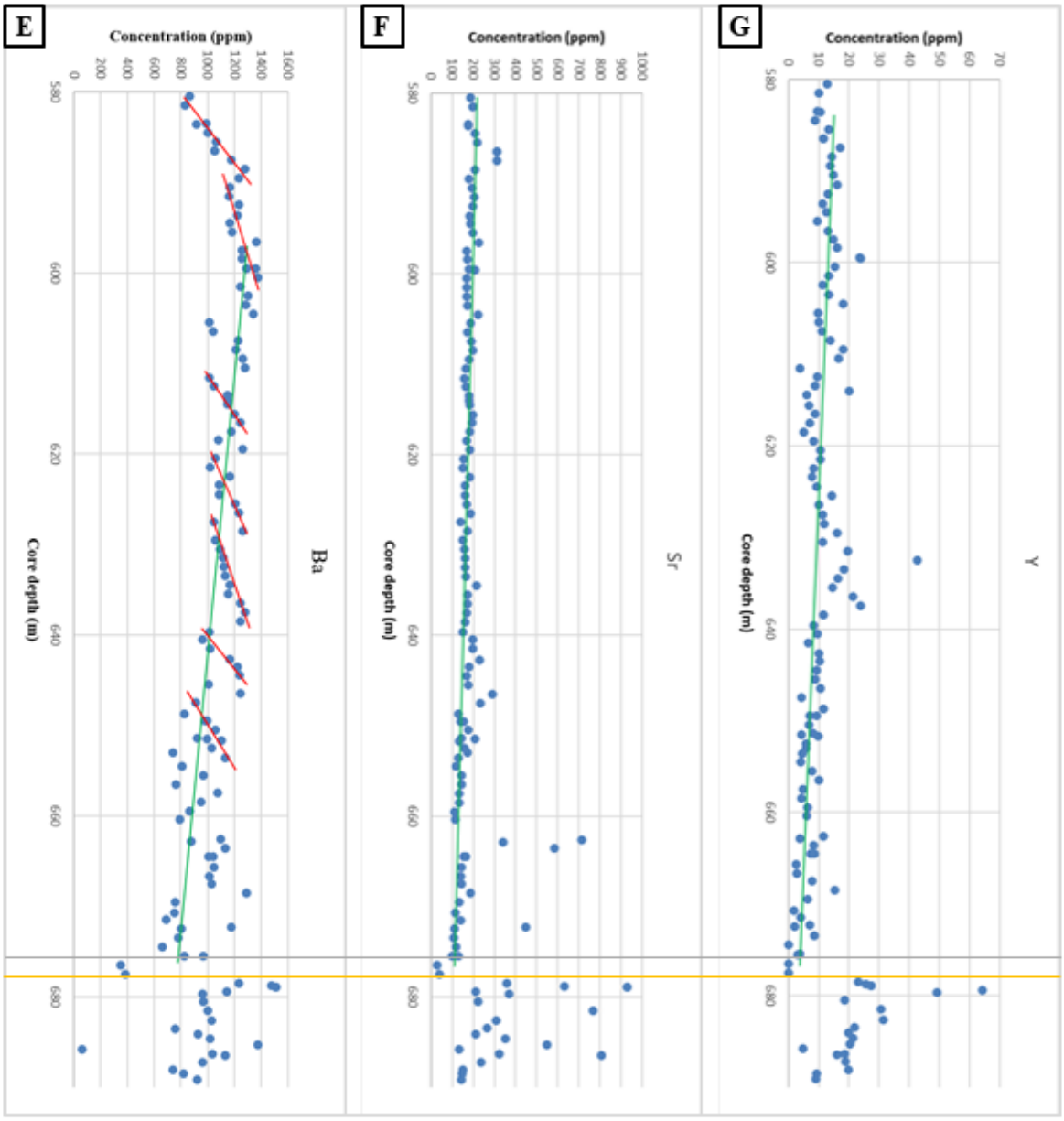

Figure II.5: (A)-(D) Full-profile plots of Al, Rb, K and Si (presented in chapter 5). (E)-(G) Additional geochemical trends identified in the Firkanten Formation (core 7-2006).

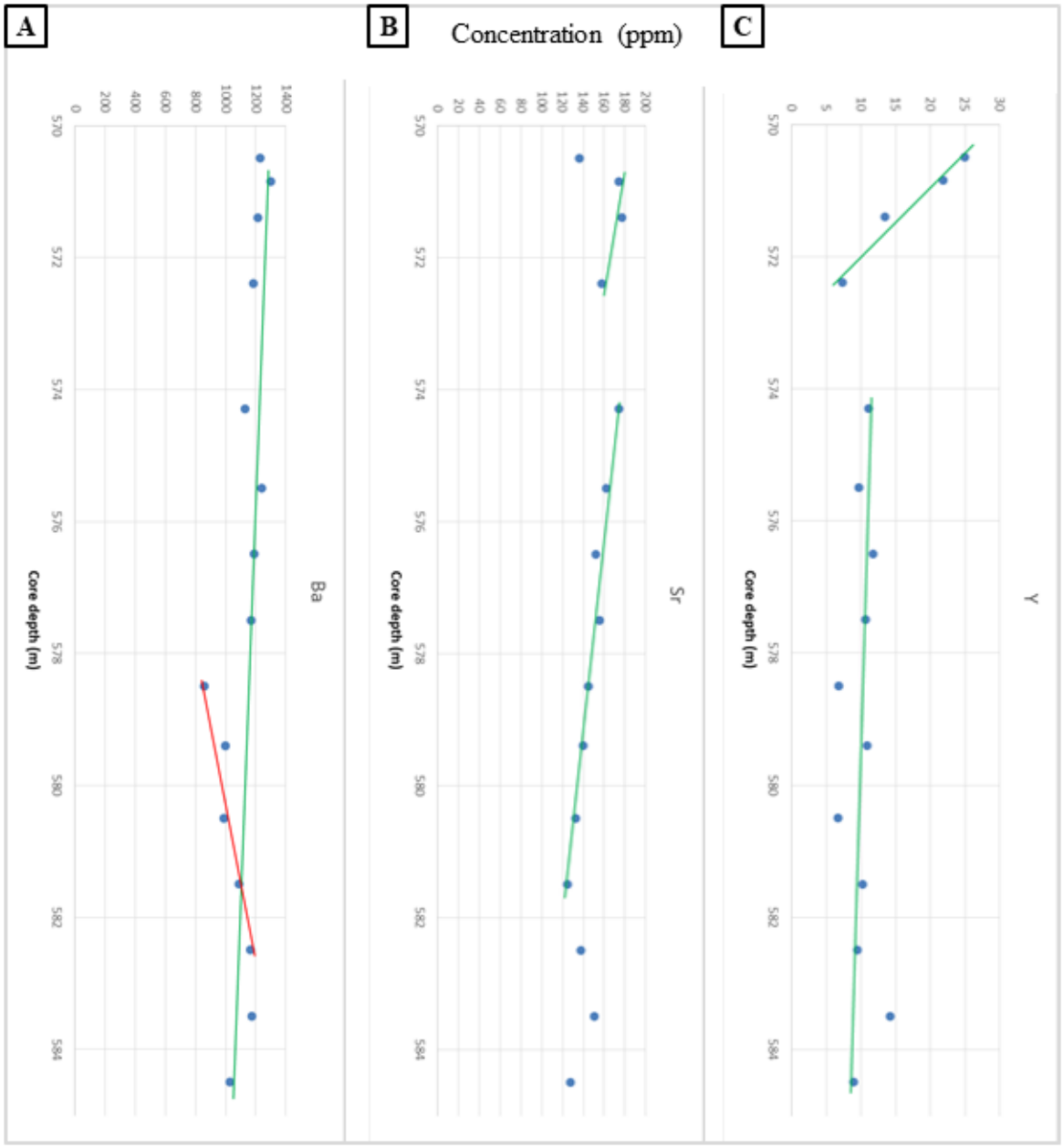

Figure II.6: (A)-(C) Additional geochemical trends identified in the Grumantbyen Formation (core 11-2003).

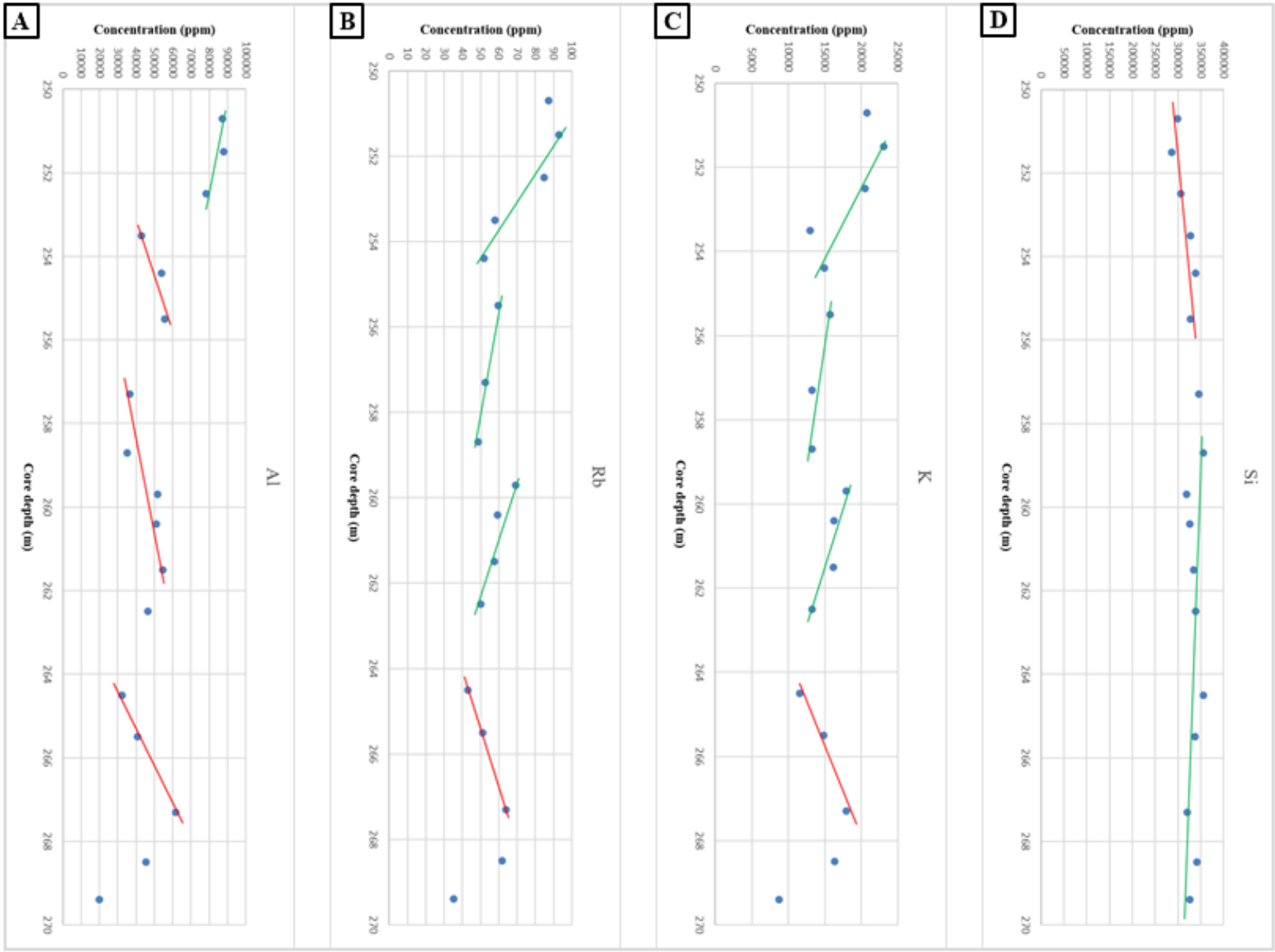
A
Concentration (ppm)
Core depth (m)
Al
B
Concentration (ppm)
Core depth (m)
Rb
C
Concentration (ppm)
Core depth (m)
K
D
Concentration (ppm)
Core depth (m)
Si

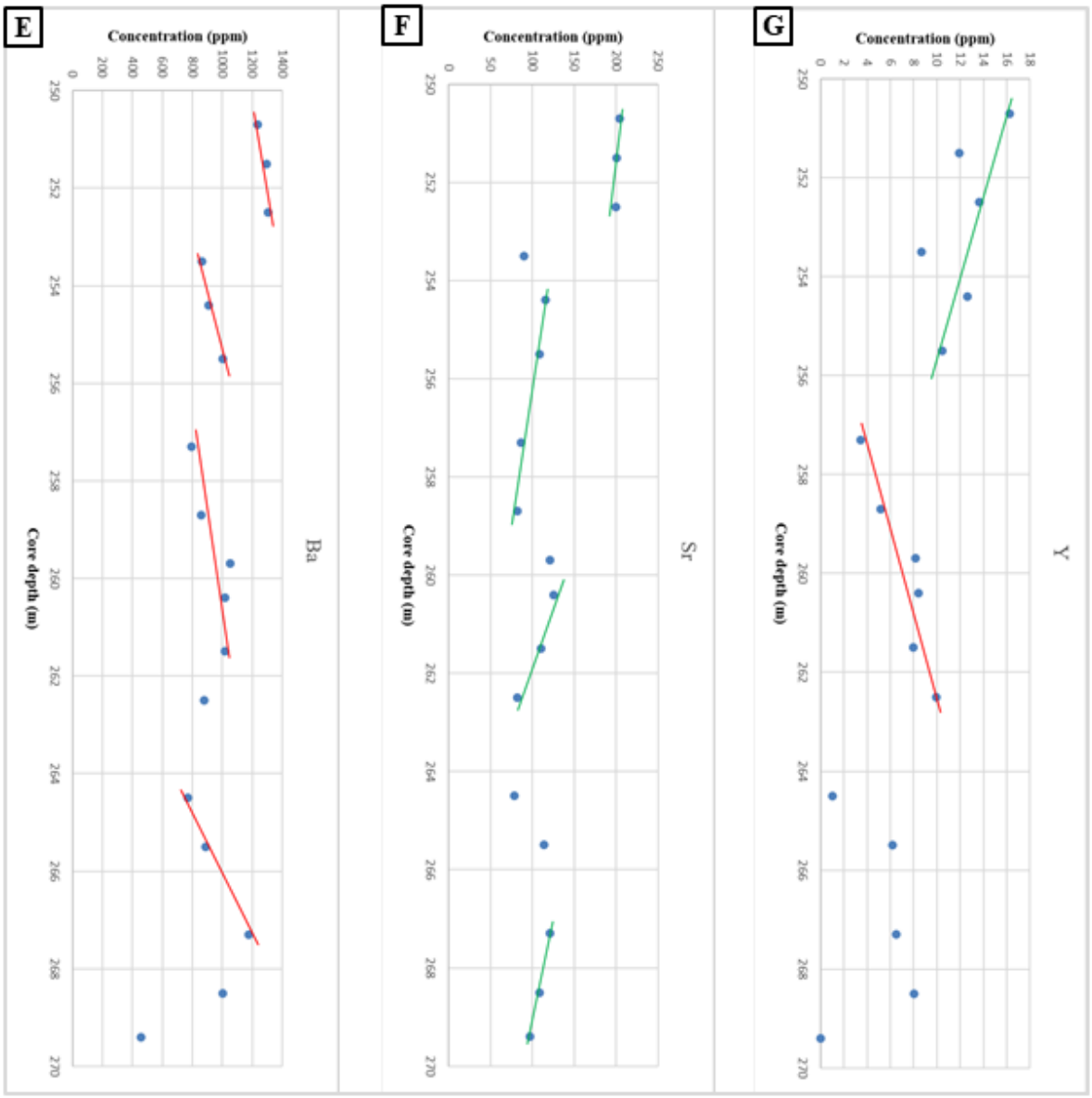

Figure II.7: (A)-(G) XRF-analysis of the Grumantbyen Formation in core 7-2006 (not presented in chapter 5).

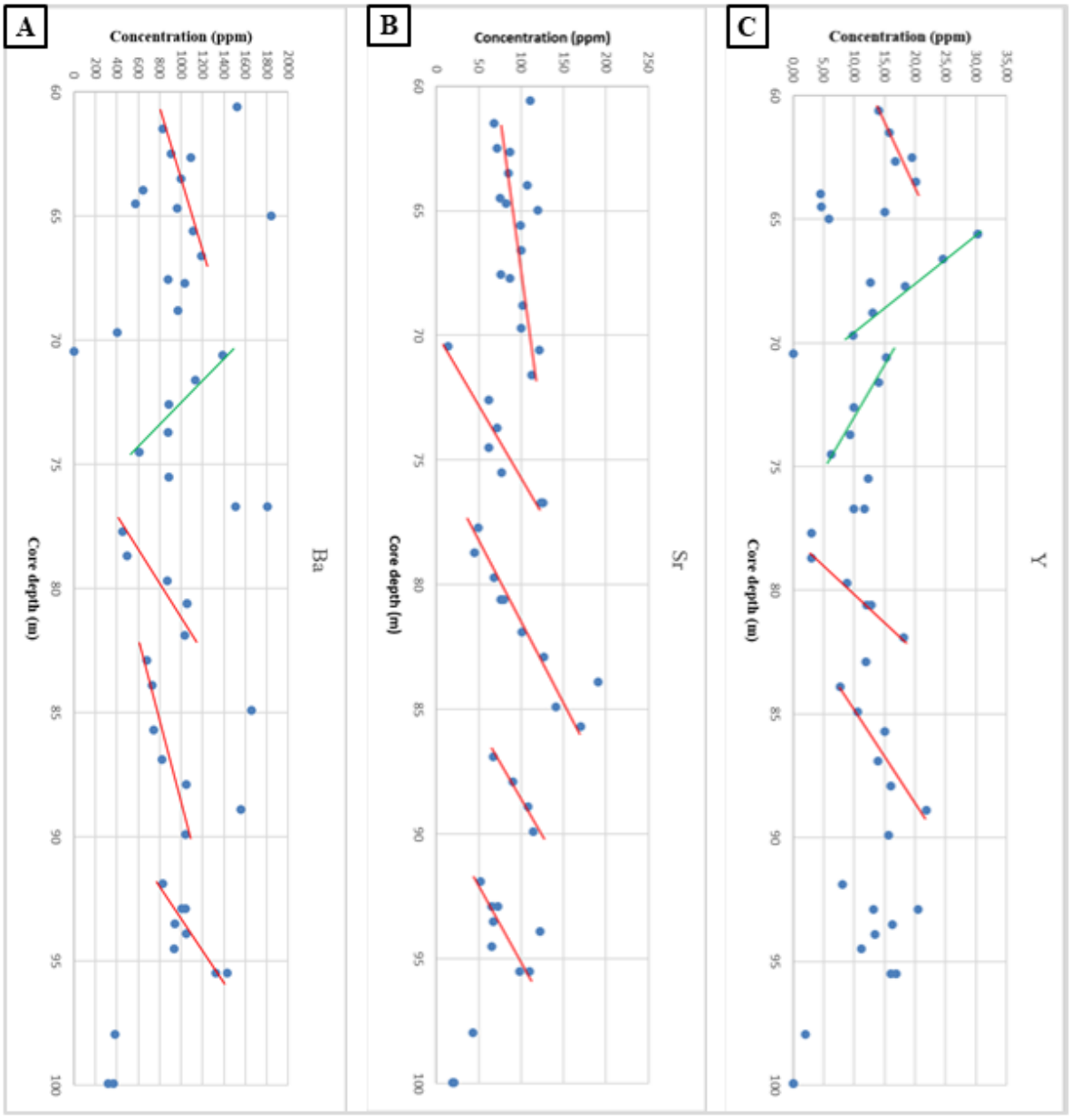

Figure II.8: (A)-(C) Additional geochemical trends identified in the Aspelintoppen Formation (core 11-2003).

APPENDIX III: *Optical micrographs*

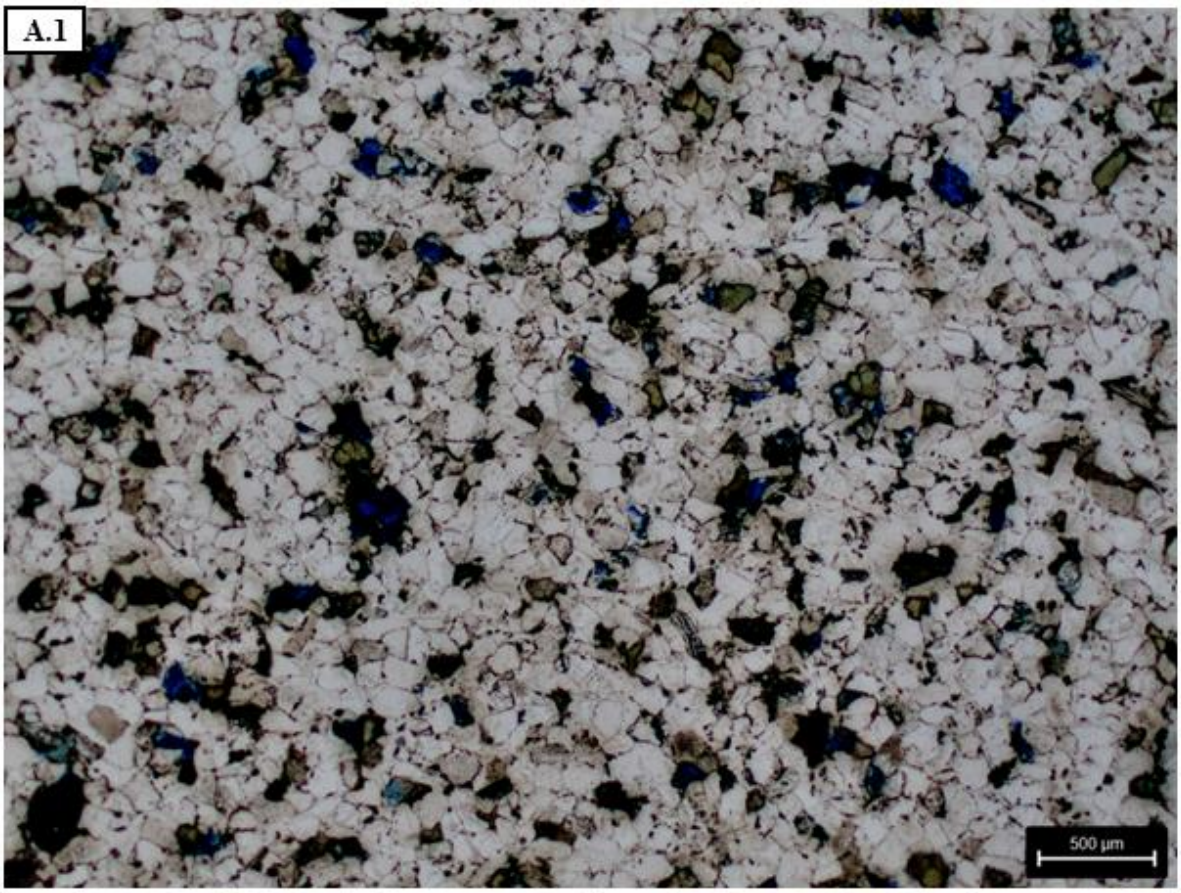
A.1
500 µm

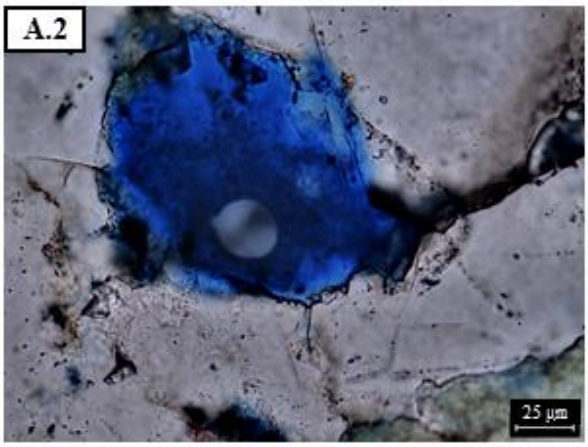
A.2
25 µm

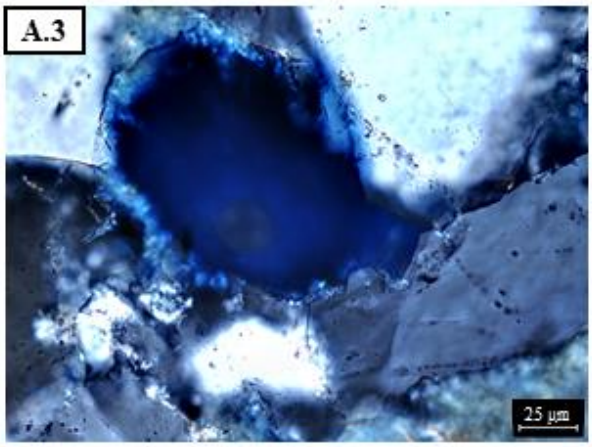
A.3
25 µm

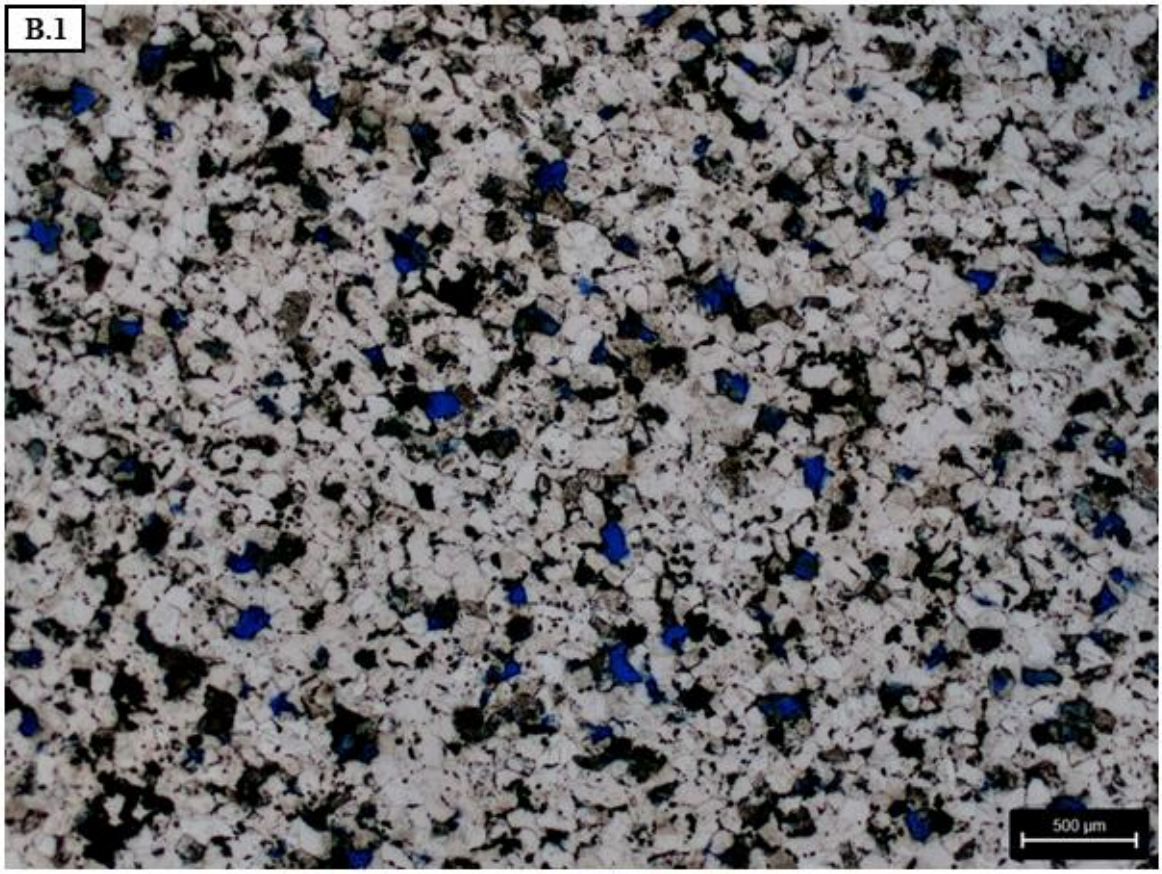
B.1
500 µm

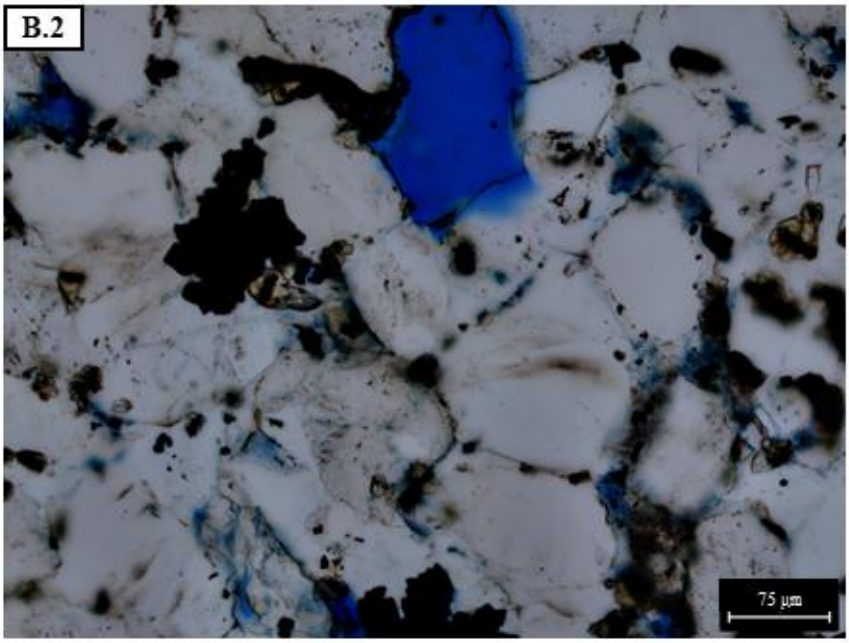
B.2
75 µm

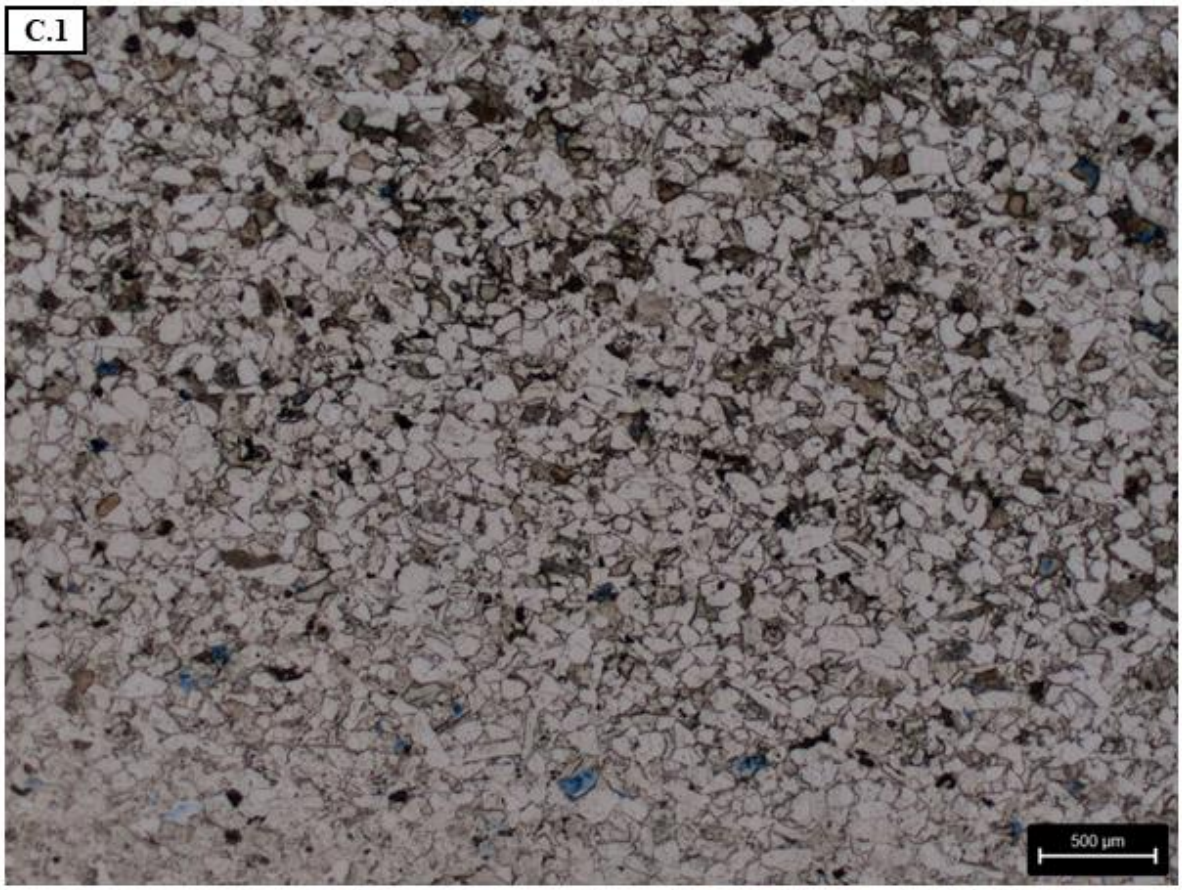
C.1
500 µm

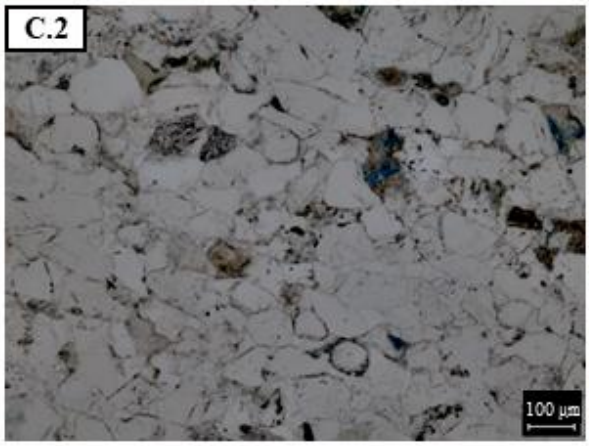
C.2
100 µm

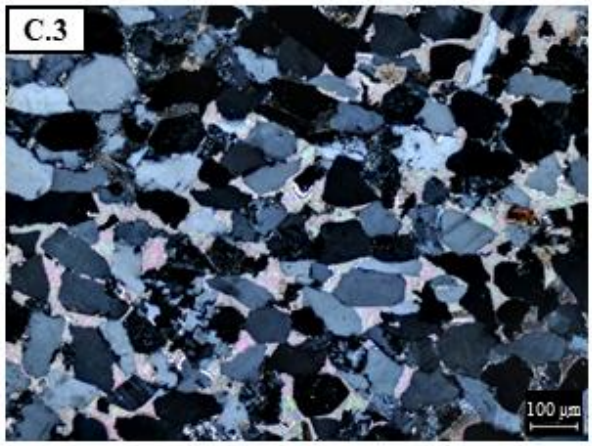
C.3
100 µm

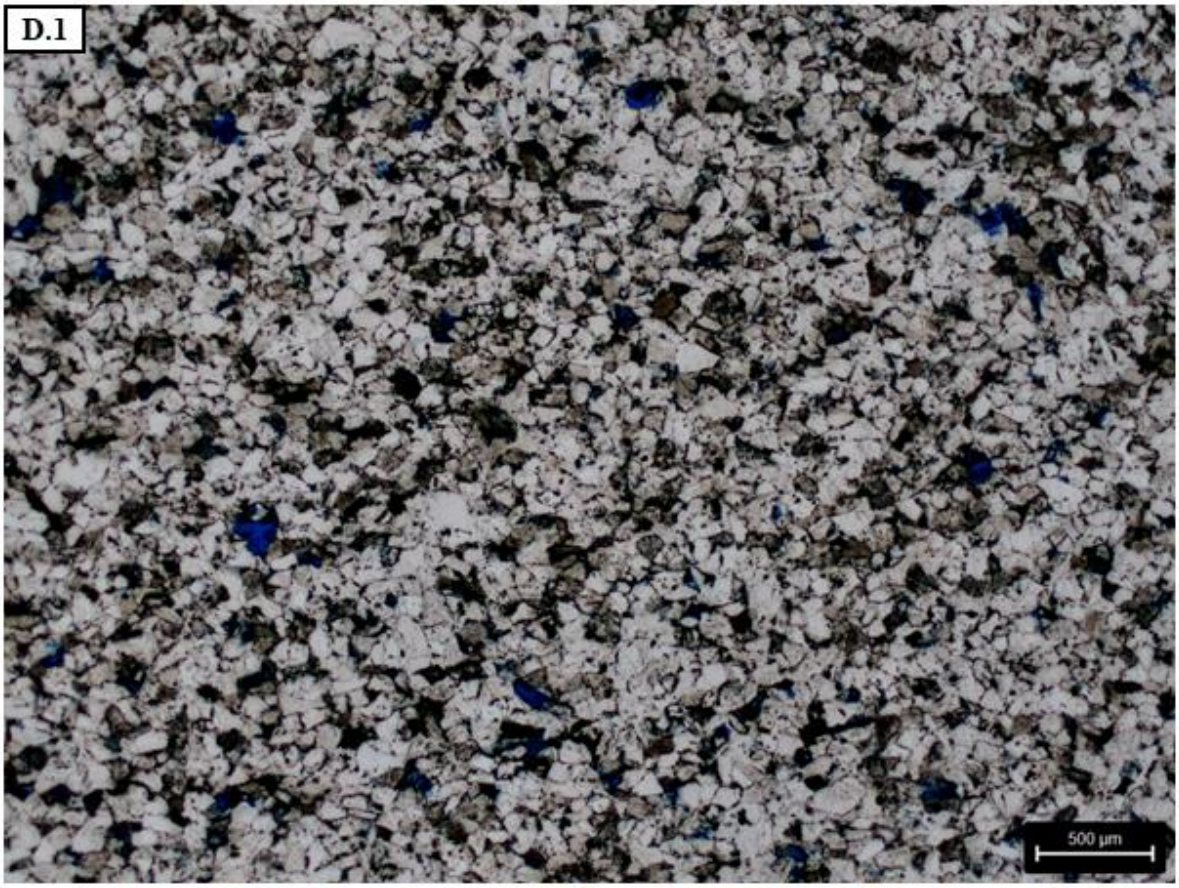
D.1
500 µm

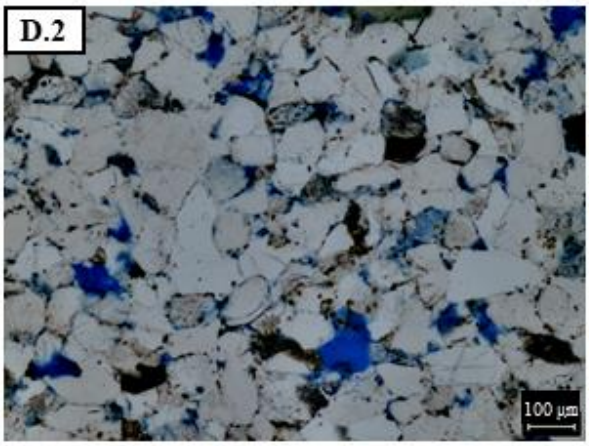
D.2
100 µm

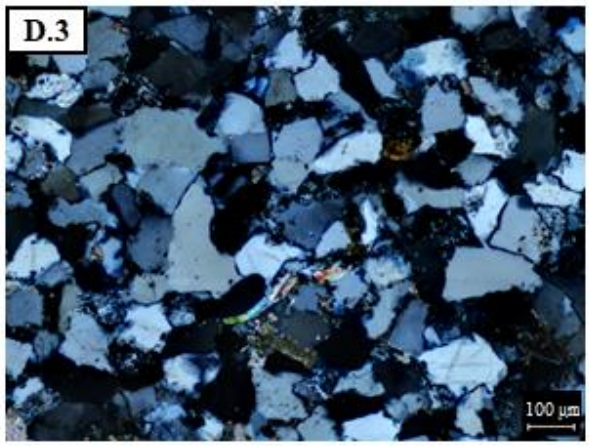
D.3
100 µm

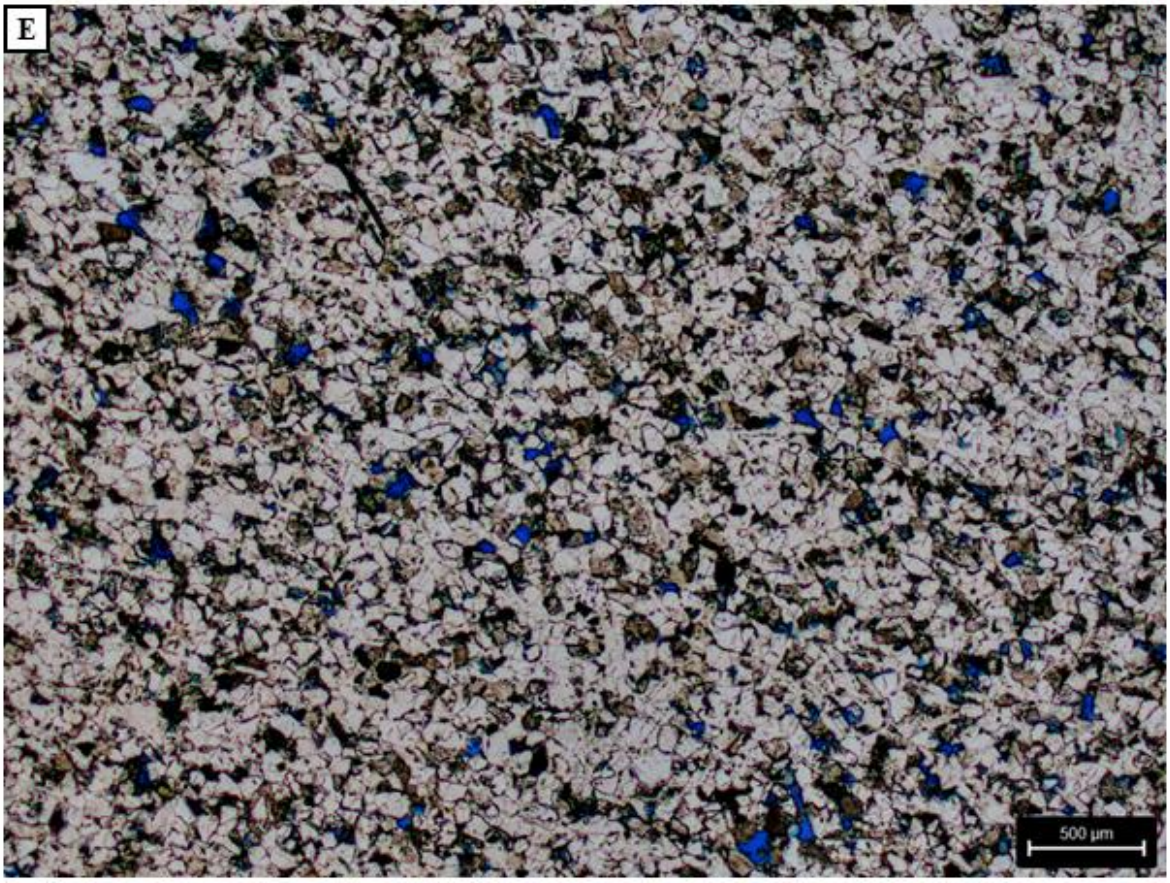
E
500 µm

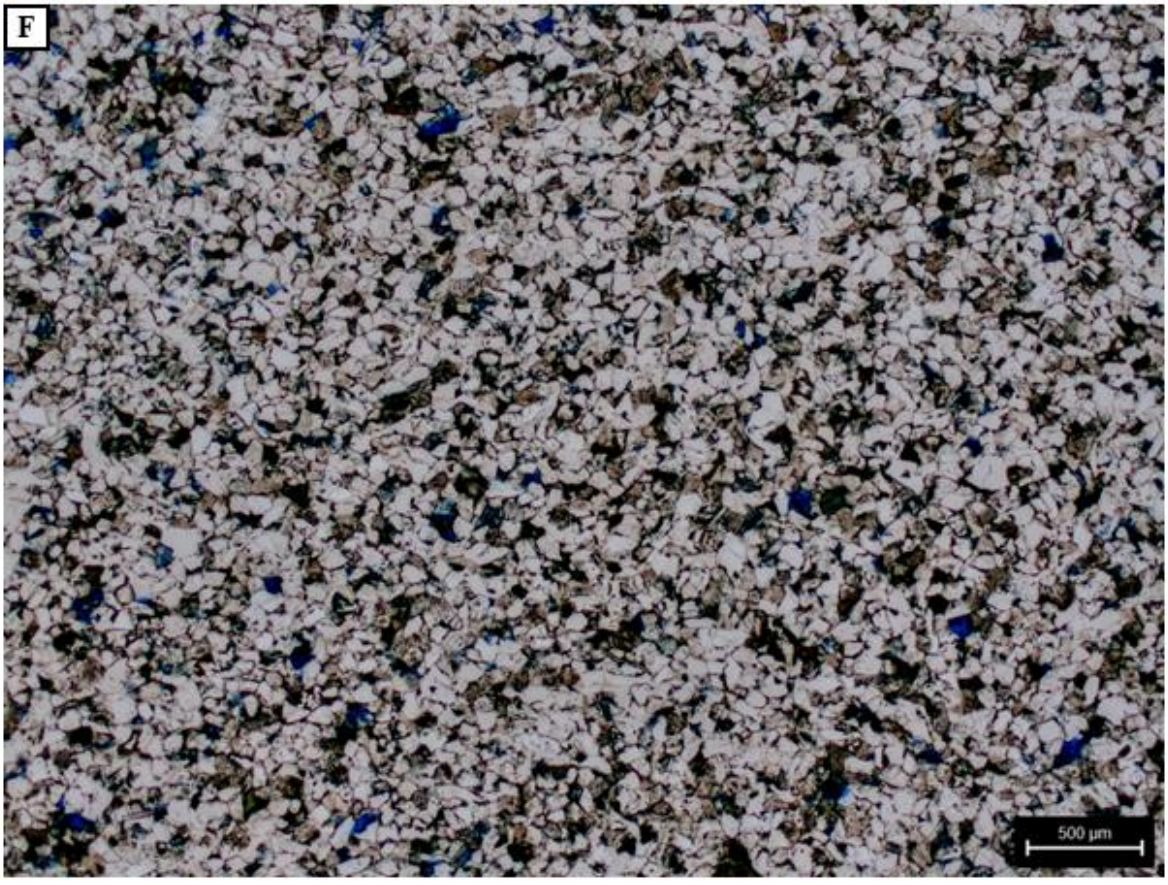
F
500 µm

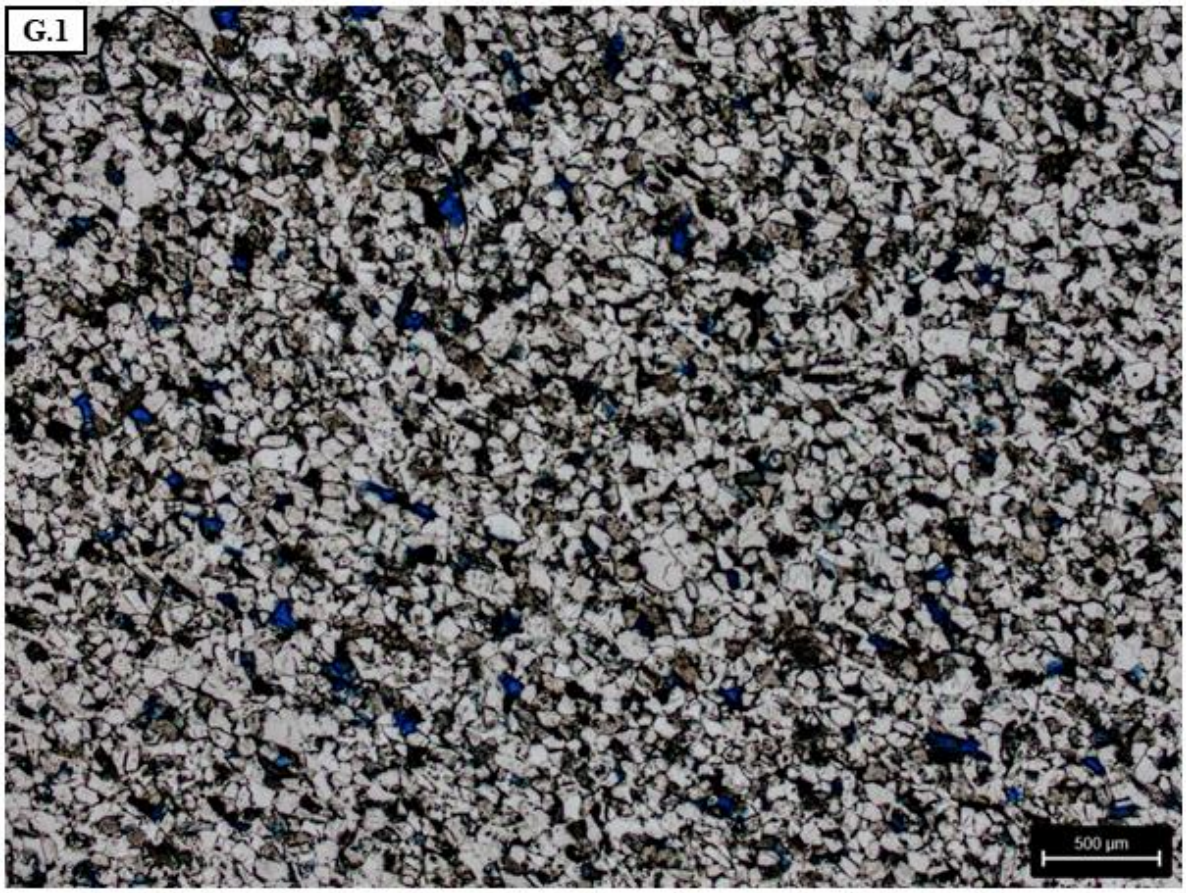
G.1
500 µm

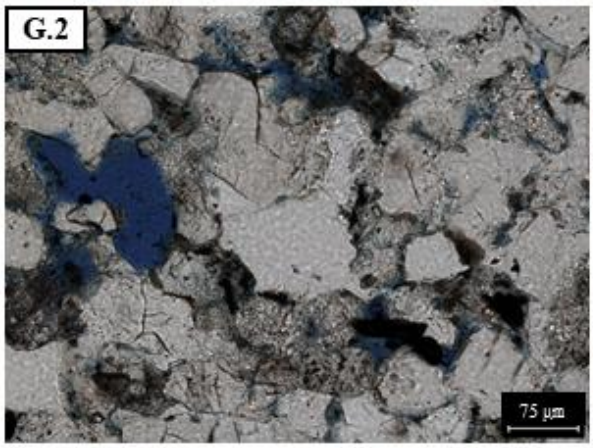
G.2
75 µm

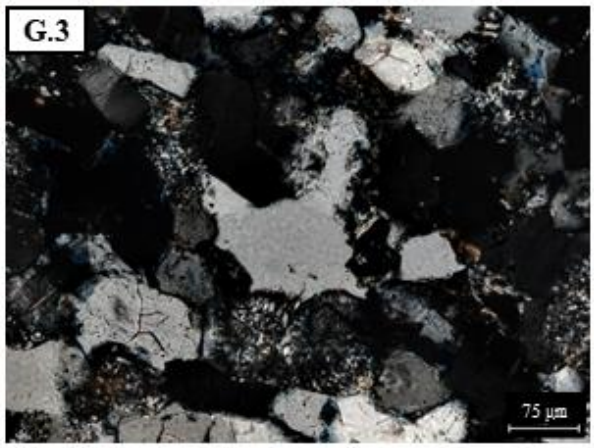
G.3
75 µm

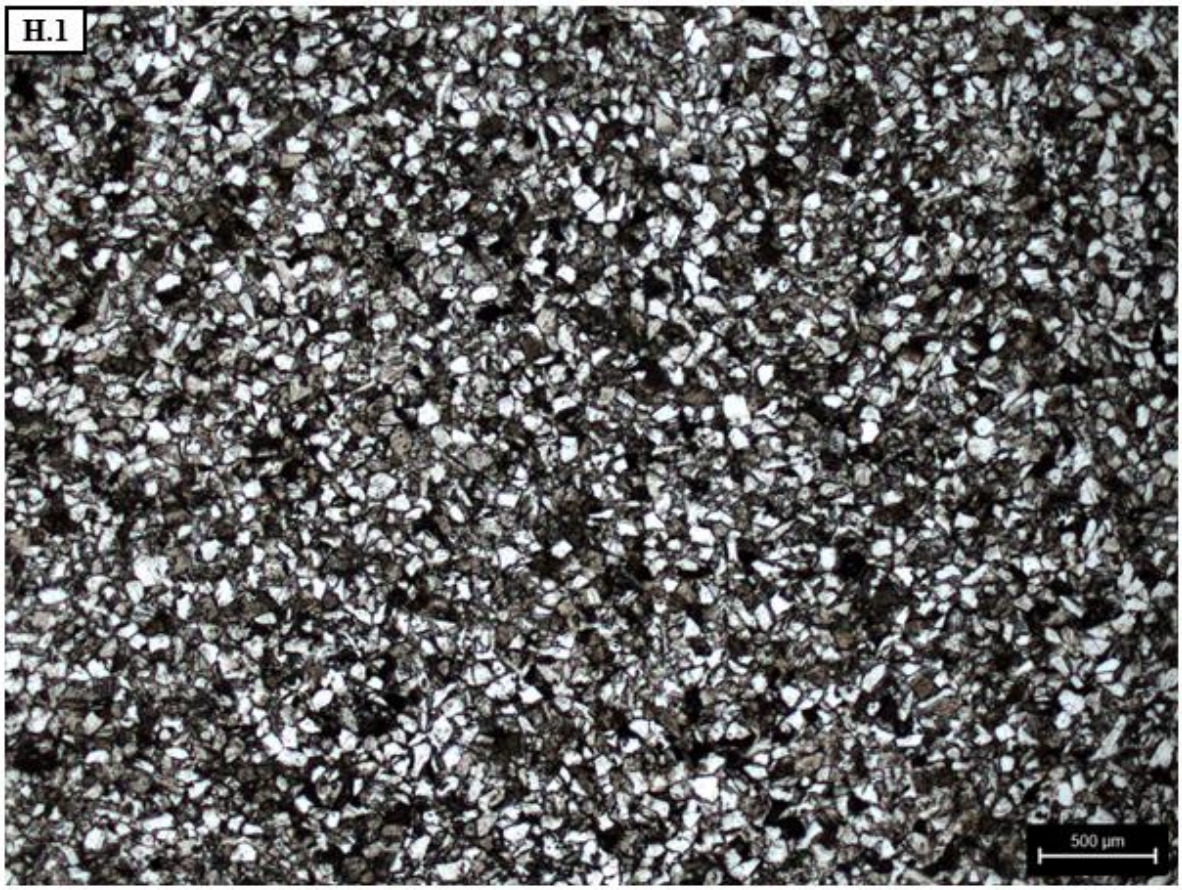
H.1
500 µm

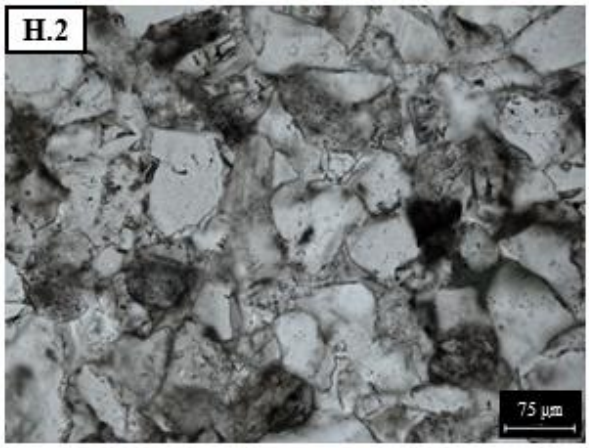
H.2
75 µm

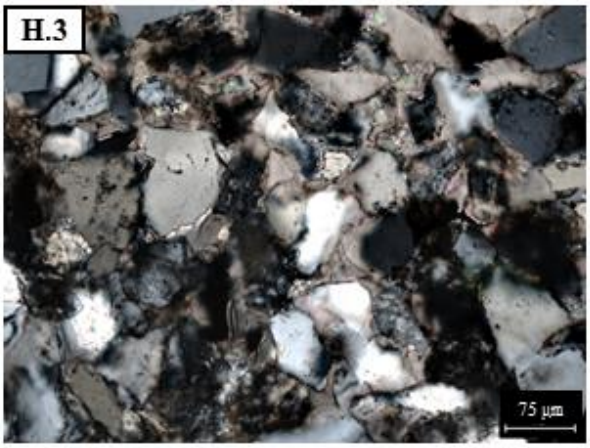
H.3
75 µm


I.1
500 µm

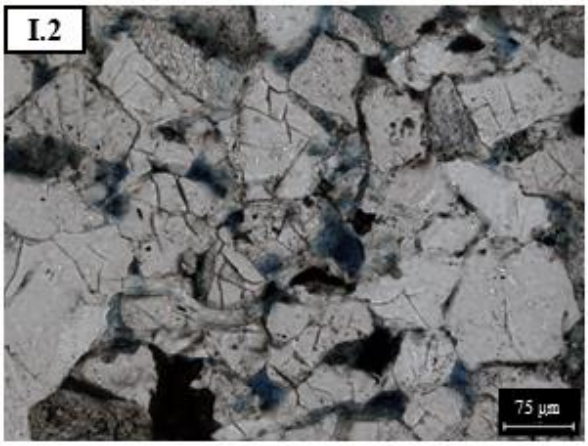
I.2
75 µm

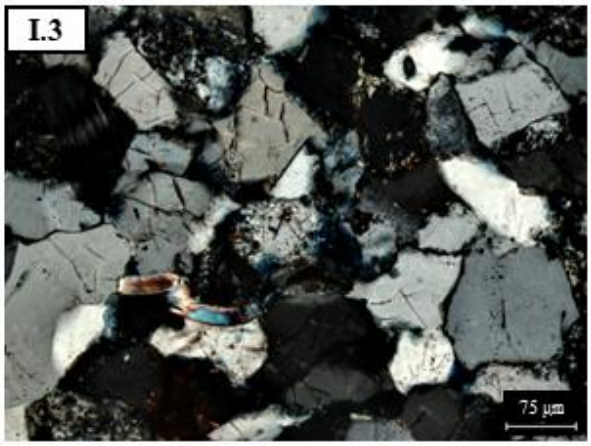
I.3
75 µm


J
500 µm


K
500 µm


L.1
500 µm

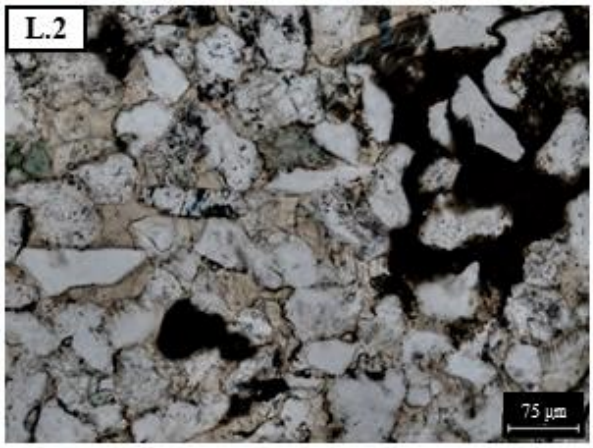
L.2
75 µm

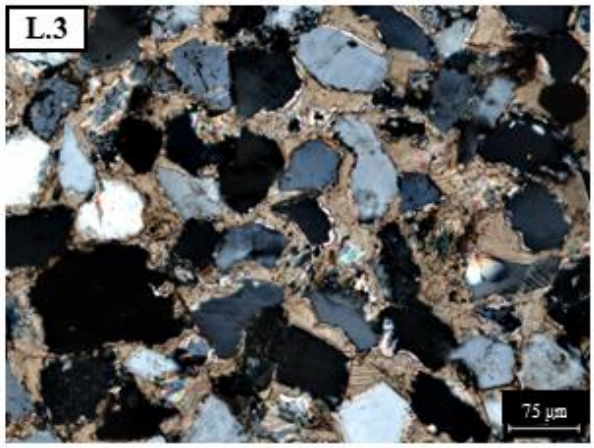
L.3
75 µm


M
500 µm


N
500 µm

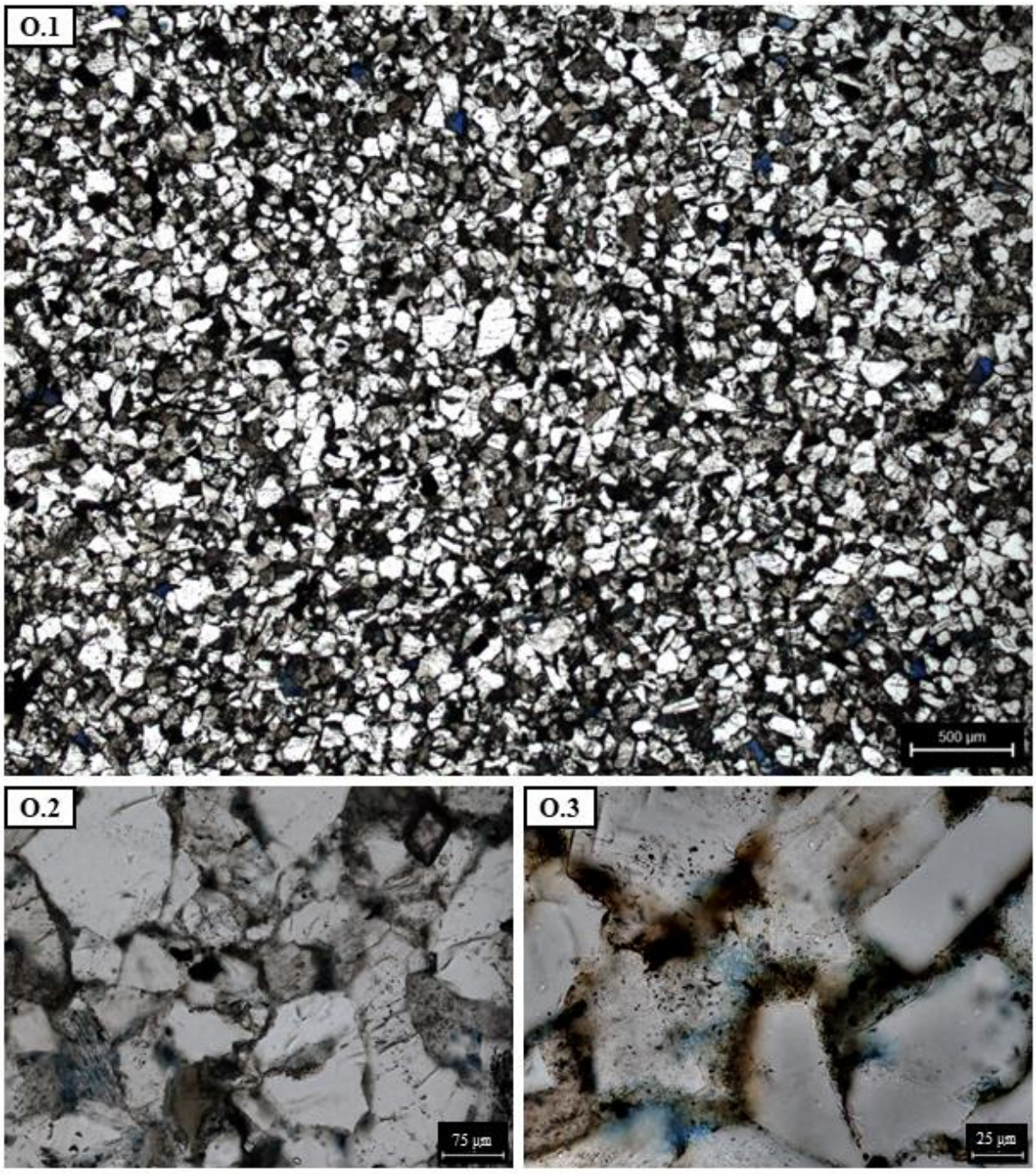
O.1
500 µm
O.2
75 µm
O.3
25 µm

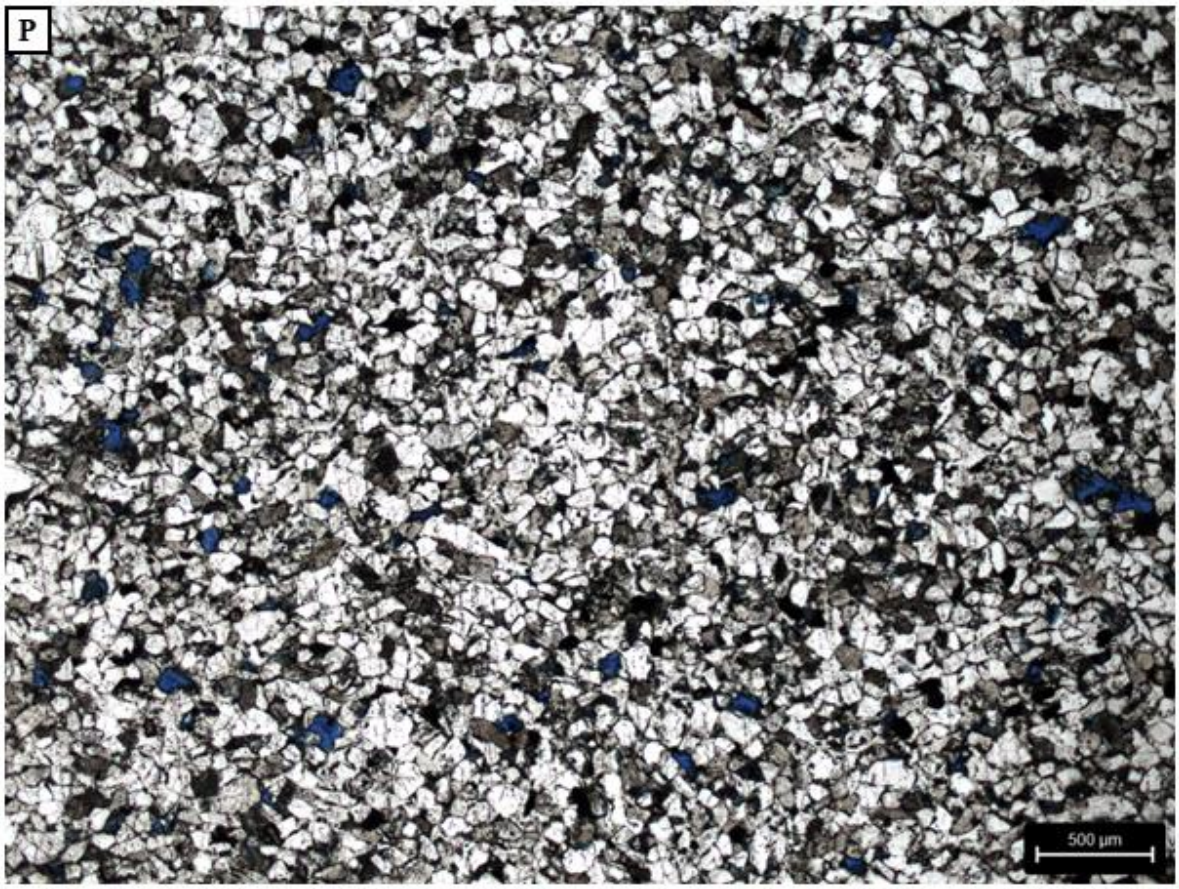
P
500 µm

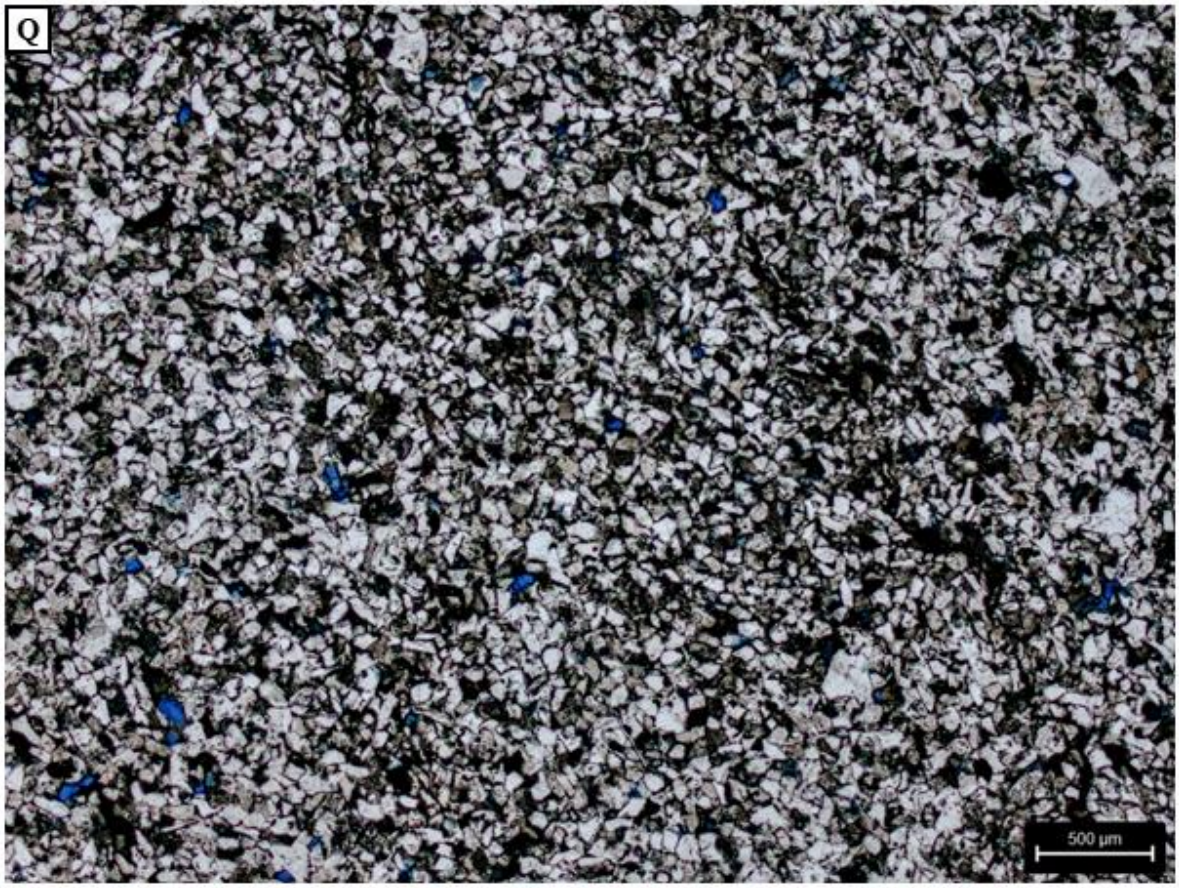
Q
500 µm

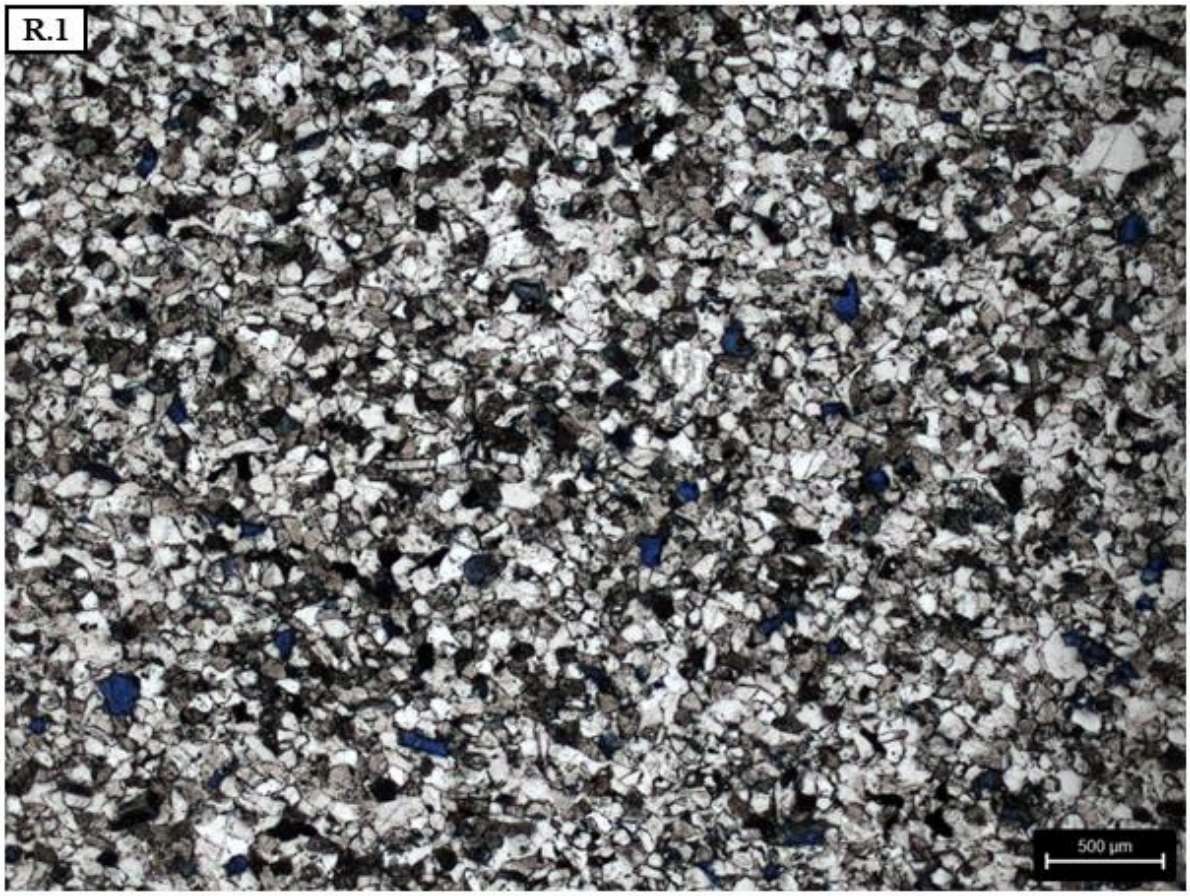
R.1
500 µm

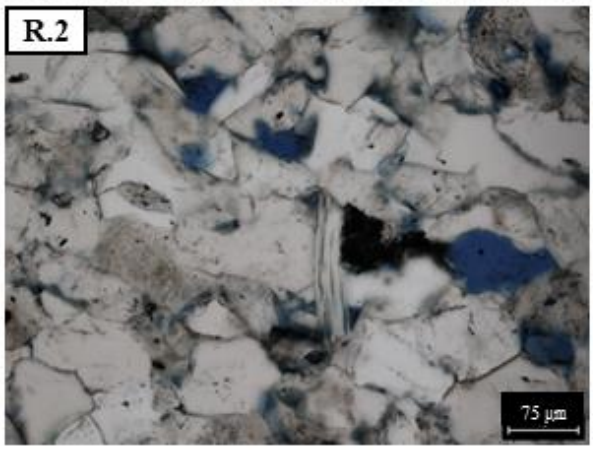
R.2
75 µm

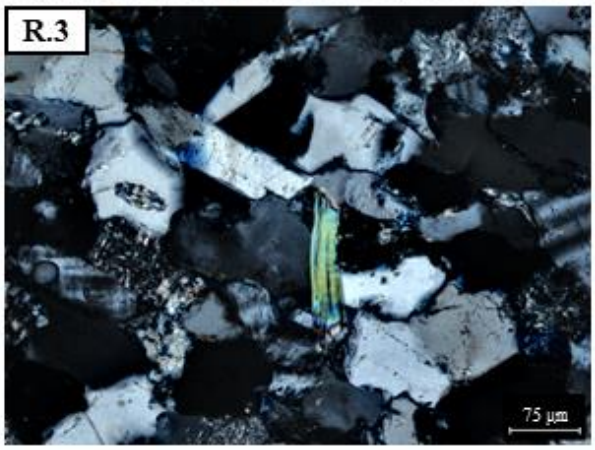
R.3
75 µm

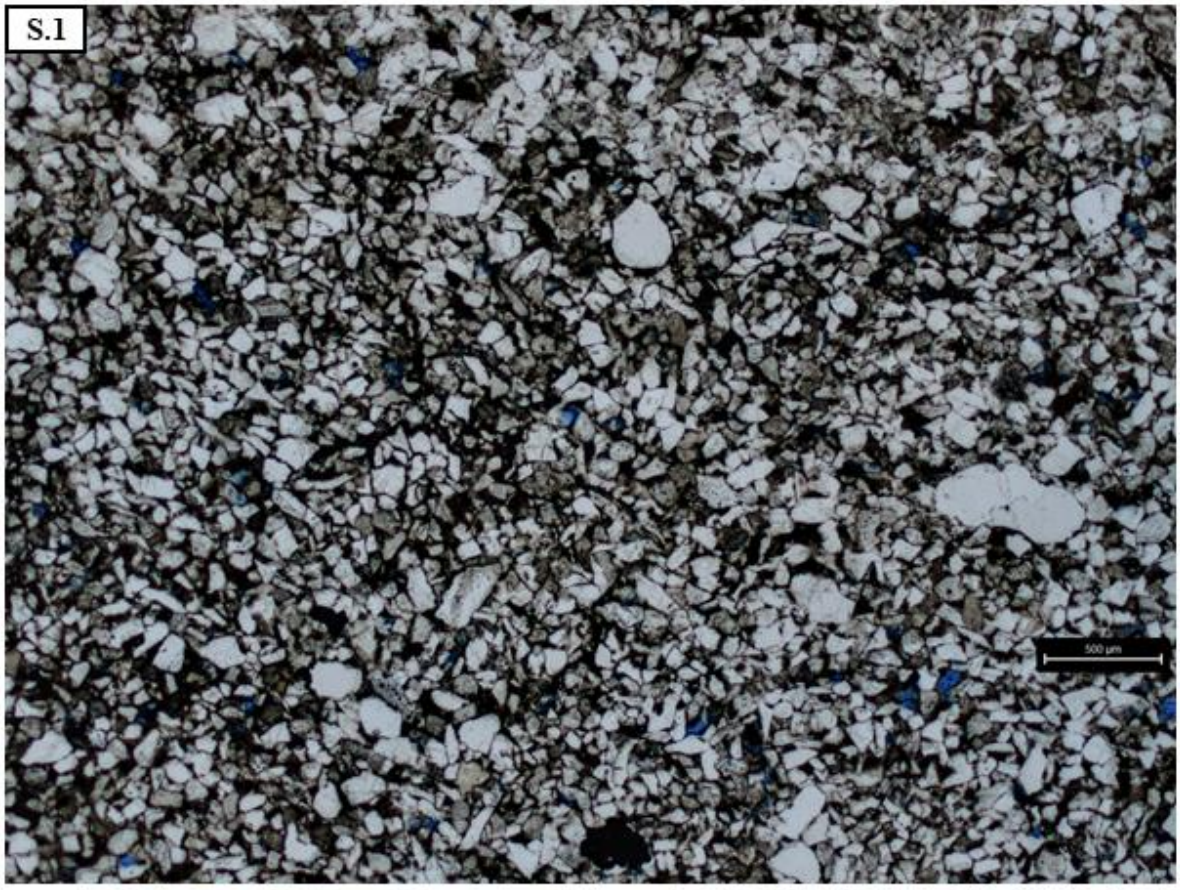
S.1
500 µm

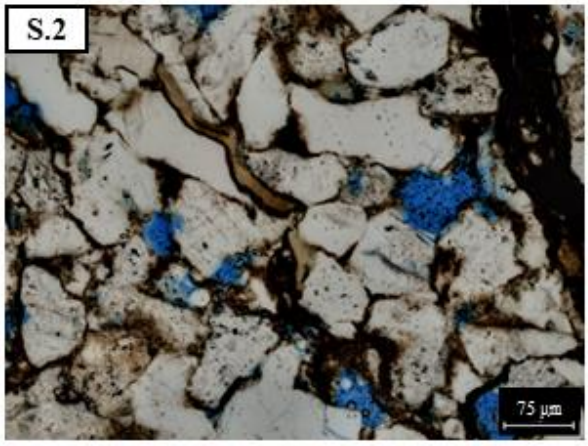
S.2
75 µm

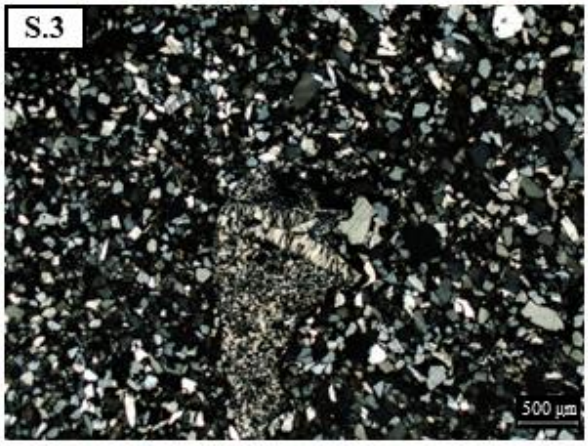
S.3
500 µm

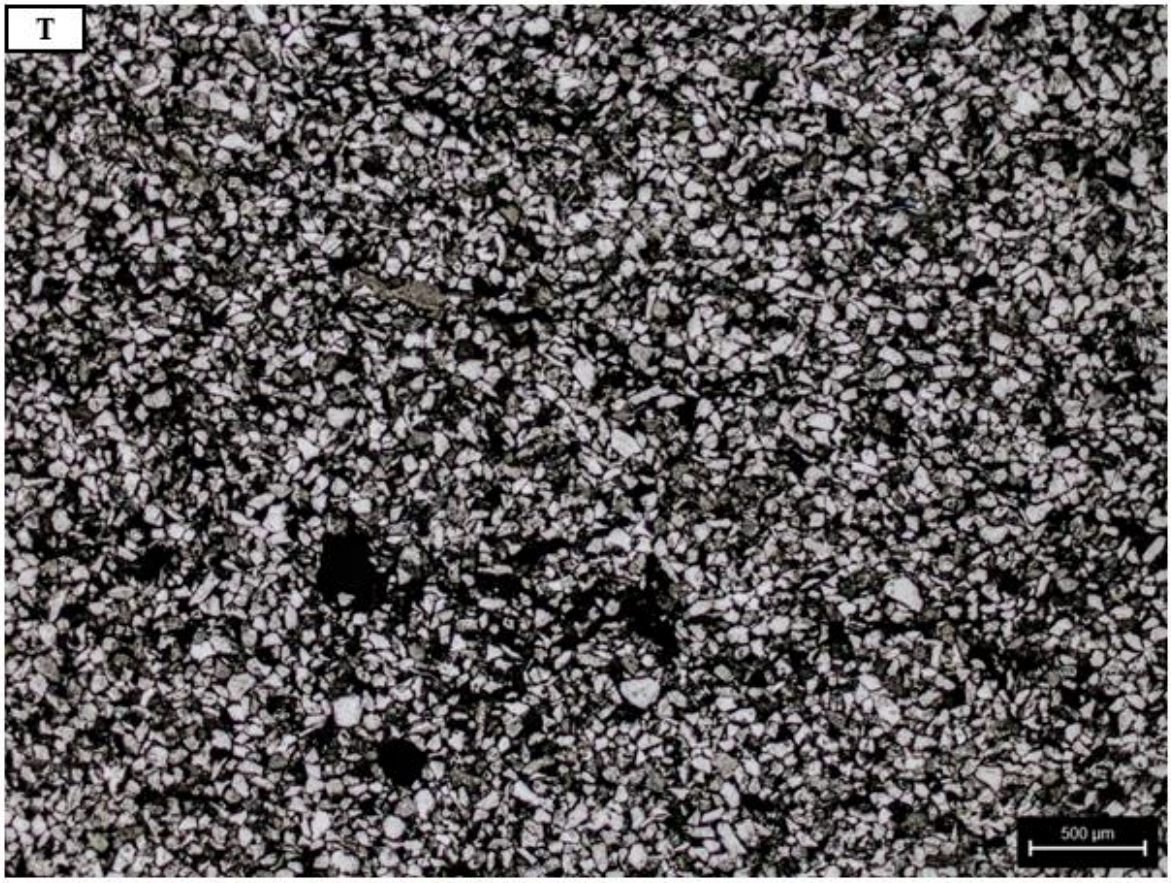
T
500 µm

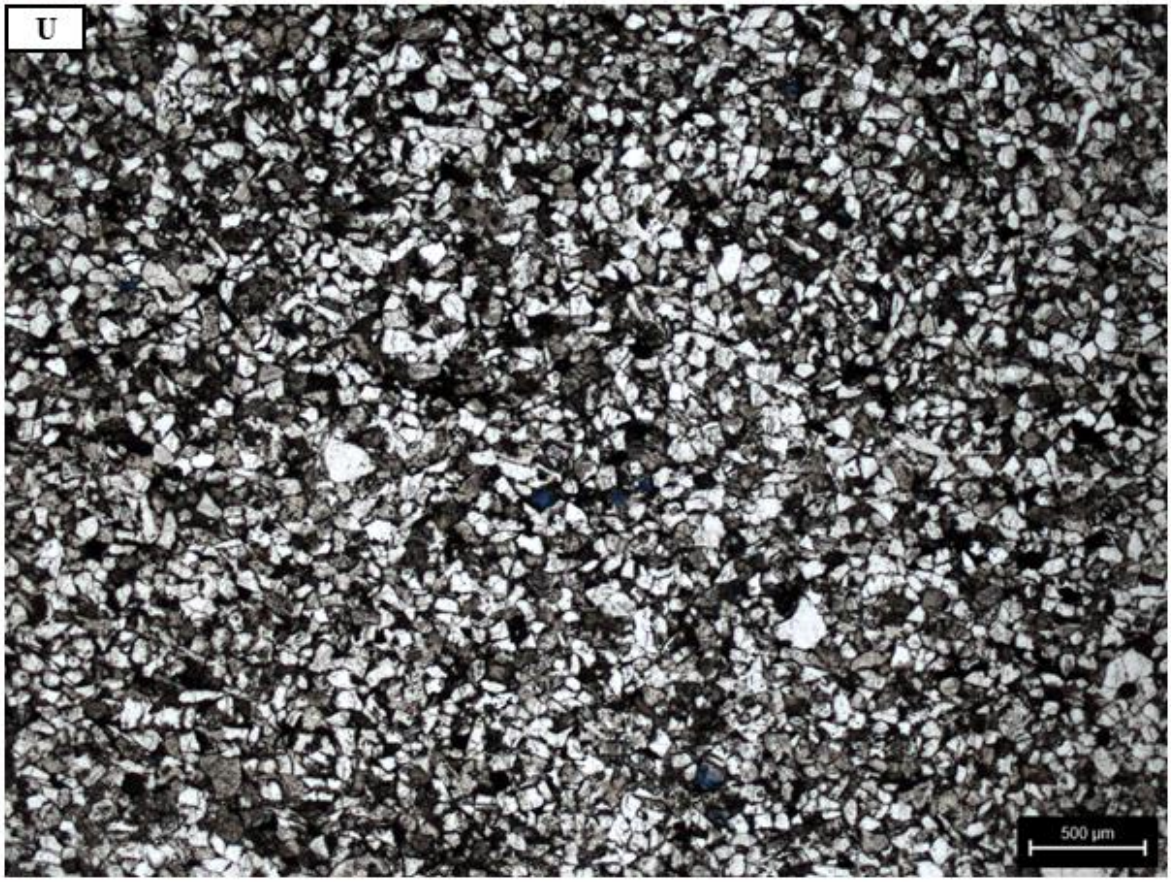
U
500 µm


V.1
500 µm

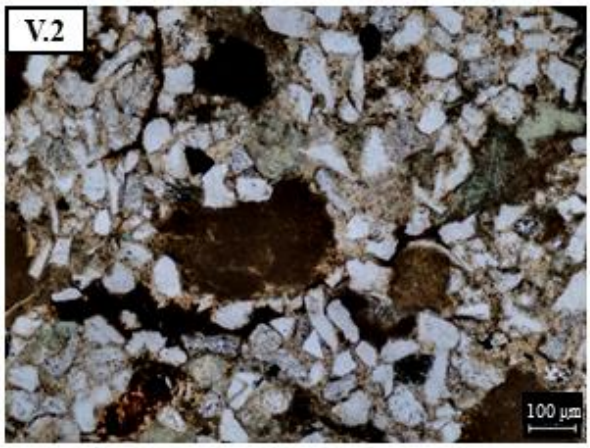
V.2
100 µm

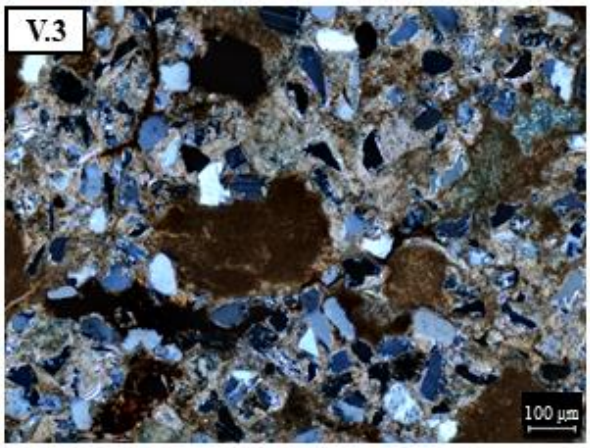
V.3
100 µm

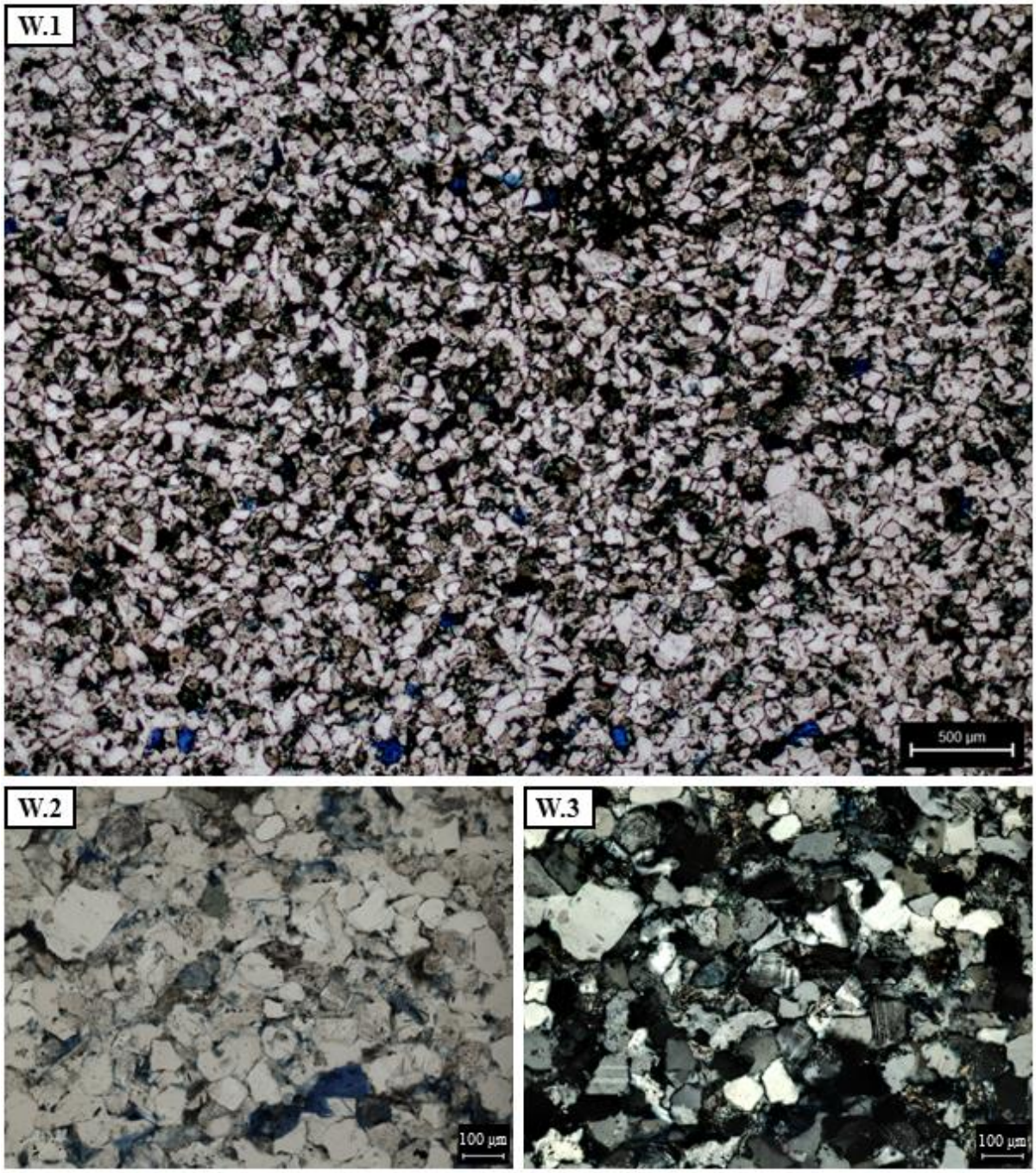

Figure III.1: Optical micrographs of most samples from the Firkanten Formation (core 7-2006). Large-scale optical micrographs (2,5x) are in PPL. (A) Sample F1. (B) Sample F2. (C) Sample F3. (D) Sample F4. (E) Sample F5. (F) Sample F7. (G) Sample F8. (H) Sample F9. (I) Sample F10. (J) Sample F11. (K) Sample F12. (L) Sample F13. (M) Sample F14. (N) Sample F15. (O) Sample F16. (P) Sample F17. (Q) Sample F18. (R) Sample F20. (S) Sample F22. (T) Sample F23. (U) Sample F24. (V) Sample F25. (W) Sample F26.

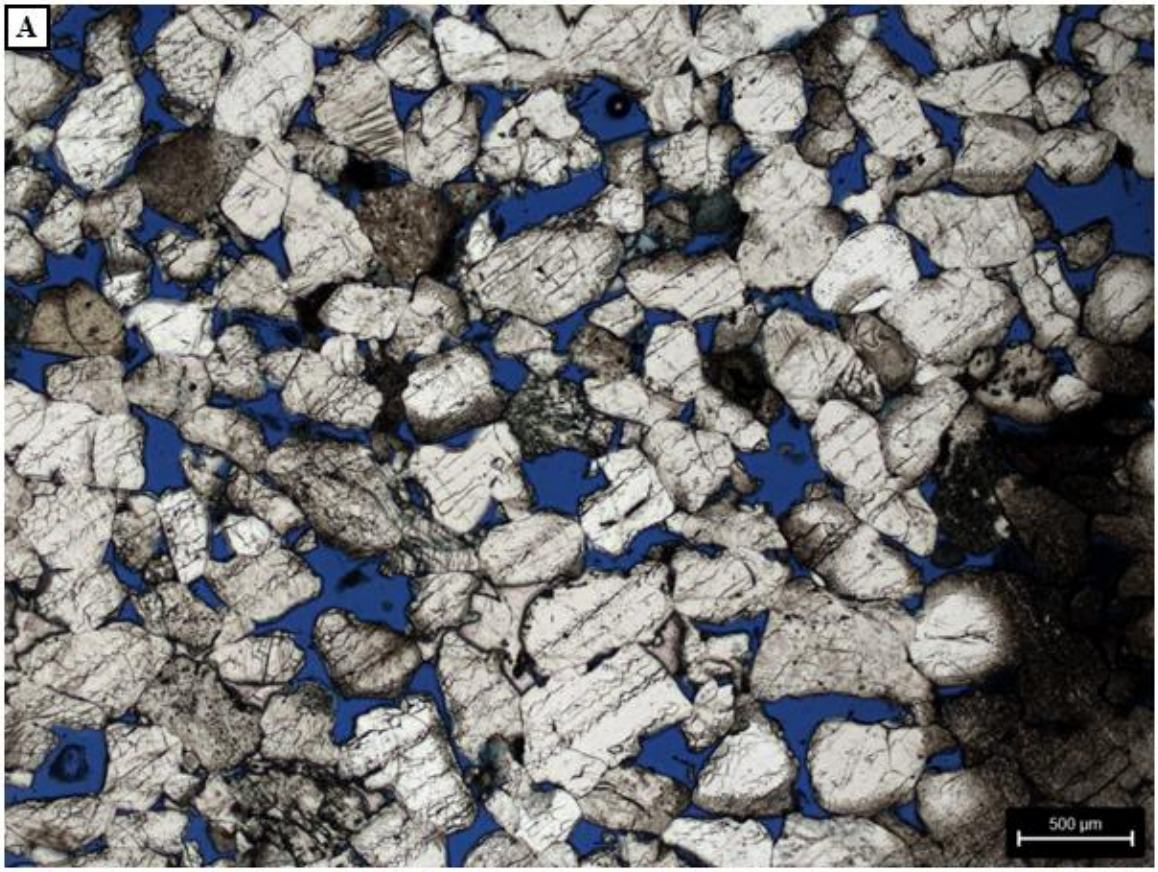
A
500 µm

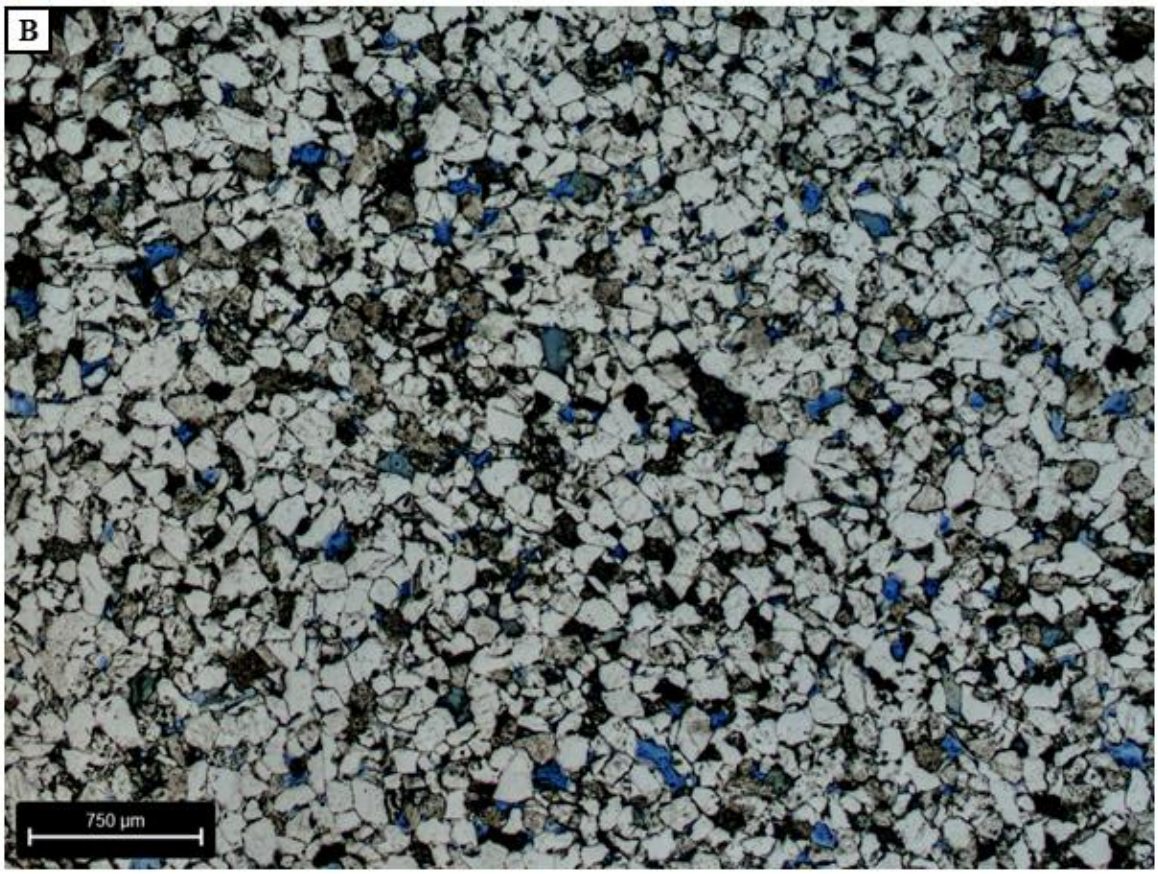
B
750 µm

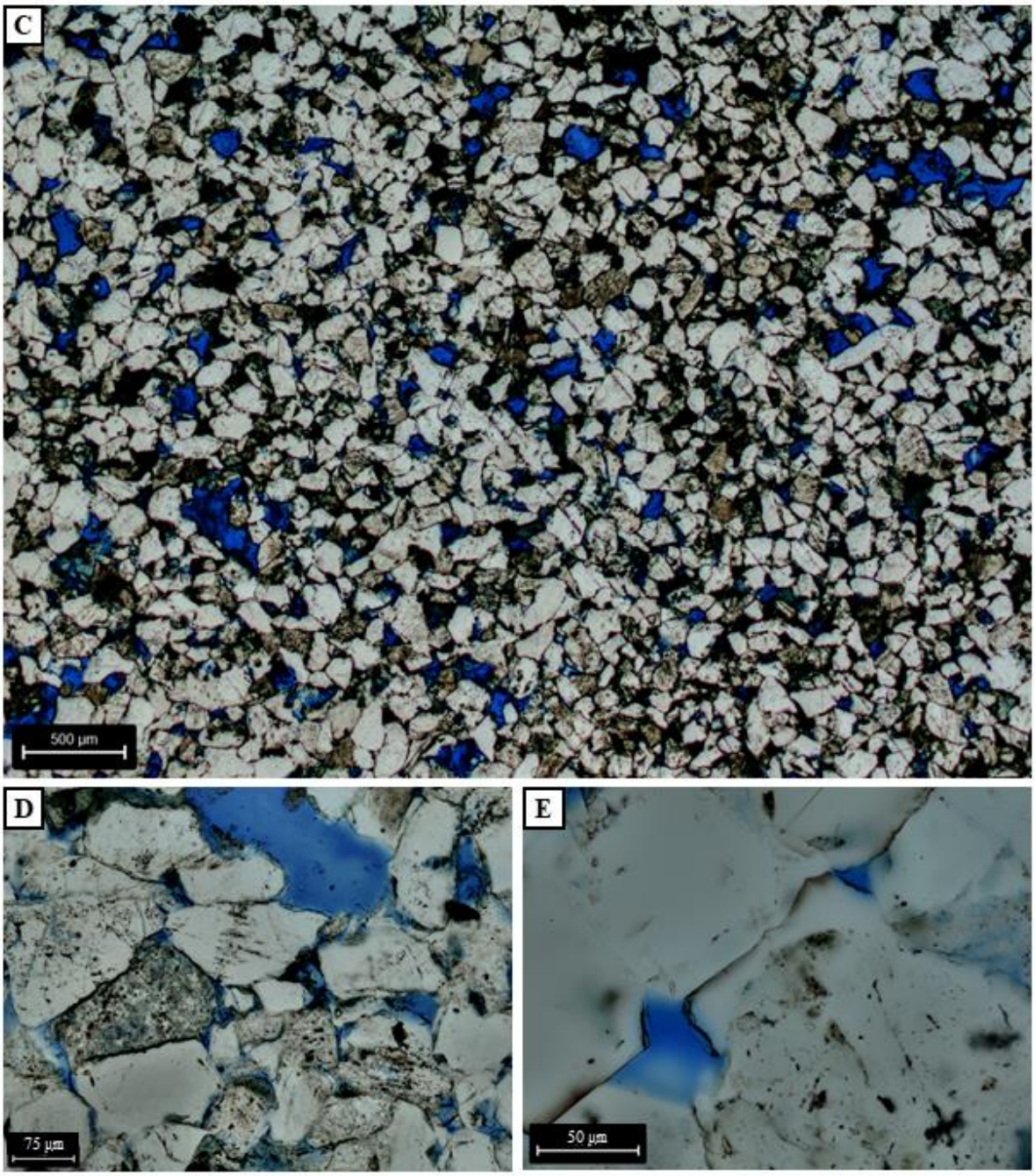

Figure III.2: Optical micrographs of samples from the Grumantbyen Formation in core 7-2006. Large-scale optical micrographs (2,5x) are in PPL. (A) Sample G1. (B) Sample G2. (C)-(E) Sample G3.

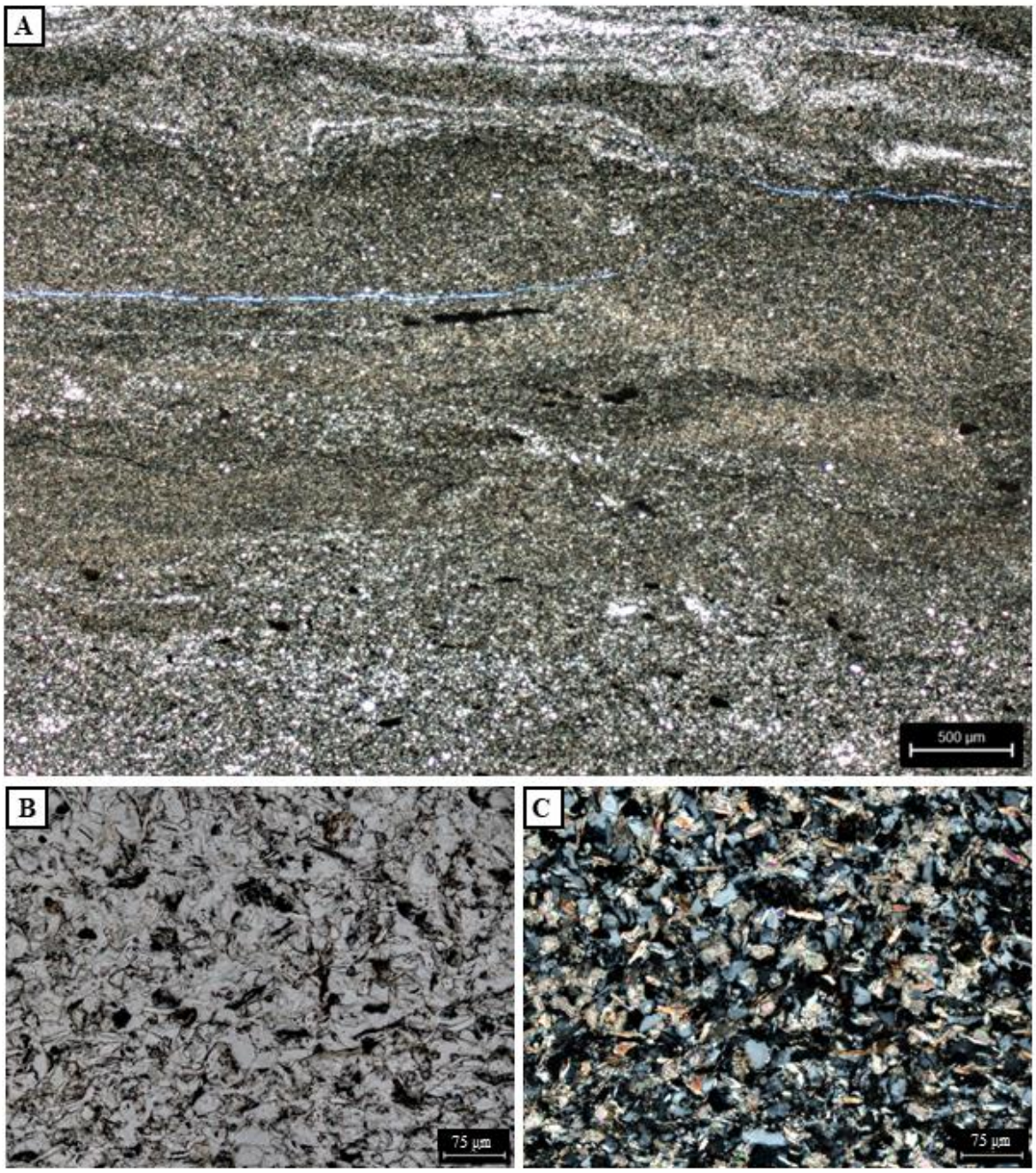
A
500 µm
B
75 µm
C
75 µm

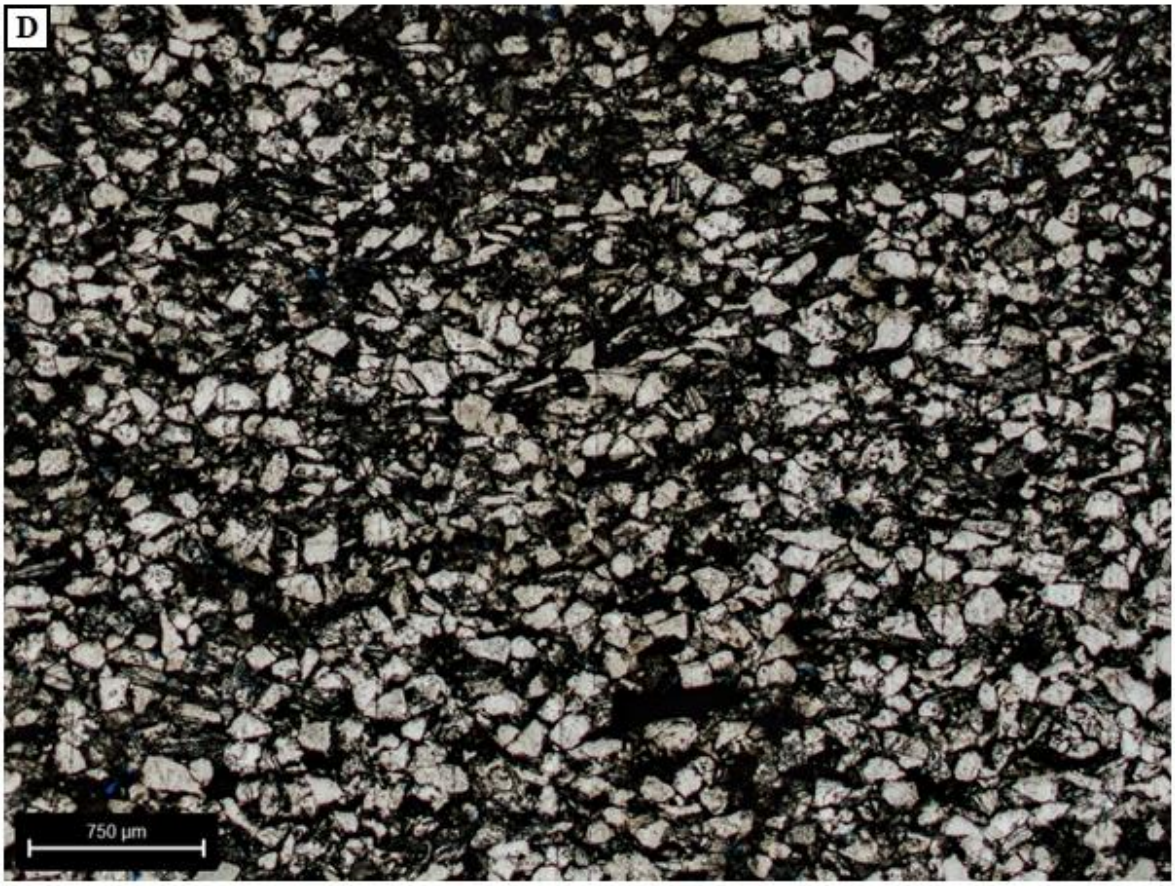
D
750 µm


E
100 µm

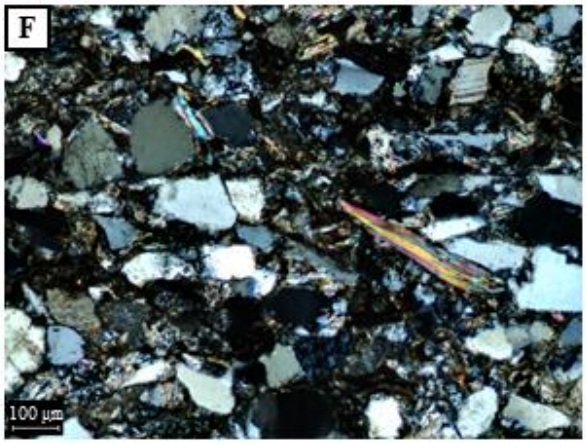
F
100 µm

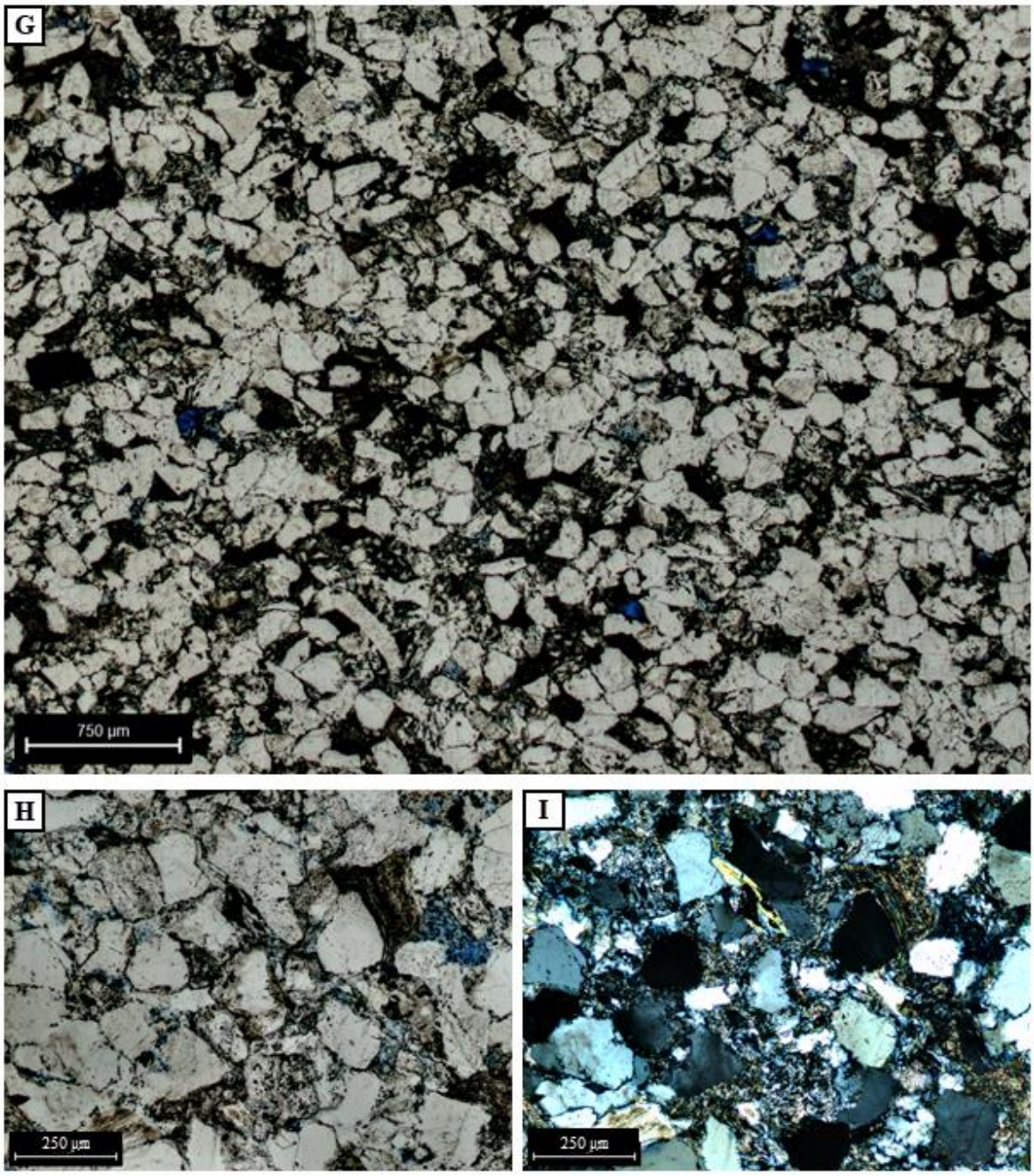

Figure III.3: Optical micrographs of samples A3, A6 and A7 from the Aspelintoppen Formation (core 11-2003). Large-scale optical micrographs (2,5x) are in PPL. (A)-(C) Sample A3. (D)-(F) Sample A6. (G)-(I) Sample A7.